# Protein and epigenetic biomarkers for variability in epidermal growth factor receptor inhibition in cancer treatment and characterization of the inhibitor-induced skin toxicity in an *in vitro* model

**Dissertation**

zur

Erlangung des Doktorgrades (Dr. rer. nat.)

der

Mathematisch-Naturwissenschaftlichen Fakultät

der

Rheinischen Friedrich-Wilhelms-Universität Bonn

vorgelegt von

**Vivien Sandra Hichert**

aus

Köln

Bonn 2018

Angefertigt mit Genehmigung der Mathematisch-Naturwissenschaftlichen Fakultät der Rheinischen Friedrich-Wilhelms-Universität Bonn.

1. Gutachter/in: Prof. Dr. Julia Stingl

2. Gutachter/in: Prof. Dr. Ulrich Jaehde

Tag der Promotion: 08.01.2019

Erscheinungsjahr: 2019

Die vorliegende Arbeit wurde in der Zeit von 2013 bis 2018 in der Forschungsabteilung des Bundesinstituts für Arzneimittel und Medizinprodukte (BfArM) unter Leitung von Frau Prof. Dr. Julia Stingl angefertigt.

„Man muss nicht alles wissen,

man muss nur wissen, wo es steht!“

Gerd Hichert
(frei nach Albert Einstein)

## Abstract

Epidermal growth factor receptor (EGFR) is often over-expressed or over-activated in cells of solid tumors and can be targeted by specific inhibitors (EGFRIs), like erlotinib, gefitinib, cetuximab and panitumumab. Unfortunately, EGFRIs only seem to work in a subset of patients suffering from EGFR-expressing tumors. Efficient biomarkers to reliably select patients who will benefit from an EGFRI therapy and determine their optimal dosage are still needed. One of the most common adverse drug reactions observed during therapy with all approved EGFRIs is the development of a typical skin rash. It has been shown in various studies that occurrence and severity of this EGFRI-induced rash are positively correlated with patient outcome (prolonged overall and progression-free survival). However, the rash usually takes several weeks to manifest and is usually treated with topical or systemic medication. Hence, its severity may be suppressed, rendering it unsuitable as a clinical predictive marker. Therefore, the aim of this study was to identify rapidly determinable predictive biomarkers for the severity of EGFRI-induced skin rash, which would be helpful to allow early preventive treatment of the rash while at the same time still allowing prediction of EGFRI efficacy early on and facilitate optimization of personalized cancer therapy for individual patients. They can also help to prevent exposure of patients to substances which are ineffective but still cause discomforting side effects.

Since previous work revealed evidence for genetic, pharmacokinetic and cytokine markers, the intention of this work was to identify functional biomarkers that are able to measure EGFR inhibition variability in the periphery, especially in blood plasma and skin cells. Therefore, molecules that interact with, regulate or functionally modulate EGFR inhibition were selected and their levels determined in plasma samples from patients treated with an EGFRI by enzyme-linked immunosorbent assay (ELISA) and it was checked for correlations with the development of EGFRI-induced skin toxicity. The EGFRI cetuximab, the EGFR ligand amphiregulin (AREG) and the growth factors hepatocyte growth factor (HGF) and 25-OH-vitamin D were selected as candidates following these criteria.

Since miRNAs have recently been shown to be very important in the response to cancer therapy, investigating the suitability of specific mature or precursor miRNA molecules as functional, epigenetic biomarkers for the development of EGFRI-induced skin toxicity was of special interest. Therefore, next generation sequencing (NGS) was performed in keratinocyte and fibroblast cultures from healthy donors to compare miRNA profiles

between cells previously identified as rather erlotinib-sensitive and those identified as rather erlotinib-insensitive.
Results show that plasma levels of the EGFRI cetuximab were not significantly associated with development of EGFRI-induced rash.
While the investigated candidates AREG and 25-OH-vitamin D also failed to show a significant correlation with the rash, the plasma concentration of the MET ligand HGF was significantly inversely correlated with severity of EGFRI-induced skin rash. This inverse correlation was also seen with overall survival (OS) in patients who developed EGFRI-induced rash but not in patients with no rash. HGF seems to be a promising biomarker, whose predictive and/or prognostic value should definitely be validated in a larger and well-controlled patient cohort.
In this study primary human dermal keratinocytes as well as fibroblasts have proven to be suitable as *in vitro* models for studying EGFRI-induced skin rash and associated potential biomarkers. Comparison of miRNA profiles between erlotinib-sensitive and rather -insensitive cells combined with a literature review to identify the miRNAs with the most supporting data, led to identification of the precursor miRNAs mir-146a, mir-31, mir-221, mir-520e and mir-944 as most promising predictive biomarkers in keratinocytes, with mir-146a, mir-520e and mir-944 having known targets and a plausible suggested mechanism of action and mir-31 and mir-221 having already been shown to be associated with sensitivity to an EGFRI in at least one previously published study. In fibroblasts the precursor miRNA mir-34a was identified as the by far most promising predictive biomarker with MET reported as direct target and an associated plausible mechanism of action and two confirmatory previous studies. Further identified promising miRNAs in fibroblasts were mir-382, mir-494, mir-520e and mir-7-1, also with plausible suggested targets.

Overall, the final conclusion of this study is that it might be possible to develop a kind of “predictive profile” consisting of several different biomarkers which taken together may have a predictive value on individual extent of EGFR inhibition in patients. The results of this study suggest that parameters like the plasma concentration of HGF, the expression of mir-146a and mir-31 in dermal keratinocytes and the expression of mir-34a in dermal fibroblasts might be promising parameters to include in such a predictive profile. However, all suggested parameters need to be further confirmed and validated in clinical settings. Eventually, such a predictive score might be used in the future to predict the requirement for changes in dosage of a specific EGFRI, closer monitoring of therapy efficacy by more frequent tumor imaging or maybe even change in therapy away from using an EGFRI or at least adding an adjuvant drug to the EGFRI for better efficacy.

# Table of contents

## List of Figures

## List of Tables

## List of Abbreviations

| | |
|---|---|
| 25(OH)D | 25-hydroxyvitamin D |
| 5-FU | fluorouracil |
| AMPKα1 | catalytic subunit of 5’ adenosine monophosphate-activated kinase |
| ANOVA | analysis of variance |
| AREG | amphiregulin |
| ATP | adenosine triphosphate |
| BMI | body mass index |
| bp | base pairs |
| cDNA | complementary deoxyribonucleic acid |
| CK | cytokeratin |
| CP | crossing point |
| CTCAE | Common Toxicity criteria for Adverse Events |
| DMSO | dimethyl sulfoxide |
| DNA | deoxyribonucleic acid |
| dNTPs | deoxyribonucleotide triphosphate |
| EDTA | ethylenediaminetetraacetic acid |
| EGF | epidermal growth factor |
| EGFR | epidermal growth factor receptor |
| EGFRI | epidermal growth factor receptor inhibitor |
| ELISA | enzyme-linked immunosorbent assay |
| ErbB | erythroblastic leukemia viral oncogene homolog |
| ERK | extracellular receptor-regulated kinase |
| EU | European Union |
| FB | fibroblasts |
| FGF | fibroblast growth factor |
| FOLFIRI | folinic acid fluorouracil irinotecan |
| FOLFOX | folinic acid fluorouracil oxaliplatin |
| FU | fluorescence units |
| GTP | guanosine triphosphate |
| HER | human epidermal growth factor receptor |
| HGF | hepatocyte growth factor |
| HK | human keratinocytes |
| HPLC | high performance liquid chromatography |
| HRP | horse radish peroxidase |

| | |
|---|---|
| Ig | Immunoglobulin |
| IUPAC | International Union of Pure and Applied Chemistry |
| JNK | c-Jun amino-terminal kinase |
| KRAS | Kirsten rat sarcoma virus oncogene homolog |
| lnme | linear and non-linear mixed effects models |
| mAb | monoclonal antibody |
| MAPK | mitogen-activated protein kinase |
| mCRC | metastatic colorectal cancer |
| miRNA | micro ribonucleic acid |
| MKK | mitogen-activated protein kinase kinase |
| mRNA | messenger ribonucleic acid |
| n | number |
| NCI | National Cancer Institute |
| NGS | next generation sequencing |
| NSCLC | non-small cell lung cancer |
| nt | nucleotides |
| OCT | organic cation transporter |
| OS | overall survival |
| p | passage |
| PAGE | polyacrylamide gel electrophoresis |
| PBS | phosphate buffered saline |
| PCR | polymerase chain reaction |
| PFS | progression-free survival |
| PI3K | phosphoinositide 3-kinase |
| PKC | protein kinase C |
| PLCγ | phospholipase Cγ |
| PTEN | phosphatase and tensin homolog |
| PVDF | polyvinylidene fluoride |
| qRT-PCR | quantitative real-time polymerase chain reaction |
| RAF | rapidly accelerated fibrosarcoma |
| RAS | rat sarcoma |
| RNA | ribonucleic acid |
| RT | room temperature |
| SD | standard deviation |
| SDS | sodium dodecyl sulfate |
| SE | standard error |
| STAT3 | signal transducer and activator of transcription 3 |

| | |
|---|---|
| TE | Tris ethylenediaminetetraacetic acid |
| TKI | tyrosine kinase inhibitor |
| TMB | 3,3',5,5'-tetramethylbenzidine (C16H20N2) |
| TOR | target of rapamycin |
| USA | United States of America |
| UTR | untranslated region |
| UV | ultraviolet |
| VDRE | vitamin D responsive element |
| WT | wild type |

# Chapter I: Introduction

## I.1 Personalized drug therapy

It has been known from the beginning of human medicine that drug efficacy and safety varies to a great extent among individual patients. However, it has taken until the late 1950s to recognize genetic variations as one cause for this variability and to start forming the research area of “pharmacogenetics”, which investigates these genetic variations[1]. Differences in the sequences of genes encoding drug target proteins, drug-metabolizing enzymes or drug transporters can have an effect on drug efficacy and safety. On top of that, there are also indirect effects, meaning that the genetic variation changes proteins which function in the biological context of the drug target/metabolizing enzyme/transporter, which can also alter the drug response. Such indirect effects make it difficult to identify single phenotype-genotype associations in drug response. In addition, various none-genetic factors can also influence drug response, adding to the complexity of the subject. The overall goal of the research area of pharmacogenetics and one of the most important goals of the current field of human medicine in general, is to achieve treatment of patients with target-specific drugs at the optimal dose for this patient to reach maximal therapeutic benefit with minimal adverse effects, which is called “individualized medicine” or “personalized medicine”.

In this regard it is of uttermost importance to first understand the molecular mechanisms behind a disease as well as the pharmacokinetic and pharmacodynamic properties of a drug and next to genomics also other approaches like transcriptomics, proteomics, epigenetics and metabolomics have to be used to identify and develop individualized treatment strategies. After the decades of genetic research, the role of RNA came more and more into focus and the importance of gene regulation and RNA modification of gene function was recognized, which created the field of epigenetics.

To date in cancer therapy there are already several targeted agents used, which are directed against specific molecular structures, which are found in the tumor of a patient but ideally not in his/her normal cells or at least to a lesser extent[2]. Epidermal growth factor receptor inhibitors (EGFRIs) for example target the epidermal growth factor receptor (EGFR), which is expressed in almost all cells of the body but which is often over-expressed or over-activated in tumor cells, especially in non-small cell lung cancer (NSCLC), colorectal cancer, pancreatic cancer and head and neck cancer. Unfortunately, EGFRIs only seem to work in a subset of patients suffering from EGFR-expressing tumors. Today there are some genetic variants (e.g. of *EGFR* itself or of downstream signaling molecules such as *KRAS* [Kirsten rat sarcoma virus oncogene homolog]) known

to be partially predictive for response to EGFRIs in a subgroup of patients. However, there are still no methods or characteristics known which could be used to reliably select all patients who will benefit from an EGFRI therapy and determine their optimal dosage. There is still more research needed to identify the causes for the variability in response to EGFRIs among patients.

## I.2 Epidermal growth factor receptor inhibitors (EGFRIs)

EGFR is a receptor tyrosine kinase, which is expressed on the surface of almost all cell types and regulates fundamental cell functions. Its signaling pathways will be further described in chapter I.5.

Frequently administered inhibitors which are specific for EGFR are the tyrosine kinase inhibitors (TKIs) erlotinib and gefitinib and the monoclonal antibodies (mAbs) cetuximab and panitumumab.

### I.2.1 Tyrosine kinase inhibitors

TKIs are small-molecular-weight molecules, which enter the cell by passive as well as active transport mechanisms. *In vitro* studies have shown that for uptake of erlotinib and gefitinib the active transport plays a much larger role than the passive one[3]. Erlotinib and gefitinib are lipophilic and have been shown in different studies to be substrates of different organic cation transporters (OCTs), like hOCT1 (erlotinib)[4], hOCT2 (erlotinib)[5] and hOCT3 (gefitinib)[3]. Efflux of TKIs is mediated by adenosine triphosphate (ATP)-dependent efflux pumps, such as P-glycoprotein (P-gp, also called ATP-binding cassette sub-family B member 1, ABCB1)[6]. TKIs act by reversibly binding to the intracellular ATP-binding site and therefore blocking ATP-binding and signal transduction[7].

Erlotinib hydrochloride, International Union of Pure and Applied Chemistry (IUPAC) name N-(3-ethynylphenyl)-6,7-bis(2-methoxyethoxy)quinazolin-4-amine (tradename Tarceva) -in this thesis referred to as erlotinib- is approved in the European Union (EU) since September 2005[8]. This study mainly focuses on erlotinib as representative for the class of EGFRIs. Its structural formula is presented in figure 1. Erlotinib is indicated as first-line treatment of patients with locally advanced or metastatic NSCLC with *EGFR* activating mutations, for switch maintenance treatment in patients with locally advanced or metastatic NSCLC with *EGFR* activating mutations and stable disease after first-line chemotherapy and for treatment of patients with locally advanced or metastatic NSCLC after failure of at least one prior chemotherapy regimen. It is also indicated in combination with gemcitabine for treatment of patients with metastatic pancreatic cancer.

Gefitinib, IUPAC name N-(3-chloro-4-fluorophenyl)-7-methoxy-6-(3-morpholin-4-ylpropoxy)quinazolin-4-amine;hydrochloride (tradename Iressa) is approved in the EU since June 2009[8]. Its structural formula is presented in figure 1. It is indicated for the treatment of adult patients with locally advanced or metastatic NSCLC with activating mutations of *EGFR*.

Treatment with erlotinib and gefitinib leads to dramatic antitumor activity in a subset of NSCLC patients: for patients with activating *EGFR* mutations in the tumor the initial response rate was shown to be approximately 75% (reviewed by Stewart et al. 2015[9]). The frequency of *EGFR* mutations is 10-30 %, depending on the studied populations. The majority of initially responsive patients will eventually acquire resistance because of an acquired T790M mutation in exon 20 of *EGFR* or other still largely unknown mechanisms. However, resistance to EGFRIs will not be subject of this thesis.

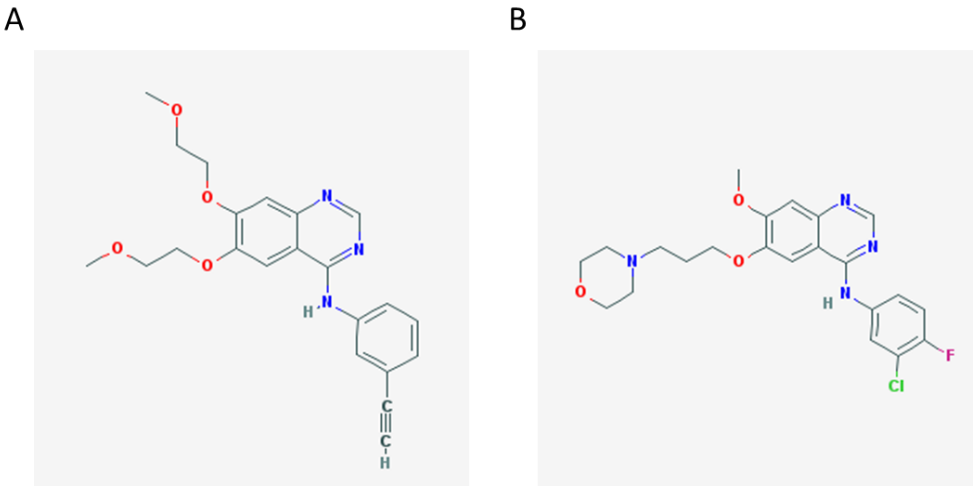


**Figure 1 Structural formulas of tyrosine kinase inhibitors erlotinib and gefitinib**

A) Structural formula of erlotinib, N-(3-ethynylphenyl)-6,7-bis(2-methoxyethoxy)quinazolin-4-amine. B) Structural formula of gefitinib, N-(3-chloro-4-fluorophenyl)-7-methoxy-6-(3-morpholin-4-ylpropoxy)quinazolin-4-amine. Source: National Center for Biotechnology Information. PubChem Compound Database; CID=176870 and CID=123631, https://pubchem.ncbi.nlm.nih.gov/compound.

### I.2.2 Monoclonal antibodies

The anti-EGFR mAbs act by irreversibly binding to the extracellular domain of EGFR and inhibiting ligand binding. Several randomized clinical trials demonstrated the effectiveness of the mAbs cetuximab and panitumumab in combination with fluorouracil (5-FU) and either oxaliplatin (FOLFOX) or irinotecan (FOLFIRI) in patients with metastatic colorectal cancer (mCRC) and wild-type (WT) *RAS* (rat sarcoma)[10-13].

Cetuximab (tradename Erbitux) is a chimeric monoclonal IgG1 antibody produced in a mammalian cell line (Sp2/0, mouse spleen) by recombinant deoxyribonucleic acid (DNA) technology. It is approved in the EU since June 2004[8]. It is indicated for the treatment of patients with EGFR-expressing, *RAS* WT mCRC in combination with FOLFOX or FOLFIRI or as a single agent in patients who have failed oxaliplatin- and irinotecan-based therapy.
Panitumumab (tradename Vectibix) is a fully human monoclonal IgG2 antibody produced in a mammalian cell line (CHO, Chinese hamster ovary) by recombinant DNA technology. It is approved in the EU since December 2007 (first conditional marketing authorization, full authorization granted in January 2015)[8]. It is indicated for the treatment of adult patients with WT *RAS* mCRC in first-line in combination with FOLFOX or FOLFIRI, in second-line in combination with FOLFIRI for patients who have received first-line fluoropyrimidine-based chemotherapy (excluding irinotecan) or as monotherapy after failure of fluoropyrimidine-, oxaliplatin-, and irinotecan-containing chemotherapy regimens.

### I.2.3 Newer epidermal growth factor receptor inhibitors

Next to erlotinib, gefitinib, cetuximab and panitumumab there are additional EGFRIs also approved for clinical use, which either target mutant EGFR instead of WT or have additional targets next to EGFR and were therefore not studied here.
The TKI lapatinib (tradename Tyverb) targets EGFR and human epidermal growth factor receptor 2 (HER2)[14] and is indicated for the treatment of adult patients with breast cancer, whose tumors overexpress HER2. It is used in combination with capecitabine, trastuzumab or an aromatase inhibitor depending on the disease stage, expression of hormone receptor and previous treatment regimens[8]. The TKI afatinib (Tradename Giotrif) targets EGFR, HER2 and HER4[15] and is indicated as monotherapy for the treatment of EGFR TKI-naïve adult patients with locally advanced or metastatic NSCLC with activating *EGFR* mutation(s); and for the treatment of locally advanced or metastatic NSCLC of squamous histology progressing on or after platinum-based chemotherapy[8].
The mAb pertuzumab (tradename Perjeta) targets HER2 and prevents dimerization with EGFR[16] and is indicated for use in combination with trastuzumab and docetaxel in adult patients with HER2-positive metastatic or locally recurrent unresectable breast cancer, who have not received previous anti-HER2 therapy or chemotherapy for their metastatic disease and for use in combination with trastuzumab and chemotherapy for the neoadjuvant treatment of adult patients with HER2-positive, locally advanced, inflammatory, or early stage breast cancer at high risk of recurrence[8].
The mAb necitumumab (tradename Portrazza) targets EGFR[17] and in combination with gemcitabine and cisplatin chemotherapy is indicated for the treatment of adult patients

with locally advanced or metastatic EGFR expressing squamous NSCLC who have not received prior chemotherapy for this condition[8]. This antibody was approved in February 2016 in Germany, after patient enrolment for the Dermatoxgen study and is therefore not studied here.
Recently, also EGFRIs have become available which specifically target mutant EGFR, such as the TKI osimertinib (tradename Tagrisso), which is indicated for the treatment of adult patients with locally advanced or metastatic EGFR T790M mutation-positive NSCLC.

## I.3 Predictive and prognostic biomarkers

In targeted cancer therapy it often takes some time (several weeks) until it can be clearly seen, e.g. by tumor imaging, whether the treatment is working sufficiently. In late stages of a tumor disease or for especially aggressive types by the time the possible insufficiency of a therapy is detected by such imaging techniques, it might be too late for the patients to optimize drug dosing or initiate an alternative treatment strategy. Therefore, it is of high value to have so called biomarkers available, which can predict therapy efficacy and patient outcome early on and facilitate optimization of personalized cancer therapy for individual patients. They can also help to prevent exposure of patients to substances which are ineffective but still cause discomforting side effects.
A biomarker is a clinical or biologic parameter which can be objectively measured and which provides information about disease outcome[18,19]. The World Organization of Health (WHO) defines a biomarker as "[…] any substance, structure or process that can be measured in the body or its products and influences or predicts the incidence of outcome or disease"[20]. A biomarker can be a single variable or a combination of different measurements, e.g. a signature consisting of expression values of various genes. One example of a biomarker already used in the clinics is the expression of the HER2 receptor in breast cancer cells. High expression of this receptor suggests a high success rate of treatment with the anti-HER2 antibody trastuzumab and would indicate that anthracycline-based adjuvant chemotherapy might be supportive[21,22].

Biomarkers can be divided into predictive and prognostic ones. A predictive biomarker allows for an in-advance evaluation of the efficacy of a therapy, e.g. an EGFRI therapy. In contrast, a prognostic biomarker allows for an in-advance evaluation of the outcome of a disease for a patient independent of the treatment[19].

For efficacy of EGFRIs the straightest potential biomarker might be *EGFR* expression on the surface of tumor cells. Unfortunately, there was no clear association found between

*EGFR* expression and response to EGFRIs, as shown for cetuximab in colorectal cancer[23] and squamous cell cancer of the head and neck[24] and for gefitinib in NSCLC[25]. Further potential therapy-associated predictive biomarkers for EGFRIs could be genetic variants of the *EGFR* gene or of other genes encoding proteins involved in the EGFR signaling network. In NSCLC driver mutations of *EGFR* (e.g. deletions in exon 19 or the missense mutation L858R in exon 21) are known positive predictive biomarkers for efficacy of erlotinib and gefitinib[26,27]. In metastatic colorectal cancer mutations in exons 2/3/4 of the GTPases (guanosine triphosphate) *KRAS* and *NRAS* are known negative biomarkers for efficacy of cetuximab and panitumumab[28]. The predictive role of EGFR inhibition reactivity might not be fully discriminable from the prognostic role. In older studies a small number of patients with skin rash, who were later diagnosed with *KRAS* mutations, had a better course of disease if treated with an EGFRI[29]. This points to an additional prognostic role of skin rash as reaction to EGFRI effects outside the tumor. Overall, in none of the numerous conducted studies mutation status of *EGFR* or *RAS* genes was sufficient to predict EGFRI efficacy for all patients (see for example the study by Lièvre et al. where 68 % of non-responders to cetuximab had WT *KRAS*[29]). Hence, new biomarkers are still needed.

Various serum/plasma proteins like growth factors which influence EGFR signaling might be suitable predictive biomarkers. Especially ligands of the EGFR could be promising in this regard. In addition, in recent years gene regulatory molecules, such as miRNAs have been in the focus of research in several research areas. MiRNAs are also conceivable as potential predictive biomarkers for efficacy of EGFRIs.

## I.4 EGFRI-induced skin toxicity

The most common adverse drug reactions observed during therapy with all approved EGFRIs are diarrhea and skin toxicities. Diarrhea is observed in around 17% of patients treated with cetuximab[30]. In patients treated with erlotinib the incidence of diarrhea is very variable, ranging from 18 % to 68 % across different phase III clinical studies (reviewed by Hirsh et al. 2014[31]). Diarrhea is a rather unspecific side effect, which was not found to have a strong correlation with patients' outcome[32]. Mild to moderate forms are commonly treated with loperamide, an opioid which acts locally in the colon, to decrease its dose-limiting properties. For more severe forms temporary discontinuation of EGFRI treatment is recommended.

Skin toxicities typically induced by EGFRIs include nail changes (e.g. paronychia or pyogenic inflammation or cracking of nails and cuticles)[33], xerosis and pruritus, hair changes (e.g. alopecia or increased growth or change in texture) and papulopustular

(acneiform) rash[34,35]. An example for the EGFRI-induced papulopustular rash is presented in figure 2. Incidences of the dermatologic side effects range from 14 % for paronychia to 80 % for papulopustular rash. Reported numbers slightly differ across clinical studies depending on study population, applied EGFRI, system used for toxicity grading, tumor types etc.

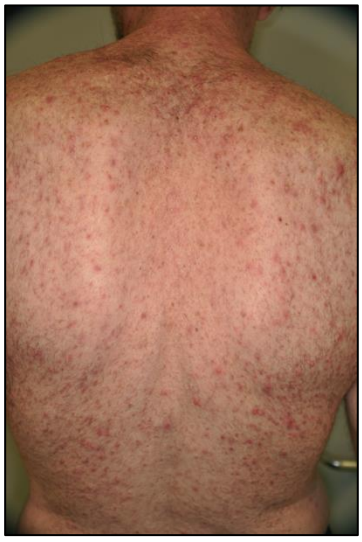

**Figure 2 Papulopustular rash induced by an epidermal growth factor receptor inhibitor**

Papulopustular (acneiform) rash on the back of a patient treated with the epidermal growth factor receptor inhibitor (EGFRI) erlotinib. Picture by Prof. Dr. Ralf Gutzmer, Medical School Hannover, Department of Dermatology, Allergology and Venereology, adapted from Hichert et al.[36].

The described skin toxicities are typically observed for all approved EGFRIs and seem to be a class effect of this group of inhibitors. Interestingly, occurrence and severity of the EGFRI-induced skin toxicity have been shown in numerous independent studies to be positively correlated with patients' progression-free and overall survival (PFS and OS)[37-39]. The molecular mechanism behind the development of EGFRI-induced skin toxicity is not fully elucidated today but is of high interest with regard to the identification of biomarkers predictive for efficacy and safety of EGFRIs.

In the clinics health care professionals already use the occurrence of EGFRI-induced skin rash as clinical marker for the efficacy of EGFRI tumor therapy and in case that no rash develops, they often try to increase the dosage of the inhibitor until rash development is obtained[40,41].

However, in many cases EGFRI-induced skin toxicities also lead to substantial physical discomfort for the patients, limit their daily activities and have a severe psychological impact, resulting in dose reduction or discontinuation of EGFRI treatment. Since the skin

toxicities are such disturbing side effects for the patients, they are often treated with various topical or systemic medications. A systematic review performed by Brown and colleagues in 2016 reported on the most commonly recommended treatment strategies for EGFRI-induced rash, taking into account 59 articles including recommendations from expert opinions, randomized-controlled trials and case report studies[42]. The most commonly recommended treatments are topical antibiotics and corticosteroids for mild rash, oral antibiotics, corticosteroids and antihistamines for moderate to severe rash and delay or dose reduction of EGFRI for very severe rash. Hence, due to medications severity of EGFRI-induced skin toxicity may be suppressed, rendering it unsuitable as predictive marker. On top of that, EGFRI-induced skin rash usually takes two to three weeks to reach its maximal manifestation after initiation of therapy or in some cases even longer[43]. Rapidly determinable predictive biomarkers for the severity of EGFRI-induced skin rash would allow to start early with preventive treatment of the rash and still also allow prediction of efficacy of EGFRI therapy. Such biomarkers might indicate whether clinicians should intensify therapy and monitoring, e.g. by more frequent tumor imaging.

## I.5 EGFR and its signaling pathways

The EGFR belongs to the erythroblastic leukemia viral oncogene homolog (ErbB) family of receptor tyrosine kinases and is also called ErbB1 or HER1. The other three ErbB receptors are ErbB2 (HER2, Neu), ErbB3 (HER3) and ErbB4 (HER4)[44]. EGFR is a 170 kDa transmembrane glycoprotein, which possesses an extracellular domain with a ligand-binding cleft and a dimerization loop, a single transmembrane domain and an intracellular kinase domain which also contains an ATP-binding site (depicted in figure 3)[45,46].

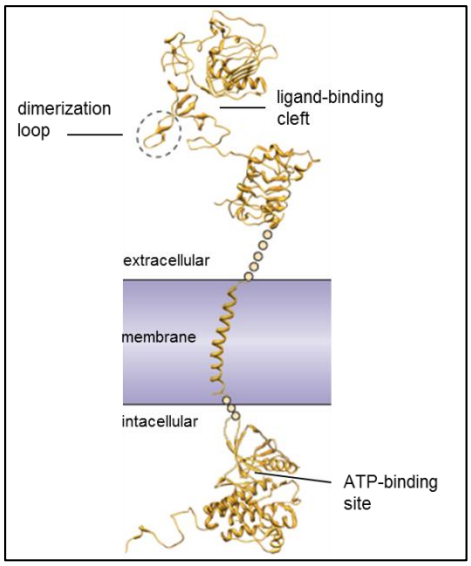


**Figure 3 Crystal structure of the epidermal growth factor receptor**

EGFR possesses an extracellular domain with a ligand-binding cleft for interaction with one of seven possible ligands, which activates the receptor. There is also a dimerization loop (dashed circle) in the extracellular domain, which is needed to form a dimer with another EGFR monomer (homodimer) or with one of the other three ErbB receptors (heterodimer). Following the single transmembrane domain there is also an intracellular kinase domain which contains an ATP-binding site and is activated via cross-phosphorylation of the two receptor monomers following ligand-binding and dimerization. Adapted from Tebbutt *et al.*[46], originally published by Yarden and Pines[45]. Abbreviations: ATP, adenosine triphosphate; EGFR, epidermal growth factor receptor; ErbB, erythroblastic leukemia viral oncogene homolog.

EGFR regulates fundamental cell functions, like survival, proliferation and migration, via numerous signaling pathways, including the MAPK cascade (RAS/RAF/MAPKK/MAPK), the phospholipase C (PLCγ/PKC), the Akt (PI3K/Akt) and the STAT3 pathways. These pathways are depicted in figure 4 and are further described in sections I.5.1 to I.5.4, including explanations of abbreviations of involved proteins.

In mammals a variety of EGFR ligands exist, which can bind to the receptor and activate its down-stream signaling cascades. Next to epidermal growth factor (EGF) there are six additional ligands known. In distinct cell types and contexts different combinations and amounts of the various ligands are expressed, facilitating fine-tuned regulation and specificity of EGFR signaling[47]. Moreover, each ligand has its own binding characteristics leading to distinct homo- or hetero-dimerization of ErbB receptors [48].

Dimerization leads to autophosphorylation of the receptor at specific tyrosine residues (cross-phosphorylation by the two monomers), which then recruit various signal transducer proteins, leading to the activation of numerous signaling cascades[49].

### I.5.1 MAPK pathway

One of the best characterized signaling cascades induced via EGFR is the mitogen-activated protein kinase (MAPK) cascade. MAPKs are enzymes which covalently attach phosphate to specific serines and threonines of certain target proteins[44]. Upon autophosphorylation of EGFR following ligand binding, a complex of adaptor proteins (growth factor receptor-bound protein 2 [Grb2], son of sevenless [SOS] and sometimes also Shc) binds to the phosphorylated tyrosine residues of EGFR[50]. A subsequent conformational change of the guanine nucleotide exchange factor SOS facilitates recruitment of the GTPase RAS (RAS-GDP). SOS induces the release of guanosine diphosphate (GDP) from RAS, which facilitates binding of guanosine triphosphate (GTP) to RAS. This activated form of RAS (RAS-GTP) in turn activates the protein kinase rapidly accelerated fibrosarcoma (RAF) by phosphorylation. RAF subsequently phosphorylates various other protein kinases, known as MAPK kinases (MAPKK) or MKKs, namely e.g. MKK4, MKK7 and MEK1/2. These proteins again phosphorylate further downstream proteins. MKK4 and MKK7 primarily phosphorylate c-Jun amino-terminal kinase (JNK) while MEK1/2 preferably targets extracellular receptor-regulated kinase (ERK)1/2[51]. The MAPKs JNK and ERK1/2 themselves phosphorylate specific transcription factors, which act in the nucleus. A prominent target of JNK is c-Jun, which is part of a complex (AP-1), which binds to specific DNA sequences and alters expression of the respective genes[52].

### I.5.2 PI3K/Akt pathway

Another prominent signaling cascade activated by EGFR is the PI3K/Akt pathway. Phosphoinositide 3-kinase (PI3K) binds to activated (autophosphorylated) EGFR and can then phosphorylate phosphatidylinositol-4,5-bisphosphate ($PIP_2$) to yield phosphatidylinositol-3,4,5-trisphosphate ($PIP_3$)[50,53]. $PIP_3$ mediates translocation of the serine/threonine kinase Akt to the plasma membrane, where it is activated via phosphorylation. Activated Akt can in turn activate different effector proteins, like mechanistic target of rapamycin (mTOR), which can become part of different complexes, which have functions at various cell organelles and on gene transcription and translation[54,55].

### I.5.3 STAT3 pathway

EGFR can also activate transcription factor signal transducer and activator of transcription 3 (STAT3). Upon ligand-mediated kinase activation and autophosphorylation of EGFR, STAT3 is recruited from the cytosol to phosphorylated tyrosines of EGFR (Y1068 and

Y1086) via its SH2 domain and is itself phosphorylated at a tyrosine residue (Y705)[56]. This phosphorylation leads to dimerization of STAT3 and translocation to the nucleus, where the STAT3 dimers can bind to their specific target DNA sequences and enhance gene expression leading to increased proliferation and survival of the cell.

### I.5.4 PLCγ/PKC pathway

The last prominent signaling pathway which can be activated by EGFR is the phospholipase Cγ (PLCγ) pathway. PLCγ directly interacts with activated EGFR and hydrolyzes $PIP_2$ to inositol 1,3,5-triphosphate ($IP_3$) and 1,2-diacylglycerol (DAG)[50]. $IP_3$ further acts on the membrane of intracellular calcium reservoirs and provokes release of calcium ions ($Ca^{2+}$)[57]. DAG on the other hand mediates activation of protein kinase C (PKC), which itself is able to initiate several signaling cascades to finally alter proliferation and inflammatory responses. These numerous cascades cannot be further covered within the scope of this thesis.

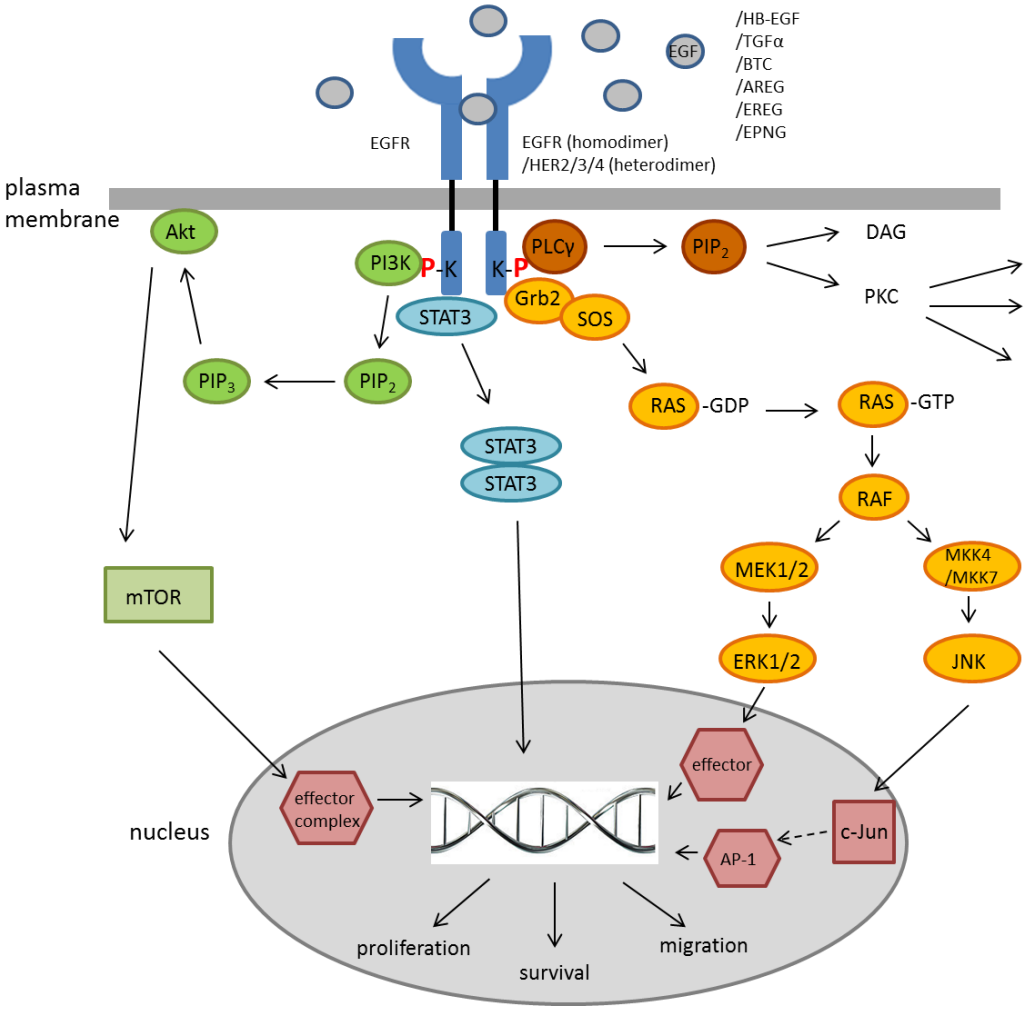


**Figure 4 Epidermal growth factor receptor signaling pathways**

When one of the seven known EGFR ligands EGF, HB-EGF, TGFα, BTC, AREG, EREG, or EPNG (grey) binds to EGFR, receptor homodimers or heterodimers (with HER1, HER2 or HER3) form, leading to autophosphorylation (red P) of EGFR at specific tyrosine residues. Different signaling cascades are initiated. Green: PI3K/Akt pathway; blue: STAT3 pathway; orange: MAPK pathway; brown: PLCγ pathway; red: effector proteins/transcription factors which alter gene transcription.
Abbreviations: AREG, amphiregulin, BTC, betacellulin; DAG, 1,2-diacylglycerol; EGF, epidermal growth factor; EGFR, epidermal growth factor receptor; EPNG, epigen; EREG, epiregulin; ERK, extracellular signal-regulated kinase; GDP, guanosine diphosphate; Grb2, growth factor receptor-bound protein 2; GTP, guanosine triphosphate; HB-EGF, heparin-binding EGF-like growth factor; HER, human epidermal growth factor receptor; JNK, c-Jun amino-terminal kinase; K, tyrosine; MAPK, mitogen-activated protein kinase; MKK, MAPK kinase; mTOR, mechanistic target of rapamycin; P, phosphate; PI3K, phosphoinositide 3-kinase; $PIP_2$, phosphatidylinositol-4,5-bisphosphate; $PIP_3$, phosphatidylinositol-3,4,5-trisphosphate; PKC, protein kinase C; PLCγ, phospholipase Cγ; RAF, rapidly accelerated fibrosarcoma; RAS, rat sarcoma; SOS, son of sevenless; STAT3, signal transducer and activator of transcription 3; TGFα, transforming growth factor α.

## I.6 EGFR signaling in skin

The human skin is composed of three layers: the hypodermis, the dermis and the outermost epidermis[58,59]. The dermis and the epidermis are separated by the basement membrane. The structure is depicted in figure 5.

The hypodermis is made up of loose connective tissue and fat.
The dermis mainly consists of fibroblasts, which produce collagen, elastin and structural proteoglycans to produce a tough and supportive cell matrix and also of immunocompetent mast cells and macrophages. The dermis also contains blood and lymphatic vessels, nerve fibers, sweat and sebaceous glands and hair roots. Dermal fibroblasts are derived from mesenchymal stem cells and are not fully differentiated cells[60]. Unlike other fibroblast cell types, dermal fibroblasts are far less likely to differentiate, which makes them popular cell models in all kinds of different research areas.
The epidermis mainly consists of keratinocytes and there are four distinct epidermal layers with characteristic physical appearances and functions (reviewed in Lacouture 2006[58]). From inside to outside there are the stratum basale (mainly keratinocyte stem cells, also melanocytes and Merkel cells), stratum spinosum (mainly differentiating keratinocytes, also immune cells like Langerhans cells), stratum granulosum (mainly keratinocytes who start to flatten and whose cytoplasm appears granular) and stratum corneum (keratinocytes become non-viable, cornified cells known as corneocytes). The later functions as protective barrier for the body and consists of structural proteins like involucrin and loricrin. Keratinocyte stem cells are present in the stratum basale and allow the epidermis to constantly renew[61]. These stem cells generate keratinocytes which exit the basal layer, stop growing and instead differentiate and migrate towards the skin surface, where they finally lose their nucleus and fuse to squamous sheets before being shed from the surface. The epidermis is completely renewed within around 48 days[62].

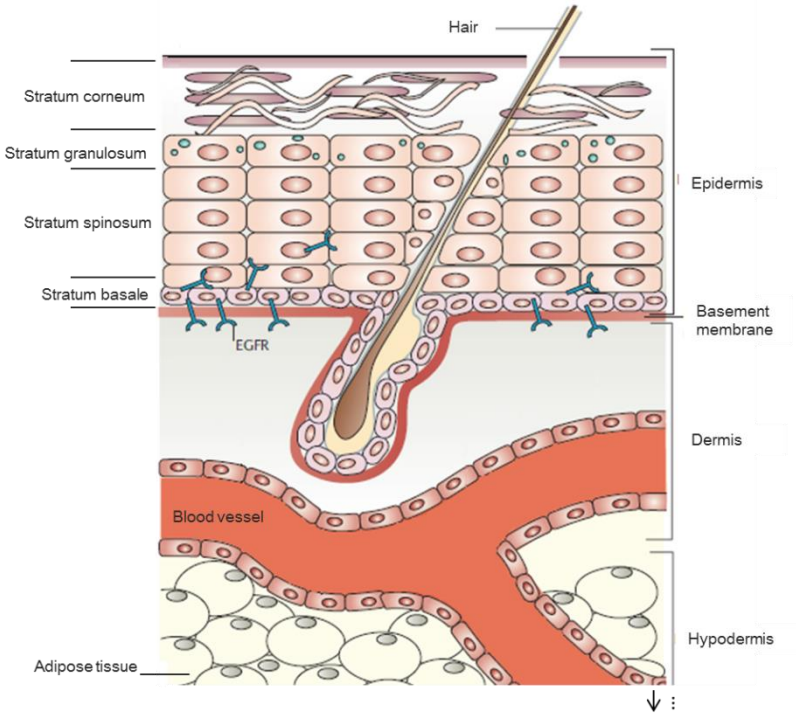


**Figure 5 Structure of human skin**

The human skin consists of three layers: the hypodermis, the dermis and the outermost epidermis. Dermis and epidermis are separated by the basement membrane. The hypodermis is mainly composed of lose connective and adipose tissue. The dermis is mainly composed of fibroblasts, which produce collagen, elastin and structural proteoglycans to produce a tough and supportive cell matrix and it also contains structures like blood and lymphatic vessels and hair roots. The epidermis mainly contains keratinocytes and is composed of four distinct layers: stratum basale, stratum spinosum, stratum granulosum and stratum corneum. EGFR is mainly expressed in the basal cell layer and the directly adjacent layers of the stratum spinosum. Figure adapted from Lacouture 2006[58].
Abbreviations: EGFR, epidermal growth factor receptor.

The proliferation, differentiation and migration of keratinocytes are highly regulated by numerous growth factors and cytokines. EGFR is mainly present in the basal cell layer and the directly adjacent layers of the stratum spinosum and EGFR signaling has been shown to be especially important in this regulation[63]. EGFR knockout mice lacking EGFR especially in the epidermis ($EGFR^{\Delta ep}$) show a phenotype of impaired epidermal stratification, skin inflammation and hair follicle abnormalities[64]. In adult $EGFR^{\Delta ep}$ mice elevated numbers of keratin 1-positive suprabasal layers of cells were detected, indicating epidermal hyperplasia. In addition, the terminal differentiation marker loricrin, which should normally mainly be found in the stratum corneum, was also detected in the basal layer. Taken together, $EGFR^{\Delta ep}$ mice show deregulated growth and differentiation of keratinocytes and therefore impaired stratification of the epidermis.
During treatment with an EGFRI, EGFR signaling is also blocked in epidermal cells, resulting in growth arrest of basal keratinocytes and premature differentiation. However,

so far it has not been elucidated which specific pathways of the various EGFR-triggered pathways and which signaling proteins in particular are involved in keratinocytes. Decreased EGFR signaling also leads to increased production of pro-inflammatory cytokines (via various pathways which under normal conditions are probably blocked via pathways involving active EGFR). Among other cytokines, increased levels of CCL2, CCL5 and CXCL10 have been found upon EGFRI treatment in skin biopsies from patients as well as in cultured keratinocytes and mice[58,64]. These cytokines cause vasodilation and edema and recruit immune cells like dendritic cells, neutrophils and T lymphocytes which release enzymes causing loss of intercellular attachments of keratinocytes and apoptosis of epidermal cells. These cellular processes cause the typical clinical manifestations of EGFRI-induced skin toxicities.

## I.7 Criteria for selection of biomarker candidates

The criteria for selection of molecules as biomarker candidates for this study were existing literature data about an effect on the function of EGFRIs or on the regulation of EGFR itself as well as known expression/function in skin cells.

The EGFR ligand amphiregulin (AREG) is particularly interesting with regard to EGFRI-induced skin rash because of its pivotal role in skin homeostasis [65]. It was found to be the most abundant EGFR ligand present in cultured human keratinocytes with over 19 times more messenger RNA (mRNA) and over seven times more soluble protein than any of the other ligands [47]. In the same study neutralization of AREG with specific antibodies resulted in significant inhibition of keratinocyte proliferation and decreased phosphorylation of ERK, which was not the case for antibodies against the other ligands, illustrating the importance of AREG in normal keratinocyte growth. In addition, Rittié and colleagues have shown that induction of AREG (by retinoids) leads to activation of EGFR and an increase in proliferation of human keratinocytes, which in turn can lead to hyperplasia of the epidermis [66]. Ishikawa et al. previously also observed a significant correlation between high serum concentrations of AREG and poor response to gefitinib in patients with NSCLC[67]. Because of these observations it is conceivable that AREG could be involved in the development of EGFRI-induced skin rash and the plasma/serum concentration of AREG might serve as a reliable prognostic or maybe even a predictive biomarker specific for the efficacy of EGFRI therapy.

The cytokine hepatocyte growth factor (HGF) has also been shown to influence the function of EGFRIs. It is a direct ligand of the receptor tyrosine kinase MET but has been

found to induce resistance to EGFRIs and is therefore thought to be able to influence EGFR signaling indirectly, via cross-talk of signaling pathways [68]. Activation of the MET receptor can in turn activate the PI3K/Akt, RAS/RAF/MAPK, STAT3/JNK and PLCγ1 pathways (reviewed in [69]). HGF/MET signaling mediates disruption of cadherin-based contacts between cells resulting in cell motility and can also induce proliferation and survival of cells [70-72]. A synergistic effect of MET and EGFR activation on cell proliferation and motility of NSCLC cells has been found, as well as a synergistic effect of MET and EGFR inhibition on apoptosis [73]. This suggests a cross-talk between the two pathways. In addition, Hammond and colleagues found a high degree of overlap of effector molecules which were phosphorylated (indicating activation) by EGF and HGF [74].
The role of dysregulated HGF/MET signaling in tumorigenesis and especially in invasive growth and metastasis has been intensively studied [75-78]. However, little is known about the influence of HGF on EGFRI therapy and its role in the development of EGFRI-induced skin rash. First associations of serum levels of HGF with EGFRI-induced skin toxicity have been found in a small cohort (n = 103) of metastatic colorectal cancer patients (inverse correlation) by Takahashi and colleagues in 2015 [79]. Therefore, HGF was selected as biomarker candidate for EGFRI efficacy here.

Interesting literature data with regard to a role in EGFR regulation has also been found for vitamin D. A putative vitamin D responsive element (VDRE) has
been found in the *EGFR* promoter region (GGGTCCAGAGGGGCA), which has high sequence similarity to a known functional VDRE in the human osteocalcin gene (GGGTGAACGGGGCA) and was shown to bind vitamin D in electrophoretic mobility shift assays [80-82]. Another VDRE has been found in intron 1 of the *EGFR* gene (AGTTGAATAAGTTGA) and its functionality was confirmed in gene reporter analyses in ovarian cancer cells[83].
An increasing effect of the main metabolite of vitamin D, called cholecalcitriol ($1\alpha,25(OH)_2D_3$) on EGFR mRNA levels has been observed in osteoblast-like cells[80] and a decreasing effect in some breast cancer cells[82]. These results from previous studies concerning the effect of $1\alpha,25(OH)_2D_3$ on EGFR suggest that vitamin D might also play a role in cancer therapy involving EGFRIs.
There are two types of vitamin D, vitamin $D_2$ (ergocalciferol) and $D_3$ (cholecalciferol). Vitamin $D_3$ is mainly (85%) produced in the skin from 7-dehydrocholesterol by ultraviolet-B light and gets transported to the liver where it is hydroxylated to cholecalcidiol (also called 25-hydroxyvitamin $D_3$, $25(OH)D_3$ or 25-OH-vitamin $D_3$) by 25-hydroxylases. The $25(OH)D_3$ is the storage form of vitamin $D_3$. It is transported to the kidney and is further hydroxylated

by 25-hydroxyvitamin $D_3$-1α-hydroxylase to yield the hormonally active metabolite cholecalcitriol (1α,25$(OH)_2D_3$).

In this context it is also interesting that the enzyme 25$(OH)D_3$-1α-hydroxylase is not just expressed in the kidney but also at several extrarenal tissues, including skin (basal keratinocytes and hair follicles)[84]. Therefore, local conversion of 25$(OH)D_3$ into the active metabolite 1α,25$(OH)_2D_3$ is possible in skin cells and it has been shown *in vitro* as well as *in vivo* that human keratinocytes can produce substantial amounts of active 1α,25$(OH)_2D_3$[85,86] Therefore, it is conceivable that vitamin D might has an influence on EGFR signaling in skin cells and could affect the development of EGFRI-induced skin rash and was chosen as biomarker candidate in this study.

## I.8 Epigenetics and functional gene regulation in association with EGFRI efficacy

MiRNAs are short RNA molecules, which do not encode proteins but can regulate gene expression at the post-transcriptional level. They play a role in nearly every biological pathway[87].

### I.8.1 MiRNA biogenesis

MiRNA biogenesis is depicted in figure 6. MiRNA molecules are 19 to 25 nucleotides (nt) long and can bind to partially complementary sequences in the 3' untranslated region (UTR) of mRNA molecules. They are transcribed as primary transcripts called pri-miRNAs and then excised by the RNase Drosha to produce so called pre-miRNAs, which are hairpin-containing miRNA precursors with a length of 60 to 110 nt[88]. The pre-miRNA molecules are exported to the cytoplasm and subsequently processed to yield mature duplex miRNA molecules. One of the two strands of these duplex miRNA molecules - the guide strand - is loaded into the RNA-induced silencing complex. The other strand - the passenger strand - can also be incorporated but at a lower frequency[89,90]. It is currently unclear at which point of the miRNA biogenesis pathway regulation is most important and has the greatest influence on miRNA-mediated epigenetic regulation. Therefore, in addition to the mature miRNA molecules, the precursor miRNAs will be included in the analyses in this study as well.

Upon binding of their target mRNA molecules (with partially complementary sequence in the 3' UTR), miRNAs can either mechanically block translation or facilitate mRNA degradation. The identification of targets of individual miRNAs has been the subject of innumerable studies and it has been learned that the impact of certain miRNAs on certain

target mRNAs can differ substantially under different conditions, like cell and tissue type, developmental stage and stress (including treatment with pharmaceutical substances).

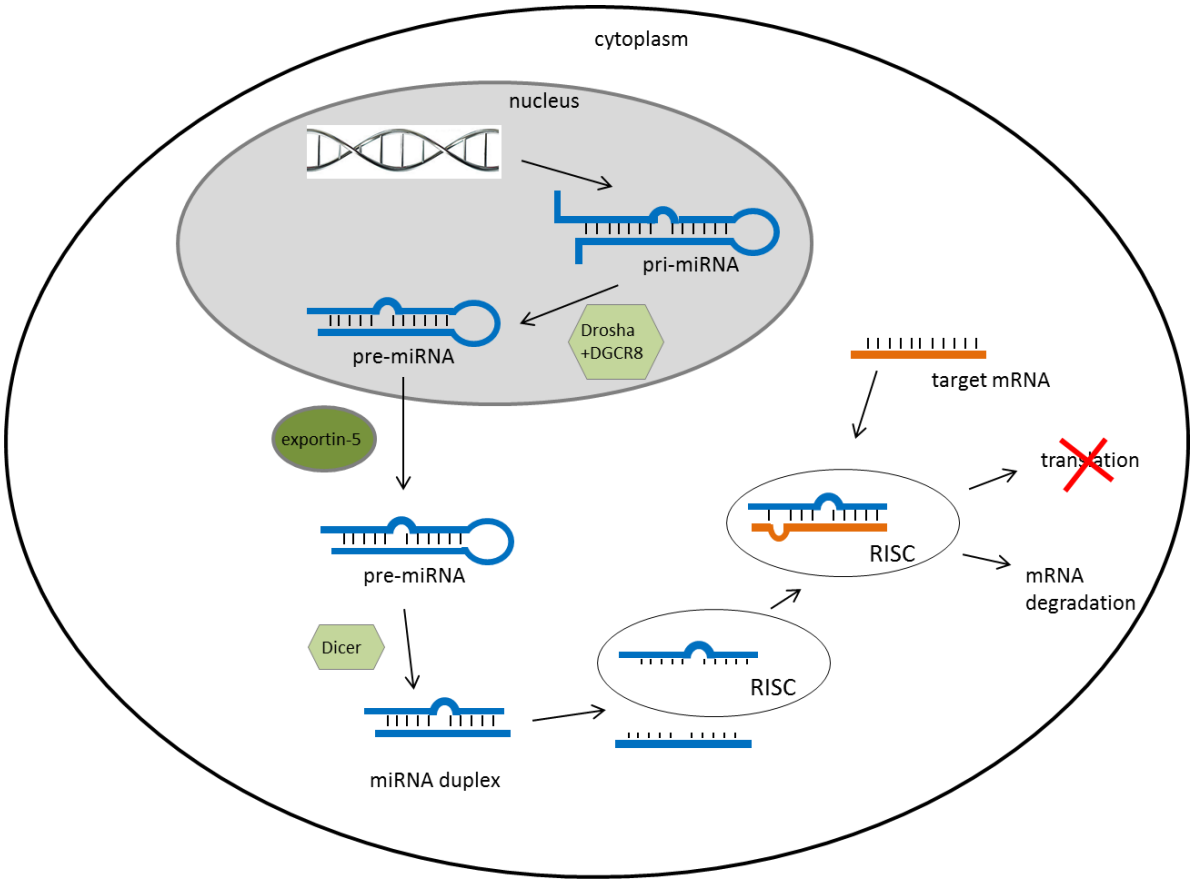


**Figure 6 MiRNA biogenesis**

MiRNAs are transcribed as primary transcripts called pri-miRNAs. These transcripts are excised by the RNase Drosha and its cofactor DGCR8 and hairpin-containing pre-miRNAs are produced (length: 60 to 110 nt). Pre-miRNAs are exported to the cytoplasm by exportin-5 and processed by Dicer to yield mature duplex miRNAs. One of the two strands (length: 19 to 25 nt) is loaded into RISC. Upon binding of their target mRNA molecules with partially complementary sequence in the 3' UTR, miRNAs can either mechanically block translation or facilitate mRNA degradation.
Abbreviations: miRNA, micro ribonucleic acid; mRNA, messenger ribonucleic acid; nt, nucleotides; RISC, ribonucleic acid-induced silencing complex; UTR, untranslated region.

The database miRBase, which provides a searchable online repository for published miRNA sequences (Griffiths-Jones laboratory, Faculty of Life Sciences, University of Manchester, UK)[91,92], contains 28645 entries of hairpin precursor miRNAs, which express 35828 mature miRNA products and are found in 223 different species (data of version 21, released in June 2014).

Each distinct miRNA has a name/identifier. The first three letters indicate the organism, e.g. hsa for human or mmu for mouse. Since in this thesis only human miRNAs are

discussed, the “hsa” will be omitted when naming the miRNAs. The mature miRNA is designated miR-x in the miRBase database and in the majority of publications, with x being a unique sequential number. On the other hand, mir-x refers to the miRNA gene as well as to the predicted stem-loop portion of the primary transcript (hairpin miRNA). Different precursor sequences and genomic loci which express identical mature miRNA sequences are named in the form hsa-mir-x-1 and hsa-mir-x-2. Lettered suffixes denote closely related mature sequences, e.g. hsa-miR-34a and hsa-miR-34b. If there are two ~22nt sequences miRNAs which originate from the same predicted precursor, the predominantly expressed mature miRNA receives the name of the form miR-x while the other miRNA produced from the opposite arm of the precursor is named miR-x*. In case that it is unclear which product is the more abundant one, names like miR-x-5p (from the 5' arm) and miR-x-3p (from the 3' arm) are assigned.

### I.8.2 MiRNAs as biomarkers

Numerous studies indicate that the deregulation of miRNA biogenesis and activity plays an important role in development and progression of cancer. Such deregulation can for example occur through genomic alterations like deletions[93] or mutations (e.g. collected in the database SomamiR[94]) or through aberrant miRNA processing[95].

Several miRNAs have also been found to drive cancer development, maintenance or metastasis by regulating EGFR signaling pathways. In addition, certain miRNAs were shown to increase resistance to EGFRIs. MiR-21 for example targets negative regulators of EGFR pathways, namely PTEN, Pdcd4 and Spry[96]. MiR-34 is known to target the receptor tyrosine kinase MET as well as cell-cycle related proteins[96]. It can inhibit invasive growth induced by MET, which was shown in breast[97], lung[98] and colon[99] cancer. In hepatocellular cancer cells, treatment with miR-34a together with the MET inhibitor SU11274 led to decreased cell proliferation and induction of apoptosis. In addition, administration of miR-34 to mice with adenocarcinomas, showing mutations in the *Kras* and *p53* genes and resistance to previous therapy, reduced lung tumor initiation and progression[100]. In certain tumors miR-7 was found downregulated and studies showed that it can directly target EGFR and some of its downstream proteins and under normal conditions negatively regulates EGFR signaling, thereby inhibiting tumorigenesis and metastasis. In colorectal cancer patients, low expression of miR-7 was an independent prognostic factor for poor survival[101]. Interestingly, in *KRAS* mutant, cetuximab resistant colorectal cancer cell lines, miR-7 also enhanced susceptibility to cetuximab. In addition,

in a different study about head and neck cancer, miR-7 rendered erlotinib-resistant cells susceptible to growth inhibition by erlotinib[102].
These results suggest miRNAs as promising targets in cancer therapy, either as direct anti-cancer agents or as supportive treatment to enhance efficacy of other anti-cancer drugs, e.g. EGFRIs and also indicate that miRNAs might be promising candidates as biomarkers, not just as prognostic ones for cancer outcome but also as predictive ones for efficacy of certain therapies, especially with EGFRIs.

Since single miRNAs typically have various target genes, they can be seen as kind of master regulators of gene expression and they might be more stable biomarkers for efficacy of certain drugs than their target mRNAs or proteins[90].
It is hypothesized that in tumor tissues miRNA profiles are probably highly variable and subject to constant changes as the tumor grows and develops. In healthy peripheral tissues, e.g. in the skin, miRNA profiles might be more stable and therefore more suitable to find reliable biomarkers. Those networks of miRNAs which are essential for cell survival and functioning will most likely stay intact, even in tumor cells. Hence, those miRNAs with essential functions for successful EGFR signaling in skin cells will probably also be comparably expressed in tumor cells which are dependent on EGFR. Therefore, it is suggested that miRNA biomarkers predictive for EGFRI efficacy might be identifiable in skin cells.
Since to date very little data about potential candidates for such miRNA biomarkers from skin cells exists in the literature, we decided to perform a screening of miRNA profiles in skin cells with different phenotypes of *in vitro* sensitivity towards erlotinib, in order to identify suitable candidate miRNA biomarkers for efficacy of EGFRIs in this study.

# Chapter II: Previous work and aim of the project

## II.1 Previous work of the research group

Based on data from the Dermatoxgen study (described in chapter III.2.1.1) the following results have been obtained and published prior to this work:

Fuerst et al. 2012[103]

A possible immunological role for EGFRIs in addition to direct antagonistic downstream effects was investigated by analyzing different polymorphisms in HLA genes. A significantly lower incidence of skin rash was found in patients carrying the HLA-A*02:01 or HLA-A*03:01 alleles; however, no association with worse survival was observed.

Parmar et al. 2013[104]

A significant association between the *EGFR* 497 G/A variant and the occurrence of skin toxicity was observed (common 497 G/G genotype: significantly more often skin toxicity than with at least one A-allele). In addition, the *EGFR* -216/-191 GC haplotype and the *PIK3CA* haplotype H4 were correlated with decreased occurrence of skin toxicity.

Hasheminasab et al. 2015[105]

To identify genomic variants in the EGFR pathway and in cytokines predisposing to skin toxicity, *EGFR* and inflammatory pathway genes were analyzed by deep sequencing. 1437 single nucleotide polymorphisms (SNPs) were found in the target region. Three SNPs in *EGFR* intron 1 were found exclusively in patients without skin rash and an *EGFR* intron 23 SNP was associated with skin rash, OS and interleukin-8 plasma concentrations.

Paul et al. 2014[106]

Potential protein biomarkers measured in serum samples of the Dermatoxgen patients were examined. It was shown that low serum concentrations of interleukin-8 were associated with increased severity of EGFRI-induced skin rash and prolonged OS.

Steffens et al. 2016[107]

As marker for individual drug metabolism the metabolic ratio of erlotinib/O-desmethyl-erlotinib in serum from Dermatoxgen patients was found to be correlated with severity of skin rash and PFS as well as OS.

## II.2 Aim of the project

The occurrence and severity of the typical skin toxicity which is induced as an adverse reaction by EGFRIs have been shown to be correlated with prolonged OS and PFS of patients[37-39]. However, since the rash is a disturbing side effect for the patients, it is often treated with topical or systemic medication (corticosteroids, antibiotics, antihistamines)[42]. Hence, its severity may be suppressed, rendering it unsuitable as a clinical predictive marker in EGFRI therapy. Therefore, rapidly determinable predictive biomarkers for the severity of EGFRI-induced skin rash would be helpful to allow early preventive treatment of the rash while at the same time still allowing prediction of EGFRI efficacy. Such biomarkers might indicate whether clinicians should intensify therapy and monitoring (e.g. by more frequent tumor imaging).

Since previous work revealed evidence for genetic, pharmacokinetic and cytokine markers, the intention to my work was to identify functional biomarkers that are able to measure EGFR inhibition variability in the periphery, especially in blood plasma and skin cells. Therefore, molecules that interact with, regulate or functionally modulate EGFR inhibition were selected and determined in plasma or in keratinocyte and fibroblast culture. Since miRNAs have recently been shown to be important not just in mechanisms leading to the development of cancer but also in the response to cancer therapy, investigating the suitability of specific mature or precursor miRNA molecules as predictive biomarkers for the development of EGFRI-induced skin toxicity was of special interest. Suitable biomarkers should be easily and rapidly measurable and would save valuable time in determining the efficacy and safety of an EGFRI therapy for an individual patient.

Since it has not been elucidated so far, which specific EGFR-triggered pathways and which signaling molecules in particular are the ones involved in the function of EGFRIs in keratinocytes or fibroblasts, characterization of the respective cell models with regard to phenotypes was also an important intermediate aim of this work.

# Chapter III: Material and methods

## III.1 Material

### III.1.1 Instruments

Instruments used in this study are listed by their field of application in table 1, including the suppliers.

**Table 1 Instruments used in this study, listed by field of application**

| Instrument | Supplier |
|---|---|
| **ELISAs** | |
| Safire² microplate reader | Tecan, Männedorf, Switzerland |
| Thermomixer comfort MTP | Eppendorf, Hamburg, Germany |
| **Cell culture** | |
| Centrifuge 5702 R | Eppendorf, Hamburg, Germany |
| $CO_2$ Incubator | Binder, Tuttlingen, Germany |
| Inverse light microscope Axiovert 40C | Zeiss, Oberkochen, Germany |
| Laminar flow cabinet Herasafe | Heraeus, Kendro, Hanau, Germany |
| **Gel electrophoreses** | |
| Criterion™ gel chamber | Bio-Rad, Hercules, USA |
| PowerPac™ Universal | Bio-Rad, Hercules, USA |
| **Western blots and phospho-kinase arrays** | |
| Trans-Blot® SD Semi-Dry Transfer Cell | Bio-Rad, Hercules, USA |
| Imaging system Stella 3200 | Raytest, Straubenhardt, Germany |
| **miRNA preparations** | |
| Avanti J-26 XP Centrifuge | Beckman Coulter, Krefeld, Germany |
| Intelli-Mixer RM-2 L, Rotator and Vortex | ELMI, Riga, Latvia |
| Diana II digital CCD imaging system (height adjustable UV table) | Raytest, Staubenhardt, Germany |
| Centrifuge 5415 R | Eppendorf, Hamburg, Germany |
| Centrifuge 5804 | Eppendorf, Hamburg, Germany |
| Mastercycler gradient | Eppendorf, Hamburg, Germany |
| Qubit® 2.0 Fluorometer | Invitrogen™, Life Technologies, Carlsbad, USA |
| **Next generation sequencing** | |
| 2100 Bioanalyzer | Agilent Technologies, Santa Clara, USA |
| MiSeq® Sequencer | Illumina®, San Diego, USA |
| **qRT-PCR** | |
| LightCycler® 480 | Roche Diagnostics, Mannheim, Germany |

### III.1.2 Kits

All kits used in this study are listed by their field of application in table 2, including the suppliers.

**Table 2 Kits used in this study, listed by field of application**

| Kit | Supplier |
|---|---|
| **Cell culture** | |
| Coating Matrix Kit | Life Technologies, Carlsbad, USA (now Thermo Fisher Scientific) |
| **ELISAs** | |
| Pierce™ BCA Protein Assay Kit | Thermo Fisher Scientific, Waltham, USA |
| Cetuximab (Erbitux®) PK ELISA | Somru BioScience, Charlottetown, Canada |
| Human Amphiregulin ELISA Kit | Sigma-Aldrich, St. Louis, USA |
| Human HGF Quantikine® ELISA Kit | R&D systems™, Minneapolis, USA |
| 25-OH-Vitamin-D-ELISA | EUROIMMUN Medizinische Labordiagnostika AG, Lübeck, Germany |
| Phospho-Erk1 ($pThr^{202}$ / $pTyr^{204}$) + Erk2 ($pTyr^{185/187}$) and pan-Erk1 / 2 ELISA Kit | Sigma-Aldrich, St. Louis, USA |
| Human/Mouse/Rat Phospho-c-Jun (S63) Cell-Based ELISA Kit | R&D systems™, Minneapolis, USA |
| Human Phospho-EGF R/ErbB1 (Y1068) Cell-Based ELISA | R&D systems™, Minneapolis, USA |
| Phospho-JNK (Thr183/Tyr185) Cell-Based ELISA Kit, human/mouse/rat | PromoKine, PromoCell, Heidelberg, Germany |
| **Western blots and phospho-kinase arrays** | |
| Proteome Profiler™ Human Phospho-Kinase Array Kit | R&D systems™, Minneapolis, USA |
| **miRNA preparations** | |
| Qubit® RNA HS Assay Kit | Life Technologies, Carlsbad, USA (now Thermo Fisher Scientific) |
| NEBNext® Multiplex Small RNA Library Prep Set for Illumina® (Set 1) | New England BioLabs, Ipswich, USA |
| QIAquick PCR Purification Kit | Qiagen, Hilden, Germany |
| **Next generation sequencing** | |
| Qubit® dsDNA HS Assay Kit | Life Technologies, Carlsbad, USA (now Thermo Fisher Scientific) |
| Agilent High Sensitivity DNA Kit | Agilent Technologies, Santa Clara, USA |
| MiSeq® Reagent Kit v2 (50 cycles) | Illumina®, San Diego, USA |
| **qRT-PCR** | |
| miScript II RT Kit | Qiagen, Hilden, Germany |
| miScript SYBR Green PCR Kit | Qiagen, Hilden, Germany |

### III.1.3 Chemicals

Chemicals used in this study are listed by their field of application in table 3, including the suppliers.

**Table 3 Chemicals used in this study, listed by field of application**

| Chemical | Supplier |
|---|---|
| **Various applications** | |
| Dulbecco's PBS w/o Magnesium, w/o Calcium, sterile | Biowest, Nuaillé, France |
| Dimethyl sulfoxide (DMSO) | Sigma-Aldrich, St. Louis, USA |
| Ethanol for molecular biology | Merck, Darmstadt, Germany |
| Erlotinib hydrochloride | Santa Cruz Biotechnology, Dallas, USA |
| Recombinant Human EGF | Peprotech, Rocky Hill, USA |
| Phospho-stop easypack phosphatase inhibitor cocktail tablets | Roche Diagnostics, Mannheim, Germany |
| Complete Ultra Tablets, mini easypack protease inhibitor cocktail tablets | Roche Diagnostics, Mannheim, Germany |
| Nuclease-free water | Ambion, Life Technologies, Carlsbad, USA, (now Thermo Fisher Scientific) |
| **Cell isolation and culture** | |
| Deoxyribonuclease I from bovine pancreas (DNase) | Sigma-Aldrich, St. Louis, USA |
| Trypsin from bovine pancreas | Sigma-Aldrich, St. Louis, USA |
| VLE-RPMI 1640 liquid medium (very low endotoxin) | Biochrom, Merck, Berlin, Germany |
| Fibroblast Growth Medium 2 including 0.02 ml/ml fetal calf serum, 1 ng/ml FGF, 5 µg/ml insulin | PromoCell, Heidelberg, Germany |
| EpiLife™ medium | Gibco, Life Technologies, Carlsbad, USA (now Thermo Fisher Scientific) |
| Human Keratinocyte Growth Supplement (HKGS), sterile | Gibco, Life Technologies, Carlsbad, USA (now Thermo Fisher Scientific) |
| Penicillin-Streptomycin solution 100x, sterile | Biowest, Nuaillé, France |
| Amphotericin B solution 250 mg/ml, sterile | Sigma-Aldrich, St. Louis, USA |
| FBS Superior | Biochrom, Merck, Berlin, Germany |
| TrypLE Express, no phenol red | Gibco, Life Technologies, Carlsbad, USA (now Thermo Fisher Scientific) |
| Trypan Blue solution | Sigma-Aldrich, St. Louis, USA |
| **Cell-based phospho-ELISAs** | |
| Formaldehyde solution | Sigma-Aldrich, St. Louis, USA |
| **Gel electrophoreses for Western blots** | |
| Laemmli Sample Buffer | Bio-Rad, Hercules, USA |
| β-mercaptoethanol | Sigma-Aldrich, St. Louis, USA |
| Precision Plus Protein WesternC Standards | Bio-Rad, Hercules, USA |
| 10 x Tris/Glycerin/SDS (TGS) Buffer | Bio-Rad, Hercules, USA |
| **Gel electrophoreses for miRNA** | |

| | |
|---|---|
| **preparation** | |
| Rotiphorese® 10x TBE Buffer | Carl Roth, Karlsruhe, Germany |
| Ethidium bromide aqueous solution 10 mg/ml | Sigma-Aldrich, St. Louis, USA |
| **Western blots** | |
| 10 x Tris/Glycerin Buffer | Bio-Rad, Hercules, USA |
| SDS solution 10 % | Bio-Rad, Hercules, USA |
| PVDF Membranes for Western Blotting | Thermo Fisher Scientific, Waltham, USA |
| Methanol | |
| Blotting Grade Blocker, Non Fat Dry Milk | Bio-Rad, Hercules, USA |
| 10 x Tris Buffered Saline (TBS) | Bio-Rad, Hercules, USA |
| 10 % Tween 20 | Bio-Rad, Hercules, USA |
| SuperSignal™ West Femto Maximum Sesitivity Substrate (Substrate A and B) | Thermo Fisher Scientific, Waltham, USA |
| **miRNA preparations** | |
| Wasserstoffperoxid 30 % (hydrogen peroxide) | Carl Roth, Karlsruhe, Germany |
| PeqGold TriFast™ | Peqlab, VWR international, Erlangen, Germany |
| Chloroform | Sigma-Aldrich, St. Louis, USA |
| 2-Propanol | Sigma-Aldrich, St. Louis, USA |
| Sodium acetate (≥ 99%, p.a.) ACS | Carl Roth, Karlsruhe, Germany |
| **Next generation sequencing** | |
| Sodium hydroxide (ultra) | Fluka Analytical, Sigma-Aldrich Chemie, Steinheim, Germany |

### III.1.4 Gels

Gels used for gel electrophoreses in this study are listed in table 4.

**Table 4 Gels used for gel electrophoreses in this study listed by field of application**

| Gel | Supplier |
|---|---|
| **Western blots** | |
| Criterion™ Tris-HCl Gel (10–20% polyacrylamide gel, 12+2 well, 45 µl) | Bio-Rad, Hercules, USA |
| **miRNA preparations** | |
| Criterion™ TBE Gel (10% polyacrylamide gel, 18-well) | Bio-Rad, Hercules, USA |

### III.1.5 Antibodies

Antibodies used for Western blots in this study are listed in table 5.

**Table 5 Antibodies used for Western blots in this study**

| Antibody | Source | Size | Supplier | Dilution used |
|---|---|---|---|---|
| **Primary** | | | | |
| anti-CK10 | mouse | 60 kDa | Abcam, Cambridge, UK | 1:1000 |
| anti-CK14 | mouse | 50 kDa | Abcam, Cambridge, UK | 1:100 |
| anti-involucrin | mouse | 120 kDa | Abcam, Cambridge, UK | 1:1000 |
| **Secondary** | | | | |
| anti-mouse IgG poly-HRP 0.5 mg/ml | goat | not specified | Thermo Fisher Scientific, Waltham, USA | 1:20000 |

### III.1.6 Primers

All primers used for quantitative real-time polymerase chain reaction (qRT-PCR) in this study were ordered from Qiagen, Hilden, Germany and are listed in table 6.

**Table 6 Primer assays used in this study with respective target sequence (all supplied by Qiagen, Hilden, Germany)**

| Primer assay | Target (mir=stem loop, miR=mature) |
|---|---|
| Hs_mir-7-1_PR_1 miScript Precursor Assay (MP00003500) | hsa-mir-7-1 |
| Hs_mir-17_PR_1 miScript Precursor Assay (MP00001064) | hsa-mir-17 |
| Hs_mir-30b_PR_1 miScript Precursor Assay (MP00001827) | hsa-mir-30b |
| Hs_mir-31_PR_1 miScript Precursor Assay (MP00008757) | hsa-mir-31 |
| Hs_mir-34a_PR_1 miScript Precursor Assay (MP00002044) | hsa-mir-34a |
| Hs_mir-138-2_PR_1 miScript Precursor Assay (MP00000889) | hsa-mir-138-2 |
| Hs_mir-146a_PR_1 miScript Precursor Assay (MP00000938) | hsa-mir-146a |
| Hs_mir-191_PR_1 miScript Precursor Assay (MP00001211) | hsa-mir-191 |
| Hs_mir-200c_PR_1 miScript Precursor Assay (MP00001414) | hsa-mir-200c |
| Hs_mir-221_PR_1 miScript Precursor Assay (MP00001617) | hsa-mir-221 |
| Hs_mir-382_PR_1 miScript Precursor Assay (MP00002177) | hsa-mir-382 |
| Hs_mir-484_PR_1 miScript Precursor Assay (MP00002338) | hsa-mir-484 |
| Hs_mir-494_PR_1 miScript Precursor Assay (MP00002408) | hsa-mir-494 |
| Hs_mir-520e_PR_1 miScript Precursor Assay (MP00002716) | hsa-mir-520e |
| Hs_mir-944_PR_1 miScript Precursor Assay (MP00003801) | hsa-mir-944 |
| Hs_miR-7-1*_1 miScript Primer Assay (MS00010535) | hsa-miR-7-1-3p |
| Hs_miR-31*_1 miScript Primer Assay (MS00009415) | hsa-miR-31-3p |
| Hs_miR-34a_1 miScript Primer Assay (MS00003318 ) | hsa-miR-34a-5p |
| Hs_miR-146a_1 miScript Primer Assay (MS00003535) | hsa-mir-146a-5p |
| Hs_miR-200c_1 miScript Primer Assay (MS00003752) | hsa-miR-200c-3p |
| Hs_miR-3182_1 miScript Primer Assay (MS00020909) | hsa-miR-3182 |
| Hs_miR-4455_1 miScript Primer Assay (MS00041181) | hsa-miR-4455 |

### III.1.7 Special labware

Special labware used in this study is listed by field of application in table 7, including the suppliers.

**Table 7 Special labware used in this study, listed by field of application**

| Special labware | Supplier |
|---|---|
| **Cell-based phospho-ELISAs** | |
| Cell culture microplate, 96 well, PS; F-bottom, µClear®, black, Cellstar®, TC | Greiner Bio-One, Kremsmünster, Austria |
| **Cell culture** | |
| Neubauer counting chamber 0.1 mm depth | LO Laboroptik, Lancing, UK |
| Tissue culture flasks 75 | TPP, Trasadingen, Switzerland |
| 6-well tissue culture test plates | TPP, Trasadingen, Switzerland |
| **miRNA preparations** | |
| cell scrapers 30 cm, sterile | TPP, Trasadingen, Switzerland |
| Qubit® assay tubes, 500 µl | Thermo Fisher Scientific, Waltham, USA |
| Non-stick RNase-free 1.5 and 2 ml microfuge tubes | Ambion, Life Technologies, Carlsbad, USA, (now Thermo Fisher Scientific) |
| Spin-X centrifuge tube filter 0.45 µm cellulose acetate RNase/DNase free | Corning Incorporated, Corning, USA |

### III.1.8 Software

Software used in this study is listed by field of application in table 8, including suppliers.

**Table 8 Software used in this study, listed by field of application**

| Software | Supplier |
|---|---|
| **Various applications** | |
| Excel™ 2010 | Microsoft, Washington, USA |
| Word 2010 | Microsoft, Washington, USA |
| Powerpoint™ 2010 | Microsoft, Washington, USA |
| Gimp 2.8.10 | The Gimp-Team, www.gimp.org |
| R v3.2.5 | R Foundation for Statistical Computing, Vienna, Austria |
| Linear and Nonlinear Mixed Effects Models (lnme) package for the R environment | Pinheiro J et al. (2016)[108] |
| **ELISAs** | |
| Magellan™ v 6.6 | Tecan, Männedorf, Switzerland |
| XFluor4 v 4.51 for Microsoft Excel™ | Tecan, Männedorf, Switzerland |
| **Western blots and phospho-kinase arrays** | |
| AIDA Image Analyzer | Raytest, Straubenhardt, Germany |
| **Next generation sequencing** | |
| 2100 Expert Software (Bioanalyzer) | Agilent Technologies, Santa Clara, USA |
| Illumina® Experiment Manager 1.6 | Illumina®, San Diego, USA |
| Cutadapt 1.9 | Marcel Martin 2011[109] |
| Bowtie 1.0.1 | John Hopkins University, Baltimore, USA Langmead 2009[110] |
| DESeq 2, package for the R environment | Love 2014[111] |
| **qRT-PCR** | |
| LightCycler® 480 software release 1.5.0 | Roche Diagnostics Mannheim, Germany |

### III.1.9 Databases

Databases used in this study are listed by field of application in table 9.

**Table 9 Databases used in this study, listed by field of application**

| Database | Operator | Website |
|---|---|---|
| **Next generation sequencing** | | |
| miRBase | **Griffiths-Jones lab, Faculty of Life Sciences, University of Manchester**[91,92] | http://www.mirbase.org |
| PubChem Compound Database | **National Center for Biotechnology Information** | https://pubchem.ncbi.nlm.nih.gov/compound |

## III.2 Methods

An overview of the methods which were used in the two parts of this work - the investigation of plasma biomarkers in patient samples from the Dermatoxgen cohort and the identification of epigenetic biomarkers in an *in vitro* cell model of keratinocytes and fibroblasts – is presented in figure 7. Details for each method are provided in the following chapters.

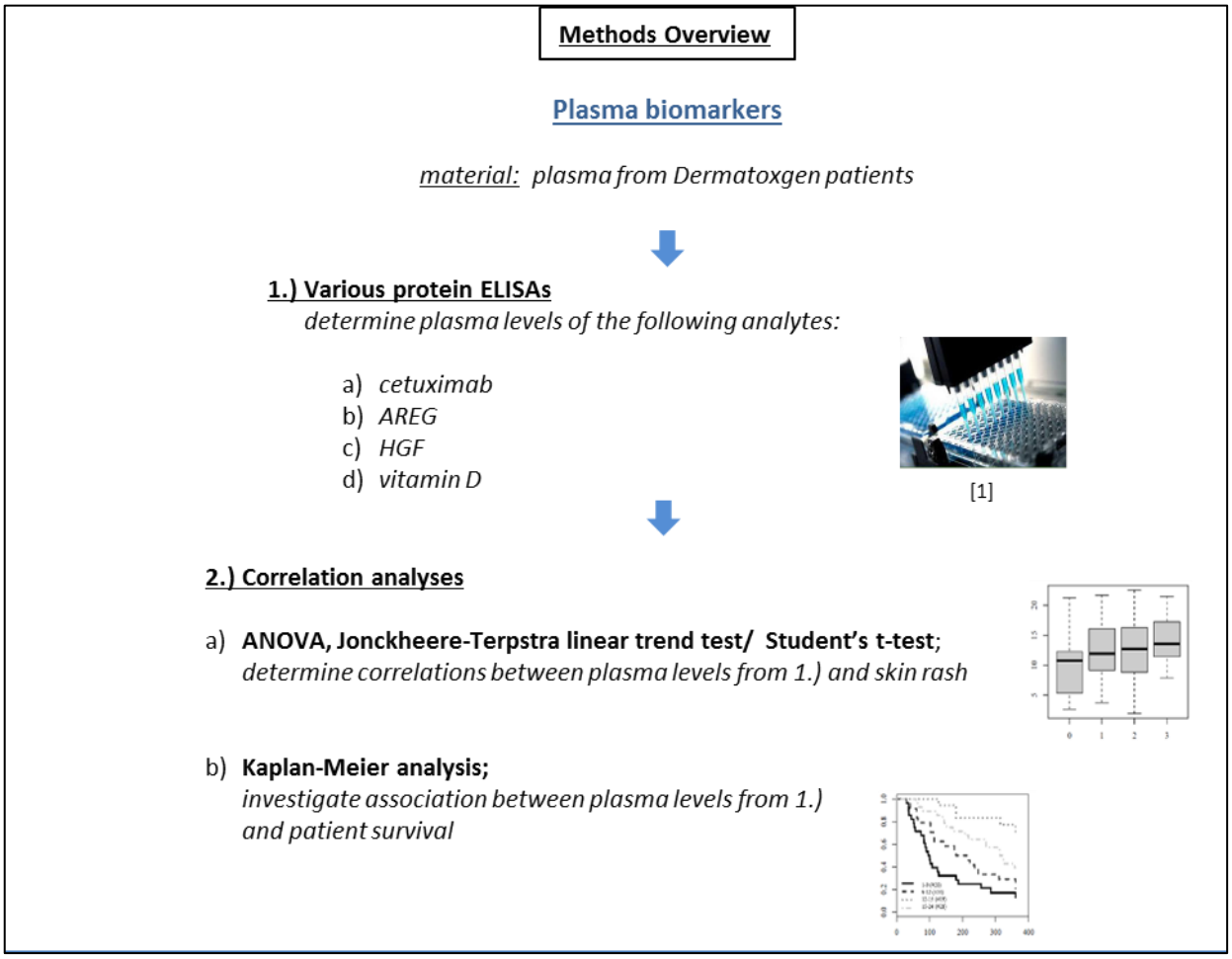

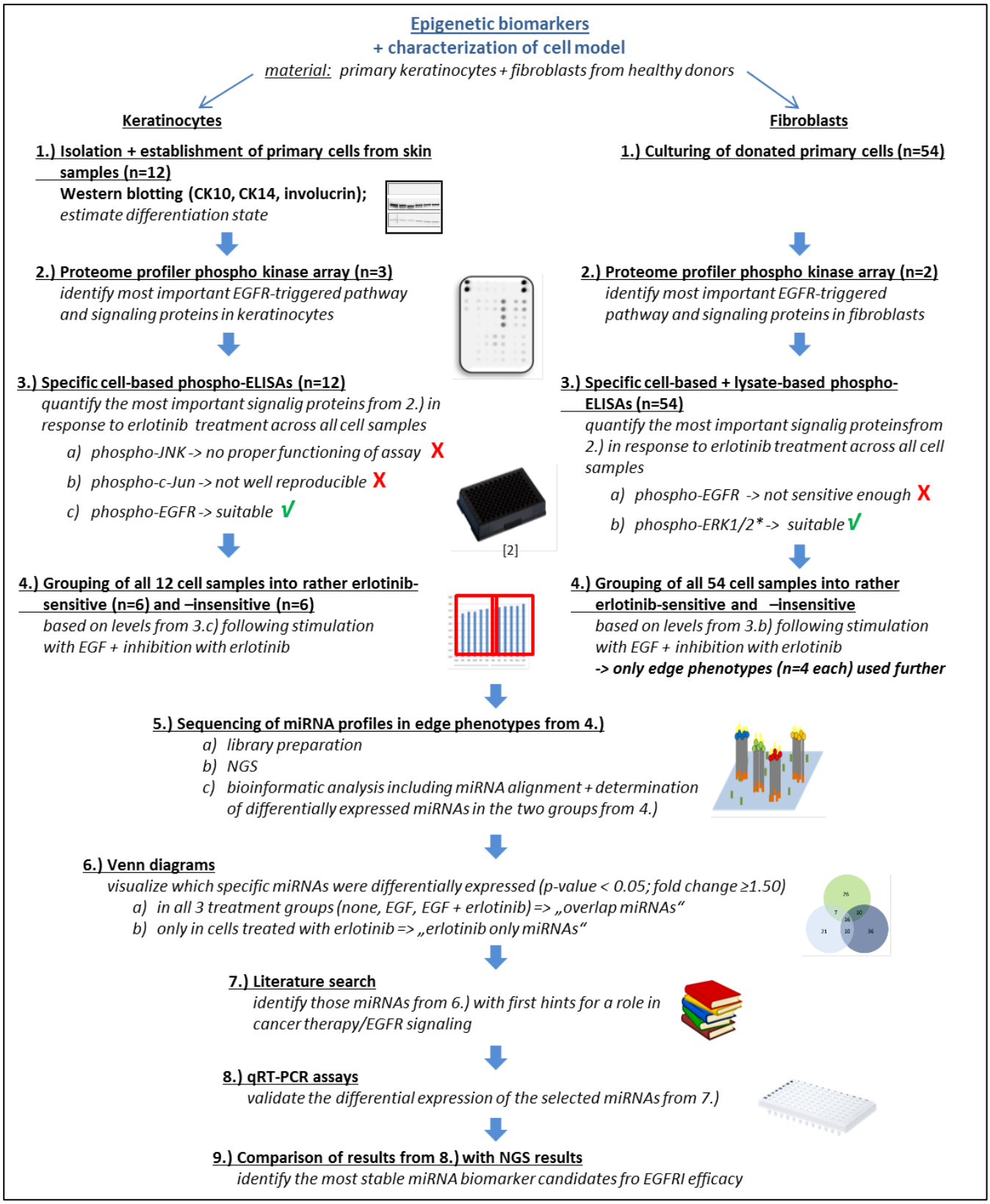


**Figure 7 Overview of methods used for this study**

* Since the EGFR-ELISA was found not sensitive enough, a lysate based assay was tried for ERK1/2. [1] Somru Bioscience cetuximab ELISA user manual, [2] Sarstedt product catalogue.

### III.2.1 Clinical study (investigations with patient plasma)

#### III.2.1.1 Dermatoxgen study

The Dermatoxgen study is a prospective, multicenter study which was conducted to investigate pharmacogenetic factors of skin toxicity induced by EGFRIs. For the patient case recruitment phase, the study received financial support by the Wilhelm Sander Stiftung (grant numbers: 2008.017.01 and 2008.017.2). The patient cohort included patients who received treatment with an EGFRI for cancer of different solid tumor types (pancreatic, colon, head and neck or lung cancer). Patients were included before they were first-time treated with an EGFRI (erlotinib, gefitinib, cetuximab or panitumumab). Written informed consent was obtained from all patients and the study was reviewed by the ethical boards of Ulm University and the Ludwig-Maximilians-University of Munich. Patients were recruited during the active recruitment period (2008-2014) at four different study sites, namely the Departments of Internal Medicine I (Prof. Dr. Thomas Seufferlein) and II (Prof. Dr. Christian Schumann, Dr. Stefan Rüdiger) at Ulm University, a hematology-oncology practice (Hämato-Onkologische Schwerpunkt-Praxis) in Ulm (Dr. Volker Kächele) and the Department of Internal Medicine III at the Klinikum Grosshadern, Ludwig-Maximilians-University of Munich (Prof. Dr. Stefan Böck, Prof. Dr. Volker Heinemann).

Clinical assessment – performed by the clinicians at the study sites listed above

Over the first four weeks of EGFRI treatment, the patients visited a physician once a week and the occurrence and severity of dermal adverse effects as well as diarrhea were documented together with any conducted treatments. The severity of skin toxicity was graded according to the Common Toxicity Criteria for Adverse Events of the American National Cancer Institute (NCI CTCAE version 3.0, 2006)[112].

Rash/desquamation

Grade 1: Macular or papular eruption or erythema without associated symptoms
Grade 2: Macular or papular eruption or erythema with pruritus or other associated symptoms; localized desquamation or other lesions covering < 50% of body surface area
Grade 3: Severe, generalized erythroderma or macular, papular or vesicular eruption; desquamation covering ≥ 50% body surface area
Grade 4: Generalized exfoliative, ulcerative, or bullous dermatitis

General patient parameters were also determined including age, gender, body mass index (BMI) and smoking status. In addition, doses of administered EGFRIs and all other

medication were documented. At the fifth visit (four weeks after initiation of EGFRI therapy) a blood sample was drawn from each patient for genetic analyses and serum and plasma samples were generated at the respective study site. Blood samples were drawn directly before application of the next scheduled dose of the respective EGFRI. Follow-up visits were conducted at three, six and twelve months after start date of treatment to document PFS and OS of patients.

Patients enrolled in the study were diagnosed with either of the following tumor types: pancreatic, colon, head and neck or non-small cell lung cancer. EGFRIs were administered in combination with different chemotherapeutic agents. Doses and application schemes of EGFRIs are listed in table 10.

**Table 10 EGFRI dosages and application schemes used in the Dermatoxgen study**

| EGFRI | Initial dose | Application scheme | dose |
|---|---|---|---|
| erlotinib | - | daily | 50, 100 or 150 mg |
| gefitinib | - | daily | 150 or 250 mg |
| cetuximab | 250, 400, 450 or 500 mg/m² | weekly (250 mg/m²) or bi-weekly (500 mg/m²) | 250 or 500 mg/m² depending on application scheme |
| panitumumab | - | bi-weekly (6 mg/kg body weight) or every three weeks (9 mg/kg body weight) | 6 or 9 mg/kg body weight depending on application scheme |

### III.2.1.2 Enzyme-linked immunosorbent assays (ELISAs) with patient plasma

An ELISA is an antibody-based detection assay for the quantitative measurement of a target substance. In this study different ELISA kits were used to quantify cetuximab, calcidiol, HGF and AREG in plasma samples of patients from the Dermatoxgen study. These ELISAs employ the quantitative sandwich immunoassay technique.

Procedure

ELISAs were conducted according to the respective manufacturer's instructions.
A capture antibody specific for the respective target protein had been pre-coated on a 96-well plate by the manufacturer. Plasma samples were added to the wells and the target protein was bound by the immobilized antibody. Furthermore, different known concentrations of the target protein were added to some wells, so called standards. To some wells only buffer was added, so called blanks. After a washing step, a detection antibody was added which was specific for the target protein. The detection antibody was

either directly linked to an enzyme or it was biotinylated and in an additional step streptavidin was added which was in turn linked to an enzyme and bound to the biotin. After an additional washing step, a substrate solution was added and the enzyme catalyzed a reaction leading to color development. The amount of color is proportional to the amount of target protein present. A stop solution was applied and the intensity of the color was read with a microplate reader. Absorbance was also measured at a reference wavelength to correct for optical imperfections in the plate.

Analysis

Absorbance values measured at the reference wavelength were subtracted from the absorbance values measured at the target wavelength to correct for optical imperfections in the plate. If blanks had been included in the experiment their readings were also subtracted from the sample and standard readings to correct for unspecific signals originating from the reagents not the target protein. If replicates had been measured the mean absorbance was calculated for each set. A standard curve was plotted with standard concentration on the x-axis and measured absorbance on the y-axis. A four or five parameter curve fit was drawn. The concentration of target protein within the plasma samples could be calculated by inserting the measured absorbance values in the equation of the standard curve. The calculations were performed with the programs Magellan™, XFluor4 and R, as specified in the following table 11.

**Table 11 Characteristics of the different protein ELISAs used in this study**

| **Target protein** | Cetuximab | Calcidiol (25-OH-vitamin D) | Amphiregulin (AREG) | Hepatocyte growth factor (HGF) |
|---|---|---|---|---|
| **ELISA kit** | Cetuximab (Erbitux®) PK ELISA, Somru BioScience | 25-OH-Vitamin-D-ELISA, EUROIMMUN Medizinische Labordiagnostika AG | Human Amphiregulin ELISA Kit, SIGMA-ALDRICH | Quantikine® ELISA Human HGF, R&D systems |
| **Replicates (samples)** | Duplicates | Duplicates | Duplicates | Duplicates |
| **Concentrations of standards [ng/ml]** | 156, 312, 625, 1250, 2500, 5000, 7500, 10000 | 0, 4, 10, 25, 60, 120 | 16.46, 49.38, 148.1, 444.4, 1333, 4000 | 125, 250, 500, 1000, 2000, 4000, 8000 |
| **Capture antibody** | Monoclonal anti-cetuximab antibody | Monoclonal antibody specific for cholecalcidiol and ergocalcidiol | Anti-amphiregulin antibody | Monoclonal anti-HGF antibody |
| **Detection antibody** | Polyclonal anti-cetuximab antibody linked to an enzyme | Enzyme-linked streptavidin | Biotinylated anti-amphiregulin antibody | Polyclonal anti-HGF antibody linked to an enzyme |
| **Enzyme** | Not specified | Peroxidase | Horseradish peroxidase linked to streptavidin | Horseradish peroxidase |
| **Substrate** | 3,3',5,5'-tetramethylbenzidine (TMB) | | | |
| **Target wavelength** | 450 nm | | | |
| **Reference wavelength** | 650 nm | 640 nm | 540 nm | 540 nm |
| **Curve fit** | 4-parameter curve fit | | | |
| **Calculations** | Absorbance was measured using the program Magellan™. All calculations including subtraction of reference absorbance, calculation of mean values from duplicates, plotting of standard curves, drawing of curve fits and determination of target protein concentrations were performed automatically by the software Magellan™. | | Absorbance was measured using the program XFluor4. Subtraction of reference absorbance and calculation of mean values from duplicates was conducted in MS-Office Excel™. Plotting of standard curves, drawing of curve fits and calculation of target protein concentrations were conducted with the lnme package in the R environment for statistical techniques. | |
| **Assay specialities** | | Unlabeled calcidiol in the samples and biotin-labeled calcidiol specifically added to the wells compete for binding sites of the capture antibodies. | | |

### III.2.2 Cell model (experiments with cells from healthy human donors)

#### III.2.2.1 Isolation of primary human keratinocytes

Primary adult human keratinocytes were isolated from excess skin obtained from plastic surgery at the University Women's Clinic Bonn (Universitätsfrauenklinik). The skin was kindly provided by the working group of Prof. Dr. med. Dr. ès sci. Thomas Bieber at the Dermatology and Allergology Department (Klinik und Poliklinik für Dermatologie und Allergologie). Within the same group, Dr. Kazumasa Iwamoto and Tim Stroich prepared a 0.4 mm split-thickness skin using an electric dermatome and washed the skin two times in phosphate buffered saline (PBS).

The subsequent protocol was adapted from the one published by Aasen and Belmonte in 2010[113]. The skin was incubated in 0.5 % trypsin in PBS with 1 % antibiotics and antimycotics (penicillin-streptomycin and amphotericin B) at 37 °C for 1 h with the epidermis facing up. The epidermis was peeled off from the dermis using forceps and the epidermis was cut into small pieces of approx. 1 $cm^2$. The pieces were transferred to a centrifuge tube containing 50 ml VLE-RPMI 1640 cell culture medium with 10 % fetal bovine serum, 1 % antibiotics and antimycotics and 100 U/ml DNase I. The solution was thoroughly resuspended and filtered through a cell strainer. The cells were washed two times with VLE-RPMI 1640 medium using centrifugation at 300 x g for 10 min each. The cells were counted in a Neubauer counting chamber and seeded at 4 x $10^5$ cells per well of a 6-well plate in 2 ml EpiLife™ cell culture medium. This serum-free medium has a defined concentration of calcium chloride (60 µM) which slows down differentiation of keratinocytes while at the same time removing contamination of other cell types such as fibroblasts, because they do not grow well under these conditions. Prior to use, the 6-well plates were coated with type I collagen by adding 800 µl dilution medium and 8 µl coating matrix per well and incubating the plates at 22 °C for 30 min. Coating of the culture plates is important for maximum yield with initial seeding of cells but was found to be unnecessary during subsequent passages. After cell seeding the medium had to be changed after 3 days and subsequently every 2 to 3 days. Under these culture conditions it took several days before healthy colonies of cells were visible. Cells were not allowed to become more than 75 % confluent to prevent differentiation. Cell aliquots were frozen at a concentration of 1 to 1.5 x $10^6$/ml in freezing medium (90 % fetal bovine serum + 10 % dimethyl sulfoxide [DMSO]).

### III.2.2.2 Culturing of cells

All cell culture work was carried out under a sterile laminar flow hood.

In this project primary adult human epidermal keratinocytes and dermal fibroblasts were used for *in vitro* studies. Keratinocytes were obtained as described in section III.2.2.1 Fibroblasts were obtained from healthy tissue by dermal excision from patients at the Clinical Pharmacology Department of the University Medicine Göttingen (kindly provided by Dr. med. Markus Schirmer).

Cell stocks were stored in liquid nitrogen. Prior to any experiments, in our laboratory all cell cultures were routinely tested for contaminations with *Mycoplasma*.
The medium used for culturing of keratinocytes was EpiLife™ supplemented with Human Keratinocyte Growth Supplement and for fibroblasts Basal Fibroblast Growth Medium 2 supplemented with 0.02 ml/ml fetal calf serum, 5 µg/ml Insulin and 0.001 µg/ml fibroblast growth factor (FGF). Both types of media were also supplemented with penicillin-streptomycin (x 1) and in addition the keratinocyte medium contained 250 ng/ml amphotericin B as an antimycotic. All cells were grown at 37 °C and 5 % $CO_2$. The medium was changed every 2 to 3 days and cells were passaged every 7 to 10 days.

For passaging, the medium was aspirated and the cells were washed with 10 ml PBS per flask. The cells were then incubated with 1 ml of the recombinant enzyme TrypLE Express for 5 min to detach them from the culture flask. 10 ml of fresh medium were added and the cells were transferred to 50 ml centrifuge tubes and centrifuged at 600 x g (keratinocytes) or 300 x g (fibroblasts) and room temperature (RT) for 5 min. The supernatant was discarded, the pellet resuspended in 10 ml PBS and centrifuged again as before. The supernatant was discarded and cells resuspended in 1 ml fresh medium. Living cells were counted by mixing 10 µl of cell suspension with 10 µl trypan blue, applying it to a Neubauer counting chamber and counting all cells which were able to exclude the blue dye indicating they were alive. Cells were seeded into fresh 75 cm² culture flasks at concentrations between 2 x $10^5$ and 4 x $10^5$ cells per flask.

### III.2.2.3 Sodium dodecyl sulfate-polyacrylamide gel electrophoresis (SDS-PAGE)

SDS-PAGE was performed to achieve separation of denatured proteins according to their electrophoretic mobility, which is determined by their molecular weight. To exclude an influence of the proteins' secondary and tertiary structures on the separation, proteins are denatured by applying heat (95 °C) which leads to destruction of hydrogen bonds and

disulfide bonds are reduced by using ß-mercaptoethanol. To ensure a similar relation between charge and size for each of the proteins, they are treated with SDS, which covers them and provides a negative charge. In an electric field the negatively charged proteins migrate through the polyacrylamide gel towards the anode. Small polypeptides migrate faster than larger ones resulting in separation of the proteins. This was necessary for later Western blot analyses.

Procedure

Cell lysates were prepared exactly as described in section III.2.2.6 (also using the lysis buffer from the Erk1/2 ELISA kit) but without any prior *in vitro* treatment. The concentration of total protein in the cell lysates was determined by a bicinchoninic acid assay as described by the manufacturer. To the total protein solution a mixture of Laemmli Buffer and ß-mercaptoethanol (1:20) was added to yield a concentration of 0.4 µg/µl. The Laemmli Buffer reduces disulfide bonds. The proteins were then denatured at 95 °C for 5 min. The samples were cooled on ice for 1 min and 20 µl were loaded per wells of a ready-to-use 10-20 % tris-HCl gel. As a marker 10 µl of Precision Plus Protein WesternC Standards was added to one well. The gel chamber was filled with 1 x tris/glycerin/SDS (TGS) buffer containing 0.1 % SDS and the electrophoresis was run at 100 V for 20 min (stacking phase) followed by 200 V for 30 min.

### III.2.2.4 Western blot (tank-blot procedure)

After electrophoretic separation the proteins were transferred to a polyvinylidene fluoride (PVDF)-membrane to allow for detection of certain proteins by specific antibodies. Protein transfer is achieved by placing a PVDF-membrane next to the gel containing the separated proteins and applying an electric field. The cathode has to be next to the gel and the anode next to the membrane allowing for the negatively charged proteins to migrate towards the anode and thereby being blotted onto the membrane. After protein transfer the free protein binding sites on the membrane have to be blocked, e. g. by incubating it in skim milk solution. The proteins of interest can then be detected by incubation with specific primary antibodies, followed by incubation with a secondary antibody coupled to an enzyme and subsequent addition of a chemiluminescent substrate and detection with an appropriate imaging system.

Procedure

A PVDF-membrane was incubated in methanol for 1 min for activation and then equilibrated in transfer buffer (150 ml 10 x tris-glycerin, 150 ml methanol, 1.5 ml 10 %

SDS). A complex was formed, consisting of the membrane and the protein gel with a filter paper and sponge on each side, which was then soaked in transfer buffer and blotting was performed in a blotting tank in transfer buffer for 60 min with a constant electric current of 350 mA. A cooling pack (-20 °C) was included in the tank during the run. The membrane was then blocked by incubation with 5% skim milk in wash buffer (tris buffered saline with 10% Tween 20 (1:200); TBS-T) for 1 h. The membrane was cut into three strips so it could be incubated with three different primary antibodies. The size of the target proteins was taken into account and the membrane was cut at the appropriate places with the help of the protein standard which had been run with the gel. The membrane strips were incubated overnight at 4 °C with gentle shaking with a primary antibody solution against the respective protein of interest diluted in TBS-T. For dilution factors for specific antibodies see table 5. On the next day the membranes were washed three times for 10 sec and then three times for 10 min each with TBS-T and then incubated with an HRP-conjugated secondary antibody solution diluted in 5% skim milk in TBS-T for 1 h at RT. The membranes were washed again as before and incubated with a chemiluminescent substrate (reagent A + reagent B 1:1) for 5 min. The protein bands were visualized with a chemiluminescent imaging system (CCD camera). Exposure time was varied for optimization of signal visualization.

#### III.2.2.5 Human phospho-kinase array

To investigate the influence of *in vitro* incubation with erlotinib and stimulation with EGF on the different EGFR signaling pathways in keratinocytes and fibroblasts, Proteome Profiler™ Human Phospho-Kinase Arrays were conducted with cell lysates. With this array relative levels of phosphorylation of 43 kinase phosphorylation sites and two related total proteins of EGFR signaling pathways are detected simultaneously. Higher amounts of phosphorylation correspond to stronger signaling activity and therefore indicate which pathways are most important in the different cell types.

Procedure

Primary adult human dermal keratinocytes and fibroblasts were cultured as described in section III.2.2.2. For each experiment three different treatment conditions were applied. Each treatment was carried out in duplicate. Therefore, six 75 $cm^2$ cell culture flasks were used per experiment. The cells were cultured to 75 % confluency. The cells were washed with PBS and starved for 2 h, meaning that the complete culture medium was replaced by supplement-free medium to reduce the presence of growth factors which could influence or mask the effect of erlotinib or EGF on the cells. Subsequently, to two flasks 10 µl of 10

mM erlotinib hydrochloride dissolved in 100 % DMSO were added resulting in a final erlotinib concentration of 10 µM and 0.1 % DMSO in the medium. Since DMSO can be harmful for cells, 10 µl of 100 % DMSO were added to the other four flasks (final concentration 0.1 %) to create equal DMSO conditions and rule out that possible effects seen later on are due to DMSO. All cells were incubated for 2 h and then stimulated with EGF. For stimulation, EGF was added to the erlotinib-containing flasks and two of the other flasks at a final concentration of 4 nM. All cells were incubated for 5 min. An overview of cell treatments is given in table 12. The concentrations of the substances were chosen according to previous experiments conducted by other members of our research group prior to my work.

**Table 12 Incubation and stimulation conditions for cells in human phospho-kinase arrays**

| Abbreviated name of sample | 2 h incubation | 5 min stimulation |
|---|---|---|
| no treatment (negative control) | medium with DMSO | - |
| EGF | medium with DMSO | 4 nM EGF |
| erlotinib + EGF | medium with 10 µM erlotinib in DMSO | 4 nM EGF |

After stimulation with EGF, the cells were detached from the flasks and counted as described before. Cells from the two flasks with equal treatment conditions were pooled. Cell lysates were prepared by solubilizing the cells at 1 x $10^7$ cells/ml in the lysis buffer provided with the kit. The cells were properly resuspended and rocked gently at 4 °C for 40 min. The samples were centrifuged at 14000 x g and 4 °C for 5 min to sort out the cell debris from the protein lysates. The supernatants were transferred to clean tubes and further used in the assay. The total protein concentration in the lysates was determined by bicinchoninic acid assay.

In the phospho-kinase array kit nitrocellulose membranes are provided on which capture and control antibodies have been spotted in duplicate. A list of all target proteins of the capture antibodies with their relevant phosphorylation sites is given in table 13.

**Table 13 Target proteins of the capture antibodies spotted on the nitrocellulose membranes of the Proteome Profiler™ Human Phospho-Kinase Arrays and their phosphorylation sites relevant for the array**

| Target | Phosphorylation site |
|---|---|
| p38α | T180/Y182 |
| ERK1/2 | T202/Y204, T185/Y187 |
| JNK 1/2/3 | T183/Y185, T221/Y223 |
| GSK-3α/β | S21/S9 |
| p53 | S392 |
| EGFR | Y1086 |
| MSK1/2 | S376/S360 |
| AMPKα1 | T183 |
| Akt 1/2/3 | S473 |
| Akt 1/2/3 | T308 |
| p53 | S46 |
| TOR | S2448 |
| CREB | S133 |
| HSP27 | S78/S82 |
| AMPKα2 | T172 |
| β-Catenin | - |
| p70 S6 Kinase | T389 |
| p53 | S15 |
| c-Jun | S63 |
| Src | Y419 |
| Lyn | Y397 |
| Lck | Y394 |

| Target | Phosphorylation site |
|---|---|
| STAT2 | Y689 |
| STAT5a | Y694 |
| p70 S6 Kinase | T421/S424 |
| RSK1/2/3 | S380/S386/S377 |
| eNOS | S1177 |
| Fyn | Y420 |
| Yes | Y426 |
| Fgr | Y412 |
| STAT6 | Y641 |
| STAT5b | Y699 |
| STAT3 | Y705 |
| p27 | T198 |
| PLC-γ1 | Y783 |
| Hck | Y411 |
| Chk-2 | T68 |
| FAK | Y397 |
| PDGF Rβ | Y751 |
| STAT5a/b | Y694/Y699 |
| STAT3 | S727 |
| WNK1 | T60 |
| PYK2 | Y402 |
| PRAS40 | T246 |
| HSP60 | - |

All reagents were brought to RT before use and prepared according to the manufacturer's instructions. Samples were kept on ice prior to use. The phospho-kinase array is divided into two membranes (A and B) to decrease cross-reactivity and increase sensitivity. The membranes were placed into an 8-well multi-dish. Membrane A and B were placed in separate wells and 1 ml blocking buffer (1 x Array Buffer 1) was added to each well. The dish was incubated for 1 h at RT on a rocking platform shaker. After incubation the blocking buffer was aspirated. The cell lysate samples were prepared by using 200 µg of total protein and diluting it with blocking buffer to a final volume of 2 ml. 1 ml was then added to each membrane (A and B). A separate set of membranes A and B was used for each sample (no treatment, EGF and erlotinib + EGF; for treatment conditions see table 12). The membranes were incubated overnight at 4 °C on a rocking platform shaker. Each membrane set was placed in a separate plastic container (A and B together in one container) and washed three times with 10 ml of 1 x Wash Buffer. During each washing step the membranes were incubated on a rocking platform shaker for 10 min. For each A membrane 20 µl of reconstituted Detection Antibody Cocktail A were added to 1 ml of 1 x

Array Buffer 2/3 and 1 ml of the mixture was added to each A membrane in the 8-well dish. The same was done for all B membranes but with reconstituted Detection Antibody Cocktail B instead of A. All membranes were incubated for 2 h at RT on a rocking platform shaker. The membranes were washed as before but this time corresponding A and B membranes were washed in separate containers to avoid cross-reactivity of the detection antibodies.
Streptavidin-HRP was diluted with 1 x Array buffer 2/3 using the dilution factor on the label and 1 ml was added to each membrane in the 8-well dish. The membranes were incubated for 30 min at RT on a rocking platform shaker. The membranes were washed as before but this time corresponding A and B membranes were washed in the same container again.
Excess buffer was drained from the membranes and they were placed on the lid of one of the wash containers. 1 ml of Chemi Reagent Mix was added to each set of membranes (A and B) and incubated for 1 min. The Chemi Reagent Mix was removed again and signals were detected using a chemiluminescent imaging system (CCD camera).

Analysis

The image analysis software AIDA was used to determine the pixel density for each spot on the membranes corresponding to the amount of the respective phosphorylated protein present in the sample. The signal values were exported to a spreadsheet program (Excel™). The average pixel density was calculated for each set of duplicate spots. The pixel density at a clear area of the membrane was used as a background value and subtracted from all sample values. The amounts of the different phosphorylated proteins were compared between the different samples (no treatment, EGF and erlotinib + EGF).

### III.2.2.6 Cell-based and lysate-based phospho-ELISAs

Cell-based or lysate-based phospho-ELISAs were used to measure the relative amount of certain phosphorylated proteins in human primary fibroblasts or keratinocytes under different *in vitro* treatment conditions. For each protein to be analyzed there is an antibody specific for the phosphorylated protein and also a different antibody specific for the whole protein regardless of the phosphorylation status (pan-protein). Hence, the amount of phosphorylated protein present can be normalized to the total amount of that protein.

Procedure

For the cell-based ELISAs, cells were seeded into 96-well plates at a concentration of 1 x $10^5$ cells/ml. 100 µl of cell suspension were used per well. The cells were grown overnight

and then starved for either 2 or 20 h. The cells were then incubated with 5 or 10 µM erlotinib for 2 h and subsequently stimulated with 4 or 40 nM EGF for 5 min. For each experiment three different *in vitro* treatment conditions were used: no treatment, EGF and erlotinib + EGF (for details see table 12). All samples and conditions were used in triplicates on the plates.

After stimulation the cells were fixed and permeabilized in the wells by replacing the culture medium with 100 µl of 4 % formaldehyde in 1 x PBS or Fixing Solution provided with the kit respectively and incubating them for 30 min at RT. For the lysate-based ELISAs instead of growing the cells directly in the 96-well plates they are grown in 75 $cm^2$ culture flasks as usual and after the desired treatment cell lysates are prepared and then used for the ELISA. In this study a phospho-Erk1/2 and pan-Erk1/2 ELISA was used as a lysate-based phospho-ELISA. These cell lysates were prepared exactly as described for the human phospho-kinase array in section III.2.2.5. The only changes in procedure were the use of the lysis buffer provided with this ELISA kit, which was mixed 1:2 with sterile water containing phosphatase and protease inhibitors (tablets dissolved according to protocol provided by the manufacturer) and cells were solubilized at a concentration of 4 x $10^6$ cells/ml.
Primary anti-phospho- and anti-pan-antibody solution were added to each well. Depending on the assay, the primary antibody specific for the phospho-protein and the one specific for the pan-protein were either added to the same well or to separate ones. In the c-Jun and the EGFR assays the primary antibodies are derived from different species enabling the use of two different secondary antibodies without cross-reactivity. The two secondary antibodies are labeled with different enzymes and two spectrally distinct fluorogenic substrates can be used for detection. Therefore the measurement of phospho- and pan-protein could be performed in the same well. In the JNK assay the measurements were performed in separate wells. The cells were incubated with the primary antibodies overnight at 4 °C or for 2 h at RT, depending on the assay. Negative controls were also included, for which blocking buffer was added to the wells instead of primary antibody solutions. The cells were washed again and 50 µl of each secondary antibody solution were added per well and incubated for 2 or 3 h at RT.
The cells were washed again with 1 x wash buffer or PBS and substrate solution was added to each well (c-Jun and EGFR assays: 75 µl of the first substrate; JNK assay: 100 µl of substrate). Incubation times varied from 30 to 60 min depending on the intensity of the developing signal (rosy color). Incubation was conducted at RT and in the dark. For the c-Jun and EGFR assays 75 µl of the second substrate were then added to each well and incubated for further 30 min at RT in the dark.

Subsequently, for the c-Jun and EGFR assays **fluorescence** was measured with excitation at a wavelength of 540 nm and emission at 600 nm representing the amount of phosphorylated target protein in the cells and subsequently with excitation at 360 nm and emission at 450 nm representing the amount of total target protein.
For the JNK assay after incubation with the substrate 50 µl of stop solution were added to each well and **absorbance** was measured at 450 nm with a microplate reader. The specific conditions for the different ELISA kits are presented in table 14. The programs XFluor4 and Excel™ were used for data collection and analysis.

Analysis

Depending on the assay type, mean **absorbance** or **fluorescence** values of the negative controls (no primary antibodies used) were calculated from the triplicate measurements and subtracted from each sample reading to correct for unspecific reactivity of the secondary antibodies.
Following this correction, for the c-Jun and EGFR assays the amount of phosphorylated target protein was normalized to the amount of total target protein by dividing the phospho-value by the pan-value. From the normalized triplicate values the mean was calculated for each sample.
For the JNK assay following the negative control correction, first the mean absorbance values were calculated for each triplicate set of sample readings. Afterwards the amount of phosphorylated target protein was normalized to the amount of total target protein by dividing the mean phospho-value by its corresponding mean pan-value for each sample. Normalized amounts of phospho-protein were compared between the different *in vitro* treatment conditions for each sample.

**Table 14 Characteristics of the cell-based and lysate-based phospho-ELISAs used in this study**

| **Target protein** | Phosphorylated c-Jun (S63) | Phosphorylated JNK (Thr183/Tyr185) | Phosphorylated EGFR (Y1068) | Phosphorylated Erk1 (T202/Y204) and Erk2 (T185/187) |
|---|---|---|---|---|
| **ELISA kit** | Human/Mouse/Rat Phospho-c-Jun (S63) Cell-Based ELISA Kit | Phospho-JNK (Thr183/Tyr185) Cell-Based ELISA Kit, human/mouse/rat | Human Phospho-EGF R/ErbB1 (Y1068) Cell-Based ELISA | Phospho-Erk1 (pThr202 / pTyr204) + Erk2 (pTyr185/187) and pan-Erk1 / 2 ELISA Kit |
| **Starvation time** | 2 h | 20 h | 2 h | 2 h |
| **Erlotinib concentration for incubation** | 5 µM | 5 µM | 10 µM | 5 µM |
| **EGF concentration for stimulation** | 4 nM | 4 nM | 40 nM | 40 nM |
| **Conditions for blocking** | 1 h, RT | 1 h, 37 °C | 1 h, RT | No blocking |
| **Primary antibodies** | Rabbit anti-phospho-c-Jun (S63) | Mouse anti-phospho-JNK (Thr183/Tyr185) | Mouse anti-phospho-EGFR (Y1068) | Rabbit anti-phospho-Erk1(T202/Y204)/Erk2(T185/Y187) |
| | Mouse anti-c-Jun | Mouse anti-JNK | Goat anti-EGFR | Anti-pan-Erk1/2 |
| **Phospho- and pan-protein measured in one well or separate?** | One well | Separate wells | One well | Separate wells |
| **Secondary antibodies** | HRP-conjugated goat anti-rabbit IgG | HRP-conjugated anti-mouse IgG | HRP-conjugated donkey anti-mouse IgG | HRP-conjugated anti-rabbit IgG |
| | AP-conjugated goat anti-mouse IgG | | AP-conjugated donkey anti-goat IgG | HRP-Streptavidin |
| **Substrates** | Fluorogenic substrate for HRP | 3,3',5,5'-tetramethylbenzidine (TMB) | Fluorogenic substrate for HRP | 3,3',5,5'-tetramethylbenzidine (TMB) |
| | Fluorogenic substrate for AP | | Fluorogenic substrate for AP | |
| **Incubation conditions** | Primary antibodies: 16 h, 4 °C<br>Secondary antibodies: 2 h, RT | Primary antibodies: 2h, RT<br>Secondary antibodies: 3 h, RT | Primary antibodies: 16 h, 4 °C<br>Secondary antibodies: 2 h, RT | Primary antibodies: 1 h, RT<br>Secondary antibodies: 1 h, RT |

### III.2.2.7 Isolation of total RNA

Total RNA was isolated from primary human dermal keratinocytes and fibroblasts by the guanidinium thiocyanate-phenol-chloroform extraction method developed by Chomczyński and Sacchi in 1987[114]. The chaotropic salt guanidine isothiocyanate is used to lyse the cells and denature proteins, which also leads to the inactivation of RNases. The aqueous samples containing the lysed cells are mixed with phenol and chloroform and centrifuged. This results in the formation of three phases. The proteins and hydrophobic lipids partition into the lower organic phase while the RNA remains in the upper aqueous phase and the DNA is found in the interphase. The aqueous phase contains the whole range of cellular RNAs including small RNAs. The RNA is precipitated with 2-propanol, washed with ethanol and dissolved in nuclease-free $H_2O$.

Procedure

To avoid contamination with RNases, gloves were worn at all times during isolation of RNA and tubes used for preparation of reagents were rinsed with 3 % $H_2O_2$ and ultrapure water.

For isolation of RNA cells were cultured in 6-well plates to a confluency of approx. 75 %. On the day of RNA isolation cells were starved for 2 h and then incubated for 2 h either with medium containing 5 µM erlotinib in DMSO or with medium only containing DMSO followed by stimulation with 4 nM EGF for 5 min. For an overview on the *in vitro* treatment conditions see table 12. Each condition was applied to four separate wells.

After stimulation the culture medium was aspirated and wells were washed with 2 ml PBS each. 1 ml of peqGOLD TriFast™ containing guanidine isothiocyanate and phenol was added to each well and incubated for 5 min at RT. The cells were detached from the plates with cell scrapers and the cell solutions were transferred to microcentrifuge tubes. 200 µl of chloroform were added per tube, vigorously shaken for 15 sec and incubated for 5 min at RT. The samples were centrifuged at 12000 x g and 4 °C for 10 min. The upper aqueous phase was transferred to fresh tubes and 500 µl of 2-propanol were added per tube. The samples were incubated for 10 min on ice and then centrifuged at 12000 x g and 4 °C for 10 min. The supernatants were discarded and the pellets washed with 500 µl of 75 % ethanol each. The samples were centrifuged at 12000 x g and 4 °C for 5 min. The pellets were left to dry and dissolved in nuclease-free water. Replicate samples were pooled and the concentration of total RNA was measured with a fluorometer as described in section III.2.2.8. The total RNA samples were stored at -80 °C until further use.

### III.2.2.8 Quantification of total RNA and DNA

The concentration of total RNA and complementary DNA (cDNA) produced during library preparation for next generation sequencing (NGS) was determined with a fluorometer and specific RNA and dsDNA high sensitivity assays designed by the manufacturer of the instrument. The assays contained an advanced RNA- or dsDNA-selective dye, which only fluoresced when bound to their target. Each assay contained two standard samples. From the fluorescence values of these standards the instrument generated a standard curve and applied a curve-fitting algorithm (modified Hill plot) to obtain a line from which concentration values could be calculated for the samples. In a special thin-walled tube 1 µl of sample was mixed with 199 µl of the reagent and incubated for 2 min at RT. Fluorescence was then measured.

### III.2.2.9 Library preparation for next generation sequencing (NGS)

In order to determine miRNA profiles of cells by NGS on the Illumina® platform, RNA transcripts have to be converted into barcoded cDNA libraries. The workflow consists of 3' adapter ligation, hybridization of the reverse transcription primer, 5' adapter ligation, reverse transcription, polymerase chain reaction (PCR) amplification and purification of the PCR amplified cDNA. During PCR amplification there is also a different index primer used for each sample to individually label each sample, allowing for multiplexing in later NGS runs. The maximal number of samples which can be included in one sequencing run is twelve. In addition, the cDNA originating from miRNA transcripts as opposed to other types of RNA has to be isolated by size selection on a poly acrylamide gel.

<u>Procedure</u>

All steps were conducted according to the manufacturer's instructions. Between 400 and 900 ng of total RNA were used per sample.

For 3' adaptor ligation 6 µl of input RNA (diluted with variable volumes of nuclease-free $H_2O$ for equal amounts of input RNA among samples) were mixed with 1 µl of 3' adaptor, incubated for 2 min at 70 °C and transferred to ice. 10 µl of 2 x 3' ligation reaction buffer and 3 µl of 3' ligation enzyme mix were added and incubated for 1 h at 25 °C.
To prevent adaptor-dimer formation, the reverse transcription primer was hybridized to the excess of 3' adaptor resulting in double-stranded DNA molecules which are not substrates for the ligase used for 5' adaptor ligation in the next step. For this hybridization 4.5 µl $H_2O$ and 1 µl reverse transcription primer were added to the samples, heated for 5 min at 75 °C, transferred to 37 °C for 15 min and then incubated for 15 min at 25 °C.

For 5’ adaptor ligation the 5’ adaptor was denatured by incubating it at 70 °C for 2 min. Then 1 µl of denatured 5’ adaptor, 1 µl of 10 x 5’ ligation reaction buffer and 2.5 ml of 5’ ligation enzyme mix were added to the ligation mixture from before and the samples were incubated for 1 h at 25 °C.

Reverse transcription was performed by adding 8 µl of first strand synthesis reaction buffer, 1 µl of murine RNase inhibitor and 1 µl of ProtoScript II Reverse Transcriptase to the adaptor-ligated RNA from before and incubating the samples for 1 h at 50 °C.

PCR amplification was performed by adding 50 µl of LongAmp *Taq* 2 x master mix, 2.5 µl of SR Primer for Illumina®, 5 µl of $H_2O$ and 2.5 µl of one of twelve different indexed PCR primers to each cDNA sample and running the PCR reaction under the conditions listed in table 15.

**Table 15 PCR cycling conditions used for amplification of cDNA transcripts during library preparation for next generation sequencing on the Illumina® platform**

| Cycle step | Temperature | Time | Number of cycles |
|---|---|---|---|
| Initial denaturation | 94 °C | 30 sec | 1 |
| Denaturation<br>Annealing<br>Extension | 94 °C<br>62 °C<br>70 °C | 15 sec<br>30 sec<br>15 sec | 14 |
| Final extension | 70 °C | 5 min | 1 |
| Hold | 4 °C | until further use | |

The amplified cDNA was purified by use of a PCR purification kit with columns for DNA binding according to the manufacturer’s instructions. The PCR reaction mixture was mixed with 5 volumes of Buffer PB containing a pH indicator. If the samples turned purple 10 µl of 3 M sodium acetate with pH 5.0 were added. The yellow color indicated a pH of ≤ 7.5 which was needed for optimal DNA binding to the columns. To elute the DNA from the columns, 30 µl of nuclease-free $H_2O$ were added to each column and the samples were incubated for 1 min at RT and then centrifuged again for 1 min. The cDNA samples were stored at -20 °C until further use.

The purified cDNA was size selected on a 10 % polyacrylamide gel to isolate the adapter-ligated constructs originating from miRNA transcripts as opposed to other types of RNA. For all subsequent steps tubes with low DNA and RNA binding properties were used (non-stick tubes).

The wells of the ready-to-use gel were rinsed with 1 x TBE buffer and the gel was run without samples at 100 V for 20 min to remove residual gel pieces and salts from the wells. All twelve samples from one library preparation set were pooled (4 µl per sample) and 10 µl of 6 x loading dye were added. A small part of 5 µl of the mixture was added to one well of the gel for later cutting under UV-light ("cutting sample"). The rest of the mixture was distributed evenly into three wells of the gel. 5 µl of the marker Quick-Load pBR322 DNA-MspI Digest were added to two wells, one close to the "small cutting" sample and one close to the other samples. The gel was run at 100 V for 1.5 h. Subsequently, the gel was incubated with 50 ml of ultrapure $H_2O$ containing 4 µl of the nucleic acid stain ethidium bromide for 5 min in the dark to allow the stain to intercalate into the DNA allowing for fluorescent detection of DNA bands on the gel. The gel was rinsed with 50 ml of ultrapure $H_2O$ and the part of the gel containing the "cutting sample" was cut off from the rest of the gel and placed on a UV-light table. The marker served to identify the 140 bp DNA band representing the adapter-ligated constructs derived from the 21 nucleotide-long miRNA transcripts. The band was cut out under UV-light. The "cutting sample" part of the gel was placed next to the rest of the gel again and the 140 bp band was cut out from the three sample lanes (without UV-light, meaning without seeing the bands) at the same height as from the "cutting sample". This way UV-light was not used on the samples which could have altered the cDNA and affected further analyses.
Each piece of gel was transferred to a 500 µl sample tube with small holes placed in a larger tube to serve as a strainer to shred the gel pieces. The samples were centrifuged in the strainers at 16,000 x g for 2 min. Each gel sample was mixed with 250 ml of gel elution buffer and rotated end-to-end for 2 h with shaking. The samples were centrifuged at 14,000 x g for 2 min in gel filtration columns and 1 µl of linear acrylamide, 25 µl of 3 M sodium acetate pH 5 and 750 µl of 100 % ethanol were added. The samples were vortexed and incubated at -80 °C for 45 min to precipitate the DNA. The samples were centrifuged at 14,000 x g and 4°C for 30 min and the resulting pellets were washed with 400 µl of 80 % ethanol. After another centrifugation step as before the supernatants were discarded again and the pellets were left to dry before dissolving them in 6 µl of TE buffer each and pooling all three samples. The DNA concentration was measured as described in section III.2.2.8.

#### III.2.2.10 Quality control and quantification of library cDNA

The purified and size-selected cDNA libraries for NGS were quantified and purity and size of the cDNA molecules were checked on microfluidic chips with a bioanalyzer. A high

sensitivity DNA kit developed by the manufacturer of the instrument was used which covered a range of 50 – 7000 bp.
With the bioanalyzer the sample components are electrophoretically separated according to their size. There is a fluorescent dye which intercalates into the DNA and whose fluorescence signals are translated into gel-like images and electropherograms. The usage of a DNA ladder and two markers allows for sizing of the cDNA samples.

Procedure

Dye-concentrate was added to a gel matrix vial (15 µl). The gel-dye mix was vortexed, applied to a spin filter and centrifuged at 2,300 x g for 10 min. A volume of 9 µl of the mix was loaded onto a high sensitivity DNA microfluidic chip and distributed evenly along all wells by leaving the chip in the chip priming station with the plunger pressed down for 1 min. Gel-dye mix was loaded onto three more wells of the chip (9 µl each) and 5 µl of marker solution were added to the remaining twelve wells. The well designated to the ladder was filled with 1 µl of high sensitivity DNA ladder. Into the eleven sample wells 1 µl of sample or $H_2O$ (for unused wells) were added and the chip was vortexed at 2400 rpm for 1 min. The chip was run on the bioanalyzer.

Analysis

The quality of the run was checked by examining the amount, size and shape of the DNA ladder and marker peaks. The size, concentration and molarity of the sample components were determined by the bioanalyzer software. The peak for the correctly adapter-ligated, size-selected cDNA constructs was expected at 147 bp. The peak at this size was further examined with regard to its shape. A stand-alone, well-resolved peak represents a pure sample. A representative electropherogram for a keratinocyte library is presented in figure 8.

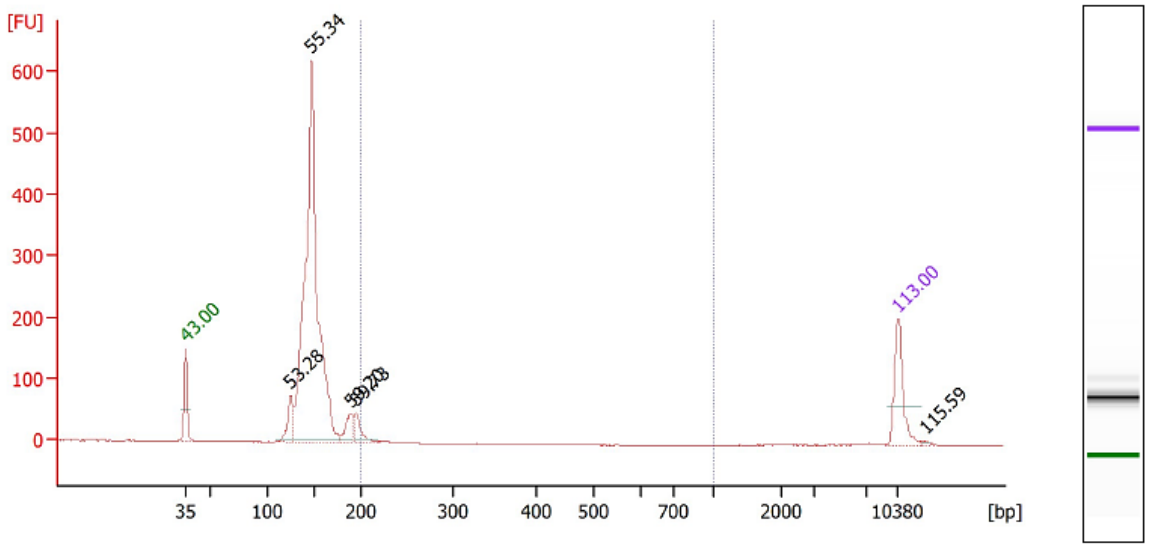


| Peak | Size [bp] | Conc. [pg/µl] | Molarity [pmol/l] | Observations |
|---|---|---|---|---|
| 1 | 35 | 125.00 | 5,411.3 | Lower Marker |
| 2 | 125 | 77.03 | 931.4 | |
| 3 | 147 | 1,227.74 | 12,617.4 | |
| 4 | 189 | 46.22 | 370.1 | |
| 5 | 195 | 48.76 | 379.0 | |
| 6 | 10,380 | 75.00 | 10.9 | Upper Marker |
| 7 | 13,109 | 0.00 | 0.0 | |

**Figure 8 Example of an electropherogram and gel-like image for a keratinocyte barcoded cDNA library used in a bioanalyzer analysis**

The size, quantity and purity of cDNA library constructs generated for next generation sequencing were analyzed on a microfluidic high sensitivity DNA chip with a bioanalyzer. Here an example electropherogram for a keratinocyte library is shown. A high sensitivity DNA ladder was used for size determination. The peak for correctly adapter-ligated, size-selected cDNA constructs is expected at 147 bp. To each sample and the ladder well there were also two markers added which are shown in green and purple here. Abbreviations: bp, base pairs; FU, fluorescence units.

If the peak at 147 bp was the highest one and the molarity was at least 3 nM the sample was considered pure enough and suitable for NGS.

### III.2.2.11 Next generation sequencing (NGS)

NGS was conducted on the Illumina® platform which uses sequencing by synthesis chemistry. In comparison to capillary electrophoresis sequencing, in NGS there is not just one DNA fragment sequenced at a time but millions of fragments in parallel.

A specifically prepared cDNA library is loaded onto a flow cell which contains a lawn of oligonucleotides complementary to the library adapters. The library fragments are

captured on the flow cell as depicted in step 1 of figure 9 and bridge amplification results in the generation of clonal clusters as depicted in step 2 of figure 9. During the actual sequencing process a DNA polymerase catalyzes the incorporation of deoxyribonucleotide triphosphates (dNTPs) into DNA strands complementary to the cDNA fragments captured on the flow cell (see step 3 of figure 9). The dNTPs are labeled with fluorescent dyes (each of the four different dNTPs with a different dye) and bound to reversible terminators. The terminators allow for single sequential cycles of DNA synthesis. During each cycle the incorporated nucleotides are identified by fluorophore excitation and the signal is recorded as depicted in step 4 of figure 9.

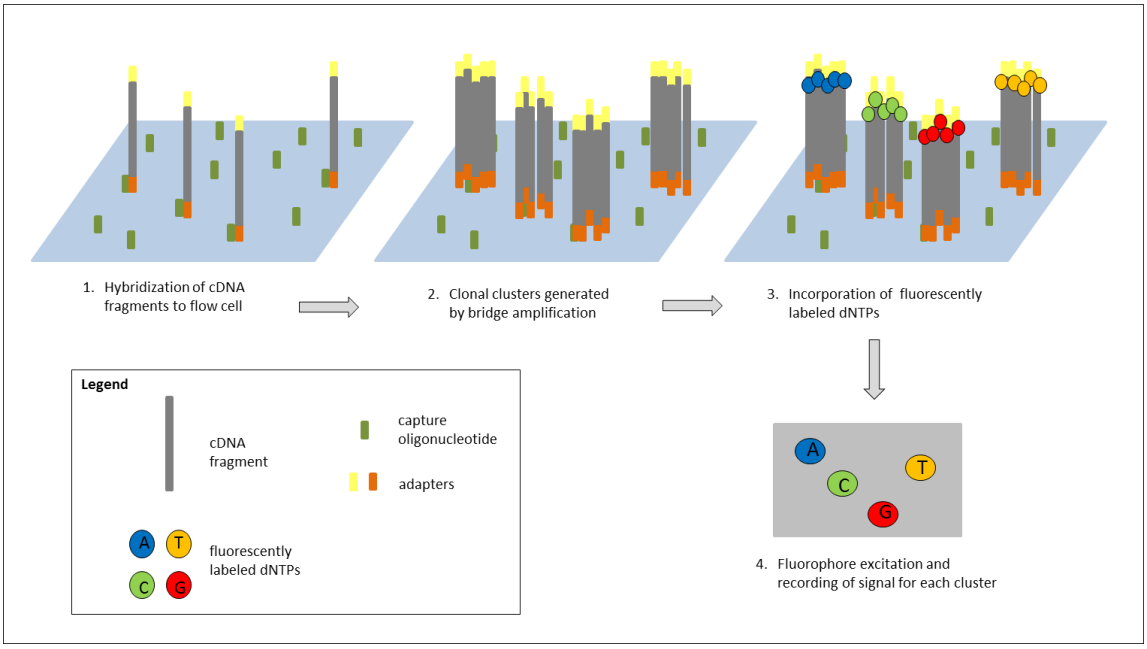


**Figure 9 NGS method on the Illumina® platform**

On the Illumina® platform sequencing by synthesis chemistry is used for next generation sequencing. 1. Adapter-ligated fragments of a cDNA library are captured on the surface of a flow cell by capture oligonucleotides complementary to the adapters (cDNA fragments shown in grey, capture oligonucleotides in green and adapters in orange and yellow). 2. Clonal clusters are generated from the fragments by bridge amplification. 3. A DNA polymerase catalyzes the incorporation of fluorescently labeled dNTPs during synthesis of DNA strands complementary to the fragments of the clusters (dNTPs shown as circles in blue, green, red and yellow, each corresponding to one of the 4 possible bases contained; adenosine (A), cytidine (C), guanosine (G), thymidine (T)). The dNTPs are linked to reversible terminators allowing for single sequential cycles of DNA synthesis. 4. During each cycle of dNTP incorporation the incorporated base is identified for each cluster by fluorophore excitation and the signal is recorded. Figure modified from the MiSeq® user manual form Illumina®.
Abbreviations: cDNA, complementary deoxyribonucleic acid; dNTP, deoxyribonucleotide triphosphate; NGS, next generation sequencing.

The determined sequencing reads can be aligned to a reference genome to allow identification of known sequences and in case of miRNA profiling the identified miRNAs can be counted for each sample. De-multiplexing is achieved by sorting the sequencing reads according to the attached indices.

Procedure

For NGS the library sample had to be denatured. A stock of 1.0 N NaOH was freshly diluted to a concentration of 0.2 N with ultra-pure $H_2O$. The cDNA library sample was diluted to a concentration of 3 nM with TE buffer (from the library preparation kit) and 10 µl were mixed with 10 µl of 0.2 N NaOH for denaturation. The sample solution was vortexed, centrifuged at 300 x g for 1 min and incubated for 5 min at RT. A volume of 980 µl HT1 Buffer was added to the sample. Subsequently, 500 µl of the resulting solution were mixed with 500 µl of HT1 Buffer for further dilution. Final concentrations in the sample were 15 pM cDNA and 1 mM NaOH. Finally, 600 µl of the resulting solution were loaded onto the sequencing cartridge purchased from the manufacturer of the sequencer. The cartridge contained all reagents necessary for the sequencing run.
A fresh flow cell was cleaned with 100 % ethanol and ultra-pure $H_2O$ and inserted into the sequencer. The cartridge and wash buffer were also loaded onto the sequencer. The sequencing run was performed with the program for small RNA and 36 cycles.

Analysis

After the sequencing run the MiSeq® Reporter software was used to generate fastq-files containing the determined sequence reads. For each of the twelve samples included in one sequencing run a separate file was generated. Some of the sequence reads still contained parts of the 3' adapters ligated to the RNA transcripts during library preparation. These adapter sequences had to be trimmed to allow proper alignment to reference genomes. Adapter trimming was performed with the program cutadapt. Reads which were shorter than 15 bp after adapter trimming were discarded to minimize false positive alignment results.
After adapter trimming, the sequencing reads were aligned to reference genomes using the program bowtie. First the reads were aligned to the whole human genome. Only those reads successfully aligned were used for further analysis. The reads were then aligned to published mature or precursor (hairpin) miRNAs collected in the miRBase data base. In figure 10 the alignment success is depicted, which also shows how well the library preparation and sequencing worked. The figure shows representative results from one sequencing run. For each sample contained in the run, the total number of reads is set to 100 %.

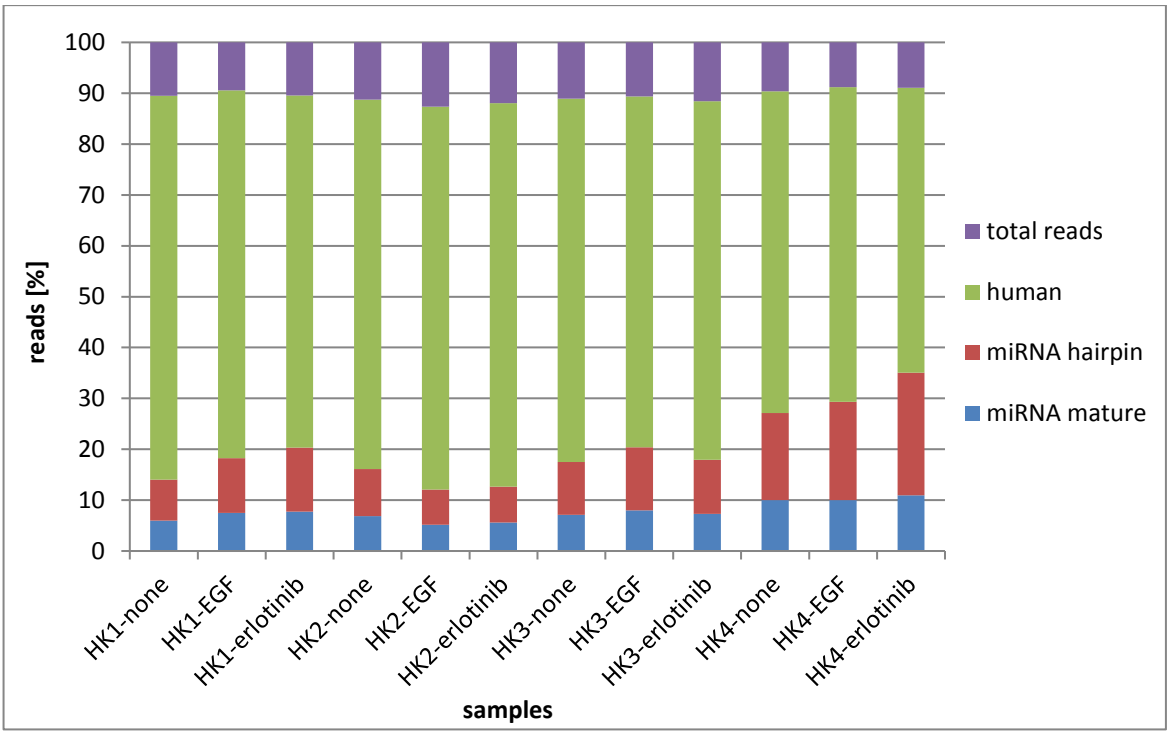


**Figure 10 Alignment success for reads determined by NGS from a keratinocyte library**

Representative results from sequencing run 2. After NGS performed with a cDNA library from keratinocytes (size-selected for miRNA), the determined reads were aligned to the whole human genome. Successfully aligned reads were then aligned to two different miRBase databases containing either published precursor (hairpin) or mature miRNAs. For each individual sample the number of total reads is set to 100 % (purple). Reads aligned to the human genome (green), hairpin miRNA (red) and mature miRNA (blue) are shown in % of total reads. Abbreviations: HK, human keratinocytes; NGS, next generation sequencing.

In table 16 the alignment success is summarized for each sequencing run. The aligned reads in % are given as a range for each run, considering all twelve samples within each run respectively.

**Table 16 Alignment success of reads determined by NGS for all sequencing runs (keratinocytes and fibroblasts)**

After NGS performed with cDNA libraries from keratinocytes or fibroblasts (size-selected for miRNA), the determined reads were aligned to the whole human genome. Successfully aligned reads were then aligned to two different miRBase databases containing either published precursor (hairpin) or mature miRNAs. For each sequencing run the number of total reads is given as a range (considering all twelve samples of that run). Reads aligned to the human genome are given as % of total reads. Reads aligned to hairpin miRNA or mature miRNA are given in % of reads aligned to the human genome. Abbreviations: FB, fibroblasts; HK, human keratinocytes; NGS, next generation sequencing.

| Sequencing run | Samples included | Total reads | Human [% of total reads] | miRNA hairpin [% of human] | miRNA mature [% of human] |
|---|---|---|---|---|---|
| Run 1, keratinocytes | HK1, HK2, HK3, HK4 (each with incubation: none, EGF, and erlotinib+EGF) | 56270 - 132828 | 87 - 90 | 14 - 38 | 6 - 13 |
| Run 2, keratinocytes | HK1, HK2, HK3, HK4 (each with incubation: none, EGF, and erlotinib+EGF) | 173456 - 433721 | 87 - 91 | 14 - 39 | 6 - 12 |
| Run 3, keratinocytes | HK5, HK6, HK7, HK8 (each with incubation: none, EGF, and erlotinib+EGF) | 879837 - 2274129 | 92 - 95 | 30 - 54 | 13 - 24 |
| Run 4, keratinocytes | HK9, HK10, HK11, HK12 (each with incubation: none, EGF, and erlotinib+EGF) | 189470 - 526177 | 76 - 78 | 40 - 58 | 14 - 22 |
| Run 5, fibroblasts | FB57, FB64, FB99, FB136 (each with incubation: none, EGF, and erlotinib+EGF) | 1104763 - 2701038 | 92 - 95 | 24 - 39 | 14 - 26 |
| Run 6, fibroblasts | FB76, FB79, FB80, FB93 (each with incubation: none, EGF, and erlotinib+EGF) | 728592 - 2317572 | 92 - 94 | 18 - 43 | 10 - 26 |

For each sample a list of identified mature and hairpin miRNAs was transferred to the spreadsheet program Excel™ and all reads were counted.
The package DESeq2 for use with the statistical software environment R was used to normalize the read counts and determine specific mature or hairpin miRNAs which were differentially expressed between two groups of samples (e.g. untreated erlotinib-sensitive versus untreated erlotinib-insensitive cells).

Some of the differentially expressed miRNAs identified with the DESeq2 program were chosen for further analysis. Those miRNAs which were significantly differentially expressed in the two groups of erlotinib-sensitive and -insensitive cells with a p-value < 0.05 and a fold change ≥ 1.50 (up-regulated) or ≤ 0.66 (down-regulated) respectively,

were regarded as especially interesting. For a better overview, the overlap of significantly differentially expressed miRNAs ($p < 0.05$) between erlotinib-sensitive and -insensitive cells across all three different *in vitro* treatment groups (no treatment, EGF and EGF + erlotinib) was determined. Venn diagrams were prepared to visualize which specific miRNAs were significantly differentially expressed in all three treatment groups and therefore represent a "baseline" difference between erlotinib-sensitive and -insensitive cells (see figure 11). It was also determined, which miRNAs were only significantly differentially expressed in cells treated with erlotinib and therefore represent a difference in response to erlotinib in the sensitive as compared to the -insensitive cells. Numbers in overlapping parts of the Venn diagram circles represent the numbers of specific miRNAs which were significantly differentially expressed ($p < 0.05$) in both or all three treatment groups, respectively.

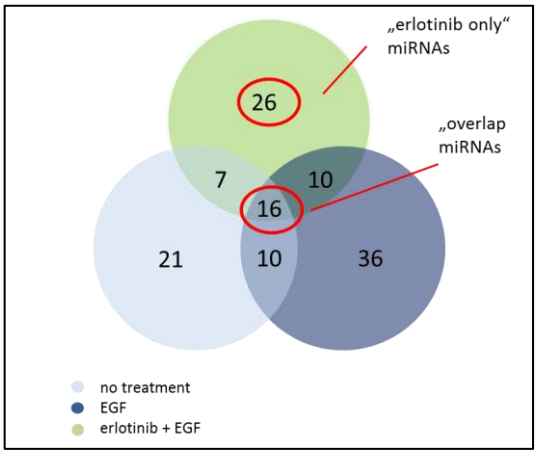


**Figure 11 Example of a Venn diagram used to visualize the overlap of differentially expressed miRNAs in erlotinib-sensitive as compared to -insensitive cells between different *in vitro* treatments**

Numbers in overlapping parts of the circles represent the numbers of specific miRNAs which were significantly differentially expressed ($p < 0.05$) in both or all three treatment groups, respectively.

For the "overlap" miRNAs from all three treatment groups and the "erlotinib only" miRNAs a structured literature search was conducted (but with non-strict criteria) and publications concerning their roles in cancer and cancer therapy, association with EGFR or similar tyrosine kinases and erlotinib or other EGFRIs and specific functions in keratinocytes, fibroblasts and skin homeostasis were reviewed. Those miRNAs for which a role in the aforementioned areas had already been suggested in previous studies were chosen, to strengthen the evidence for them as suitable candidate miRNAs. Their differential

expression in erlotinib-sensitive versus -insensitive samples was validated using qRT-PCR. The results of the literature search are presented in the appendix (table 38). Since pre-experiments had shown that greater differences in expression could be identified for precursor (hairpin) miRNAs than for mature miRNAs, in NGS as well as qRT-PCR, mainly Precursor Assays were chosen for analyses. Only for the most interesting miRNAs also the mature forms were tested. Those miRNAs whose expression was analyzed in keratinocytes by PCR were also investigated in fibroblasts and vice versa to determine potential differences in those two cell types.

#### III.2.2.12 MiRNA expression analysis by quantitative real time polymerase chain reaction (qRT-PCR)

Differential expression of candidate mature and precursor miRNA molecules determined by NGS was further analyzed using qRT-PCR with the miScript PCR system by Qiagen (Hilden, Germany). This system enables specific quantification of multiple mature as well as precursor miRNAs from a single cDNA preparation. Total RNA is used as starting material. Messenger RNA (mRNA) is reverse transcribed into cDNA using oligo-deoxythymine (oligo-dT) and random primers. Mature miRNA, precursor miRNA and other noncoding RNA are not polyadenylated in nature, so the enzyme poly(A) polymerase has to be used for polyadenylation before reverse transcription, in order for the oligo-dT primers to be able to bind. The oligo-dT primers have a degenerate anchor at the 3' end and a universal tag sequence at the 5' end to ensure that later on only cDNA from miRNA and no genomic DNA is detected.

For detection of specific mature and precursor miRNAs, qRT-PCR was performed with miScript Primer Assays and Precursor Assays each including a forward primer specific for the respective miRNA and a universal reverse primer. The DNA double strand dye SYBR Green was also needed for the quantification. Upon binding to the amplified PCR products, SYBR Green increases its fluorescence up to 1000-fold. A thermal cycler equipped with fluorescence detection modules can be used to monitor fluorescence during log-linear phase of PCR amplification. The measured fluorescence reflects the amount of amplified product in each cycle. The crossing point (CP) is the point at which there is enough PCR product accumulated to give a fluorescent signal above background. CP values correlate with the amount of PCR template and therefore are the basis for quantification. If there is a large amount of template at the start of the PCR reaction, relatively few amplification cycles will be needed for the fluorescent signal to rise above background. Hence, a low or early CP will be measured. In contrast, if a small amount of template is present, a high or late CP will be measured.

In order to correct for sample-to-sample variations, the amount of target miRNA has to be normalized by also quantifying the amount of an endogenous reference RNA within each sample. Here the small nuclear RNA (snRNA) RNU6B was used as reference RNA.

Procedure

Total RNA was isolated as described in section III.2.2.7. All reactions were set up on ice to prevent degradation of RNA. For reverse transcription a master mix was prepared using the reagents listed below. The amount of water added depended on the volume of template RNA which had to be added in the subsequent step (250 ng of template RNA were used per reaction).

| **Reagent** | **Volume per reaction** |
|---|---|
| 5x miScript HiFlex Buffer | 4 µl |
| 10x miScript Nucleics Mix | 2 µl |
| miScript Reverse Transcriptase Mix | 2 µl |
| RNase-free water | variable |
| Template RNA 250 ng (not added directly but in the subsequent step!) | variable |
| Total volume | 20 µl |

To each reaction (tube) the appropriate volume of template RNA was added (corresponding to 250 ng RNA) and the mixture was incubated at 37 °C for 60 min followed by 95 °C for 5 min to inactivate the transcriptase. As negative controls one sample containing no reverse transcriptase and one sample containing 5 µl $H_2O$ instead of the template RNA were included.

For qRT-PCR the cDNA samples from the previous step were diluted 1:10 with RNase-free water. A master mix was prepared using the reagents listed below.

| Reagent | Volume per reaction |
|---|---|
| 2x QuantiTect SYBR Green Master Mix | 12.5 µl |
| 10x miScript Universal Primer | 2.5 µl |
| 10x miScript Primer or Precursor Assay | 2.5 µl |
| RNase-free water | variable |
| cDNA 17 ng (not added directly but in the subsequent step!) | variable |
| Total volume | 25 µl |

Twenty-five (25) µl of the master mix were used per well of a 96-well plate and the appropriate volume of diluted cDNA was added to each well (corresponding to 17 ng cDNA). The plate was sealed with heat-sealing film and centrifuged at 1000 x g and RT for 1 min to remove bubbles. The following PCR program was run on a LightCycler® 480 (Roche Diagnostics, Mannheim, Germany).

**Table 17 PCR program run in this study**

| Step | Cycles | Temperature | Time |
|---|---|---|---|
| **Initial activation step (for HotStarTaq DNA Polymerase)** | 1 | 95 °C | 15 min |
| **Amplification** | 45 | | |
| Denaturation | | 94 °C | 15 s |
| Annealing | | 55 °C | 30 s |
| Extension | | 70 °C | 30 s |

Analysis

For analysis, relative expression (RE) levels (fold-changes) were calculated from CP values with the function $RE = 2^{-\Delta\Delta CP}$. In this equation $\Delta CP$ is the difference between the sample's CP value obtained for the target RNA and the sample's CP value obtained for the reference RNA RNU6B. In turn, $\Delta\Delta CP$ is the difference between the afore-mentioned normalized value and the CP value of the control sample (e.g. erlotinib sensitive cells as compared to erlotinib-insensitive cells). All CP values were calculated from duplicate replicates. Analyses were performed with the LightCycler® 480 software and Microsoft Excel™.

### III.2.3 Statistical analysis

Plasma biomarker analyses in patient samples from the Dermatoxgen study

First of all, the concentrations of the plasma analytes cetuximab, AREG, HGF and 25-OH-vitamin D were tested for association with the multinomial end-point maximal (max) skin rash and max diarrhoea using analysis of variance (ANOVA) and the Jonckheere-Terpstra linear trend test. In case the endpoints were dichotomized, associations were calculated by Student's t-test. The hypothesis was that the plasma concentrations would correlate with the occurrence and grade of EGFRI-induced skin rash in patients.
The influence of covariates such as tumor type, tumor stage, age and BMI had previously been analysed by multiple regression and had been excluded as published by Steffens et al. [107] and were excluded again for the data sub set used here.

The above mentioned plasma proteins were also tested for association with the end-points OS and PFS. Therefore, survival distributions between different patient groups were compared using Kaplan-Meier analysis. OS times were restricted with an upper limit = 360 days. Data from patients lost to follow-up were censored at the day last known alive. Due to the nature of our censored data, the non-parametric log-rank test was used. All p-values are reported as nominal p-values and p-values $< 0.05$ were regarded as significant. Since some of the survivor functions do not fall below a survival portion of 0.5, median OS and 95 % confidence intervals cannot be calculated. Therefore, mean OS times with standard error (SE) are provided for comparisons. OS data was found to be more expressive than PFS data in this study, meaning that differences in survival times between the different analysed patient groups were more profound. Therefore, only OS data is presented throughout this thesis.

All statistical analyses were performed with R v3.2.5 including the libraries coin v1.1-2 and survival 2.39-5 (R Foundation for Statistical Computing, Vienna, Austria).

Epigenetic biomarker analyses in the human skin cell model

Following miRNA profiling by NGS the package DESeq2 for use with the statistical software environment R was used to normalize the detected miRNA read counts and determine specific mature or hairpin miRNAs which were differentially expressed between two groups of samples (e.g. untreated erlotinib-sensitive versus untreated erlotinib-insensitive cells).
The package uses shrinkage estimation for dispersions and fold changes to determine stable estimates for differential miRNA expression. The fold change as logarithm of the basis 2 (log2 fold change) is given with its standard error (log fold change standard error,

lfcSE). The program performs a hypothesis test (Wald test) to check whether there is enough evidence to reject the null hypothesis, stating that the effect is only due to experimental variability and not due to the treatment or differential characteristics of the sample groups. The result of the Wald test together with the corresponding p-value is also listed by the program. In addition, DESeq2 uses Benjamini-Hochberg adjustment (false discovery rate) to calculate adjusted p-values, taking into account that if multiple testing is performed, the significance level has to be corrected stepwise (more strict with each test) to prevent detection of an increasing amount of false positives.

Mean differences in miRNA expression determined in qRT-PCR experiments are presented together with standard error of the mean (SEM) in bar diagrams (error bars), as calculated with the program Excel™. One-sided, unpaired Student's t-test was used to test these differences for significance.

# Chapter IV: Results

## IV.1 Patient samples from the Dermatoxgen study

### IV.1.1 Patient characteristics

The aim of this study was to identify biomarkers for the occurrence and severity of EGFRI-induced skin toxicity. Samples from 248 patients of the Dermatoxgen cohort were used for the analyses in this thesis. Clinical parameters were determined prior to this work at the respective study sites. Characteristics of the patients whose plasma samples were used for this work are listed in table 18.

**Table 18 Characteristics of patients from the Dermatoxgen study**

All Dermatoxgen patients whose clinical data and plasma samples were analyzed within this thesis are included in this table.

| Characteristics | Category | Count (Total: n = 248) | % |
|---|---|---|---|
| Sex | female | 92 | 37.1 |
| | male | 156 | 62.9 |
| Age median* [years] (range) | | 68.5 (31-87) | |
| BMI median* [kg/m²] (range) | | 24.7 (14.2-48.9) | |
| Smoking status* | never | 90 | 36.3 |
| | former | 122 | 49.2 |
| | present | 29 | 11.7 |
| | unknown | 7 | 2.8 |
| Tumor* | lung cancer | 143 | 57.7 |
| | colon cancer (*KRAS* WT) | 46 | 18.5 |
| | head and neck cancer | 10 | 4.0 |
| | pancreatic cancer | 49 | 19.8 |
| Metastasis* | yes | 123 | 49.6 |
| | no | 68 | 27.4 |
| | unknown | 57 | 23.0 |
| EGFRI applied during observation period | erlotinib | 150 | 60.5 |
| | gefitinib | 13 | 5.2 |
| | cetuximab | 74 | 29.8 |
| | panitumumab | 11 | 4.4 |
| Maximal skin rash during observation period (grade after NCI-CTCAE)[112] | 0 | 53 | 21.4 |
| | 1 | 93 | 37.5 |
| | 2 | 90 | 36.3 |
| | 3 | 12 | 4.8 |
| Maximal diarrhea during observation period (grade after NCI-CTCAE)[112] | 0 | 156 | 62.9 |
| | 1 | 60 | 24.2 |
| | 2 | 24 | 9.7 |
| | 3 | 7 | 2.8 |
| | 4 | 1 | 0.4 |

* at beginning of observation period

Abbreviations: BMI, body mass indexr; EGFRI, epidermal growth factor receptor inhibitor; NCI-CTCAE, National Cancer Institute - Common Terminology Criteria for Adverse Events; WT, wild type.

There were 92 (37.1 %) female and 156 (62.9 %) male patients analyzed with a median age of 68.5 years (range 31 – 87 years). The majority of patients were diagnosed with lung cancer (57.7 %) but there were also patients included diagnosed with pancreatic (19.8 %), colon (18.5 %) and head and neck (4.0 %) cancer. In accordance with the indications of the single EGFRIs, the majority of patients were treated with erlotinib (60.5 %), followed by cetuximab (29.8 %), gefitinib (5.2 %) and panitumumab (4.4 %). BMI and smoking status of the patients were also considered.

Since skin rash is the main form of skin toxicity induced by treatment with an EGFRI, the maximal grade of skin rash developed during the observation period was used as measure for skin toxicity in all analyses. Within the patient population described here, 53 patients (21.4 %) developed no skin rash, while 93 (37.5 %) showed grade 1, 90 (36.3 %) grade 2 and twelve (4.8 %) even grade 3 skin rash.

Diarrhea is also a common adverse effect of EGFRIs, which was not shown to stably correlate with treatment efficacy or OS in previous studies[32]. Within the patient population described here, 156 patients (62.9 %) showed no diarrhea, while 60 patients (24.2 %) had grade 1, 24 (9.7 %) grade 2, seven (2.8 %) grade 3 and one patient (0.4 %) even grade 4 diarrhea.

### IV.1.2 Correlation between plasma concentrations of cetuximab and skin rash and survival

As shown in a publication by our research group, there is an association between a metabolic ratio of erlotinib and occurrence of skin rash as well as OS of patients [107]. The calculations performed by Michael Steffens showed that patients with a low ratio of erlotinib serum concentration divided by serum concentration of the metabolite O-desmethyl-erlotinb developed lower grades of EGFRI-induced skin rash and had shorter OS times. In this work it was investigated whether a correlation between plasma concentrations of cetuximab and development of skin rash and survival time could be identified. Following erlotinib, cetuximab was the next most frequently used EGFRI in the Dermatoxgen study cohort. For the patients who received this EGFRI, the plasma concentrations of cetuximab were determined by a specific ELISA. The correlation between the concentration of cetuximab and the occurrence and severity of EGFRI-induced skin rash were investigated. The results are depicted in figure 12.

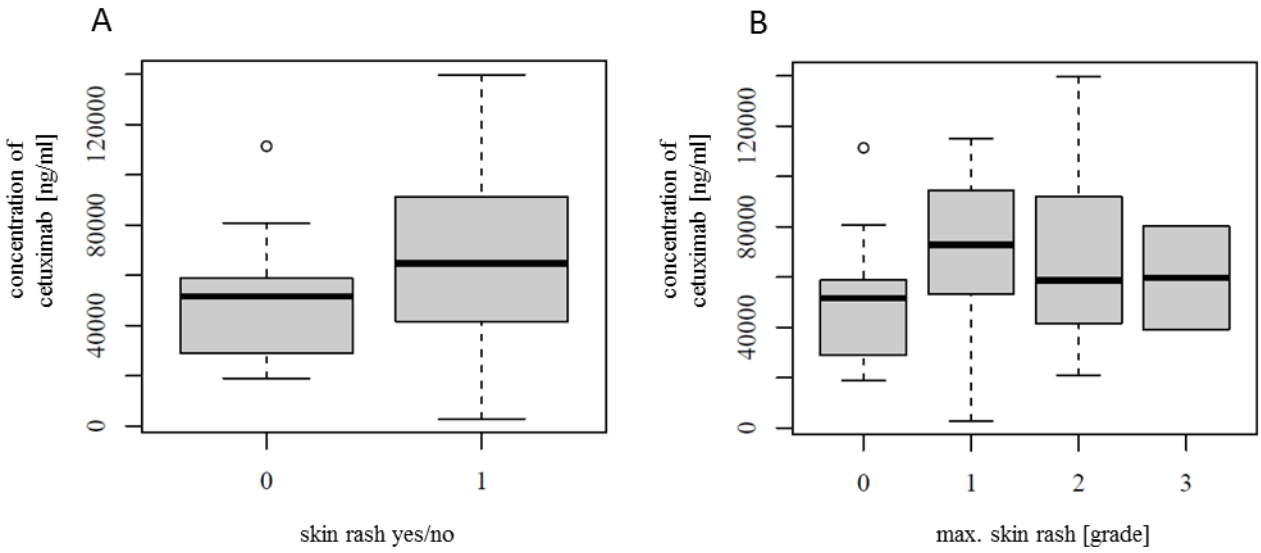


**Figure 12 Correlation between plasma concentration of cetuximab and EGFRI-induced skin rash**

The concentration of cetuximab was determined in plasma of patients from the Dermatoxgen study by ELISA. n = 54. **A**) Cetuximab concentration plotted against the occurrence of skin rash during the observation period (0 = no rash, 1 = rash); Welch Two-Sample t-Test, **p-value = 0.159**. **B**) Cetuximab concentration plotted against the max grade of skin rash developed during observation period; ANOVA, **p-value = 0.526**.
Abbreviations: ANOVA, analysis of variance; ELISA, enzyme-linked immunosorbent assay; EGFRI, epidermal growth factor receptor inhibitor; max, maximal; n. number [of patients].

The plasma concentration of cetuximab was not significantly correlated with the occurrence (p-value = 0.159) or the grades (p-value = 0.526) of EGFRI-induced skin rash. The association with OS of the patients was also analyzed, as depicted in figure 13.

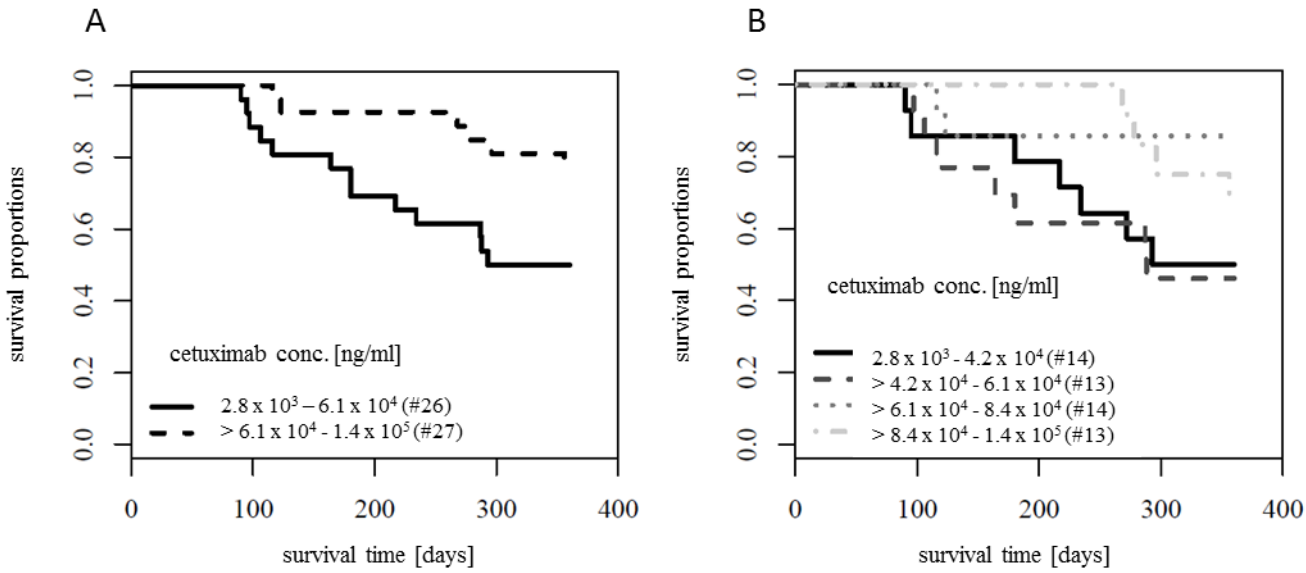


**Figure 13 Association between plasma concentration of cetuximab and overall survival**

Patients from the Dermatoxgen study were followed-up for 360 days after initiation of the EGFRI therapy. The proportion of patients still alive is plotted over the observation period in the Kaplan-Meier plots. Patients are grouped according to their plasma conc. of cetuximab. **A**) Dichotomized, mean OS of patients with low cetuximab conc. 270 days (SE: 20.4), for patients with high cetuximab conc. 333 days (SE: 12.6); log rank test, **p-value = 0.027**; **B**) Quartered, mean OS for group 1 279 days (SE: 25.9), group 2 261 days (SE: 29.6), group 3 326 days (SE: 22.5), group 4 340 days (SE: 10.0); log rank test, **p-value = 0.110**. OS times are restricted with an upper limit = 360 days.
Abbreviations: conc., concentration; EGFRI, epidermal growth factor receptor inhibitor; OS, overall survival; SE, standard error; #, number of patients.

The plasma concentration of cetuximab was significantly associated with OS when patients were dichotomized (p-value = 0.027). When patients were sorted into four groups according to the plasma concentration of cetuximab, the association between the cetuximab concentration and OS was not significant (p-value = 0.110).

### IV.1.3 Correlation between plasma concentrations of growth factors AREG and HGF and skin rash and survival

Following the analysis of serum/plasma concentrations of EGFRIs themselves, the plasma concentrations of the selected biomarker candidates EGFR ligand AREG and MET ligand HGF were determined as well. The correlation between the plasma concentrations of AREG and HGF and EGFRI-induced skin rash are shown in figure 14. Figure 14 B and D have similarly also been published in the article published by the author of this thesis [Hichert et al. 2017][115].

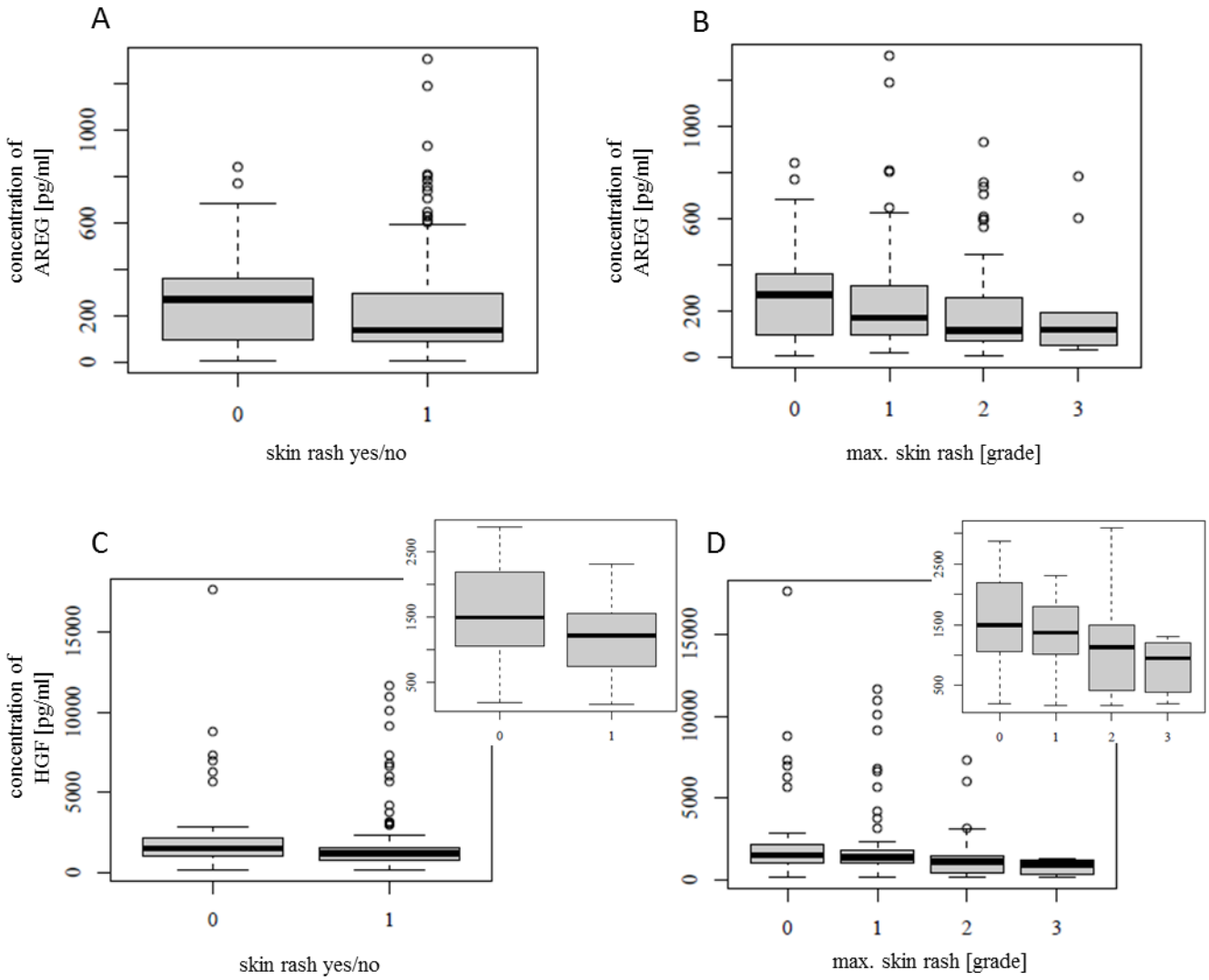


**Figure 14 Correlation between plasma concentrations of AREG and HGF and EGFRI-induced skin rash**

The concentrations of AREG and HGF were determined in plasma of patients from the Dermatoxgen study by ELISA (AREG n = 190; HGF n = 197). **A**) AREG concentration plotted against the occurrence of skin rash during the observation period (0 = no rash, 1 = rash); Welch Two-Sample t-Test, **p-value = 0.18**. **B**) AREG concentration plotted against the max grade of skin rash developed during observation period; Linear Trend Test, **p-value = 0.0763**. **C**) HGF concentration plotted against the occurrence of skin rash during the observation period (0 = no rash, 1 = rash); Welch Two-Sample t-Test, **p-value = 0.0769**. **D**) HGF concentration plotted against the max grade of skin rash developed during observation period; Linear Trend Test, **p-value = 0.00124.** For better visualization, in Figures **C**) and **D**) the plots are also presented without the outliers. In these cases outliers were still used for the calculations but excluded during plotting.
Abbreviations: AREG, amphiregulin; ELISA, enzyme-linked immunosorbent assay; EGFRI, epidermal growth factor receptor inhibitor; HGF, hepatocyte growth factor; max, maximal; n, number [of patients].

The plasma concentration of AREG was not significantly correlated with the occurrence (p-value = 0.18) or the grade (p-value = 0.0763) of EGFRI-induced skin rash. The plasma

concentration of HGF was not significantly correlated with skin rash when only looking at the occurrence (skin rash yes/no; p-value = 0.0769) but when considering the grade of the developed skin rash (grades 0 to 3) the correlation was significant (p-value = 0.00124). The association with OS of the patients was also analyzed, as depicted in figure 15. Figure 15 has similarly also been published in the article published by the author of this thesis [Hichert et al. 2017][115].

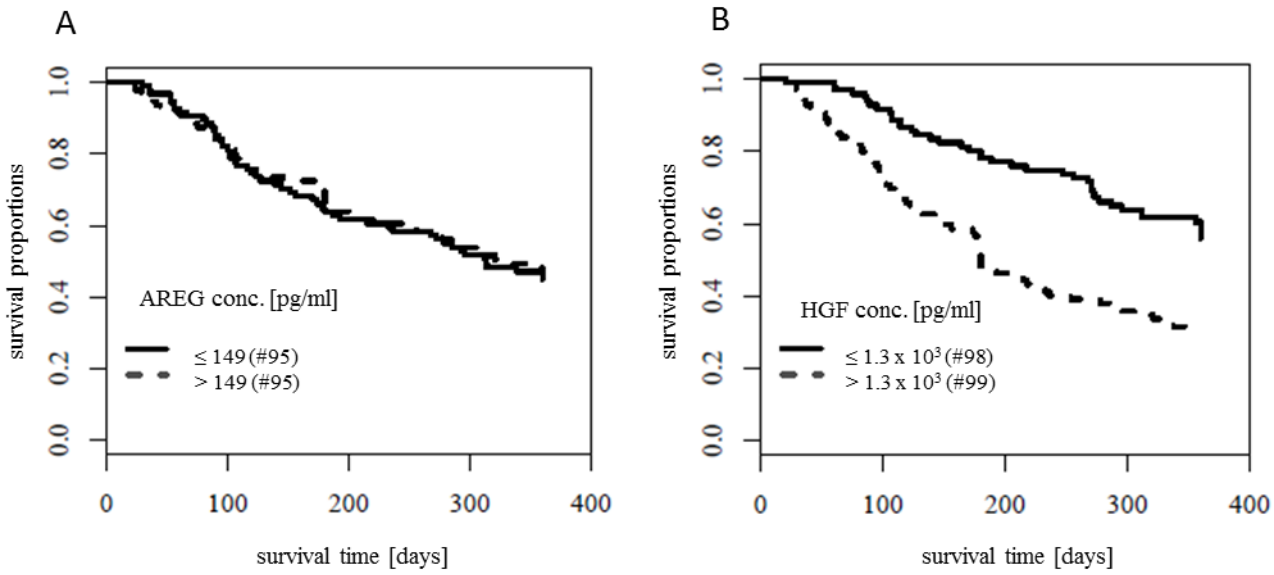


**Figure 15 Association between plasma concentrations of AREG and HGF and overall survival**

Patients from the Dermatoxgen study were followed-up for 360 days after initiation of the EGFRI therapy. The proportion of patients still alive is plotted over the observation period in the Kaplan-Meier plots. Patients are grouped according to their plasma concentration of **A**) AREG, dichotomized, mean OS for patients with low AREG conc. 252 days (SE: 12.5), for patients with high AREG conc. 255 days (SE: 12.6); log rank test, **p-value = 0.86** and **B**) HGF, dichotomized, mean OS for patients with low HGF conc. 290 days (SE: 10.5), for patients with high HGF conc. 210 days (SE: 12.4); log rank test, **p-value = 2 x $10^{-5}$**. OS times are restricted with an upper limit = 360 days.
Abbreviations: AREG, amphiregulin; conc., concentration; EGFRI, epidermal growth factor receptor inhibitor; HGF, hepatocyte growth factor; OS, overall survival; SE, standard error; #, number of patients.

The plasma concentration of AREG was not significantly correlated with OS of the patients (p-value = 0.86) while the association of the plasma concentration of HGF with OS was significant (p-value = 2 x $10^{-5}$), with a mean of 290 days for patients with low HGF levels and 210 days for patients with high levels.

The survival curve for the plasma concentration of HGF was further divided according to the type of tumor the patients were suffering from. Separate survival curves were drawn for patients with bronchial, colon, head and neck, and pancreatic cancer respectively, which are presented in figure 16.

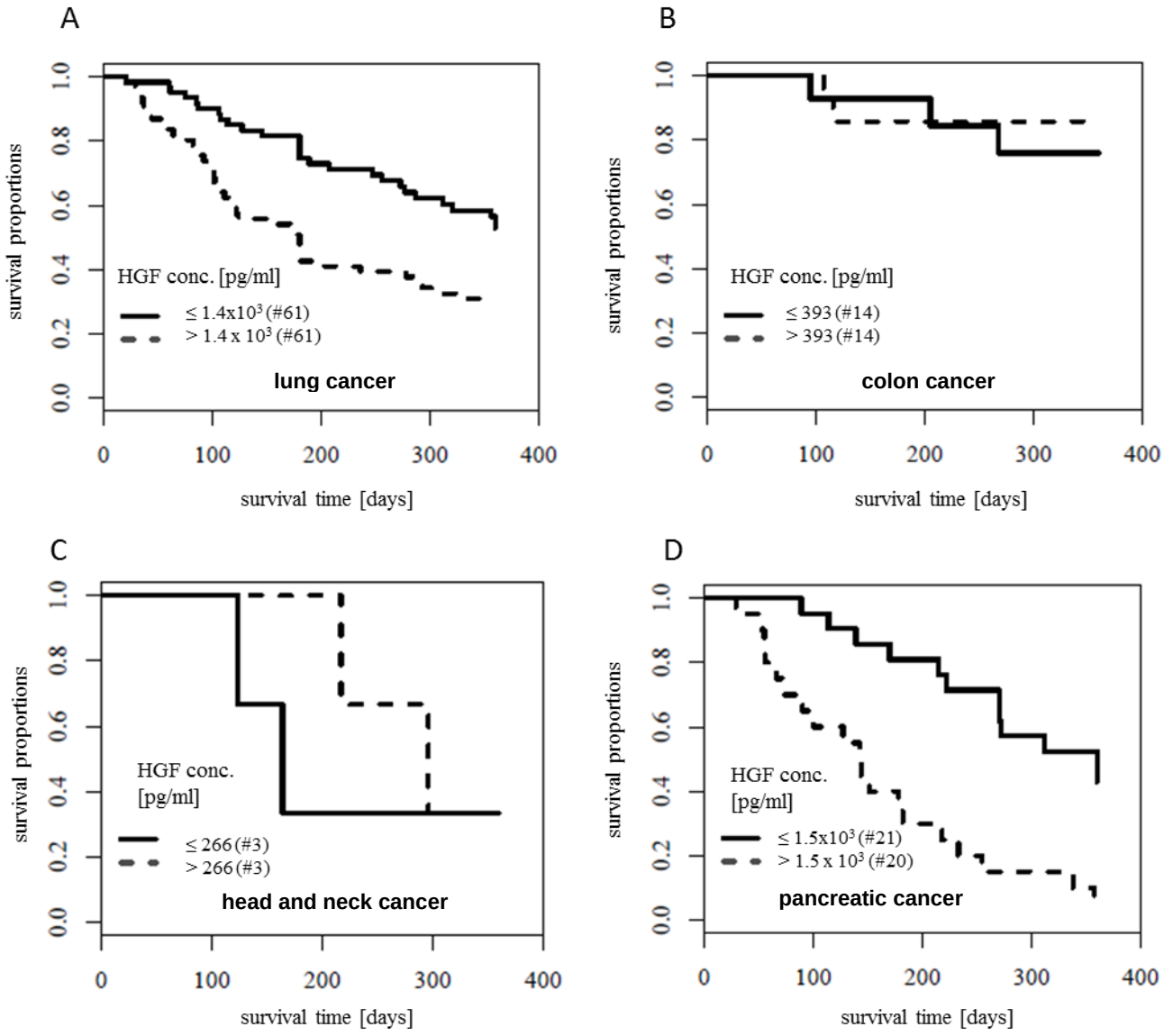


**Figure 16 Association between the plasma concentration of HGF and overall survival separated according to tumor type**

Patients from the Dermatoxgen study were followed-up for 360 days after initiation of the EGFRI therapy. The proportion of patients still alive is plotted over the observation period in the Kaplan-Meier plots. Patients are grouped according to their plasma conc. of HGF. **A**) Patients with lung cancer, mean OS for patients with low HGF conc. 282 days (SE: 14.0), for patients with high HGF conc. 200 days (SE: 16.2); log rank test, **p-value = 0.0018**. **B**) Patients with colon cancer, mean OS for patients with low HGF conc. 320 days (SE: 21.7), for patients with high HGF conc. 324 days (SE: 23.2); log rank test, **p-value = 0.63**. **C**) Patients with head and neck cancer, mean OS for patients with low HGF conc. 212 days (SE: 56.5), for patients with high HGF conc. 287 days (SE: 31.1); log rank test, **p-value = 0.59**. **D**) Patients with pancreatic cancer, mean OS for patients with low HGF conc. 287 days (SE: 19.9), for patients with high HGF conc. 160 days (SE: 22.7); log rank test, **p-value = 0.00014**. OS times are restricted with an upper limit = 360 days.
Abbreviations: concentration; EGFRI, epidermal growth factor receptor inhibitor; HGF, hepatocyte growth factor; OS, overall survival; SE, standard error; #, number of patients.

When sorting patients according to their tumor type, the significant association between the plasma concentration of HGF and OS observed in figure 15 can only be shown for lung (p-value = 0.0018) and pancreatic (p-value = 0.00014) but not for colon (p-value = 0.63) and head and neck (p-value = 0.59) cancer.

We then subdivided the patient cohort into two groups, according to whether they had developed an EGFRI-induced skin rash or not. This allowed investigating whether the increased OS in patients with low plasma concentrations of HGF was specific for patients with EGFRI-induced skin rash or rather a general observation for all patients. Results are depicted in figure 17. Figure 17 has similarly also been published in the article published by the author of this thesis [Hichert et al. 2017][115].

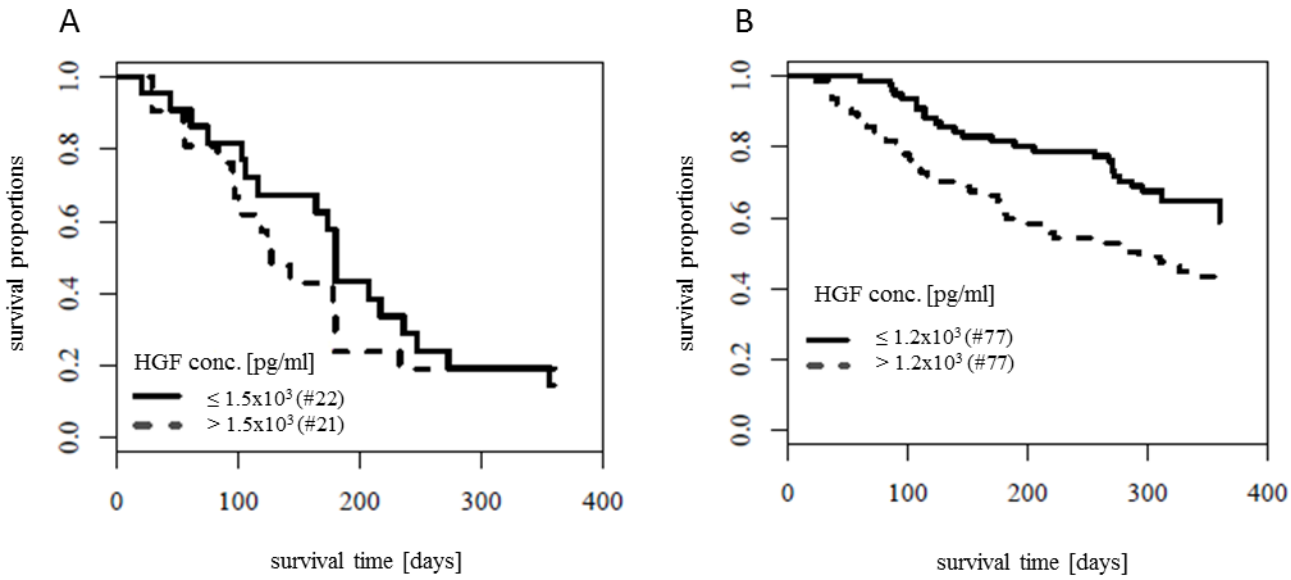


**Figure 17 Association between plasma concentration of HGF and overall survival in patients with or without skin rash**

Patients from the Dermatoxgen study were followed-up for 360 days after initiation of the EGFRI therapy. The proportion of patients still alive is plotted over the observation period in the Kaplan-Meier plots. Patients are grouped according to their plasma concentration of HGF. **A**) Patients who did not develop EGFRI-induced skin rash; log rank test, **p-value = 0.56**; mean OS for patients with low HGF conc. 193 days (SE: 22.5), for patients with high HGF conc. 164 days (SE: 23.6). **B**) Patients who developed EGFRI-induced skin rash (grades 1 to 3); log rank test, **p-value = 0.0075**; mean OS for patients with low HGF conc. 299 days (SE: 11.2), for patients with high HGF conc. 240 days (SE: 14.5). OS times are restricted with an upper limit = 360 days.
Abbreviations: conc., concentration; EGFRI, epidermal growth factor receptor inhibitor; HGF, hepatocyte growth factor; OS, overall survival; SE, standard error; #, number of patients.

The association between increased OS in patients and low plasma concentrations of HGF was only significant in the subgroup of patients with skin rash (p-value = 0.0075) but not for the ones without rash (p-value = 0.56). In the subgroup of patients with skin rash, the mean OS time was 299 days (SE: 11.2) for patients with low HGF levels (≤ 1220 pg/ml) and 240 days (SE: 14.5) for patients with high levels (> 1220 pg/ml).

### IV.1.4 Correlation between plasma concentrations of 25-OH-vitamin D and skin rash, survival and metastasis

Following the analyses regarding the plasma concentrations of the EGFRI cetuximab, the EGFR ligand AREG and the MET ligand HGF, the role of the plasma concentration of the selected biomarker candidate 25-OH-vitamin D with regard to EGFRI-induced skin rash and OS was also investigated. The results are depicted in figures 18 and 19. Figure 18 B has similarly also been published in the article published by the author of this thesis [Hichert et al. 2017][115].

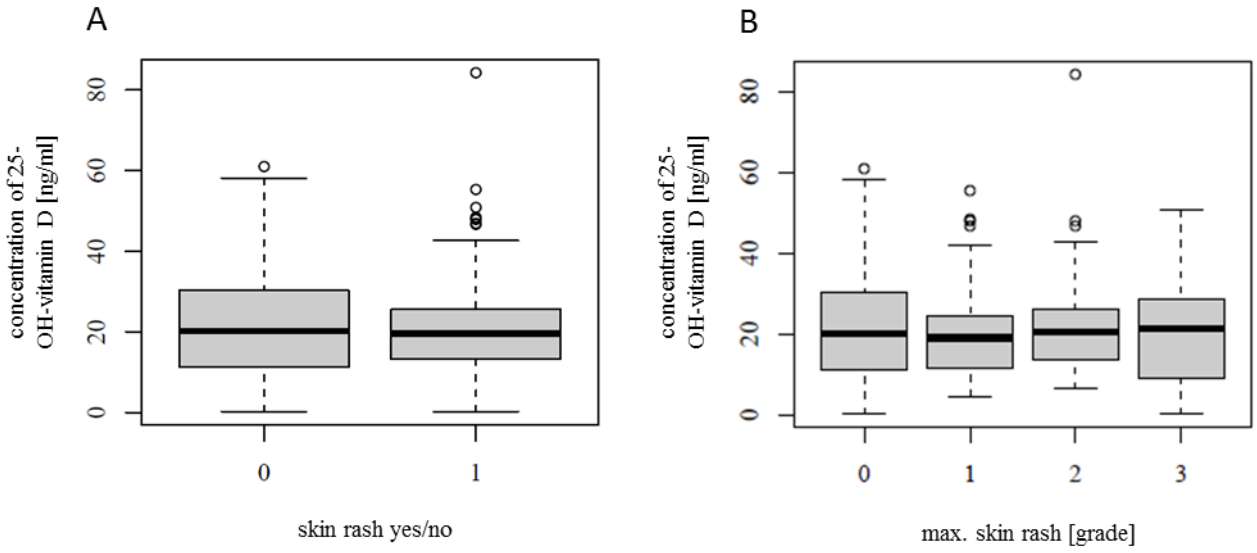


**Figure 18 Correlation between plasma concentration of 25-OH-vitamin D and EGFRI-induced skin rash**

The concentration of 25-OH-vitamin D was determined in plasma of patients from the Dermatoxgen study by ELISA. n = 211. **A**) 25-OH-vitamin D concentration plotted against the occurrence of skin rash during the observation period (0 = no rash, 1 = rash); Welch Two-Sample t-Test, **p-value = 0.251**. **B**) 25-OH-vitamin D concentration plotted against the max grade of skin rash developed during observation period; ANOVA, **p-value = 0.415**.
Abbreviations: ANOVA, analysis of variance; ELISA, enzyme-linked immunosorbent assay; EGFRI, epidermal growth factor receptor inhibitor; max, maximal; n, number [of patients].

The plasma concentration of 25-OH-vitamin D was not significantly correlated with the occurrence (p-value = 0.251) or the grade (p-value = 0.415) of EGFRI-induced skin rash. The association with OS of the patients was also analyzed, as depicted in figure 19.

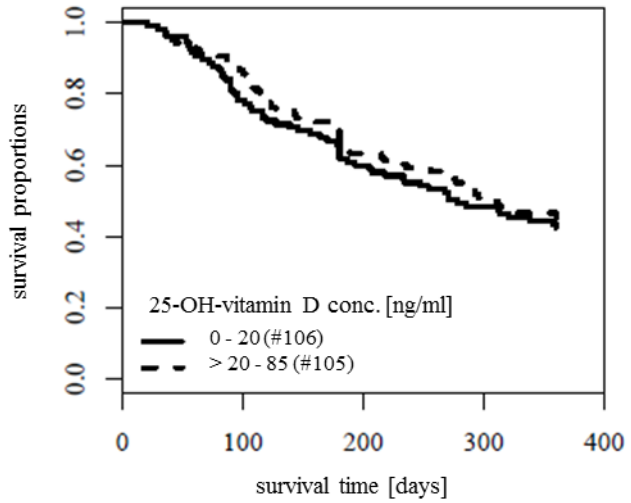


**Figure 19 Association between plasma concentration of 25-OH-vitamin D and overall survival**

Patients from the Dermatoxgen study were followed-up for 360 days after initiation of the EGFRI therapy. The proportion of patients still alive is plotted over the observation period in the Kaplan-Meier plots. Patients are grouped according to their plasma conc. of 25-OH-vitamin D. Dichotomized, mean OS of patients with low 25-OH-vitamin D conc. 243 days (SE: 12.0), for patients with high 25-OH-vitamin D conc. 255 days (SE: 11.6); Log rank test, **p-value = 0.67**. OS times are restricted with an upper limit = 360 days.
Abbreviations: conc., concentration; EGFRI, epidermal growth factor receptor inhibitor; OS, overall survival; SE, standard error; #, number of patients.

25-OH-vitamin D is the storage form of vitamin D and measurement of its plasma concentration is most suitable to detect vitamin D status. In our study the plasma levels varied between 0.3 and 84.0 ng/ml (median: 19.7 ng/ml; mean: 21.3 ng/ml). In the literature there is no standardized cut-off value defining vitamin D sufficiency and deficiency. However, most studies suggest that plasma levels of ≥ 20 ng/ml are sufficient for calcidiol to have a beneficial effect on health, e.g. with regard to bone mineral density and cancer-related as well as all-cause mortality[116,117]. Therefore, in our study we defined 25-OH-vitamin D levels ≤ 20 ng/ml as low and > 20 ng/ml as high levels. When comparing OS times between patients with low and those with high 25-OH-vitamin D levels, there was no significant difference (p-value = 0.67).

As a control for the quality of the Dermatoxgen plasma samples and the correct conduction of the assays, the association of the plasma concentration of 25-OH-vitamin D with metastasis was also investigated. A significant association had previously been shown in various studies[118,119]. The result is shown in figure 20.

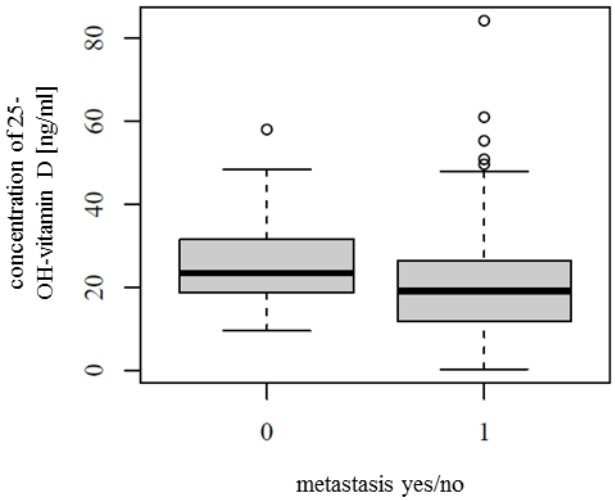


**Figure 20 Correlation between plasma concentration of 25-OH-vitamin D and metastasis**

The concentration of 25-OH-vitamin D was determined in plasma of patients from the Dermatoxgen study by ELISA. n = 207. The concentration is plotted against the presence of metastases at the beginning of the observation period (0 = no metastasis, 1 = metastasis); Welch Two-Sample t-Test, **p-value = 0.0109**.
Abbreviations: ELISA, enzyme-linked immunosorbent assay; n, number [of patients].

The plasma concentration of 25-OH-vitamin D was significantly correlated with metastasis (p-value = 0.0109). Patients who showed metastases at the beginning of the observation period had lower plasma concentrations of 25-OH-vitamin D than those who showed no metastases.

## IV.2 Epigenetic biomarker analyses in the human skin cell model

To enable epigenetic analyses and investigations of functional biomarkers, a major aim of this study was the establishment of a suitable cell model for *in vitro* studies of molecular mechanisms underlying and influencing EGFRI-induced skin toxicity. Primary human epidermal keratinocytes and primary human dermal fibroblasts from healthy donors were isolated, brought into culture and evaluated for their suitability as such a cell model.

### IV.2.1 Keratinocytes

#### IV.2.1.1 Establishment of primary epidermal keratinocytes

As described in section I.6 the main type of skin cells involved in the development of EGFRI-induced skin toxicity are epidermal keratinocytes. Therefore, these cells were chosen for the investigation aiming at finding a suitable cell model. Primary epidermal keratinocytes were isolated from twelve healthy human donors and brought into culture. The cells had to be monitored closely during sub-culturing by visual examination to ensure that the right cell type was cultured and that the keratinocytes did not differentiate too far prior to any experiments. Figure 21 illustrates the formation of mainly pure epidermal keratinocyte clusters. At passage (p) 0 there are different cell types present in the sample (Figure 21 A) including keratinocytes, fibroblasts and melanocytes. Due to the application of optimal culture conditions for keratinocytes, the other cell types die during subculturing making the keratinocyte clusters purer over time (Figure 21 B and C). Only then further analyses of only the keratinocytes are possible.

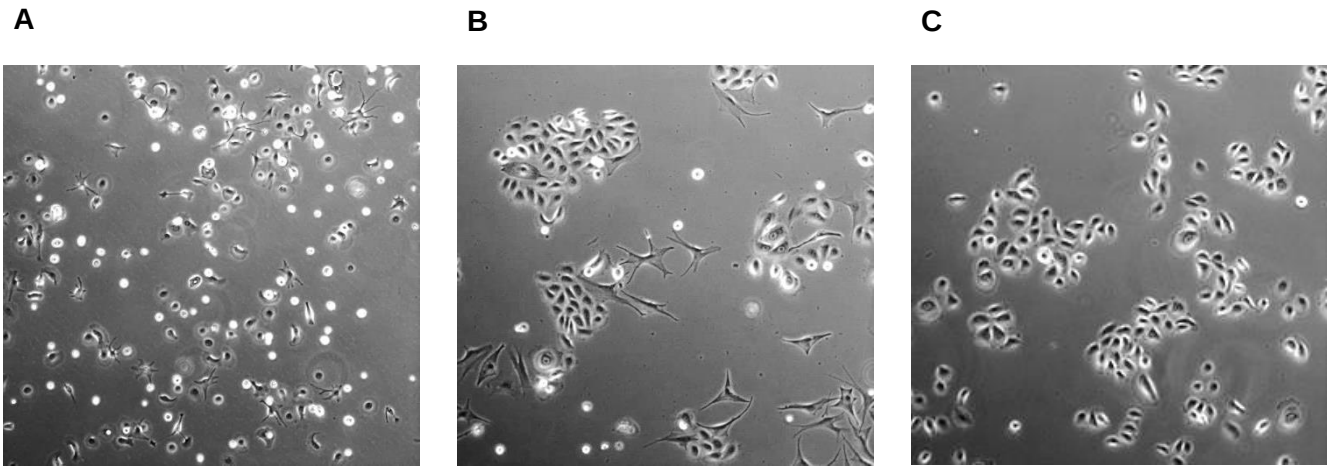


**Figure 21 Isolation and cultivation of primary human epidermal keratinocytes**

The cells were obtained from healthy excess skin removed during plastic surgery. A) Three days after isolation, cells in passage 0. Different types of cells are present distinguishable by their shapes (elongated: fibroblasts, stellar: melanocytes, small and polygonal: keratinocytes, round: dead or damaged cells). B) Ten days after isolation, cells in passage 1; clusters of keratinocytes are forming. C) 25 days after isolation, cells in passage 5; mainly keratinocytes remaining in the culture.

In addition to visual identification by cell morphology, the presence of certain keratinocyte marker proteins (CK10, CK14 and involucrin) was also checked using Western blotting, which is shown in Figure 22.

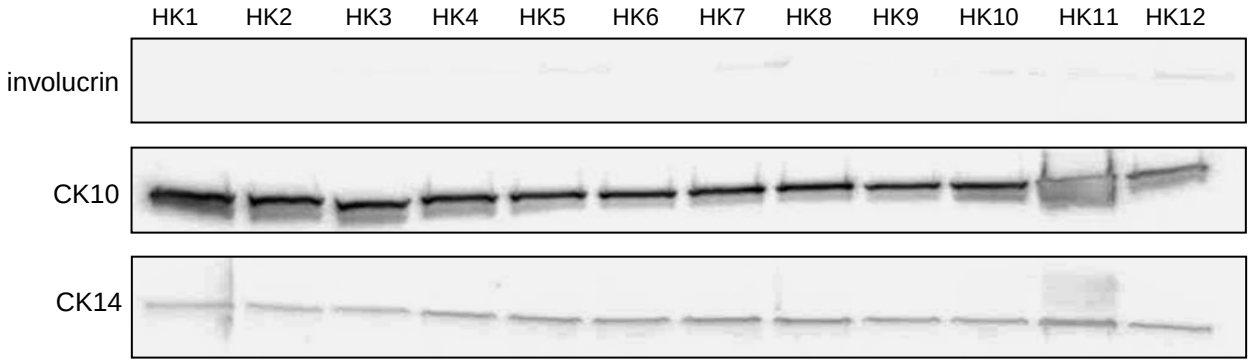


**Figure 22 Detection of keratinocyte marker proteins in human keratinocytes by Western blot**

Primary human keratinocytes were isolated from healthy excess skin removed during plastic surgery. The keratinocyte marker proteins CK14 (50 kDa), CK10 (60 kDa) and involucrin (120 kDa) were detected by Western blot. Cells were in passage 3 to 6. Abbreviations: CK, cytokeratin; HK, human keratinocytes; kDa, kilo Dalton.

The cytokeratins CK10 and CK14 were detected in all twelve keratinocyte samples, while the signal for CK10 was stronger than for CK14. Involucrin, which is mainly found in the two outer epidermal layers, was not detected in any of the twelve samples. No controls were available for the assay, since for commercially available primary keratinocytes no information about differentiation status was provided. Therefore, results have to be interpreted with caution (refer to chapter IV.2.1). Specificity of the assays was at least confirmed by inclusion of lanes with either no primary or no secondary antibody.

#### IV.2.1.2 Effect of erlotinib on EGFR signaling in keratinocytes *in vitro*

To further evaluate the suitability of epidermal keratinocytes as cell model for studying EGFRI-induced skin toxicity, the *in vitro* effect of incubation with the EGFRI erlotinib was investigated. The relative phosphorylation levels of different kinase phosphorylation sites and related proteins involved in EGFR signaling cascades were compared between keratinocytes incubated with erlotinib and stimulated with EGF (Figure 23 C) and keratinocytes only stimulated with EGF (Figure 23 B). Concentrations were chosen analogous to the ones established for other methods (e.g. Western blotting) by other members of this research group prior to this work and were found to be suitable also for this method. Phosphorylation indicates activation. As a control untreated keratinocytes were also included (Figure 23 A). Human phospho kinase arrays were conducted and three separate experiments were performed with different cell samples (HK3 p6, HK4 p5, HK4 p8). Figures 23 and 24 show representative results for HK4 p8.

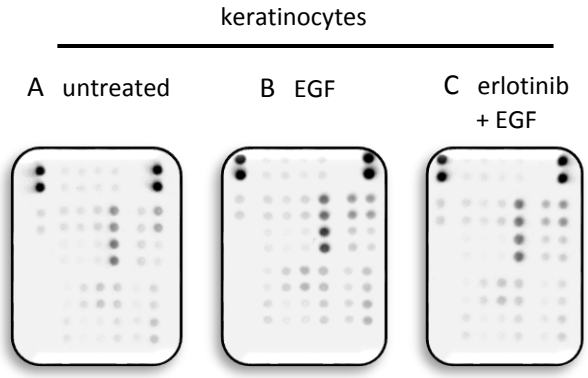


**Figure 23** ***In vitro*** **effect of erlotinib on phosphorylation of proteins involved in EGFR signaling in keratinocytes**

Human phospho kinase arrays were conducted with keratinocyte cell lysates of HK4 p8. Some sections of the membranes after chemiluminescent visualization of the phosphorylated proteins are shown. A) No treatment. B) Stimulated with 4 nM EGF for 5 min. C) Incubated with 10 µM erlotinib for 2 h then stimulated with 4 nM EGF for 5 min. A stronger signal (pixel density) corresponds to higher amounts of phosphorylated protein present and stronger signaling activity. Abbreviations: EGF, epidermal growth factor; HK, human keratinocytes; p, passage.

.

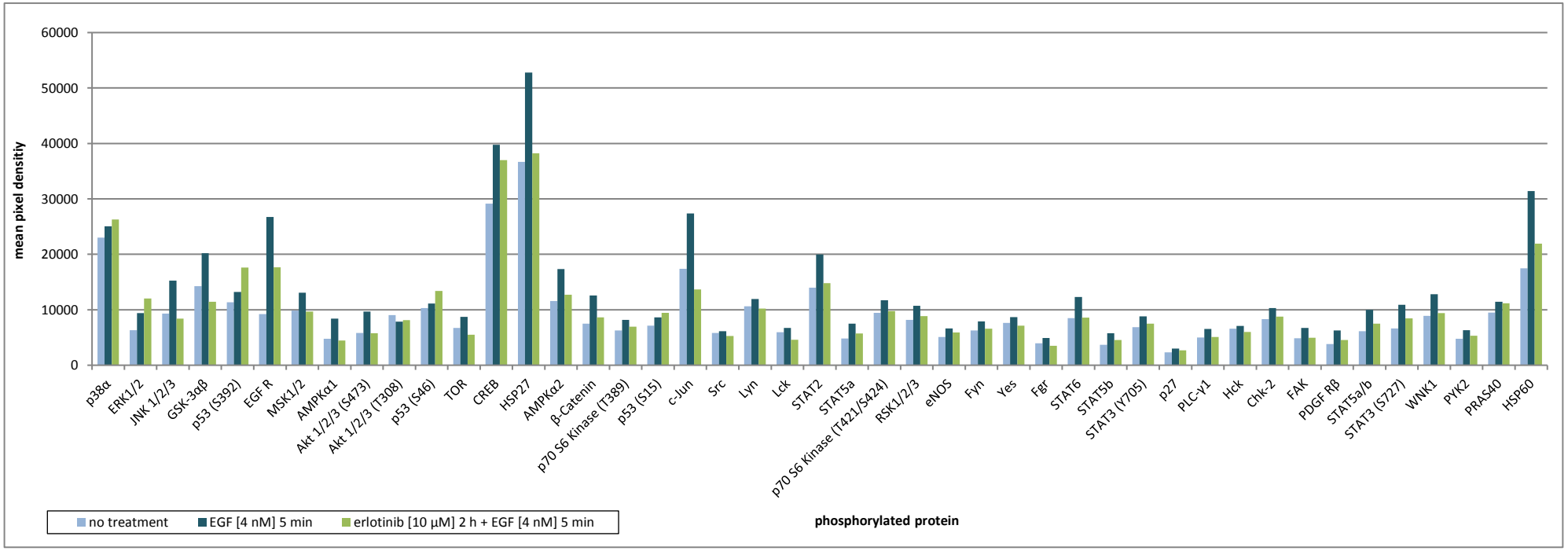


**Figure 24 Quantification of *in vitro* effect of erlotinib on phosphorylation of proteins involved in EGFR signaling in keratinocytes**

Human phospho kinase arrays were conducted with keratinocyte cell lysates of HK4 p8. The mean pixel density after chemiluminescent visualization of the 45 different phosphorylated proteins is shown. Light blue: no treatment. Dark blue: stimulated with 4 nM EGF for 5 min. Green: incubated with 10 µM erlotinib for 2 h then stimulated with 4 nM EGF for 5 min. A stronger signal (pixel density) corresponds to higher amounts of phosphorylated protein present and stronger signaling activity.
Abbreviations: EGF, epidermal growth factor; EGFR, epidermal growth factor receptor; HK, human keratinocytes; p, passage.

EGF increased phosphorylation of most of the tested proteins involved in EGFR signaling cascades while erlotinib decreased the phosphorylation. The strength of the effect was different for the various signaling proteins. For quantification of the effects two ratios were calculated for each protein as suggested by the manufacturer:

$$1)\ \ EGF/no\ treatment\ = \frac{pixel\ density\ for\ cells\ stimulated\ with\ EGF}{pixel\ density\ for\ untreated\ cells}$$

The **higher** the value for this ratio, the stronger is the stimulating effect of EGF.

$$2)\ \ erlotinib/EGF\ = \frac{pixel\ density\ for\ cells\ incubated\ with\ erlotinib\ and\ stimulated\ with\ EGF}{pixel\ densitiy\ for\ cells\ only\ stimulated\ with\ EGF}$$

The **lower** the value for this ratio, the stronger is the inhibitory effect of erlotinib.

The two ratios were calculated for all proteins and all three cell samples (HK3 p6, HK4 p5, HK4 p8). The five proteins on which erlotinib had the strongest effect across all experiments are listed in table 19 for all cell samples. The values for all other proteins are provided in appendix A).

**Table 19 Mean pixel density for selected proteins from human phospho-kinase arrays of three different keratinocyte cell samples**

Human phospho kinase arrays were conducted with three different keratinocyte cell samples (HK3 p6, HK4 p5, HK4 p8) following three *in vitro* treatment conditions (no treatment, 4 nM EGF for 5 min and 10 µM erlotinib for 2 h + 4 nM EGF for 5 min). For clearer comparison of the stimulating effect of EGF and the inhibitory effect of erlotinib between the different cell samples, ratios were calculated (EGF/no treatment and erlotinib/EGF). Results for the five phosphorylated proteins on whose abundance EGF and erlotinib had the biggest effect are listed here. Abbreviations: EGF, epidermal growth factor; HK, human keratinocytes; p, passage.

| | **mean pixel density for HK3 p6** | | | | |
|---|---|---|---|---|---|
| **protein** | **no treatment** | **EGF** | **erlotinib** | **EGF/no treatment** | **erlotinib/ EGF** |
| JNK 1/2/3 | 4254 | 13344 | 4993 | 3.14 | 0.37 |
| EGF R | 5884 | 28853 | 6687 | 4.90 | 0.23 |
| AMPKα1 | 1052 | 4001 | 2370 | 3.80 | 0.59 |
| c-Jun | 20885 | 35552 | 11892 | 1.70 | 0.33 |
| Src | 1772 | 35532 | 2232 | 20.05 | 0.06 |
| | **mean pixel density for HK4 p5** | | | | |
| **protein** | **no treatment** | **EGF** | **erlotinib** | **EGF/no treatment** | **erlotinib/ EGF** |
| JNK 1/2/3 | 11292 | 16537 | 6933 | 1.46 | 0.42 |
| EGF R | 13143 | 38779 | 18868 | 2.95 | 0.49 |
| AMPKα1 | 7833 | 10667 | 3559 | 1.36 | 0.33 |
| c-Jun | 22371 | 40513 | 14939 | 1.81 | 0.37 |
| Src | 6088 | 11194 | 2641 | 1.84 | 0.24 |
| | **mean pixel density for HK4 p8** | | | | |
| **protein** | **no treatment** | **EGF** | **erlotinib** | **EGF/no treatment** | **erlotinib/ EGF** |
| JNK 1/2/3 | 9328 | 15247 | 8401 | 1.63 | 0.55 |
| EGF R | 9225 | 26717 | 17661 | 2.90 | 0.66 |
| AMPKα1 | 4752 | 8422 | 4465 | 1.77 | 0.53 |
| c-Jun | 17372 | 27373 | 13679 | 1.58 | 0.50 |
| Src | 5823 | 6115 | 5262 | 1.05 | 0.86 |

*In vitro* erlotinib seemed to have the strongest inhibitory effect on the phosphorylation of the EGFR itself as well as on the MAPK JNK 1/2/3, its downstream transcription factor c-Jun, the kinase Src and the catalytic subunit of 5’ adenosine monophosphate-activated kinase (AMPKα1).

For further analyses of EGFR signaling across more than just the three example keratinocyte samples used for the phospho kinase arrays, specific phospho-ELISAs were conducted. According to the results from the phospho kinase arrays and considering the commercial availability of validated assays, ELISAs for phospho-JNK, phospho-c-Jun and

phospho-EGFR were chosen. In order to identify the most suitable assay to detect phenotypic differences in the *in vitro* effect of erlotinib between different cell samples, meaning differences in sensitivity towards erlotinib, important criteria were sufficient sensitivity, reproducibility and proper functioning of the assay in general.

#### IV.2.1.3 Effect of erlotinib on the phosphorylation of JNK, c-Jun and EGFR in keratinocytes *in vitro*

The relative amount of phosphorylated target protein, normalized to the amount of total target protein, was determined and compared between cells incubated with erlotinib and stimulated with EGF, cells only stimulated with EGF and cells left untreated. For better comparison between cells from different individuals, again the ratios EGF/no treatment and erlotinib/EGF were calculated as explained in the previous section (IV.2.1.2). The results for these ratios from the phospho-JNK ELISA are presented in table 20.

**Table 20** ***In vitro*** **effect of erlotinib on relative amount of phosphorylated JNK in keratinocytes**

Phospho-JNK ELISAs were conducted with six different keratinocyte cell samples following three *in vitro* treatment conditions (no treatment, 4 nM EGF for 5 min and 5 µM erlotinib for 2 h + 4 nM EGF for 5 min). The relative amount of phosphorylated JNK was determined in RFUs normalized to total protein. For clearer comparison of the stimulating effect of EGF and the inhibitory effect of erlotinib between the different cell samples, ratios were calculated (EGF/no treatment and erlotinib/EGF). Abbreviations: EGF, epidermal growth factor; ELISA, enzyme-linked immunosorbent assay; HK, human keratinocytes; JNK, c-Jun N-terminal kinase; p, passage; RFUs, relative fluorescence units.

| | **phospho-JNK** | |
|---|---|---|
| cell sample | **EGF/no treatment** | **erlotinib/EGF** |
| HK1 p8 | 1.1659 | 0.8503 |
| HK2 p6 | 1.4367 | 0.7884 |
| HK3 p6 | 0.9873 | 0.8569 |
| HK4 p8 | 0.9774 | 0.5563 |
| HK5 p6 | 0.5658 | 1.1855 |
| HK6 p8 | 1.0989 | 1.2762 |

In the phospho-JNK ELISA EGF only increased the relative amount of phosphorylated JNK in some cell samples but not all (EGF/no treatment < 1 means the relative amount of phosphorylated target protein is higher in untreated samples than in samples stimulated with EGF). In addition, erlotinib only decreased the relative amount of phosphorylated JNK in some of the cell samples (erlotinib/EGF > 1 means the relative amount of phosphorylated target protein is higher in cells incubated with erlotinib than in un-

incubated samples). Therefore, the phospho-JNK ELISA did not seem to be suitable to measure the *in vitro* effect of erlotinib on human epidermal keratinocytes. Hence, it was not used for further analyses. Instead, a phospho-c-Jun ELISA was conducted and tested for its suitability for this task. The results are presented in table 21.

**Table 21 *In vitro* effect of erlotinib on relative amount of phosphorylated c-Jun in keratinocytes**

Phospho-c-Jun ELISAs were conducted with twelve different keratinocyte cell samples following three *in vitro* treatment conditions (no treatment, 4 nM EGF for 5 min and 5 µM erlotinib for 2 h + 4 nM EGF for 5 min). The relative amount of phosphorylated c-Jun was determined in RFUs normalized to total protein. For clearer comparison of the stimulating effect of EGF and the inhibitory effect of erlotinib between the different cell samples, ratios were calculated (EGF/no treatment and erlotinib/EGF). Abbreviations: EGF, epidermal growth factor; ELISA, enzyme-linked immunosorbent assay; HK, human keratinocytes; p, passage; SD, standard deviation, RFUs, relative fluorescence units.

| | **phospho-c-Jun** | |
|---|---|---|
| cell sample | **EGF/no treatment** | **erlotinib/EGF** |
| HK1 p6 | 1.0958 | 0.8106 |
| HK2 p5 | 1.2098 | 0.5923 |
| HK3 p4 | 1.2044 | 0.5982 |
| HK4 p4 | 1.0994 | 0.6094 |
| HK5 p4 | 1.0790 | 0.5304 |
| HK6 p4 | 1.0089 | 0.7701 |
| HK7 p4 | 1.2341 | 0.7644 |
| HK8 p4 | 1.2578 | 0.7214 |
| HK9 p4 | 1.0820 | 0.7591 |
| HK10 p7 | 1.1824 | 1.0477 |
| HK11 p4 | 1.0568 | 1.0137 |
| HK12 p7 | 1.0779 | 0.8273 |

Stimulation with EGF increased the relative amount of phosphorylated c-Jun in all tested keratinocytes (EGF/no treatment > 1). Prior incubation with erlotinib decreased the relative amount of phosphorylated c-Jun in most but not all cell samples (erlotinib/EGF < 1).
The cell samples HK1, HK2, HK3, HK4, HK5 and HK6 were cultured again and used for a second independent experiment (biological duplicates) to investigate the reproducibility of the results. Mean ratios and standard deviations (SDs) are given in table 22.

**Table 22 Reproducibility of results for *in vitro* effect of erlotinib on keratinocytes from phospho-c-Jun ELISA**

Phospho-c-Jun ELISAs were conducted with six different keratinocyte cell samples following three *in vitro* treatment conditions (no treatment, 4 nM EGF for 5 min and 5 µM erlotinib for 2 h + 4 nM EGF for 5 min). The relative amount of phosphorylated c-Jun was determined in RFUs normalized to total protein. For clearer comparison of the stimulating effect of EGF and the inhibitory effect of erlotinib between the different cell samples, ratios were calculated (EGF/no treatment and erlotinib/EGF). Results are presented as mean values with SDs from two independent experiments. Abbreviations: EGF, epidermal growth factor; ELISA, enzyme-linked immunosorbent assay; HK, human keratinocytes; n, number [of independent experiments]; p, passage; SD, standard deviation, RFUs, relative fluorescence units.

| | | **phospho-c-Jun** | | | |
|---|---|---|---|---|---|
| | | **EGF/no treatment** | | **erlotinib/EGF** | |
| cell sample | n | mean | SD | mean | SD |
| HK1 p6 | 2 | 1.6068 | 0.7227 | 0.6256 | 0.2617 |
| HK2 p5 | 2 | 1.3127 | 0.1454 | 0.6032 | 0.0154 |
| HK3 p4 | 2 | 1.1892 | 0.0215 | 0.7182 | 0.1697 |
| HK4 p4 | 2 | 1.1330 | 0.0475 | 0.7758 | 0.2353 |
| HK5 p4 | 2 | 1.1413 | 0.0882 | 0.6947 | 0.2324 |
| HK6 p4 | 2 | 1.0883 | 0.1124 | 0.8407 | 0.0998 |

Some of the standard deviations calculated for the biological duplicates were quite high. Hence, the phospho-c-Jun ELISA did not seem to be suitable to provide stable and reproducible results for the *in vitro* effect of erlotinib on human keratinocytes. Next, a phospho-EGFR ELISA was conducted and tested for its suitability for this task. The results are presented in table 23.

**Table 23 *In vitro* effect of erlotinib on relative amount of phosphorylated EGFR in keratinocytes**

Phospho-EGFR ELISAs were conducted with twelve different keratinocyte cell samples following three *in vitro* treatment conditions (no treatment, 40 nM EGF for 5 min and 10 µM erlotinib for 2 h + 4 nM EGF for 5 min). The relative amount of phosphorylated EGFR was determined in relative fluorescence units normalized to total protein. For clearer comparison of the stimulating effect of EGF and the inhibitory effect of erlotinib between the different cell samples, ratios were calculated (EGF/no treatment and erlotinib/EGF). Abbreviations: EGF, epidermal growth factor; EGFR, epidermal growth factor receptor; ELISA, enzyme-linked immunosorbent assay; HK, human keratinocytes; p, passage; RFUs, relative fluorescence units.

| | **phospho-EGFR** | |
|---|---|---|
| cell sample | **EGF/no treatment** | **erlotinib/EGF** |
| HK1 p6 | 1.3538 | 0.7622 |
| HK2 p5 | 1.5424 | 0.7504 |
| HK3 p4 | 1.4562 | 0.7673 |
| HK4 p4 | 1.6011 | 0.6570 |
| HK5 p4 | 1.5005 | 0.7253 |
| HK6 p5 | 1.4800 | 0.7279 |
| HK7 p4 | 1.3491 | 0.7147 |
| HK8 p4 | 1.2517 | 0.6792 |
| HK9 p4 | 1.2783 | 0.7974 |
| HK10 p7 | 1.1858 | 0.6808 |
| HK11 p4 | 1.1649 | 0.7675 |
| HK12 p7 | 1.7210 | 0.5312 |

Stimulation with EGF increased the amount of phosphorylated EGFR (EGF/no treatment > 1), while prior incubation with erlotinib decreased it (erlotinib/EGF < 1) in all cell samples. Therefore, the phospho-EGFR ELISA seemed to be suitable to measure the *in vitro* effect of erlotinib in human keratinocytes.

The cell samples HK1, HK2, HK3 and HK 4 were cultured again and used for two additional independent experiments (biological triplicates) to investigate the reproducibility of the results. Mean ratios and SDs are given in table 24.

**Table 24 Reproducibility of results for *in vitro* effect of erlotinib on keratinocytes from phospho-EGFR ELISA**

Phospho-EGFR ELISAs were conducted with four different keratinocyte cell samples following three *in vitro* treatment conditions (no treatment, 40 nM EGF for 5 min and 10 µM erlotinib for 2 h + 4 nM EGF for 5 min). The relative amount of phosphorylated EGFR was determined in RFUs normalized to total protein. For clearer comparison of the stimulating effect of EGF and the inhibitory effect of erlotinib between the different cell samples, ratios were calculated (EGF/no treatment and erlotinib/EGF). Results are presented as mean values with SDs from three independent experiments. Abbreviations: EGF, epidermal growth factor; ELISA, enzyme-linked immunosorbent assay; HK, human keratinocytes; n, number [of independent experiments]; p, passage; SD, standard deviation, RFUs, relative fluorescence units.

| | | **phospho-EGFR** | | | |
|---|---|---|---|---|---|
| | | **EGF/no treatment** | | **erlotinib/EGF** | |
| cell sample | n | mean | SD | mean | SD |
| HK1 p6 | 3 | 1.3824 | 0.0629 | 0.7911 | 0.0921 |
| HK2 p5 | 3 | 1.5411 | 0.0633 | 0.6990 | 0.0445 |
| HK3 p4 | 3 | 1.5072 | 0.0526 | 0.7190 | 0.0440 |
| HK4 p4 | 3 | 1.4542 | 0.1553 | 0.7107 | 0.0479 |

The standard deviations calculated for the biological triplicates of the phospho-EGFR ELISA were much lower than for the phospho-c-Jun ELISA. The phospho-EGFR ELISA seemed to be the most suitable among the tested assays to detect differences in the *in vitro* effect of erlotinib (sensitivity towards erlotinib) on human epidermal keratinocytes. Therefore, the results from the phospho-EGFR ELISA (table 23) were used to group the keratinocyte cell samples according to their sensitivity towards erlotinib for further analyses. A low erlotinib/EGF ratio means higher sensitivity towards erlotinib. This grouping is depicted in figure 25.

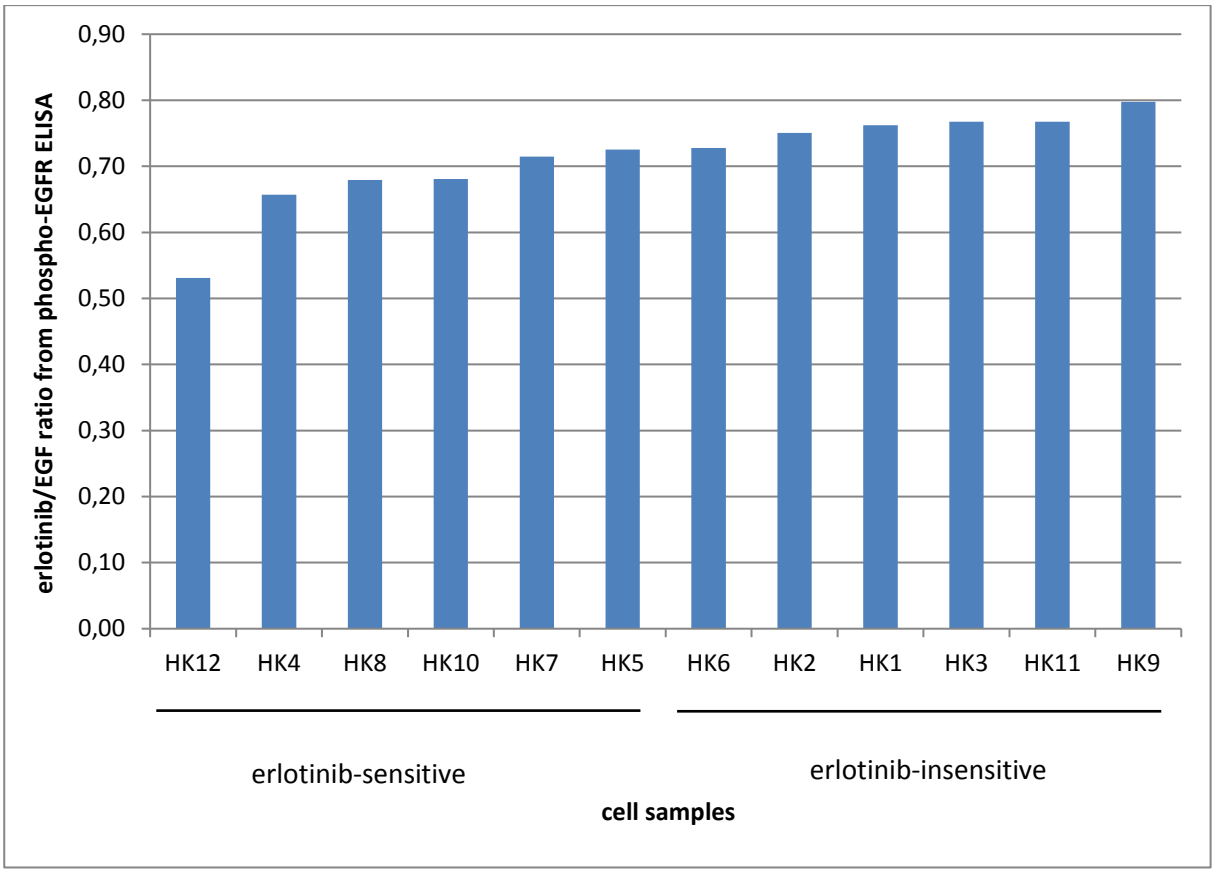


**Figure 25 Keratinocytes grouped into rather erlotinib-sensitive and -insensitive**

The results from phospho-EGFR ELISAs, which were conducted with twelve different keratinocyte cell samples following *in vitro* treatment with erlotinib (10 µM, 2 h) and subsequent stimulation with EGF (40 nM, 5 min) or stimulation with EGF alone, were used to calculate an erlotinib/EGF ratio for each cell sample. Cell samples were grouped into rather erlotinib-sensitive and erlotinib-insensitive according to the ratio. A smaller ratio means higher sensitivity towards erlotinib.
Abbreviations: EGF, epidermal growth factor; EGFR, epidermal growth factor receptor; ELISA, enzyme-linked immunosorbent assay; HK, human keratinocytes.

For all twelve keratinocyte samples the miRNA profiles were determined and compared between the six rather erlotinib-sensitive and the six rather erlotinib-insensitive samples.

### IV.2.1.4 MiRNA profiles of erlotinib-sensitive versus erlotinib-insensitive keratinocytes

In order to assess epigenetic effects of erlotinib in keratinocytes, total RNA was isolated from the epidermal keratinocyte samples and barcoded cDNA libraries were prepared for NGS. Mature as well as precursor (hairpin) miRNAs which were differentially expressed between the six rather erlotinib-sensitive and the six rather erlotinib-insensitive cell samples (both determined *in vitro* by the EGFR-ELISA, see previous section) were

identified with the program DESeq2. Both, mature as well as precursor miRNAs were investigated since they mark different time points in post-transcriptional gene regulation and it is currently unknown the amounts of which are more important in influencing EGFR inhibition or development of EGFRI-induced skin rash. It was also checked whether prior incubation with erlotinib + EGF or EGF alone had an influence on the list of differentially expressed miRNAs. Those miRNAs with a p-value < 0.05 and a fold change of ≥ 1.50 (up-regulated) or ≤ 0.66 (down-regulated) respectively, were considered interesting and are listed in table 25 for cells with no treatment.

**Table 25 Differentially expressed miRNAs in erlotinib-sensitive as compared to -insensitive keratinocytes (no treatment)**

Differentially expressed precursor and mature miRNAs in rather erlotinib-sensitive as compared to -insensitive keratinocytes (n = 6 in each group) were determined by NGS and the program DESeq2. *In vitro* sensitivity towards erlotinib was previously determined by EGFR-ELISA. miRNAs with a p-value < 0.05 and a fold change of ≥ 1.50 (up-regulated) or ≤ 0.66 (down-regulated) respectively, are listed. The fold change as logarithm of the basis 2 (log2 fold change) is given with its standard error (lfcSE, log fold change standard error). The result of the statistic Wald test (stat) together with the corresponding p-value is also listed.

| | erlotinib-sensitive vs. -insensitive treatment: none | | | | |
|---|---|---|---|---|---|
| **precursor miRNA (hairpin)** | **log2 fold change** | **lfcSE** | **fold change** | **stat** | **p-value** |
| hsa-mir-1273c | -0.5966 | 0.2028 | 0.6613 | -2.9422 | 3.26E-03 |
| hsa-mir-3911 | -0.6772 | 0.2376 | 0.6254 | -2.8500 | 4.37E-03 |
| hsa-mir-95 | 0.7409 | 0.2936 | 1.6712 | 2.5232 | 1.16E-02 |
| hsa-mir-611 | -0.6297 | 0.2619 | 0.6463 | -2.4040 | 1.62E-02 |
| hsa-mir-5189 | -0.6949 | 0.2966 | 0.6177 | -2.3428 | 1.91E-02 |
| hsa-mir-146a | -0.6348 | 0.2968 | 0.6440 | -2.1390 | 3.24E-02 |
| hsa-mir-4451 | -0.6823 | 0.3296 | 0.6232 | -2.0696 | 3.85E-02 |
| hsa-mir-485 | -0.6806 | 0.3347 | 0.6239 | -2.0332 | 4.20E-02 |
| hsa-mir-4695 | -0.6271 | 0.3145 | 0.6475 | -1.9944 | 4.61E-02 |
| hsa-mir-1973 | -0.6392 | 0.3250 | 0.6421 | -1.9669 | 4.92E-02 |
| **mature miRNA** | | | | | |
| hsa-miR-31-3p | -0.7517 | 0.2781 | 0.5939 | -2.7035 | 6.86E-03 |
| hsa-miR-4451 | -0.6517 | 0.2603 | 0.6365 | -2.5036 | 1.23E-02 |
| hsa-miR-224-5p | 0.6182 | 0.2592 | 1.5349 | 2.3849 | 1.71E-02 |

In the erlotinib-sensitive keratinocytes nine precursor and two mature miRNAs were significantly down-regulated while one precursor and one mature miRNA were significantly up-regulated when compared to erlotinib-insensitive cells. Fold changes

ranged between 1.53 and 1.67 (0.66 and 0.59 for down-regulation, respectively). The differentially expressed miRNAs differed in cells incubated with EGF or erlotinib (respective lists presented in appendix A).

Reproducibility of the sequencing results was confirmed by repeating the sequencing run with the same barcoded cDNA library including the samples HK1, HK2, HK3 and HK4. The list of differentially expressed miRNAs differed but the most significantly differentially expressed ones were still identified.

For a better overview, those miRNAs which were significantly differentially expressed ($p < 0.05$) under all three different *in vitro* treatments were determined, as depicted in figure 26. These miRNAs are referred to as “overlap miRNAs”.

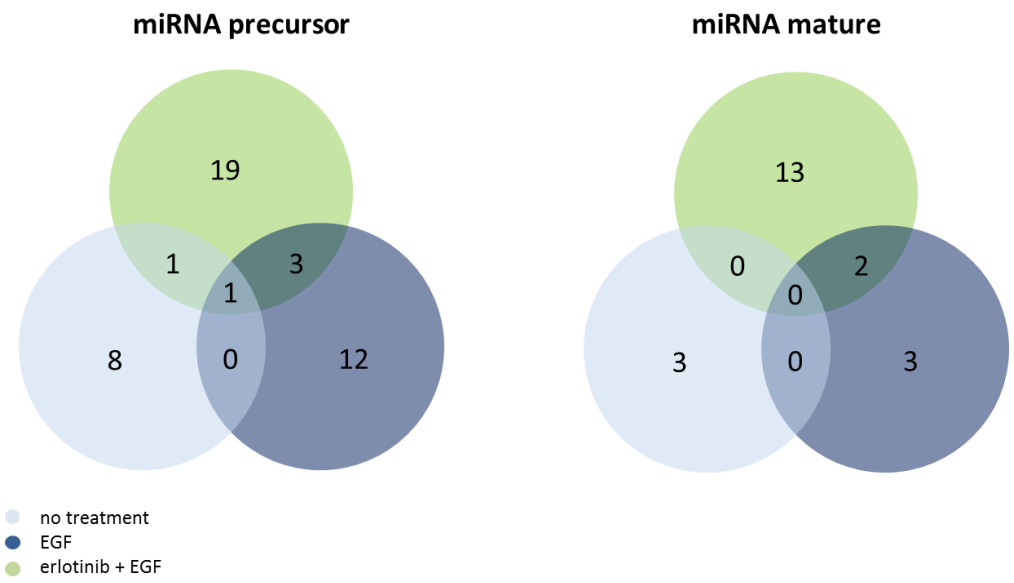


**Figure 26 Overlap of differentially expressed miRNAs in erlotinib-sensitive as compared to -insensitive keratinocytes between different *in vitro* treatments**

Significantly differentially expressed precursor (left) and mature (right) miRNAs in rather erlotinib-sensitive as compared to -insensitive keratinocytes (n = 6 in each group). MiRNA expression was determined by NGS. Cells were either incubated with 4 nM EGF (dark blue circle) or 4 nM EGF plus 5 µM erlotinib (green circle) or left untreated (light blue circle) prior to sequencing. Numbers in overlapping parts of the circles represent the numbers of specific miRNAs which were significantly differentially expressed ($p < 0.05$) in both or all three treatment groups, respectively.
Abbreviations: EGF, epidermal growth factor; miRNA, micro ribonucleic acid; NGS, next generation sequencing.

Those miRNAs which were significantly differentially expressed in rather erlotinib-sensitive as compared to -insensitive keratinocytes regardless of the *in vitro* treatment were considered especially interesting. They represent a “baseline” difference between the erlotinib-sensitive and -insensitive cells, which is independent of stimulation with EGF or incubation with erlotinib. There was no overlap of mature miRNAs in all three treatment groups. There was one overlap of precursor miRNAs, which was found to be mir-146a.

Those miRNAs which were only significantly differentially expressed in cells incubated with erlotinib and not in the other treatment groups were also considered especially interesting. They represent a difference in response to erlotinib in erlotinib-sensitive as compared to -insensitive keratinocytes. There were 19 different miRNA precursors and 13 mature miRNAs only significantly differentially expressed in cells incubated with erlotinib. For these miRNAs a thorough literature search was conducted to select those miRNAs which had already been found to be involved in response to EGFRIs in previous studies, which strengthened the evidence for these candidate miRNAs. Further analysis of all miRNAs would have exceeded the timeframe of this thesis. An overview table of the results of this literature search can be found in Appendix A). Based on the literature search, expression of the following precursor and mature miRNAs in erlotinib-sensitive as compared to -insensitive keratinocytes was verified using qRT-PCR: mir-146a, miR-146a-5p, mir-31, miR-31-3p, mir-138-2, mir-221, mir-520e, and mir-944. In addition, the following miRNAs identified from the equivalent literature search for candidate miRNAs in fibroblasts (refer to Appendix B) were also tested in keratinocytes to compare their roles in the two cell types: mir-34a, miR-34a-5p, mir-17, mir-30b, mir-382, mir-494, mir-7-1, miR-7-1-3p.
In general, in PCR analyses the differences in expression between cell samples grouped as erlotinib-sensitive and those grouped as erlotinib-insensitive were not significant for any miRNAs as tested with Student’s t-test (except for mir-944 with p-value = 0.02). Figure 27 shows a comparison of ΔCP values for expression of miRNAs in untreated erlotinib-sensitive keratinocytes and untreated erlotinib-insensitive keratinocytes.

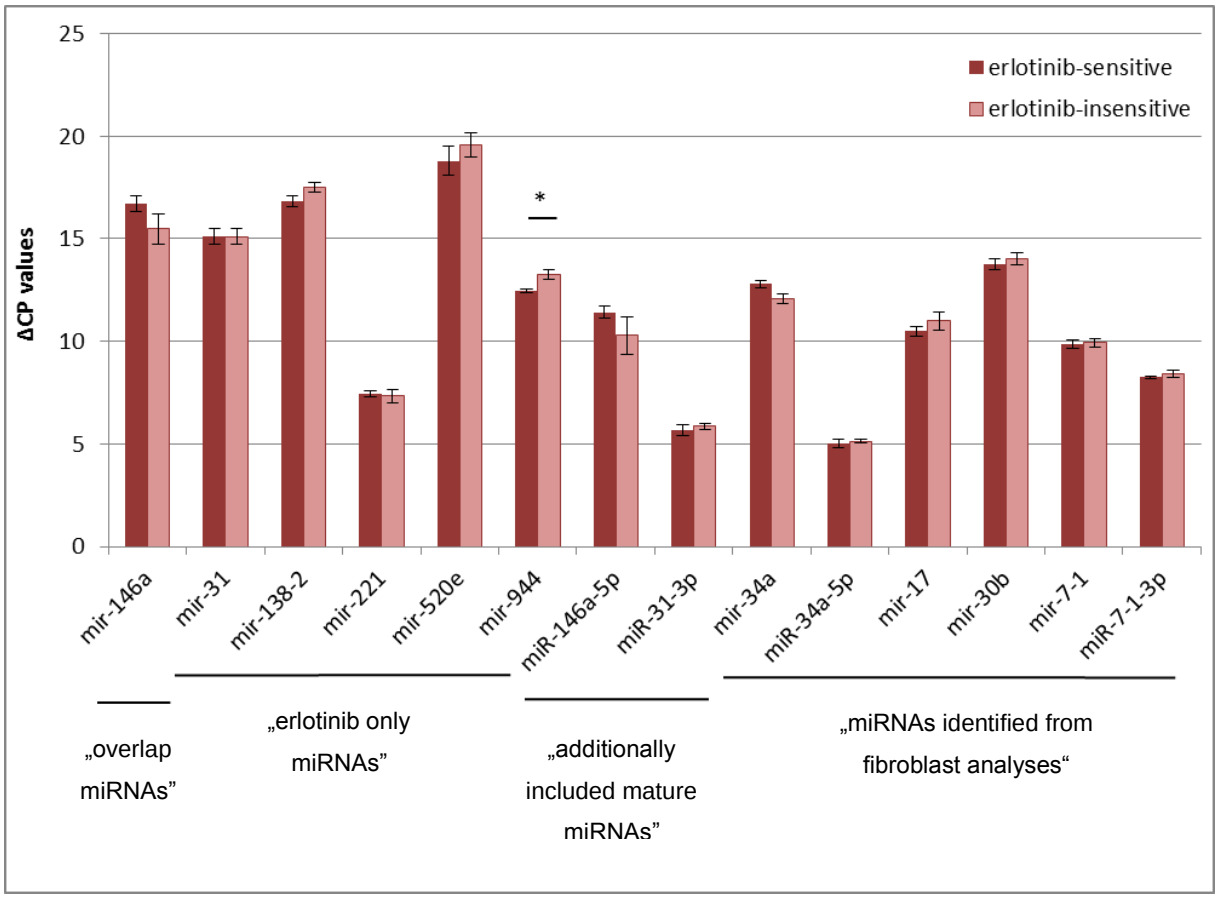


**Figure 27 Comparison of miRNA expression in untreated erlotinib-sensitive and erlotinib-insensitive keratinocytes determined by qRT-PCR**

ΔCP values representing expression of different miRNAs in untreated keratinocytes as determined by qRT-PCR. Dark red: Mean ΔCP values of erlotinib-sensitive cell samples as determined by ELISAs (n = 6). Light red: Mean ΔCP values of erlotinib-insensitive cell samples (n = 6). MiRNAs were selected due to results from NGS and a literature search. Error bars represent SEM.* represents a significant difference (p-value < 0.05, Student's t-test).
Abbreviations: ΔCP, delta crossing point; ELISA, enzyme-linked immunosorbent assay; NGS, next generation sequencing; qRT-PCR, quantitative real-time polymerase chain reaction; SEM, standard error of the mean.

Upon *in vitro* treatment with erlotinib, the difference in expression of the selected miRNAs in the group of erlotinib-sensitive cells as compared to the group of erlotinib-insensitive cells was not significant, either.

A comparison of the results from NGS and PCR is presented in table 26 with fold-changes and p-values for NGS and also fold-changes for PCR (but no p-values since in PCR analysis t-test for ΔΔCP values did not show significant differences [no p-values <0.05]). (Please note that cut-off values defining up- and down-regulation were chosen less strict than for the Venn diagrams, in order to give a better visualization also of smaller effects.)

**Table 26 Comparison of NGS and qRT-PCR results for fold-changes of specific miRNAs differentially expressed in erlotinib-sensitive and -insensitive keratinocytes**

Fold-changes in expression of specific precursor and mature miRNAs in erlotinib-sensitive as compared to -insensitive primary human keratinocytes (n = 6 in each group) were determined by NGS and qRT-PCR. Cells were either incubated with 4 nM EGF (dark blue columns) or 5 µM erlotinib plus 4 nM EGF (green columns) or left untreated (light blue columns) prior to miRNA expression analyses. Significant p-values for NGS results (< 0.05) are marked in bold. MiRNAs selected by Venn diagrams and literature search as described in chapter III. MiRNAs with higher expression in erlotinib-sensitive cells than in -insensitive cells (fold-change ≥ 1.2) are marked with a green arrow (up-regulated) while those with lower expression (fold-change ≤ 0.8) are marked with a red arrow (down-regulated). Fold-changes in between those cut-offs are not regarded as differential.
Abbreviations: EGF, epidermal growth factor; miRNA, micro ribonucleic acid; NGS, next generation sequencing; qRT-PCR, quantitative real-time polymerase chain reaction.

| | sensitive vs. insensitive (no treatment) | | | | | sensitive vs. insensitive (EGF) | | | | | sensitive vs. insensitive (erlotinib) | | | | |
|---|---|---|---|---|---|---|---|---|---|---|---|---|---|---|---|
| **miRNA** | | **NGS** | | | **PCR** | | **NGS** | | | **PCR** | | **NGS** | | | **PCR** | |
| | | fold-change | p-value | | fold-change | | fold-change | p-value | | fold-change | | fold-change | p-value | | fold-change |
| **"overlap miRNAs"** | | | | | | | | | | | | | | | |
| mir-146a hairpin | ↓ | 0.64 | **0.0324** | ↓ | 0.43 | ↓ | 0.62 | **0.0440** | ↓ | 0.45 | ↓ | 0.55 | **0.0207** | ↓ | 0.46 |
| **"erlotinib only miRNAs"** | | | | | | | | | | | | | | | |
| mir-31 hairpin | ↓ | 0.77 | **0.0423** | | 1.00 | ↓ | 0.79 | **0.0350** | | 0.92 | ↓ | 0.65 | **0.0096** | ↑ | 1.60 |
| mir-138-2 hairpin | ↓ | 0.72 | 0.1418 | ↑ | 1.59 | ↓ | 0.78 | 0.2511 | | 1.08 | ↓ | 0.40 | **0.0002** | ↓ | 0.73 |
| mir-221 hairpin | | 0.97 | 0.7817 | | 0.93 | | 0.82 | 0.1318 | | 0.92 | ↓ | 0.70 | **0.0086** | | 0.97 |
| mir-520e hairpin | | 0.81 | 0.3243 | ↑ | 1.70 | | 0.99 | NA | | 1.18 | ↓ | 0.18 | **0.0000** | ↓ | 0.74 |
| mir-944 hairpin | | 1.11 | 0.4501 | ↑ | 1.74 | ↑ | 1.57 | **0.0103** | ↑ | 1.43 | ↑ | 1.67 | **0.0020** | ↑ | 1.43 |
| **additionally included mature miRNAs** | | | | | | | | | | | | | | | |
| miR-146a-5p (mature) | ↓ | 0.71 | **0.0258** | ↓ | 0.45 | ↓ | 0.57 | **0.0055** | ↓ | 0.44 | ↓ | 0.50 | **0.0040** | ↓ | 0.39 |
| miR-31-3p (mature) | ↓ | 0.59 | **0.0069** | | 1.13 | | 1.00 | 0.9889 | | 0.93 | | 0.90 | 0.6616 | ↓ | 0.75 |
| **miRNAs identified from fibroblast analyses** | | | | | | | | | | | | | | | |
| mir-34a hairpin | | 1.00 | 0.9989 | ↓ | 0.60 | | 0.83 | 0.2828 | ↓ | 0.76 | ↓ | 0.29 | 0.7909 | | 1.18 |
| miR-34a-5p (mature) | | 0.97 | 0.8406 | | 1.08 | ↓ | 0.80 | 0.2050 | | 0.91 | ↓ | 0.79 | 0.2779 | | 1.03 |
| mir-17 hairpin | | 0.97 | 0.8311 | ↑ | 1.42 | | 1.04 | 0.7508 | ↑ | 1.27 | ↓ | 0.20 | 0.8213 | ↑ | 1.39 |
| mir-30b hairpin | | 0.91 | 0.5923 | | 1.19 | | 1.19 | 0.2697 | ↑ | 1.21 | | 0.83 | 0.9518 | | 1.11 |
| mir-7-1 hairpin | ↑ | 1.34 | 0.0809 | | 1.04 | ↑ | 1.36 | 0.0807 | | 1.14 | ↓ | 0.10 | 1.3762 | ↑ | 1.44 |
| miR-7-1-3p (mature) | | 0.89 | 0.5409 | | 1.15 | | 1.05 | 0.8190 | ↑ | 1.20 | ↓ | 0.70 | 0.1464 | ↑ | 1.51 |

Even though fold-changes greatly differed between NGS and PCR results, those miRNAs which were significantly (p-value < 0.05) up- or down-regulated in the NGS analyses were mainly also determined as up- or down-regulated in the PCR analyses, respectively, confirming the effect.

In erlotinib-sensitive keratinocytes expression of miRNA mir-146a was down-regulated as compared to erlotinib-insensitive cells, across all three treatment options, in NGS (significantly) as well as in PCR assays. This was also observed for the mature form miR-146a-5p. According to NGS results, mir-31 was also significantly down-regulated in sensitive cells; however, this effect was not confirmed by PCR. Depending on the cut-off values used to define down-regulation, mir-31 was either only differentially expressed in cells treated with erlotinib (fold-change 0.65) or also in those treated with EGF alone (fold-

change 0.79) and those left untreated (fold-change 0.77). The two miRNAs mir-138-2 and mir-520e were significantly down-regulated in sensitive keratinocytes previously incubated with erlotinib (confirmed by PCR) but not under the other treatment conditions. On the other hand, mir-944 was up-regulated in sensitive cells under EGF as well as erlotinib + EGF treatment. A trend towards up-regulation of mir-944 was also visible in untreated cells (but in NGS did not reach the cut-off value of 1.2).

Those miRNAs which were identified as significantly differentially expressed in fibroblasts were not significantly differentially expressed in keratinocytes, again indicating large differences in cellular processes in these two dermal cell types. Regulation of mir-34a and its mature form miR-34a-5p even seemed to be opposite in the two cell types. While in fibroblasts expression of mir-34a and miR-34a-5p were up-regulated in erlotinib-sensitive cells, in keratinocytes the two miRNAs were rather down-regulated in erlotinib-sensitive cells.

### IV.2.2 Fibroblasts

The amount of healthy donors for primary epidermal keratinocytes was very limited. However, a large number of samples of primary human dermal fibroblasts was available from the Clinical Pharmacology Department of the University Medicine Göttingen. Since fibroblasts are the most abundant cell type of the dermis, directly adjacent to the epidermis, and *EGFR* is also expressed in dermal fibroblasts, it was investigated whether these cells could also serve as a suitable cell model to study EGFRI-induced skin toxicity.

#### IV.2.2.1 Effect of erlotinib on EGFR signaling in fibroblasts *in vitro*

First of all, the *in vitro* effect of incubation with the EGFRI erlotinib was investigated using phospho kinase arrays, like for the keratinocytes (described in section IV.2.1.2). Two separate experiments were performed with different cell samples (FB64 p7 and FB120 p8). Figures 28 and 29 show representative results for FB120 p8.

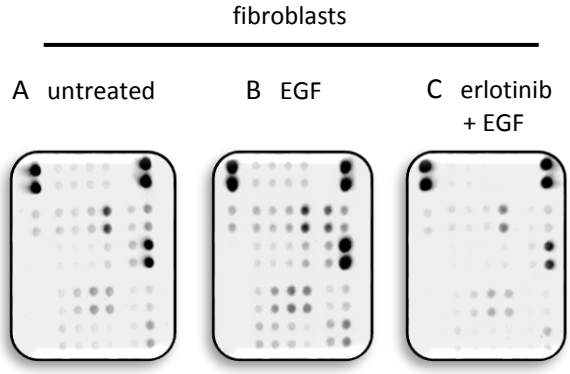


**Figure 28 *In vitro* effect of erlotinib on phosphorylation of proteins involved in EGFR signaling in fibroblasts**

Human phospho kinase arrays were conducted with dermal fibroblast cell lysates of FB120 p8. Some sections of the membranes after chemiluminescent visualization of the phosphorylated proteins are shown. **A**) No treatment. **B**) Stimulated with 4 nM EGF for 5 min. **C**) Incubated with 10 µM erlotinib for 2 h then stimulated with 4 nM EGF for 5 min. A stronger signal (pixel density) corresponds to higher amounts of phosphorylated protein present and stronger signaling activity. Abbreviations: EGF, epidermal growth factor; FB, fibroblasts; p, passage.

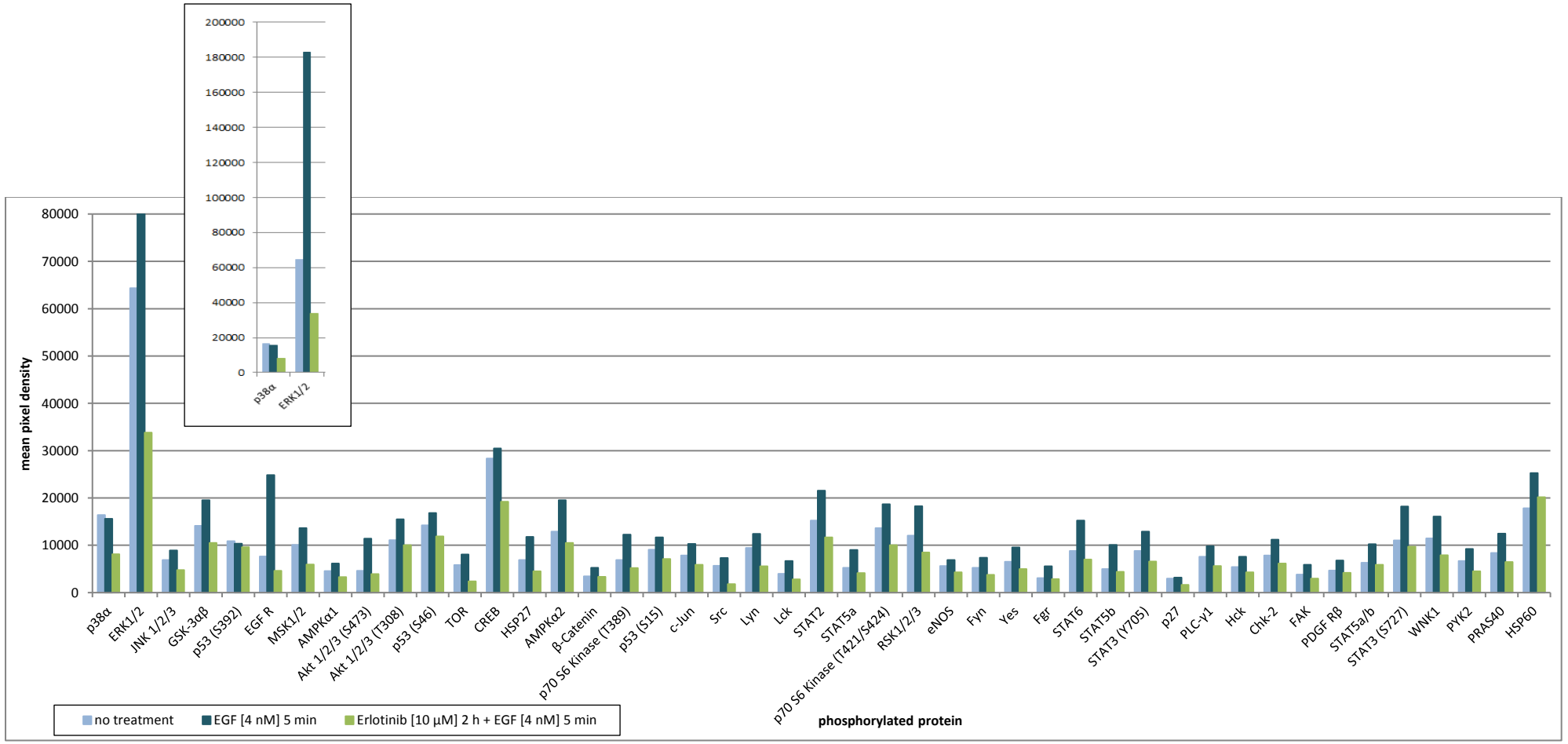


**Figure 29 Quantification of *in vitro* effect of erlotinib on phosphorylation of proteins involved in EGFR signaling in fibroblasts**

Human phospho kinase arrays were conducted with dermal fibroblast cell lysates of FB120 p8. The mean pixel density after chemiluminescent visualization of the 45 different phosphorylated proteins is shown. Light blue: no treatment. Dark blue: stimulated with 4 nM EGF for 5 min. Green: incubated with 10 µM erlotinib for 2 h then stimulated with 4 nM EGF for 5 min. The signal for the protein ERK1/2 is too strong to fit the scale and is therefore cut-off at the end of it. The real end of the bar for ERK1/2 is shown in the additional section next to the graph where a larger scale is used. A stronger signal (pixel density) corresponds to higher amounts of phosphorylated protein present and stronger signaling activity.
Abbreviations: EGF, epidermal growth factor; EGFR, epidermal growth factor receptor; ERK, extracellular signal-regulated kinase; FB, fibroblasts; p, passage.

In dermal fibroblasts EGF also increased phosphorylation of most of the tested proteins involved in EGFR signaling cascades while erlotinib decreased the phosphorylation. Again the strength of the effect was different for the various signaling proteins. For quantification of the effects the EGF/no treatment and the erlotinib/EGF ratios were calculated as described for the keratinocytes in section IV.2.1.2. The five proteins on which erlotinib had the strongest effect across the experiments are listed in table 27. The values for all other proteins are provided in the Appendix B).

**Table 27 Mean pixel density for selected proteins from human phospho kinase arrays of two different fibroblast cell samples**

Human phospho-kinase arrays were conducted with two different fibroblast cell samples (FB64 p7 and FB120 p8) following three *in vitro* treatment conditions (no treatment, 4 nM EGF for 5 min and 10 µM erlotinib for 2 h + 4 nM EGF for 5 min). For clearer comparison of the stimulating effect of EGF and the inhibitory effect of erlotinib between the different cell samples, ratios were calculated (EGF/no treatment and erlotinib/EGF). Results for the five phosphorylated proteins on whose abundance EGF and erlotinib had the biggest effect are listed here. Abbreviations: EGF, epidermal growth factor; FB, fibroblasts; p, passage.

| | **mean pixel density for FB64 p7** | | | | |
|---|---|---|---|---|---|
| **protein** | **no treatment** | **EGF** | **erlotinib** | **EGF/no treatment** | **erlotinib/ EGF** |
| ERK1/2 | 134053 | 254220 | 107268 | 1.90 | 0.42 |
| Akt 1/2/3 (S473) | 19079 | 22766 | 12611 | 1.19 | 0.55 |
| EGF R | 34264 | 74409 | 23720 | 2.17 | 0.32 |
| TOR | 17408 | 17158 | 8974 | 0.99 | 0.52 |
| Src | 14331 | 43802 | 7245 | 3.06 | 0.17 |
| | **mean pixel density for FB120 p8** | | | | |
| **protein** | **no treatment** | **EGF** | **erlotinib** | **EGF/no treatment** | **erlotinib/ EGF** |
| ERK1/2 | 64330.5 | 182975 | 33812 | 2.84 | 0.18 |
| Akt 1/2/3 (S473) | 4629 | 11387.5 | 3941.5 | 2.46 | 0.35 |
| EGF R | 7628 | 24849 | 4612 | 3.26 | 0.19 |
| TOR | 5835 | 8063 | 2369.5 | 1.38 | 0.29 |
| Src | 5677 | 7298.5 | 1791 | 1.29 | 0.25 |

The proteins on whose phosphorylation erlotinib had the strongest inhibitory effect differed in fibroblasts as compared to keratinocytes. Only EGFR and Src were among the top five in both cell types. In addition, in fibroblasts the effect seems to be strongest on the MAPK ERK 1/2 and the kinases Akt 1/2/3 and target of rapamycin (TOR).

### IV.2.2.2 Effect of erlotinib on the phosphorylation of EGFR and ERK 1/2 in fibroblasts *in vitro*

For further analyses of EGFR signaling across more than just the two example fibroblast samples used for the phospho kinase arrays, specific phospho-ELISAs were conducted. According to the results from the phospho kinase arrays and considering the commercial availability of validated assays, ELISAs for phospho-EGFR and phospho-ERK 1/2 were chosen. The relative amount of phosphorylated target protein, normalized to the amount of total target protein, was determined and compared between cells incubated with erlotinib and stimulated with EGF, cells only stimulated with EGF and cells left untreated. For better comparison between cells from different individuals, again the ratios EGF/no treatment and erlotinib/EGF were calculated as explained in section IV.2.1.2. The results for these ratios from the phospho-EGFR ELISA are presented in table 28.

**Table 28 *In vitro* effect of erlotinib on relative amount of phosphorylated EGFR in fibroblasts**

Phospho-EGFR ELISAs were conducted with six different fibroblast cell samples following three *in vitro* treatment conditions (no treatment, 40 nM EGF for 5 min and 10 µM erlotinib for 2 h + 40 nM EGF for 5 min). The relative amount of phosphorylated EGFR was determined in RFUs normalized to total protein. For clearer comparison of the stimulating effect of EGF and the inhibitory effect of erlotinib between the different cell samples, ratios were calculated (EGF/no treatment and erlotinib/EGF). Abbreviations: EGF, epidermal growth factor; EGFR, epidermal growth factor receptor; ELISA, enzyme-linked immunosorbent assay; FB, fibroblasts; p, passage; RFUs, relative fluorescence units.

| | **phospho-EGFR** | |
|---|---|---|
| cell sample | **EGF/no treatment** | **erlotinib/EGF** |
| FB19 p6 | 1.1380 | 0.8678 |
| FB21 p9 | 1.1058 | 0.8753 |
| FB25 p11 | 1.1565 | 0.8529 |
| FB26 p6 | 1.2093 | 0.8184 |
| FB33 p10 | 1.1934 | 0.8067 |
| FB43 p8 | 1.2495 | 0.8403 |

Stimulation with EGF increased the amount of phosphorylated EGFR (EGF/no treatment > 1), while prior incubation with erlotinib decreased it (erlotinib/EGF < 1) in all cell samples. Therefore, the phospho-EGFR ELISA seemed to be suitable to measure the *in vitro* effect of erlotinib. However, the results for the erlotinib/EGF ratio were very similar in all six tested cell samples. The assay did not seem to be sensitive enough to detect differences in the *in vitro* effect of erlotinib in human fibroblasts from different individuals. Therefore, it was not used for further analyses. Instead, phospho-ERK 1/2 ELISAs were tested for their

suitability for this task. Since the cell-based EGFR ELISA was found not sensitive enough, a lysate-based ELISA was tested for ERK 1/2. After establishment and optimization of the assay, the main ERK 1/2 ELISA experiments were conducted by the medical student Marcel Struß within our working group, under my supervision. The results are presented in table 29.

**Table 29** ***In vitro*** **effect of erlotinib on relative amount of phosphorylated ERK 1/2 in fibroblasts**

Phospho-ERK 1/2 ELISAs were conducted with 54 different fibroblast cell samples following three *in vitro* treatment conditions (no treatment, 40 nM EGF for 5 min and 5 µM erlotinib for 2 h + 40 nM EGF for 5 min). Relative amount of phosphorylated ERK 1/2 was determined in RFUs normalized to total protein. For clearer comparison of the stimulating effect of EGF and the inhibitory effect of erlotinib between cell samples, ratios were calculated (EGF/no treatment and erlotinib/EGF). Abbreviations: EGF, epidermal growth factor; ELISA, enzyme-linked immunosorbent assay; ERK, extracellular signal-regulated kinase; FB, fibroblasts; RFUs, relative fluorescence units.

| | phospho-ERK 1/2 | |
|---|---|---|
| cell sample | **EGF/no treatment** | **erlotinib/EGF** |
| FB19 p9 | 3.6883 | 0.2536 |
| FB21 p9 | 4.1130 | 0.3235 |
| FB26 p11 | 7.6180 | 0.4013 |
| FB33 p8 | 2.5443 | 0.5681 |
| FB40 p9 | 5.2113 | 0.4493 |
| FB43 p8 | 2.4889 | 0.3194 |
| FB46 p10 | 2.8345 | 0.3703 |
| FB53 p7 | 4.4225 | 0.4100 |
| FB57 p7 | 5.2379 | 0.1765 |
| FB64 p8 | 3.6602 | 0.0099 |
| FB72 p9 | 4.0739 | 0.4754 |
| FB74 p8 | 3.4761 | 0.5651 |
| FB75 p10 | 1.3296 | 0.6989 |
| FB76 p9 | 1.7068 | 0.9914 |
| FB79 p9 | 2.1351 | 0.9735 |
| FB80 p10 | 1.4940 | 0.8854 |
| FB81 p9 | 2.1457 | 0.7966 |
| FB82 p9 | 4.5296 | 0.3124 |
| FB83 p8 | 8.2605 | 0.3442 |
| FB84 p8 | 1.5823 | 1.1183 |
| FB85 p9 | 2.0481 | 0.6394 |
| FB86 p10 | 5.5561 | 0.7228 |
| FB87 p8 | 2.0339 | 0.7963 |
| FB90 p8 | 2.2504 | 0.6667 |
| FB92 p9 | 2.7265 | 0.4974 |
| FB93 p8 | 2.6828 | 0.8247 |
| FB95 p8 | 10.6493 | 0.3698 |

| | phospho-ERK 1/2 | |
|---|---|---|
| cell sample | **EGF/no treatment** | **erlotinib/EGF** |
| FB96 p8 | 3.9190 | 0.3792 |
| FB98 p8 | 4.8371 | 0.5564 |
| FB99 p8 | 5.1002 | 0.2039 |
| FB103 p8 | 3.2308 | 0.4803 |
| FB106 p9 | 2.7031 | 0.8185 |
| FB112 p7 | 11.1117 | 0.5878 |
| FB114 p7 | 23.5336 | 0.4553 |
| FB117 p7 | 4.0906 | 0.4949 |
| FB118 p7 | 17.7995 | 0.3088 |
| FB120 p8 | 2.5310 | 0.4599 |
| FB122 p6 | 5.9503 | 0.4863 |
| FB124 p8 | 4.3149 | 0.4250 |
| FB125 p8 | 3.1734 | 0.4846 |
| FB126 p8 | 3.0523 | 0.6255 |
| FB127 p8 | 1.9762 | 0.6909 |
| FB128 p8 | 2.5256 | 0.8201 |
| FB129 p8 | 1.6903 | 0.3254 |
| FB130 p6 | 3.6520 | 0.4188 |
| FB131 p7 | 1.0400 | 1.0513 |
| FB132 p7 | 3.3119 | 0.5480 |
| FB133 p7 | 2.8670 | 0.3172 |
| FB134 p7 | 3.9009 | 0.5068 |
| FB135 p6 | 4.0618 | 0.5765 |
| FB136 p6 | 7.8450 | 0.2129 |
| FB137 p6 | 2.1229 | 0.6699 |
| FB138 p7 | 2.0504 | 0.6206 |
| FB139 p7 | 1.6598 | 0.5859 |

Stimulation with EGF increased the amount of phosphorylated ERK 1/2 in all fibroblast samples (EGF/no treatment > 1). Prior incubation with erlotinib decreased the amount of phosphorylated ERK 1/2 in all but two cell samples (erlotinib/EGF < 1). The phospho-ERK 1/2 ELISA seemed to be suitable to measure the *in vitro* effect of erlotinib in human fibroblasts.

The cell samples FB76, FB79, FB80 and FB99 were cultured again and used for an additional independent experiment (biological duplicate) to investigate the reproducibility of the results. Mean ratios and SDs are given in table 30.

**Table 30 Reproducibility of results for *in vitro* effect of erlotinib on fibroblasts from phospho-ERK 1/2 ELISA**

Phospho-ERK 1/2 ELISAs were conducted with four different fibroblast cell samples following three *in vitro* treatment conditions (no treatment, 40 nM EGF for 5 min and 5 µM erlotinib for 2 h + 40 nM EGF for 5 min). The relative amount of phosphorylated ERK 1/2 was determined in RFUs normalized to total protein. For clearer comparison of the stimulating effect of EGF and the inhibitory effect of erlotinib between the different cell samples, ratios were calculated (EGF/no treatment and erlotinib/EGF). Results are presented as mean values with SDs from two independent experiments. Abbreviations: EGF, epidermal growth factor; ELISA, enzyme-linked immunosorbent assay; ERK, extracellular signal-regulated kinase; FB, fibroblasts; n number [of independent experiments]; p, passage; SD, standard deviation, RFUs, relative fluorescence units.

| | | phospho-ERK 1/2 | | | |
|---|---|---|---|---|---|
| | | EGF/no treatment | | erlotinib/EGF | |
| cell sample | n | mean | SD | mean | SD |
| FB76 | 2 | 1.9051 | 0.2805 | 0.8381 | 0.2169 |
| FB79 | 2 | 4.6406 | 3.5433 | 0.8956 | 0.1102 |
| FB80 | 2 | 2.7174 | 1.7301 | 0.6287 | 0.3630 |
| FB99 | 2 | 4.4099 | 0.9762 | 0.1902 | 0.0194 |

The standard deviations calculated for the biological duplicates of the phospho-ERK 1/2 ELISA were rather high for the EGF/no treatment ratio but lower for the erlotinib/EGF ratio. The phospho-ERK 1/2 ELISA seemed to be suitable to detect differences in the *in vitro* effect of erlotinib (sensitivity towards erlotinib) on human dermal fibroblasts. Therefore, the results from the phospho-ERK 1/2 ELISA (table 29) were used to sort the fibroblast samples according to their sensitivity towards erlotinib for further analyses. A low erlotinib/EGF ratio means higher sensitivity towards erlotinib. This sorting is depicted in figure 30.

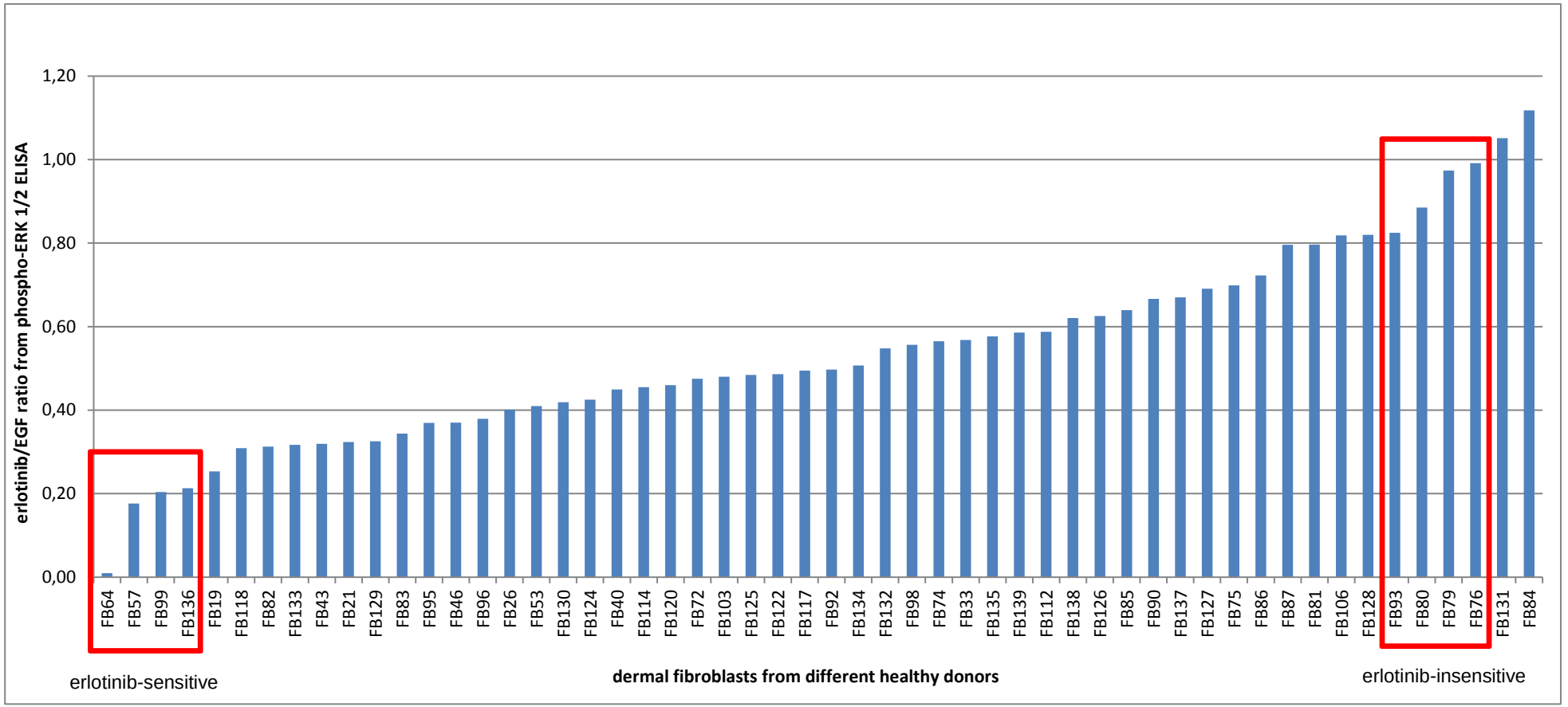


**Figure 30 Fibroblasts grouped into erlotinib-sensitive and -insensitive**

The results from phospho-ERK 1/2 ELISAs, which were conducted with 54 different fibroblast cell samples following *in vitro* treatment with erlotinib (10 µM, 2 h) and subsequent stimulation with EGF (40 nM, 5 min) or stimulation with EGF alone, were used to calculate an erlotinib/EGF ratio for each cell sample. Cell samples were grouped into rather erlotinib-sensitive and rather erlotinib-insensitive according to the ratio. Four cell samples from each edge group were chosen for further analyses, marked by the red frames. A smaller ratio means higher sensitivity towards erlotinib. Abbreviations: EGF, epidermal growth factor; ELISA, enzyme-linked immunosorbent assay; ERK, extracellular signal-regulated kinase; FB, fibroblasts.

The four fibroblast cell samples with the lowest erlotinib/EGF ratio were chosen as rather erlotinib-sensitive cells and the four fibroblast samples with the highest erlotinib/EGF ratio (but < 1) were chosen as rather erlotinib-insensitive cells. For all eight cell samples the miRNA profiles were determined and compared between the two groups.

### IV.2.2.3 MiRNA profiles of erlotinib-sensitive versus -insensitive fibroblasts

As already described for the keratinocytes, miRNA profiles were also determined for the dermal fibroblasts. Mature as well as precursor (hairpin) miRNAs which were differentially expressed between the four rather erlotinib-sensitive and the four rather erlotinib-insensitive cell samples (both determined *in vitro* by the ERK 1/2-ELISA, see previous section) were identified. Again, it was also checked whether prior incubation with erlotinib + EGF or EGF alone had an influence on the list of differentially expressed miRNAs. Since the lists of differentially expressed miRNAs obtained for the fibroblasts were a lot longer than those for the keratinocytes, miRNAs with a p-value < 0.02 instead of the usual 0.05 are listed. The results for untreated cells are presented in table 31 and respective tables for cells incubated with EGF or erlotinib + EGF are included in Appendix B). The threshold for the fold change, set at ≥ 1.50 (up-regulated) or ≤ 0.66 (down-regulated) respectively, was retained.

**Table 31 Differentially expressed miRNAs in erlotinib-sensitive as compared to -insensitive fibroblasts (no treatment)**

Differentially expressed precursor and mature miRNAs in rather erlotinib-sensitive as compared to -insensitive fibroblasts (n = 4 in each group) were determined by NGS and the program DESeq2. *In vitro* sensitivity towards erlotinib was previously determined by ERK 1/2-ELISA. MiRNAs with a p-value < 0.02 and a fold change of ≥ 1.50 (up-regulated in erlotinib-sensitive cells) or ≤ 0.66 (down-regulated in erlotinib-sensitive) respectively, are listed. The fold change as logarithm of the basis 2 (log2 fold change) is given with its standard error (lfcSE, log fold change standard error). The result of the statistic Wald test (stat) together with the corresponding p-value is also listed.

| | erlotinib-sensitive vs. -insensitive treatment: none | | | | |
|---|---|---|---|---|---|
| **precursor miRNA (hairpin)** | **log2 fold change** | **lfcSE** | **fold change** | **stat** | **p-value** |
| hsa-mir-20a | 1.2245 | 0.3097 | 2.3367 | 3.9543 | 7.68E-05 |
| hsa-mir-494 | 1.4506 | 0.3709 | 2.7333 | 3.9106 | 9.21E-05 |
| hsa-mir-199b | 1.0134 | 0.2851 | 2.0187 | 3.5545 | 3.79E-04 |
| hsa-mir-382 | 1.2959 | 0.3793 | 2.4553 | 3.4163 | 6.35E-04 |
| hsa-mir-520e | -1.6402 | 0.4907 | 0.3208 | -3.3424 | 8.31E-04 |
| hsa-mir-127 | 1.2793 | 0.3851 | 2.4273 | 3.3221 | 8.93E-04 |
| hsa-mir-450b | 1.0213 | 0.3239 | 2.0298 | 3.1537 | 1.61E-03 |

| | | | | | |
|---|---|---|---|---|---|
| hsa-mir-889 | 1.2399 | 0.3955 | 2.3618 | 3.1349 | 1.72E-03 |
| hsa-mir-148b | 0.8478 | 0.2826 | 1.7997 | 3.0000 | 2.70E-03 |
| hsa-mir-101-2 | 0.8467 | 0.2909 | 1.7984 | 2.9112 | 3.60E-03 |
| hsa-mir-411 | 1.0640 | 0.3683 | 2.0907 | 2.8888 | 3.87E-03 |
| hsa-mir-654 | 1.0489 | 0.3632 | 2.0690 | 2.8881 | 3.88E-03 |
| hsa-mir-323a | 1.0728 | 0.3759 | 2.1035 | 2.8538 | 4.32E-03 |
| hsa-mir-379 | 1.1258 | 0.3992 | 2.1823 | 2.8205 | 4.80E-03 |
| hsa-mir-30b | 0.9572 | 0.3402 | 1.9416 | 2.8138 | 4.90E-03 |
| hsa-mir-101-1 | 0.7779 | 0.2861 | 1.7146 | 2.7192 | 6.54E-03 |
| hsa-mir-17 | 0.8324 | 0.3113 | 1.7806 | 2.6742 | 7.49E-03 |
| hsa-mir-136 | 0.9454 | 0.3680 | 1.9258 | 2.5690 | 1.02E-02 |
| hsa-mir-342 | 0.9676 | 0.3804 | 1.9556 | 2.5439 | 1.10E-02 |
| hsa-mir-585 | 0.9698 | 0.3884 | 1.9586 | 2.4972 | 1.25E-02 |
| hsa-mir-106b | 0.6790 | 0.2872 | 1.6011 | 2.3641 | 1.81E-02 |
| hsa-mir-199a-2 | 0.6648 | 0.2817 | 1.5854 | 2.3599 | 1.83E-02 |
| hsa-mir-323b | 0.9831 | 0.4180 | 1.9767 | 2.3517 | 1.87E-02 |
| hsa-mir-7158 | 0.8414 | 0.3581 | 1.7918 | 2.3497 | 1.88E-02 |
| hsa-mir-199a-1 | 0.6628 | 0.2833 | 1.5831 | 2.3392 | 1.93E-02 |
| | | | | | |
| **mature miRNA** | | | | | |
| hsa-miR-22-5p | -0.9825 | 0.2618 | 0.5061 | -3.7524 | 1.75E-04 |
| hsa-miR-504-5p | 1.8510 | 0.5015 | 3.6075 | 3.6909 | 2.23E-04 |
| hsa-miR-6756-5p | -2.0247 | 0.5780 | 0.2458 | -3.5032 | 4.60E-04 |
| hsa-miR-138-5p | -1.1710 | 0.3510 | 0.4441 | -3.3359 | 8.50E-04 |
| hsa-miR-20a-5p | 1.0365 | 0.3184 | 2.0512 | 3.2553 | 1.13E-03 |
| hsa-miR-199b-5p | 1.4812 | 0.4622 | 2.7918 | 3.2045 | 1.35E-03 |
| hsa-miR-651-5p | 2.0364 | 0.6356 | 4.1021 | 3.2038 | 1.36E-03 |
| hsa-miR-145-3p | -1.4868 | 0.4789 | 0.3568 | -3.1046 | 1.91E-03 |
| hsa-miR-654-5p | 1.3471 | 0.4346 | 2.5440 | 3.0997 | 1.94E-03 |
| hsa-miR-655-3p | 1.5090 | 0.4971 | 2.8461 | 3.0356 | 2.40E-03 |
| hsa-miR-450b-5p | 0.8490 | 0.2800 | 1.8012 | 3.0319 | 2.43E-03 |
| hsa-miR-22-3p | -0.9057 | 0.3025 | 0.5338 | -2.9941 | 2.75E-03 |
| hsa-miR-4485 | -1.5206 | 0.5293 | 0.3485 | -2.8731 | 4.06E-03 |
| hsa-miR-30b-5p | 0.8988 | 0.3305 | 1.8645 | 2.7198 | 6.53E-03 |
| hsa-miR-27b-5p | -1.1321 | 0.4175 | 0.4562 | -2.7115 | 6.70E-03 |
| hsa-miR-148a-3p | 1.2919 | 0.4826 | 2.4485 | 2.6768 | 7.43E-03 |
| hsa-miR-361-3p | 0.7173 | 0.2687 | 1.6441 | 2.6697 | 7.59E-03 |
| hsa-miR-7641 | -1.2389 | 0.4764 | 0.4237 | -2.6006 | 9.31E-03 |
| hsa-miR-127-3p | 1.0281 | 0.4086 | 2.0393 | 2.5162 | 1.19E-02 |
| hsa-miR-23a-5p | -1.5575 | 0.6220 | 0.3397 | -2.5039 | 1.23E-02 |
| hsa-miR-383-5p | 1.5725 | 0.6356 | 2.9742 | 2.4741 | 1.34E-02 |
| hsa-miR-758-3p | 0.9273 | 0.3773 | 1.9017 | 2.4576 | 1.40E-02 |
| hsa-miR-380-3p | 1.5437 | 0.6285 | 2.9155 | 2.4564 | 1.40E-02 |
| hsa-miR-1268b | -1.5223 | 0.6345 | 0.3481 | -2.3991 | 1.64E-02 |
| hsa-miR-17-5p | 0.6945 | 0.2903 | 1.6183 | 2.3920 | 1.68E-02 |

| | | | | | |
|---|---|---|---|---|---|
| hsa-miR-4510 | -0.9195 | 0.3895 | 0.5287 | -2.3606 | 1.82E-02 |
| hsa-miR-143-5p | -1.0984 | 0.4664 | 0.4670 | -2.3553 | 1.85E-02 |
| hsa-miR-3135b | -0.9745 | 0.4182 | 0.5089 | -2.3301 | 1.98E-02 |

In the erlotinib-sensitive fibroblasts one precursor miRNA and 13 mature miRNAs were significantly down-regulated while 24 precursor and 15 mature miRNAs were significantly up-regulated when compared to erlotinib-insensitive cells. Fold changes ranged between 1.58 and 4.10 (0.53 and 0.25 for down-regulation respectively).

For a better overview, those miRNAs which were significantly differentially expressed ($p < 0.05$) under all three different *in vitro* treatments were determined, as depicted in figure 31. These miRNAs are referred to as “overlap miRNAs”.

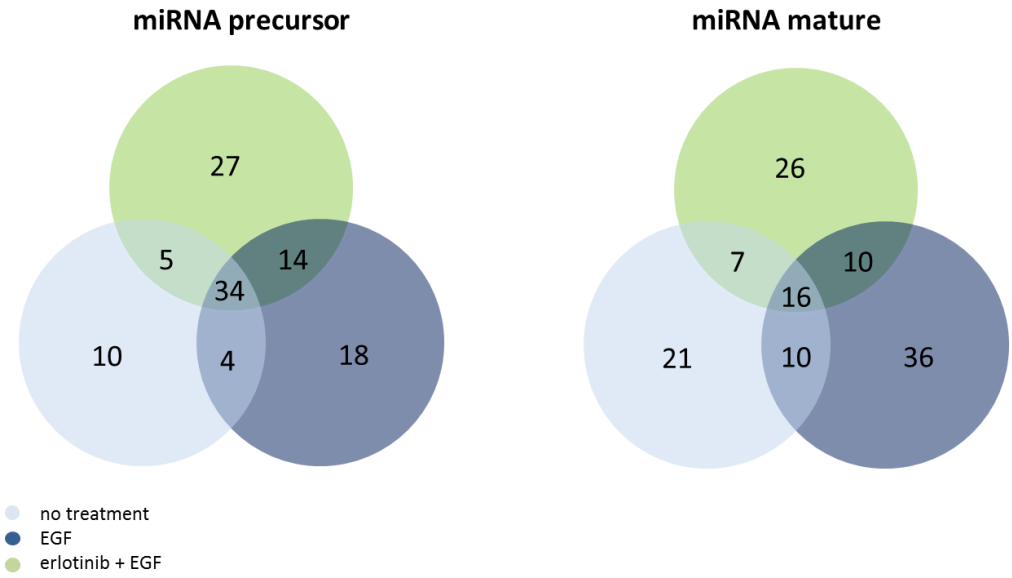


**Figure 31 Overlap of differentially expressed miRNAs in erlotinib-sensitive as compared to -insensitive fibroblasts between different *in vitro* treatments**

Significantly differentially expressed precursor (left) and mature (right) miRNAs in rather erlotinib-sensitive as compared to -insensitive fibroblasts (n = 4 in each group). MiRNA expression was determined by NGS. Cells were either incubated with 4 nM EGF (dark blue circle) or 4 nM EGF plus 5 µM erlotinib (green circle) or left untreated (light blue circle) prior to sequencing. Numbers in overlapping parts of the circles represent the numbers of specific miRNAs which were significantly differentially expressed ($p < 0.05$) in both or all three treatment groups, respectively.
Abbreviations: EGF, epidermal growth factor; miRNA, micro ribonucleic acid; NGS, next generation sequencing.

As for the keratinocytes, those miRNAs which were significantly differentially expressed in erlotinib-sensitive as compared to -insensitive fibroblasts regardless of the *in vitro* treatment were considered especially interesting. They represent a “baseline” difference between the erlotinib-sensitive and -insensitive cells, which is independent of stimulation with EGF or incubation with erlotinib. There was an overlap of 34 specific precursor miRNAs which were significantly differentially expressed in all three *in vitro* treatment groups and an overlap of 16 mature miRNAs.

Those miRNAs which were only significantly differentially expressed in cells incubated with erlotinib and not in the other treatment groups were also considered especially interesting. They represent a difference in response to erlotinib in erlotinib-sensitive as compared to -insensitive fibroblasts. There were 27 different miRNA precursors and 26 mature miRNAs only significantly differentially expressed in cells incubated with erlotinib. As already explained for the keratinocytes, also for these fibroblast miRNAs a through literature search was conducted to select those miRNAs which had already been found to be involved in response to EGFRIs in previous studies, which provided additional evidence for the suitability of the selected candidate miRNAs. Further analysis of all miRNAs would have exceeded the timeframe of this thesis. An overview table of the results of this literature search can be found in appendix B. Based on the literature search, expression of the following miRNAs in erlotinib-sensitive as compared to -insensitive fibroblasts was verified using qRT-PCR: mir-34a, miR-34a-5p, mir-17, mir-30b, mir-382, mir-494, mir-520e, mir-7-1, miR-7-1-3p, mir-31, miR-31-3p. In addition, the following miRNAs identified from the equivalent literature search for candidate miRNAs in keratinocytes (refer to Appendix A) were also tested in fibroblasts to compare their roles in the two cell types: mir-146a, miR-146a-5p, mir-138-2, mir-221.

In general, in PCR analyses the differences in expression between cell samples grouped as erlotinib-sensitive and those grouped as erlotinib-insensitive were not significant for any of the selected miRNAs as tested with Student’s t-test. Figure 32 shows a comparison of ΔCP values for expression of miRNAs in untreated erlotinib-sensitive fibroblasts and untreated erlotinib-insensitive fibroblasts. Differential expression was also not significant in cells with prior *in vitro* treatment with erlotinib.

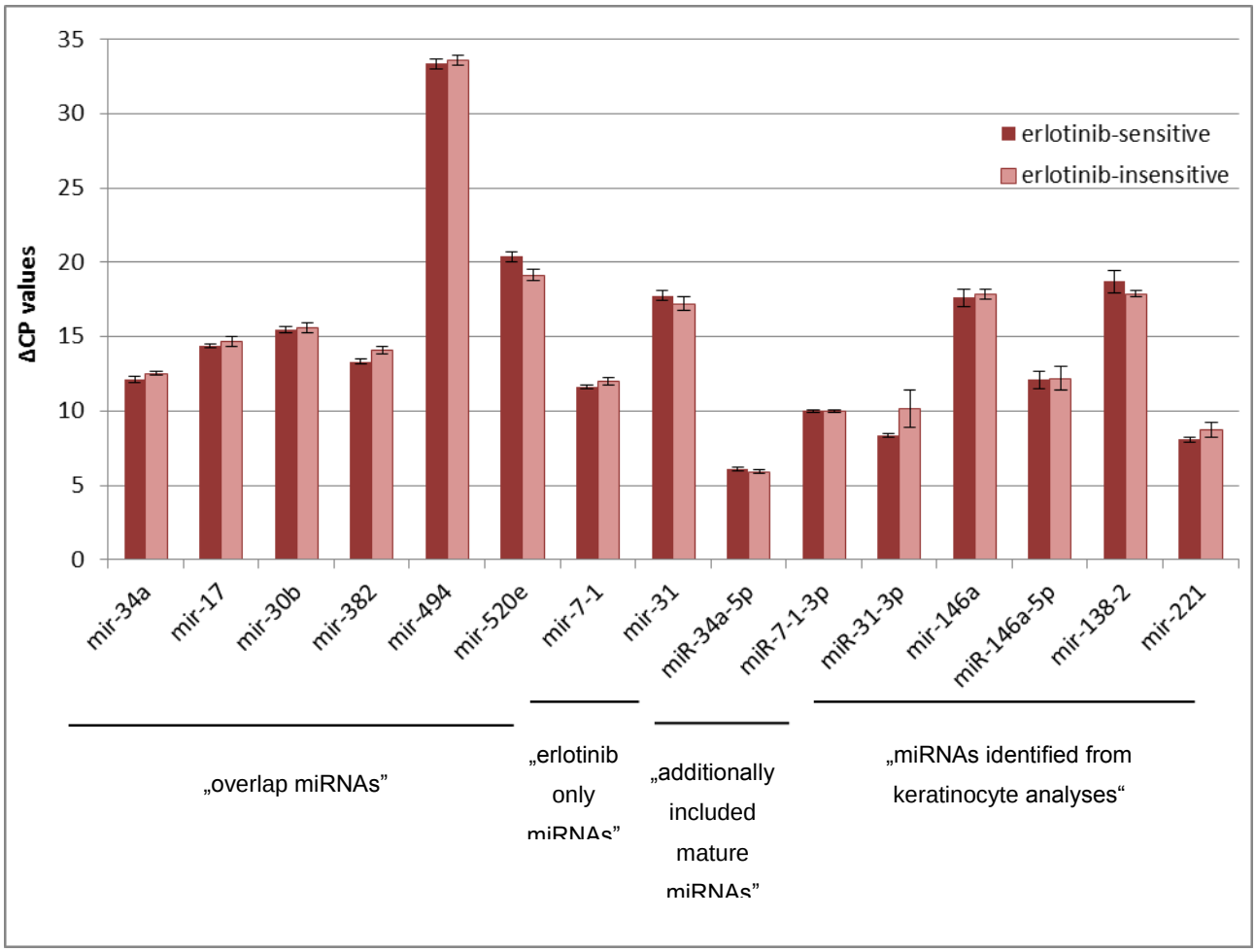


**Figure 32 Comparison of miRNA expression in untreated erlotinib-sensitive and erlotinib-insensitive fibroblasts determined by qRT-PCR**

ΔCP values representing expression of different miRNAs in untreated fibroblasts as determined by qRT-PCR. Dark red: Mean ΔCP values of erlotinib-sensitive cell samples as determined by ELISAs (n = 6). Light red: Mean ΔCP values of erlotinib-insensitive cell samples (n = 6). MiRNAs were selected due to results from NGS and a literature search. Error bars represent SEM. Student's t-test showed no significant differences (p-value < 0.05).
Abbreviations: ΔCP, delta crossing point; ELISA, enzyme-linked immunosorbent assay; NGS, next generation sequencing; qRT-PCR, quantitative real-time polymerase chain reaction; SEM, standard error of the mean.

A comparison of the results from NGS and PCR is presented in table 40 with fold-changes and p-values for NGS and also fold-changes for PCR (but no p-values since in PCR analysis t-test for ΔΔCP values did not show significant differences [no p-values <0.05]).

**Table 32 Comparison of NGS and qRT-PCR results for fold-changes of specific miRNAs differentially expressed in erlotinib-sensitive and -insensitive fibroblasts**

Fold-changes in expression of specific precursor and mature miRNAs in erlotinib-sensitive as compared to -insensitive primary human fibroblasts (n = 4 in each group) were determined by NGS and qRT-PCR. Cells were either incubated with 4 nM EGF (dark blue columns) or 5 µM erlotinib plus 4 nM EGF (green columns) or left untreated (light blue columns) prior to miRNA expression analyses. Significant p-values for NGS results (< 0.05) are marked in bold. MiRNAs selected by Venn diagrams and literature search as described in chapter III. MiRNAs with higher expression in erlotinib-sensitive cells than in -insensitive cells (fold-change ≥ 1.2) are marked with a green arrow (up-regulated) while those with lower expression (fold-change ≤ 0.8) are marked with a red arrow (down-regulated). Fold-changes in between those cut-offs are not regarded as differential.
Abbreviations: EGF, epidermal growth factor; miRNA, micro ribonucleic acid; NGS, next generation sequencing; qRT-PCR, quantitative real-time polymerase chain reaction.

| | sensitive vs. insensitive (no treatment) | | | | | sensitive vs. insensitiv (EGF) | | | | | sensitive vs. insensitive (erlotinib) | | | | |
|---|---|---|---|---|---|---|---|---|---|---|---|---|---|---|---|
| **miRNA** | **NGS** | | | **PCR** | | **NGS** | | | **PCR** | | **NGS** | | | **PCR** | |
| | | fold-change | p-value | | fold-change | | fold-change | p-value | | fold-change | | fold-change | p-value | | fold-change |
| **"overlap miRNAs"** | | | | | | | | | | | | | | | |
| mir-34a hairpin | ↑ | 1.59 | **0.0261** | ↑ | 1.30 | ↑ | 1.78 | **0.0063** | ↑ | 2.48 | ↑ | 1.79 | **0.0117** | ↑ | 2.60 |
| mir-17 hairpin | ↑ | 1.78 | **0.0075** | ↑ | 1.25 | ↑ | 1.81 | **0.0205** | ↑ | 1.73 | ↑ | 1.85 | **0.0108** | ↑ | 1.58 |
| mir-30b hairpin | ↑ | 1.94 | **0.0049** | | 1.11 | ↑ | 2.22 | **0.0001** | ↑ | 1.73 | ↑ | 1.99 | **0.0019** | ↑ | 2.00 |
| mir-382 hairpin | ↑ | 2.46 | **0.0006** | ↑ | 1.70 | ↑ | 2.41 | **0.0012** | ↑ | 1.62 | ↑ | 2.35 | **0.0038** | ↑ | 2.63 |
| mir-494 hairpin | ↑ | 2.73 | **0.0001** | | 1.17 | ↑ | 2.49 | **0.0030** | ↑ | 2.19 | ↑ | 2.70 | **0.0005** | ↑ | 2.90 |
| mir-520e hairpin | ↓ | 0.32 | **0.0008** | ↓ | 0.42 | ↓ | 0.45 | **0.0300** | ↓ | 0.79 | ↓ | 0.40 | **0.0128** | | 0.85 |
| **"erlotinib only miRNAs"** | | | | | | | | | | | | | | | |
| mir-7-1 hairpin | ↑ | 1.47 | 0.0826 | ↑ | 1.30 | ↑ | 1.44 | 0.1164 | ↑ | 2.02 | ↑ | 1.56 | **0.0427** | ↑ | 1.72 |
| mir-31 hairpin | ↑ | 1.34 | 0.1358 | ↓ | 0.69 | ↑ | 1.44 | 0.0985 | ↑ | 1.24 | ↑ | 1.55 | **0.0417** | | 0.88 |
| **additionally included mature miRNAs** | | | | | | | | | | | | | | | |
| miR-34a-5p (mature) | ↑ | 1.30 | 0.2578 | | 0.90 | ↑ | 1.57 | 0.0527 | ↑ | 1.27 | ↑ | 1.52 | 0.0509 | | 0.93 |
| miR-7-1-3p (mature) | | 0.96 | 0.9152 | | 0.97 | | 0.93 | 0.8494 | ↑ | 1.33 | | 1.10 | 0.7928 | ↑ | 1.33 |
| miR-31-3p (mature) | | 1.12 | 0.7816 | ↑ | 3.49 | | 1.13 | 0.7701 | ↑ | 1.33 | | 0.84 | 0.6308 | ↓ | 0.64 |
| **miRNAs identified from keratonocyte analyses** | | | | | | | | | | | | | | | |
| mir-146a hairpin | ↑ | 1.22 | 0.5293 | | 1.17 | ↑ | 1.48 | 0.2410 | ↑ | 2.07 | ↑ | 1.47 | 0.2472 | ↑ | 1.37 |
| miR-146a-5p (mature) | ↑ | 1.31 | 0.5259 | | 1.00 | ↑ | 1.39 | 0.4727 | ↑ | 1.26 | ↑ | 1.40 | NA | | 1.19 |
| mir-138-2 hairpin | ↓ | 0.69 | 0.1401 | ↓ | 0.57 | | 1.15 | 0.5816 | | 1.13 | | 0.83 | 0.4602 | ↑ | 1.27 |
| mir-221 hairpin | ↑ | 1.22 | 0.2861 | ↑ | 1.56 | ↑ | 1.21 | 0.3096 | ↑ | 1.60 | ↑ | 1.33 | 0.1530 | ↑ | 1.75 |

As for the keratinocytes, for the fibroblasts again those miRNAs which were significantly (p-value < 0.05) up- or down-regulated in the NGS analyses were mainly also determined as up- or down-regulated in the PCR analyses, respectively, confirming the effect (even though fold-changes differed between NGS and PCR results).

In erlotinib-sensitive fibroblasts expression of miRNA mir-34a was significantly up-regulated as compared to erlotinib-insensitive cells, across all three treatment options, in NGS as well as PCR assays. This was also observed for the mature form miR-34a-5p (partially confirmed by PCR). The miRNAs mir-17, mir-30b, mir-382 and mir-494 were also up-regulated in erlotinib-sensitive as compared to -insensitive cells, as confirmed by PCR (in untreated cells fold-changes of mir-30b and mir-494 just below cut-off value of 1.2 in PCR). Further, mir-7-1 was significantly up-regulated in sensitive cells under treatment

with erlotinib. Up-regulation of mir-7-1 was also visible in untreated cells as well as cells incubated with EGF in NGS and PCR assays (but in NGS did not reach significance). In contrast, mir-520e was significantly down-regulated in erlotinib-sensitive fibroblasts as compared to erlotinib-insensitive cells, across all three treatment options, in NGS as well as PCR assays.

Those miRNAs which were identified as significantly differentially expressed in keratinocytes were not significantly differentially expressed in fibroblasts, again indicating large differences in cellular processes in these two dermal cell types. Regulation of some miRNAs even seemed to be opposite in the two cell types. While in keratinocytes mir-146a and its mature form miR-146a-5p were down-regulated in erlotinib-sensitive cells across all treatments, in fibroblasts those two miRNAs were rather up-regulated in erlotinib-sensitive cells. Similarly, in keratinocytes mir-221 was down-regulated in erlotinib-sensitive cells, especially under treatment with erlotinib, but in fibroblasts mir-221 was upregulated in erlotinib-sensitive cells across all treatments.

# Chapter V: Discussion

## V.1 Patient samples from the Dermatoxgen study

### V.1.1 EGFRI-induced skin rash and survival

The aim of this study was to identify predictive biomarkers for the occurrence and severity of EGFRI-induced skin toxicity. To achieve this, plasma samples from patients enrolled in the Dermatoxgen study were analyzed with regard to the concentrations of various candidate analytes which are known to interact with, regulate or functionally modulate EGFR inhibition, such as ligands of EGFR or cross-reacting receptors, molecules regulating *EGFR* expression or EGFRIs themselves, which might show correlations with clinical parameters (skin rash, OS, PFS).

A significant association between occurrence of EGFRI-induced skin rash and survival of the patients in the Dermatoxgen study was already shown in previous publications by this research group[104,106,107] and confirmed the studies by Saltz *et al*[37], Wacker *et al*[38] and Perez-Soler *et al*[39] and numerous others. These results confirmed that the Dermatoxgen patient cohort is suitable to investigate EGFRI-induced skin rash and search for potential biomarkers for this rash.

### V.1.2 Association between plasma concentrations of EGFRIs and skin rash and survival

In the Dermatoxgen patient cohort the serum concentration of the EGFRI erlotinib was not significantly associated with development of skin rash or survival of the patients, as shown in the publication by Steffens et al[107]. In order to better reflect the erlotinib metabolism of the patients, rather than just measuring single serum concentrations, Steffens et al. determined a metabolic ratio by dividing the serum concentration of erlotinib by the serum concentration of its main metabolite O-desmethyl-erlotinib. The calculated metabolic ratio was significantly correlated with the occurrence of EGFRI-induced skin rash (p-value = 0.0291). The metabolic ratio was also significantly associated with OS. A lower metabolic ratio means higher metabolic activity, which was associated with decreased survival.

In this present work we now investigated whether a correlation between plasma concentrations of cetuximab and development of skin rash and survival time could also be identified. Therefore, in patients from the Dermatoxgen study who were treated with the

mAb cetuximab the plasma concentration of this EGFRI was determined by a specific ELISA. The cetuximab plasma concentration was not significantly associated with development of skin rash, but a trend of association of higher cetuximab levels with development of rash can be seen in the graphic presentations. With regard to survival, higher concentrations of cetuximab were significantly associated with increased survival of the patients, but only if the concentration values were dichotomized (not when quartered). Only very high and very low concentration values of cetuximab seem to correlate with survival (positively or negatively, respectively).
It might be beneficial if a metabolic ratio for cetuximab could be determined, as it was previously done for erlotinib. However, there is no known metabolic product of cetuximab, whose concentration could be measured. The elimination routes of exogenous mAbs are not well characterized and it is believed that various mechanisms are involved, such as the reticuloendothelial system (RES) and target-mediated elimination, as well as non-specific endocytosis[120]. The mAbs are degraded into small peptides by lysosomes, therefore, specific metabolites cannot be identified.
Overall, at present metabolic ratios can only be determined for TKIs, not for mAbs.

### V.1.3 Association between plasma concentrations of the growth factors AREG and HGF and skin rash and survival

#### V.1.3.1 AREG

The plasma concentration of the EGFR ligand AREG was not significantly correlated with the development of EGFRI-induced skin rash or survival of the patients. This finding is in contrast to the results by Takahashi and colleagues, who found that patients with higher serum levels of AREG developed lower grades of skin toxicity[79]. This discrepancy in results could be due to the fact that they analyzed pre-treatment samples while in the Dermatoxgen study plasma samples were only available from four weeks after initiation of the EGFRI therapy. In previous studies the group around Takahashi showed that the serum levels of AREG increased during EGFRI therapy in 95 % of patients, while HGF levels only increased in 58 % of patients and also to a much lesser extent[121]. This might explain why higher concentrations of AREG were measured in the Dermatoxgen cohort (5-1303 pg/ml) than in Takahashi's cohort (3-636 pg/ml) and also in a cohort analyzed by Ishikawa and colleagues (10-380 pg/ml)[67]. Both of the other groups used pre-treatment serum samples for their analyses. Our results confirm that HGF is more stable as a biomarker than AREG over the course of therapy. However, it might be advisable to use plasma taken prior to the start of the EGFRI therapy.

Further studies to investigate the role of AREG plasma concentrations in EGFRI-induced skin rash and therapy response are needed, since currently conflicting results exist. In a recent study by Wang *et al.* AREG was identified as a possible prognostic marker in pancreatic ductal adenocarcinoma[122]. In that study, protein levels of AREG in the tumor tissue were inversely correlated with disease-free and overall survival. However, Llovet and colleagues found that in patients suffering from metastatic colorectal cancer high amounts of AREG mRNA in the tumor tissue correlated with better therapy response and increased OS[123]. Another group (Yonesaka et al.) also recently showed a correlation between high plasma levels of AREG (in combination with low levels of the ErbB3 ligand heregulin) and increased objective response rate to cetuximab in metastatic colorectal cancer[124]. The working group around Ishikawa on the other hand observed a significant correlation between high serum concentrations of AREG and poor response to gefitinib in patients with NSCLC[67].These studies show that AREG might play different roles in distinct types of cancer and that its concentration might have different meanings depending on whether it was determined in tumor tissue or blood serum/plasma.

#### V.1.3.2 HGF

In the Dermatoxgen patient cohort the plasma concentration of the MET ligand HGF was inversely correlated with OS of the patients (p-value = $2 \times 10^{-5}$). This result confirms the observations reported by Takahashi and colleagues in 2014[121]. They analyzed serum levels of different growth factors in patients with metastatic colorectal cancer who were treated with an anti-EGFR antibody and also found a significant inverse correlation between serum levels of HGF and OS. The results presented in this thesis show that the correlation between HGF levels and OS is not restricted to patients suffering from colorectal cancer and being treated with mAbs. Instead it can also be observed in a patient cohort including different types of cancers (lung, colon, pancreatic and head and neck cancer) and EGFRIs (mAbs and TKIs).

Subgroup analysis showed that the correlation between HGF concentration and OS was significant in patients suffering from lung and pancreatic cancer (p-values = 0.0018 and 0.00014, respectively) but not in patients suffering from colon and head and neck cancer (p-values = 0.63 and 0.59, respectively). A lack of correlation in the two latter groups might be due to the small number of patients with head and neck cancer (n = 6) and the fact that during the rather short follow-up period (360 days) only few patients suffering from colon cancer died, which means a longer follow-up time would have been necessary to determine factors correlated with the survival time.

It is well established that over-activated HGF/MET signaling increases invasive growth and metastasis by inducing motility of tumor cells and survival in remote tissue sites[77,78]. This effect could explain why higher levels of HGF are associated with decreased survival and it would rather render HGF a prognostic biomarker. However, the correlation between plasma concentration of HGF and OS was only significant in the subgroup of patients who had developed skin rash and not in the group without rash. This suggests that HGF might rather have a predictive implication for the efficacy of EGFR inhibition.

A significant inverse correlation between HGF levels and severity of EGFRI-induced rash was also observed when considering all four grades of rash (grades 0 to 3). This finding is in accordance with a Takahashi study from 2015, which also found that patients with higher serum levels of HGF developed lower grades of skin toxicity[79]. They measured a median HGF concentration of 1337 pg/ml in serum which is in accordance with our median of 1292 pg/ml determined in plasma. It remains unclear why no significant correlation was observed between HGF concentrations and skin rash yes/no (figure 14C). However, this might be due to some single outliers, which might call for further optimization of the ELISA assay and further standardization of sample handling at the various study sites.

The mechanism behind the correlation between HGF levels and skin rash is not completely understood so far. HGF/MET signaling has been linked to resistance to EGFRI therapy in many types of cancer[68], like NSCLC (gefitinib)[125,126] and colon cancer (cetuximab)[127]. MET can activate a number of pathways which are normally also activated by EGFR, like the MAPK, PLCγ and PI3K/Akt pathways[69]. It is probable that in signaling networks as complex as the ones containing EGFR and MET, certain effectors or even pathways are redundant for certain functions under specific physiological conditions[74,128]. When EGFR is inhibited in cancer therapy, tumor cells possibly evade death by increasing MET signaling, which shares a high number of effectors with the EGFR pathways. This offers an explanation for the correlation between plasma concentration of the MET ligand HGF and OS of the patients. This compensation of EGFR inhibition by HGF/MET signaling might also happen in skin cells and could explain why higher plasma concentrations of HGF correlate with less severe EGFRI-induced skin rash.

Several studies have already investigated possible signaling mechanisms of HGF and MET in keratinocytes. Animal studies in a mouse model for diabetes (impaired wound repair) showed that treatment of wounds with HGF increases re-epithelialization and reconstruction of an intact epidermal layer via migration and proliferation of

keratinocytes[70]. In 2007 Spix and colleagues found that in human corneal epithelial cells HGF stimulates EGFR and downstream effectors like ERK1/2 via MET and activation of EGFR ligands like AREG by proteolysis[129]. They also observed that directly after stimulation with HGF the resulting phosphorylation of ERK1/2 was not dependent on EGFR. Only about an hour after the HGF stimulation the phosphorylation of ERK1/2 could be regulated by EGFR. This indicates that HGF cannot just cross-activate the EGFR itself but also effectors of the EGFR independently of the receptor. The group also found indications for these mechanisms to be present in human epidermal keratinocytes.

Overall, HGF seems to be a promising predictive biomarker for the efficacy of EGFRI therapy. It should be noted that in the subgroup of patients who developed no skin rash a trend towards an association between plasma levels of HGF and OS was also visible. Even though this association was not significant, it might indicate that the plasma concentration of HGF is not exclusively predictive for therapy efficacy but also partially prognostic for patients' outcome (OS), independently of the activity of the EGFRI. It has been shown in a previous study in metastatic colorectal cancer patients that the occurrence of EGFRI-induced rash was significantly associated with OS in patients with mutations in codon 12 of *KRAS* in tumor cells[130]. Such a mutation leads to an EGFR-independent activation of the MAPK pathway, rendering EGFRIs ineffective and making it surprising that EGFRI-induced rash was still associated with OS. This suggests that, in addition to being predictive for EGFRI efficacy, the skin rash might also partially be a prognostic marker, which would match observations in the Dermatoxgen samples for HGF. Possible mechanisms explaining this still remain to be investigated. Immunological processes might be involved.

Of course due to its pivotal role in tumorigenesis and development of resistance to certain anti-cancer drugs, HGF is also a promising target for cancer therapy itself. In 2014 a randomized phase Ib/II trial evaluated the efficacy of a combination therapy with the EGFRI panitumumab and an anti-HGF antibody called rilotumumab in patients with metastatic colorectal cancer[131]. They found an improvement in objective response rate as compared to treatment with panitumumab alone (31 vs. 21 %). Therefore, HGF should also be further studied with regard to its role as target in cancer therapy.

### V.1.4 No association between plasma levels of vitamin D and EGFRI-induced skin rash

The suitability of 25-OH-vitamin D levels as biomarkers in EGFRI therapy was also investigated. No previous studies could be identified in which 25-OH-vitamin D has ever been investigated in this context. The mean 25-OH-vitamin D plasma concentration in the Dermatoxgen patient cohort was 21 ng/ml. In comparison, this concentration is higher than the mean concentration measured by Imtiaz and colleagues in a study cohort of 90 breast cancer patients, which was 9.3 ng/ml[132]. However, this discrepancy might be due to a different role of vitamin D in breast cancer patients than in patients suffering from lung, colorectal, pancreatic or head and neck cancer, which is not elucidated so far. In the same publication a mean serum vitamin D level of 14.9 ng/ml was reported in healthy controls, indicating that vitamin D levels seem to be decreased in breast cancer patients. In addition the use of a different assay kit might have led to higher values in our study cohort. Literature values for vitamin D levels, which were determined in patients suffering from the same types of cancer as patients in the Dermatoxgen study and which were measured with an ELISA method instead of other methodologies (e.g. HPLC) could not be identified for comparison.

There was no significant association between the plasma concentration of 25-OH-vitamin D and the development of EGFRI-induced skin rash in the Dermatoxgen cohort. VDREs had been identified in the promoter region[80-82] and intron 1[83] of the *EGFR* gene in previous studies by other groups and 25-OH-vitamin D had been shown to either increase or decrease EGFR mRNA and protein levels in different cancer cells[80,81]. However, according to our results, plasma levels of 25-OH-vitamin D do not seem to have an influence on EGFR signaling in skin cells or at least not to an extend which affects EGFR inhibition by the applied drugs or development of EGFRI-induced skin rash.

The vitamin D ELISA used in this study detects 25-OH-vitamin $D_2$ and $D_3$, so both types of vitamin D were taken into account for the analyses. Unfortunately, there are no standardized threshold values to define sufficiency and deficiency in vitamin D. Some studies and meta-analyses suggest that vitamin D levels > 30 ng/ml have a beneficial effect on OS in general and on the prevention and prognosis regarding certain diseases, such as common types of cancer and cardiovascular diseases[133,134]. Therefore, they suggest that plasma levels < 30 ng/ml define vitamin D insufficiency. However, a recent study by Hansen *et al.* found no beneficial effect on bone mineral density upon vitamin D supplementation for one year raising plasma levels from < 30 ng/ml (14 – 27 ng/ml) to > 30 ng/ml in postmenopausal women[117]. They suggest that vitamin D serum concentrations

of ≥ 20 ng/ml represent vitamin D repletion and hence support the conclusion of the Institute of Medicine from 2011, stating that 20 ng/ml is the cut-off value defining vitamin D sufficiency[116]. Some experts would set this cut-off value even lower (< 10 ng/ml), especially when the plasma/serum concentrations are determined using immunological methods, because these methods are not as sensitive as others[135]. Considering the high variation in serum and plasma concentrations of vitamin D measured with different methods, such as HPLC, luminescence assays or ELISAs, it would be most advisable to postulate standardized individual reference values for each specific method, but so far such values have not been implemented[136]. Until such reference values are established, conduction of vitamin D assays and interpretation of results will remain variable and unreliable.

In the Dermatoxgen patient cohort the plasma concentration of 25-OH-vitamin D was significantly correlated with metastasis (p-value = 0.0109). Patients who showed metastases at the beginning of the observation period had lower plasma concentrations of 25-OH-vitamin D than those who showed no metastases. This association has also been shown in various other studies, e.g. in multiple melanoma patients[118] and in breast cancer cells and mouse models of breast cancer[119]. The fact that the results of these previous investigations were confirmed in our study underlines the good quality of the Dermatoxgen plasma samples and the correct conduction of the assays. Further investigations about the mechanisms by which 25-OH-vitamin D deficiency mediates metastasis, were not part of the scope of this study.

## V.2 Cell model

### V.2.1 Primary human dermal keratinocytes as cell model for studying EGFRI-induced skin rash

To date the molecular mechanisms leading to the occurrence of EGFRI-induced skin rash are not completely understood. In order to identify and establish reliable predictive biomarkers for this rash, it is of great importance to further elucidate the pathways and single signaling molecules involved in its development. Since epidermal keratinocytes are the main type of skin cells involved in the pathophysiology of EGFRI-induced rash[58], they were chosen for further experiments to test their suitability as cell model for *in vitro* studies of the rash. First investigations were performed in epidermal keratinocytes from healthy human donors.

Characterization of the primary keratinocytes by visual examination and identification of specific keratinocyte markers confirmed that isolation and cultivation of primary keratinocytes from the donated skin samples was successful. Using Western blot analysis a strong signal for cytokeratin CK10 was detected across all established keratinocytes cultures, and a slight signal for CK14, also across all cultures. Keratins are structural proteins, which form heterodimers to build strong filamentous bundles in keratinocytes. In basal cells mainly keratin 5 and 14 are expressed, while in the upper skin layers (mainly in the stratum spinosum and to some extend also in the stratum granulosum) keratin 1 and 10 are the prevailing keratins[137]. This indicates that the established keratinocyte cultures mainly contained keratinocytes which were differentiated and rather resembled cells from the intermediate skin layers instead of the basal layer. Involucrin, which is a differentiation marker mainly found in cells of the two outer skin layers, stratum granulosum and stratum corneum, could not be identified in the established keratinocyte culture, indicating that the cells were not completely differentiated. It has to be noted however that no controls were available for Western blotting since the commercially available primary keratinocytes did not contain specifications about their differentiation status. Hence, the Western blot results have to be interpreted with caution. However, they can provide hints for characterization of the cell cultures and about potential inter-sample differences. The amounts of cytokeratin proteins detected seemed to be similar in all tested keratinocyte cultures, indicating that cells were in similar differentiation stages.

### V.2.1.1 *In vitro* effect of erlotinib in keratinocytes

Incubation of the established primary human keratinocytes with the EGFRI erlotinib showed that an optimal concentration to observe changes in cell signaling *in vitro* was between 5 and 10 µM. In comparison, Lankheet and colleagues measured a mean pre-dose plasma concentration of 3.1 µM erlotinib (1222 ng/ml) in NSCLC patients treated with 150 mg erlotinib per day for three weeks[138], which is similar to the mean serum concentration determined in the Dermatoxgen study: 1079.6 ng/ml. Lankheet and colleagues also measured a pre-dose concentration of 0.37 µM erlotinib (149 ng/ml) in tumor samples. The erlotinib concentrations used in the *in vitro* cell model described here are 1.5 to 25 fold higher than the plasma/tumor tissue concentrations measured in patients by Lankheet *et al*. However, it has to be taken into account that in our study healthy dermal cells were used, which might depend on EGFR signaling to a different extent than tumor cells (with overexpressed or over-activated EGFR) and therefore higher concentrations of EGFRIs might be needed to cause measurable *in vitro* effects. The erlotinib concentrations established in our study are in accordance with the concentrations used by several other groups in their *in vitro* experiments, e.g. by Commandeur *et al* for investigations about EGFR inhibition in 3D *in vitro* models of normal skin and cutaneous carcinoma (10 µM erlotinib used)[139] and by Miyazaki *et al* for establishing two novel *in vitro* drug sensitivity tests to predict molecular target drug responses in lung cancer cells (0.2 µM - 20 µM erlotinib used)[140].

In our study we showed that *in vitro* stimulation with the EGFR ligand EGF led to a significant increase in the amount of phosphorylated proteins involved in the well-known EGFR signaling pathways, indicating increased signaling activity. Prior incubation with erlotinib resulted in a significant decrease in the amount of these phosphorylated proteins, indicating successful inhibition of EGFR signaling *in vitro*. The strength of this inhibitory effect was different for the various investigated signaling proteins and it was strongest for the proteins EGFR, JNK 1/2/3, c-Jun, Src and AMPKα1. JNK is known as kinase from the MAPK pathway and c-Jun as its target, which is part of a complex (AP-1), which upon activation by phosphorylation binds to specific DNA sequences in the nucleus and alters gene expression[52]. Src (short for sarcoma) is a tyrosine kinase which is known to be involved in numerous pathways, triggered by a variety of receptors, including receptor tyrosine kinases, G-protein coupled receptors and adhesion receptors[141], rendering it difficult to analyze its role in one specific pathway. AMPKα1 is the catalytic subunit of the serine/threonine kinase AMPK, which regulates various key metabolic enzymes and protects the cell from ATP depletion. It is activated when decreases in ATP production result in relative increases in the levels of AMP or adenosine diphosphate in the cell. It is still not clear whether there is a cross-talk between EGFR and AMPK pathways. Guo and

colleagues found that activation of AMPK results in inhibition of glioblastoma cells, which is much more effective in tumors which are EGFR-activated[142]. Similarly, in breast cancer cell lines with amplification and over-expression of EGFR, activation of AMPK led to dose- and time-dependent inhibition of EGFR and eventually cell death, as shown by Jhaveri *et al*[143]. However, none of the groups further elucidated possible underlying mechanisms of the inhibitory effect of AMPK on EGFR signaling. It also remains elusive whether some kind of inverse feedback mechanism exists which might directly link an inhibition of EGFR with a decrease in the amount of phosphorylated AMPK in the cell or whether an inhibition of EGFR signaling might just lead to a reduced requirement of ATP in the cell and therefore also to a decrease of the cellular levels of activated AMPK. For further investigations of *in vitro* EGFR inhibition the proteins EGFR, JNK and c-Jun were chosen here, since their roles in EGFR signaling are considerably better understood.

Specific ELISAs for EGFR, JNK and c-Jun conducted across all available primary keratinocyte cultures showed that the phospho-EGFR ELISA was most suitable to measure the *in vitro* effect of erlotinib in human keratinocytes, with the best reproducibility among the tested assays. Therefore, results from the phospho-EGFR ELISA were used to group all available primary keratinocyte cultures into erlotinib-sensitive and rather erlotinib-insensitive cells (six versus six cultures). For all twelve keratinocyte samples miRNA profiles were determined by using NGS and compared between the six rather erlotinib-sensitive and the six rather erlotinib-insensitive samples.

#### V.2.1.2 Differences in miRNA profiles in erlotinib-sensitive versus -insensitive keratinocytes

Differences in miRNA profiles in erlotinib-sensitive as compared to rather erlotinib-insensitive keratinocytes were investigated using the same three different treatment options as in the prior experiments: EGF, erlotinib plus EGF and no treatment. Those miRNAs which were significantly differentially expressed across all three treatment options were considered to represent a “baseline” difference between the erlotinib-sensitive and -insensitive cells, which is independent of stimulation with EGF or incubation with erlotinib. There was only one such overlap miRNA identified, which was the precursor **mir-146a.**

Those miRNAs which were only significantly differentially expressed in cells incubated with erlotinib and not in the other treatment groups were also considered interesting because they might represent a difference in response to erlotinib in erlotinib-sensitive as compared to -insensitive keratinocytes. Nineteen respective precursor miRNAs and 13

mature miRNAs were identified. A literature search revealed that some of these identified miRNAs were also identified in other studies with potential roles in EGFR signaling and inhibition, which strengthened the evidence for these candidate miRNAs. Those miRNAs were **mir-31, mir-138-2, mir-221, mir-520e** and **mir-944**.

mir-146a/miR-146a-5p

In erlotinib-sensitive keratinocytes expression of precursor mir-146a and the corresponding mature form miR-146a-5p were down-regulated as compared to erlotinib-insensitive cells, across all three treatment options, in NGS (significantly) as well as in PCR assays.

Mir-146a is known as a tumor suppressor gene, whose expression was found to be lower in tumor tissue than in healthy control tissue as shown for example in NSCLC[144] and pancreatic cancer[145] patients. In a recent bioinformatics analysis conducted by Huang and colleagues, using twelve different online software programs, target genes of miR-146a-5p were predicted[146]. EGFR and JUN were among the “Top targets” found with most of the software.

In addition, inhibition of mir-146a was found to result in up-regulation of EGFR in various cell lines, while re-expression of mir-146a led to a decrease in EGFR mRNA and protein levels (pancreatic cancer cells[147], hepatocellular cancer cells[148], NSCLC cells[144]). Interestingly, it was also shown in *in vitro* experiments that transfection with mir-146a had an additive inhibitory effect on cancer cell proliferation together with each of the TKIs afatinib, gefitinib and erlotinib as well as with the mAb cetuximab[144,148]. In our study keratinocytes in which phosphorylated EGFR was effectively down-regulated by erlotinib had lower baseline expression of mir-146a/miR-146a-5p than those in which erlotinib was rather not effective. In keratinocytes with low levels of mir-146a there might be less translational repression of EGFR, possibly resulting in higher dependence on EGFR signaling than in cells with high levels of mir-146a. Therefore, inhibition of EGFR phosphorylation by erlotinib might have a more pronounced effect in cells with previous lower levels of mir-146a. On the other hand, if due to high baseline expression of mir-146a there are low levels of EGFR, alternative signaling pathways might be up-regulated, such as the HGF/MET pathway for example, rendering later use of EGFRIs rather ineffective (e.g. because of less activation/phosphorylation of EGFR). However, this hypothesis warrants further confirmation, as the conducted cell-based phospho-ELISAs were not suitable to analyse differences in EGFR expression across cell samples.

Taken together, mir-146a shows potential with regard to its baseline levels in skin cells as possible predictive marker for efficacy of EGFRIs, as well as potential as an adjuvant inhibitor which might be effective when administered together with an EGFRI.

mir-31

According to NGS results, mir-31 was significantly down-regulated in erlotinib-sensitive keratinocytes as compared to rather erlotinib-insensitive ones. However, this effect was not confirmed by PCR and the effect was rather small in in cells treated with EGF alone (fold-change 0.79) and those left untreated (fold-change 0.77). This effect was also not observed for the mature form miR-31-3p.

Nevertheless, the observed small association between low levels of mir-31 and increased sensitivity towards erlotinib is in accordance with the results previously obtained by several other groups. Four different research groups, partially using overlapping patient cohorts but also partially using independent ones, observed a significant association between high levels of miR-31-3p and/or miR-31-5p and low response to anti-EGFR therapy (mainly with cetuximab), defined by short PFS, in patients with metastatic colorectal cancer and WT Ras[149-152].

These results indicate that mir-31 is a promising predictive marker for response to EGFRI therapy. However, at this time clear targets of mir-31 have not been identified reliably and therefore the mechanism behind the predictive value of mir-31 remains unknown.

mir-138-2/miR-138-5p

There are two genomic loci known in humans which express the mature miRNA sequence of miR-138. The respective precursor miRNAs are named mir-138-1 and mir-138-2. In this study expression of mir-138-2 was investigated in keratinocytes. Expression of mir-138-2 was down-regulated in erlotinib-sensitive as compared to -insensitive cells, which was significant in those cells which were previously treated with erlotinib.

Contrary to these results, in a study by Gao et al. miR-138-5p was found to be the most down-regulated miRNA in a gefitinib-resistant lung cancer cell line as compared to a gefitinib-sensitive cell line[153]. They confirmed this down-regulation in 20 pairs of lung adenocarcinoma specimens and adjacent non-cancerous tissue samples. Using bioinformatics analysis and luciferase reporter assay they found that the G protein-coupled receptor (GPR) 124 was a direct target of miR-138-5p. Interestingly, re-expression of miR-138-5p was sufficient to re-sensitized the cells to gefitinib. Similarly, a recent Chinese study from 2016 found that in cervical cancer cells miR-138 could directly target the receptor MET and was down-regulated in the cancer cells as compared to adjacent non-cancerous tissue[154]. Based on these results it might be expected that in our cells miR-138 would also be up-regulated in erlotinib-sensitive as compared to -insensitive cells, leading to decreased levels of MET and therefore higher dependence on the EGFR signal cascade and higher efficacy of EGFRIs. However, miR-138-2 expression was down-regulated in our keratinocyte experiments in erlotinib-sensitive as compared to -

insensitive cells, which was significant in those cells which were previously treated with erlotinib. Potential differences between miR-138 and mir-138-2 cannot be excluded, as well as differences of their functions in cancer cells as compared to skin cells. Considering the significant down-regulation of mir-138-2 only in those keratinocytes previously treated with erlotinib, it might be speculated that there could be some kind of feedback mechanism, inhibiting expression of mir-138-2 upon EGFR inhibition by erlotinib to increase levels of MET to compensate for the blockage of signaling via EGFR. However, this remains purely speculative and further insights into the regulation of miR-138/mir-138-2 expression will be essential for further investigations and conclusions. It might be more promising to investigate the therapeutic potential of mir-138-2 in future studies.

mir-221/miR-221

In the keratinocyte experiments mir-221 was downregulated in erlotinib-sensitive cells when previously treated with erlotinib. It was previously demonstrated by Garofalo and colleagues that upon silencing of EGFR and MET in NSCLC cell lines, miR-221 expression decreased, indicating regulation of this miRNA by the two receptor tyrosine kinases[155]. Interestingly, suppression of miR-221 also increased sensitivity of the cells towards the EGFRI gefitinib, presumably because miR-221 targeted apoptotic protease activating factor 1 (APAF1), which mediates gefitinib-induced apoptosis[156]. This means when expression of miR-221 is high, APAF1 is down-regulated leading to inhibition of the pro-apoptotic effect of gefitinib. Our results in keratinocytes are in accordance with the results by Garofalo et al. and suggest that upon inhibition of EGFR signaling by erlotinib, expression of miR-221 is down-regulated. It is unclear whether this inhibition of miR-221 also to some extend confers the growth inhibitory effect of erlotinib via up-regulation of certain target genes of this miRNA. Further studies are warranted to investigate this possibility. Nevertheless, it has to be kept in mind that miR-221 was not significantly down-regulated in erlotinib-sensitive keratinocytes treated with EGF alone or left untreated, indicating that it only seems to play a role after administration of erlotinib. Hence, with regard to its potential as predictive biomarker for the efficacy of erlotinib, it would not be suitable to just determine the levels of miR-221 in skin cells of patients prior to treatment with erlotinib. Instead it would be necessary to cultivate a cell sample from the patient, incubate the cells with erlotinib and then measure the amount of miR-221 to predict the sensitivity to erlotinib. Feasibility of this method has to be considered.

mir-520e

The miRNA mir-520e was significantly down-regulated in erlotinib-sensitive keratinocytes as compared to the rather erlotinib-insensitive ones, but only in cells previously incubated with erlotinib, not under the other treatment conditions.

In a publication by Li and colleagues it was shown that miR-520e (and miR-520b) can directly bind to the 3' UTR of EGFR and thereby inhibit EGFR expression[157]. The fact that mir-520e was only differentially expressed in keratinocytes previously treated with erlotinib leads to the speculation that inhibition of EGFR by erlotinib in erlotinib-sensitive keratinocytes might trigger a kind of feed-back mechanism leading to down-regulation of mir-520e and in turn less inhibition of EGFR expression to increase activation of EGFR signaling. However, at this time this assumption remains highly speculative.

mir-944

In erlotinib-sensitive keratinocytes mir-944 expression was up-regulated as compared to erlotinib-insensitive keratinocytes. mir-944 has previously been shown to target certain proteins involved in cell migration (SIAH1 and PTP4A1) in breast cancer cells and was suggested to be a tumor suppressor[158].

In a study from 2014 mir-944 was found to target the tumor suppressor protein suppressor of cytokine signaling (SOCS) 4 in NSCLC cells[159]. SOCS4 is known to regulate EGFR signaling by binding to EGFR and suppressing its signal transduction[160]. Higher levels of mir-944 lead to lower levels of SOCS4 and therefore to increased EGFR signaling and cell proliferation. However, a more recent study found that mir-944 can target the tyrosine kinase receptor ephrin type-A receptor 7 (EPHA7) and inhibit proliferation of NSCLC cells[161].

The two studies have contrary results. It is unclear which role of mir-944 is supported by our results in keratinocytes. However, it might be speculated that higher levels of mir-944, leading to increased EGFR signaling via suppression of SOCS4, could render cells more sensitive to EGFR inhibitors like erlotinib, due to a higher dependence of these cells on this signaling pathway.

Summary of identified miRNAs

A summary of data collected for each candidate miRNA including analysis of potential as predictive biomarker for efficacy of EGFRIs is provided in table 33.

**Table 33 Summary of suitability of identified miRNAs as predictive biomarkers in keratinocytes**

Summary of data collected about candidate miRNAs identified in keratinocytes in this study, including supporting and conflicting aspects concerning suitability as predictive biomarkers for efficacy of EGFRIs. Arrows mean up- or down-regulated in erlotinib-sensitive as compared to -insensitive cells, respectively.

| | **suitability as predictive biomarker for EGFRI efficacy** | | |
|---|---|---|---|
| **miRNA (expression in erlotinib-sensitive cells)** | **supporting aspects +** | **conflicting aspects -** | **future steps** |
| mir-146a/ miR-146a-5p (↓) | - differential expression observed for precursor and mature form, across all treatment options and using NGS and PCR (rather stable results)<br>- EGFR and Jun reported as direct targets in literature (plausible mechanism)[148] | | - check correlation between levels in skin cells and clinical response in patients<br>- investigate therapeutic potential |
| mir-31/ miR-31-3p (↓) | - differential expression confirms publications in metastatic colorectal cancer treated with anti-EGFR mAbs (associated with shorter PFS)[149-152] | - only small effect detected (low fold-change), not confirmed by PCR<br>- no suggested target/mechanism yet | - identify target(s)<br>- confirm results in other types of cancer and with other types of EGFRIs |
| mir-138-2 (↓) | - large fold-change and high significance of differential expression in erlotinib-treated cells | - differential expression only significant in erlotinib-treated cells<br>- opposite associated with erlotinib-sensitivity than reported in publication for gefitinib-sensitivity in lung cancer cells[153] | - potential therapeutic value could be further investigated |
| mir-221 (↓) | - differential expression in erlotinib-treated cells is in accordance with a publication about expression in lung cancer cells treated with gefitinib[155] | - association with erlotinib-sensitivity only observed upon incubation with erlotinib | - investigate down-stream effect of miRNA inhibition and correlations in skin and cancer cells<br>- confirm in patients |
| mir-520e (↓) | - large fold-change and high significance of differential expression in erlotinib-treated cells<br>- EGFR reported as direct target in literature (plausible mechanism)[157] | - association with erlotinib-sensitivity only observed upon incubation with erlotinib | - identify target(s) in skin cells and further explore why differential expression only observed upon incubation with erlotinib |
| mir-944 (↑) | - SOCS4 reported as target in literature, which can block EGFR (plausible mechanism)[159] | - differential expression not significant in untreated cells | - identify target(s) in skin cells<br>- confirm correlation of miRNA level in skin and cancer cells of patients |

Abbreviations: EGFRI, epidermal growth factor receptor inhibitor; NGS, next generation sequencing; PCR polymerase chain reaction; SOCS, suppressor of cytokine signaling.

### V.2.2 Primary human dermal fibroblasts as cell model for studying EGFRI-induced skin rash

Even though epidermal keratinocytes are thought to be the main type of skin cells involved in the pathophysiology of EGFRI-induced rash[58], dermal fibroblasts may also play a role. It has long been known that fibroblasts are involved in inflammatory processes. They can determine quantity, quality, and duration of the inflammatory infiltrate, mainly by producing and secreting a variety of cytokines, which recruit or even inhibit different immune cells, as for example experimentally shown in a mouse model for arthritis[162] and also thoroughly reviewed by Linthout *et al*[163]. In the skin of EGFRI-treated patients an immunological infiltrate can be found prior to and during the occurrence of EGFRI-induced skin toxicity[64]. Hence, dermal fibroblasts might also be involved in the development of EGFRI-induced skin rash and were therefore also further investigated in the study presented here for their suitability as cell model to study the rash.

#### V.2.2.1 *In vitro* effect of erlotinib in fibroblasts

Incubation of the established primary human dermal fibroblasts with the EGFRI erlotinib showed that, as for the keratinocytes, again an optimal concentration to observe changes in cell signaling was between 5 and 10 µM.

*In vitro* stimulation with the EGFR ligand EGF also led to a significant increase in the amount of phosphorylated proteins involved in EGFR signaling pathways in fibroblasts and prior incubation with erlotinib resulted in a significant decrease in the amount of these phosphorylated proteins, indicating successful inhibition of EGFR signaling *in vitro*. Interestingly, the strongest inhibitory effect was found for different proteins as in the keratinocytes. In the fibroblasts the effect was strongest for EGFR, ERK1/2, Akt1/2/3, TOR and Src. Phosphorylation of EGFR and Src was also strongly inhibited by erlotinib in keratinocytes. However, in fibroblasts erlotinib decreased the level of phosphorylated protein most remarkably for the MAPK ERK. *In vitro* stimulation with EGF also stimulated phosphorylation of ERK to a much higher extend than phosphorylation of the other tested proteins. In fibroblasts the MAPK ERK seems to play a more important role in the EGFR signaling pathway than the MAPK JNK, while in keratinocytes JNK seems to be more important. No publications could be identified which previously compared EGFR signaling in keratinocytes and fibroblasts.

It is also remarkable that in fibroblasts *in vitro* treatment with erlotinib has a very strong inhibitory effect on the kinases Akt (1/2/3) and TOR. These two proteins are important signaling molecules of the PI3K/Akt pathway. Erlotinib seems to have a strong inhibitory effect on this pathway in fibroblasts. In keratinocytes on the other hand erlotinib does not

seem to have such a considerable inhibitory effect on the proteins involved in the PI3K/Akt pathway. These results suggest that EGFR signaling as well as the effect of EGFRIs is different in human dermal fibroblasts as compared to keratinocytes, with different signaling molecules having distinct importance. This also has to be taken into consideration when selecting an appropriate cell model for investigations about EGFRI-induced skin toxicity.
For further investigations of *in vitro* EGFR inhibition in fibroblasts, specific ELISAs for EGFR and ERK 1/2 were conducted across all available primary fibroblast cultures. The ERK 1/2 ELISA was found to be most suitable to detect differences in EGFR inhibition upon incubation with erlotinib between the different cell samples.

The results from the phospho-ERK 1/2 ELISA were used to group the various fibroblast cultures into erlotinib-sensitive and rather -insensitive cells. The “edge groups” were selected, meaning the four most erlotinib-sensitive and the four most erlotinib-insensitive cell samples. Two cell samples were excluded from this selection (FB131 and FB84) because in these cells incubation with erlotinib resulted in a higher amount of phosphorylated ERK 1/2 than stimulation with EGF alone, indicating that either the assay did not work correctly with them or there was another unidentified problem with the cells or their signaling cascades. In the selected edge groups the miRNA profiles were determined by NGS and compared between the four rather erlotinib-sensitive and the four rather erlotinib-insensitive samples.

#### V.2.2.2 Differences in miRNA profiles in erlotinib-sensitive versus -insensitive fibroblasts

Analyses were performed analogous to the ones in keratinocytes. In fibroblasts there were 34 precursor and 16 mature miRNAs identified which were significantly differentially expressed in erlotinib-sensitive as compared to -insensitive cells across all three treatment options. A literature search revealed that some of these identified miRNAs were also identified in other studies with potential roles in EGFR signaling and inhibition, which strengthened the evidence for these candidate miRNAs. Those miRNAs were **mir-34a, mir-17, mir-30b, mir-382, mir-494,** and **mir-520e.**
Those miRNAs which were only significantly differentially expressed in cells incubated with erlotinib and not in the other treatment groups and were confirmed by literature search were **mir-7-1** and **mir-31**.

mir-34a/miR-34a-5p

In erlotinib-sensitive fibroblasts expression of mir-34a (significantly) and its mature form miR-34-5p (non-significantly) were up-regulated as compared to rather erlotinib-insensitive fibroblasts, which was observed across all three treatment options in NGS (and partially confirmed by PCR). These results agree with the results obtained by a Chinese group around Zhou, who investigated the role of miR-34a in two gefitinib-resistant lung adenocarcinoma cell lines and in a gefitinib-resistant mouse xenograft model[164]. They found that forced expression of miR-34a down-regulated the receptor tyrosine kinase MET by direct targeting and induced apoptosis in the gefitinib-resistant cell lines. In the gefitinib-resistant mouse xenograft model, the combination of miR-34a and gefitinib caused dramatic tumor regression, much more effectively than monotherapy with either one of them. In a very recent American study published in 2017 by Zhao and colleagues, a synergistic anti-proliferative effect was also observed for miR-34a together with next generation TKIs, like afatinib, and osimertinib, in EGFR mutant NSCLC cell lines[165]. Taken together, miR-34a is a promising candidate predictive biomarker for efficacy of EGFRIs, which might be worth investigating in more detail in clinical settings.

mir-17

The expression of mir-17 was up-regulated in erlotinib-sensitive fibroblasts as compared to the rather erlotinib-insensitive ones across all three treatment options. Recently published results of *in vitro* experiments with mir-17 by two different Chinese groups are contradicting. One group showed that expression of miR-17-5p was higher in gefitinib-resistant NSCLC cells (A549/GR cell line) than in gefitinib-sensitive ones (A549 cell line) and that transfection with miR-17-5p mimic reduced sensitivity to gefitinib in the A549 NSCLC cells[166]. The other group showed that expression of miR-17-5p was lower in erlotinib-resistant NSCLC cells (A549/ER) than in erlotinib-sensitive ones (A549)[167]. The second group confirmed their observation also in tumor samples and plasma of erlotinib-sensitive as compared to erlotinib-resistant NSCLC patients. Our results in fibroblasts also confirm the results by the second group around Zhang. However, it remains unclear whether the use of the EGFRI gefitinib instead of erlotinib in fibroblasts would lead to different results.

It should be noted that in 2015 low expression of mir-17 was also shown to be associated with resistance to chemotherapy with cisplatin[168]. This was suggested to be due to an up-regulation of the target proteins cyclin-dependent kinase inhibitor 1A (CDKN1A) and cohesion complex component RAD21, which leads to increased cell cycle arrest and increased DNA repair, respectively, mediating resistance to cisplatin-induced apoptosis.

Since patients who are treated with an EGFRI usually also receive a type of chemotherapy in addition, the role of miR-17 in response to chemotherapy should also be further investigated. Large patient cohorts and control groups, e.g. receiving chemotherapy alone, will be essential to clarify the predictive role of miR-17. It is also important to identify the target(s) of mir-17 and to elucidate its mechanism of action.

mir-30b

As described for miR-221 in the keratinocyte section (refer to V.2.1.2) it was shown in the same study by Garofalo et al. in NSCLC cell lines that upon silencing of EGFR and MET miR-30b expression decreased, indicating regulation of this miRNA by the two receptor tyrosine kinases[155]. This decrease in miR-30b levels also increased sensitivity of the cells towards the EGFRI gefitinib. MiR-30b can target the pro-apoptotic factor Bcl-2-like protein 11 (BIM), which was previously shown to mediate TKI-induced apoptosis[169]. The study by Garofalo et al. suggests that if expression of miR-30b is high, BIM is down-regulated leading to inhibition of the pro-apoptotic effect of gefitinib. In our fibroblast experiments however, miR-30b was up-regulated in erlotinib-sensitive as compared to rather erlotinib-insensitive cells across all three treatment options. This is not in accordance with the results of the Garofalo study. However, it confirms a study conducted by Gu and colleagues conducted in 2013, who retrospectively examined expression of miR-30b in 41 paraffin-embedded tumor samples from NSCLC patients who had been first-time treated with a TKI[170]. They observed that higher expression of miR-30b was associated with longer OS (miR-30b low expression group: median OS 7.5 months; miR-30b high expression group: median OS 17.4 months). Taken together, the results about potential functions of miR-30b in cancer and efficacy of EGFRIs as studied in cell lines and tumor samples are controversial. The Gu study has similar limitations to our study since association of miR-30b expression with patient outcome has not been studied in a control group of patients not treated with a TKI. Therefore, the predictive potential of miR-30b in EGFRI therapy remains uncertain.

mir-382

In fibroblasts the expression of mir-382 was increased in the erlotinib-sensitive group as compared to the erlotinib-insensitive one. According to literature the role of mir-382 seems to be different in different types of cancer. In breast cancer tissue miR-382-5p was found to be up-regulated[171], while in hepatocellular carcinoma tissue it was found to be down-regulated as compared to non-cancerous control tissue[172]. In the hepatocellular carcinoma study Golgi Membrane Protein 1 (GOLM1) was suggested as target of the mature miRNA

miR-382. However, this target protein does not explain the differential expression of mir-382 observed in erlotinib-sensitive as compared to -insensitive fibroblasts. In the breast cancer study Ras-related and estrogen-regulated growth inhibitor (RERG) was suggested as target protein of miR-382-5p. This protein is a Ras superfamily small GTPase, which deactivates Ras/ERK signaling effectors, and therefore its suppression by miR-382-5p would lead to increased activation of the MAPK signaling pathway, which can be activated by EGFR. This mechanism might also be present in fibroblasts and such an increase in activation of MAPK signaling might also explain why higher expression of mir-382 renders fibroblasts more susceptible to the EGFRI erlotinib. However, at this time it is unclear to what extend the protein RERG is expressed and active in fibroblasts. Therefore, further investigations about expression and activity of RERG in fibroblasts and about targets of mir-382 in general will be necessary to draw reliable conclusions about this miRNA with respect to its role in response to EGFRIs.
Interestingly, in a study in murine and human hepatocytes mir-382 was found to target the protein phosphatase and tensin homolog (PTEN), which when active dephosphorylates several signaling molecules from the PI3K-Akt pathway and therefore is an important inhibitor of this pathway[173]. It can be speculated that PTEN might also be a target of mir-382 in fibroblasts and that via this mechanism increased expression of mir-382 might lead to increased activation of the EGFR-PI3K-Akt pathway and therefore to increased susceptibility of fibroblasts to the EGFRI erlotinib.

mir-494

The expression of mir-494 was increased in the erlotinib-sensitive group of fibroblasts as compared to the erlotinib-insensitive group. In the literature mir-494 is discussed with respect to its role in various types of cancer and numerous potential targets are suggested for this miRNA depending on the type of tissue. As already suggested for mir-382 (see previous section) the phosphatase PTEN has been shown to be a direct target of mir-494, e.g. in colorectal cancer tissue[174] and NSCLC[175]. As already speculated for mir-382, PTEN might also be a target of mir-494 in fibroblasts and via this mechanism increased expression of mir-494 might lead to increased activation of the EGFR-PI3K-Akt pathway and therefore to increased susceptibility of fibroblasts to the EGFRI erlotinib.
However, there are additional hypotheses which arise from review of the abundant literature on mir-494. A study by Kwak et al. for example found that in glioma cells miR-494 directly targets the GTPase activating protein p190B, which in turn leads to stabilization of EGFR at the cell surface through decreased lysosomal degradation[176]. This mechanism could also explain why increased expression of mir-494 renders fibroblasts more sensitive to the EGFRI erlotinib.

A further study by Romano et al. suggests that miR-494 expression is up-regulated by ERK1/2 via its down-stream transcription factor AP-1 in NSCLS cells[177]. However, if this mechanism was also present in fibroblasts, erlotinib-sensitive fibroblasts should show a decrease in mir-494 levels upon incubation with erlotinib, due to an inhibition of the EGFR down-stream signaling molecule ERK1/2. Since this was not observed in our fibroblast experiments, it is questionable whether the mechanism suggested by Romano et al. is also present in skin cells.
Specific target analyses for mir-494 in fibroblasts are inevitable to draw further conclusions.

mir-520e

In fibroblasts mir-520e was significantly down-regulated in erlotinib-sensitive as compared to rather erlotinib-insensitive cells across all three treatment options. As already discussed for the keratinocyte experiments, in a publication by Li and colleagues it was shown that miR-520e (and miR-520b) can directly bind to the 3' UTR of EGFR and thereby inhibit EGFR expression in gastric cancer cells[157]. This mechanism might also be present in fibroblasts and lower levels of mir-520e would lead to increased expression of EGFR and therefore possibly also higher sensitivity towards EGFR inhibition by erlotinib. This mechanism would render mir-520e a very promising predictive biomarker for the response to erlotinib.
However, in keratinocytes mir-520e was only differentially expressed in cells previously treated with erlotinib and not across the other treatment options. Whether the role of mir-520e might be different in fibroblasts and keratinocytes or whether expression analyses did not work properly in one of the two cell types remains unknown and warrants further validation experiments.

mir-7-1

Mir-7-1 was up-regulated in erlotinib-sensitive fibroblasts as compared to -insensitive ones (significant in cells treated with erlotinib). It has been shown in a previous study that miR-7 can down-regulate EGFR mRNA and protein expression in various cancer cell lines (lung cancer, breast cancer, glioblastoma) via two different target sites in the EGFR 3'UTR[178]. Microarray and bioinformatics analysis also conducted in that study suggested that there might be additional direct targets of miR-7 down-stream of EGFR in its signaling pathways, such as the protein kinase RAF-1. This might point to a synergistic effect of miR-7 on EGFR inhibition together with erlotinib and might explain the up-regulation of miR-7 detected in erlotinib-sensitive fibroblasts. Interestingly, in a study by Suto et al.

expression of the precursor mir-7 was found to sensitize two different colon cancer cell lines harboring *KRAS* mutations to the mAb cetuximab[101]. Cells with *KRAS* mutations are usually cetuximab-resistant. It was suggested by the authors that in cells with *KRAS* mutations KRAS signals to ERK 1/2 rather through RAF-1, instead of through BRAF, like it is mainly seen in *KRAS* WT cells. MiR-7 can target RAF-1 and thus might increase the cells' sensitivity towards EGFR inhibition by cetuximab. A similar mechanism might exist in fibroblasts, which would match our results with the EGFRI erlotinib. However, the study by Suto also showed that in a cell line harboring a BRAF mutation mir-7 expression was not effective in sensitizing the cells to cetuximab. This result emphasizes that the various functions of miRNAs are highly specific and in further investigations mutation statuses of certain signaling molecules might also have to be taken into account. Nevertheless, mir-7/mir-7-1 is a promising candidate as predictive biomarker for EGFRI efficacy and might be worth studying in more detail in clinical settings.

mir-31

In fibroblasts mir-31 was up-regulated in erlotinib-sensitive cells as compared to rather erlotinib-insensitive ones. This effect was only significant for those cells previously incubated with erlotinib. This result is not in accordance with the results obtained in keratinocytes and it is also contrary to the results previously published by other groups. As already discussed in the keratinocyte section, four different research groups, partially using overlapping patient cohorts but also partially using independent ones, observed a significant association between high levels of miR-31-3p and/or miR-31-5p and low response to anti-EGFR therapy (mainly with cetuximab), defined by short PFS, in patients with metastatic colorectal cancer and WT Ras[149-152]. However, the four mentioned studies did not identify clear targets of mir-31, which makes it impossible to say whether the same targets are also present in fibroblasts.

Summary of identified miRNAs

A summary of data collected for each candidate miRNA including analysis of potential as predictive biomarker for efficacy of EGFRIs is provided in table 34.

**Table 34 Summary of suitability of identified miRNAs as predictive biomarkers in fibroblasts**

Summary of data collected about candidate miRNAs identified in fibroblasts in this study, including supporting and conflicting aspects concerning suitability as predictive biomarkers for efficacy of EGFRIs. Arrows mean up- or down-regulated in erlotinib-sensitive as compared to -insensitive cells, respectively.

| | **suitability as predictive biomarker for EGFRI efficacy** | | |
|---|---|---|---|
| **miRNA (expression in erlotinib-sensitive cells)** | **supporting aspects +** | **conflicting aspects -** | **future steps** |
| mir-34a/ miR-34a-5p (↑) | - differential expression observed for precursor and mature form, across all treatment options and using NGS and partially also PCR (rather stable results)<br>- differential expression confirms 2 publications about a synergistic effect with TKIs in cancer cells/a xenograft mouse model[164,165]<br>- MET reported as direct target (plausible mechanism)[164] | | - confirm predictive properties for efficacy of EGFRIs in patients |
| mir-17 (↑) | - differential expression significant across all treatment options<br>- differential expression confirms a publication about association of low levels with erlotinib-resistance in NSCLC patients[167] | - opposite association with erlotinib-sensitivity than reported for gefitinib-sensitivity in NSCLC cells in a Chinses study[166] | - identify target(s) and elucidate mechanism of action<br>- check predictive potential in patients and elucidate if there are differences between different EGFRIs |
| mir-30b (↑) | - differential expression confirms a previous retrospective study about association of expression in tumors with overall survival in patients treated with a TKI[170] | - opposite association with erlotinib-sensitivity than reported for gefitinib-sensitivity in NSCLC cells in a publication[155] | - identify target(s) and elucidate mechanism of action<br>- confirm predictive potential in larger patient cohorts including an adequate control arm |
| mir-382 (↑) | - large fold-change and high significance of differential expression across all treatment options, also confirmed by PCR<br>- RERG and PTEN suggested as targets (plausible mechanisms)[171,173] | | - clarify relevant target(s) (RERG and PTEN relevant in fibroblasts?)<br>- confirm predictive properties for efficacy of EGFRIs in patients |

| | | | |
|---|---|---|---|
| mir-494<br>(↑) | - large fold-change and high significance of differential expression across all treatment options, also confirmed by PCR<br>- PTEN and p190B suggested as targets (plausible mechanisms)[174-176] | | - confirm predictive properties for efficacy of EGFRIs in patients |
| mir-520e<br>(↓) | - large fold-change and high significance of differential expression, especially in untreated cells<br>- EGFR reported as direct target in literature (plausible mechanism)[157] | | - confirm predictive properties for efficacy of EGFRIs in patients |
| mir-7-1<br>(↑) | - differential expression confirms a study in colon cancer cells where this miRNA sensitized cells with *KRAS* mutation to cetuximab[101]<br>- EGFR and RAF reported as target in literature (plausible mechanism)[178] | - differential expression only observed upon incubation with erlotinib and not confirmed for mature form | - clarify mechanism of action and association with *KRAS* mutations<br>- investigate why only significant in cells treated with erlotinib<br>- confirm correlation of miRNA level in skin and cancer cells of patients |
| mir-31<br>(↑) | - differential expression significant in cells previously treated with erlotinib | - differential expression only observed upon incubation with erlotinib and not confirmed for mature form<br>- opposite regulation than in keratinocytes<br>- opposite association with erlotinib-sensitivity than reported association with response to anti-EGFR therapy in patients in 4 previous studies[149-152] | - identify target(s)<br>- rather further investigate predictive potential in keratinocytes than in fibroblasts because so far results more promising in that cell type |

Abbreviations: EGFRI, epidermal growth factor receptor inhibitor; NGS, next generation sequencing; NSCLC, non-small cell lung cancer; PCR polymerase chain reaction; PTEN, phosphatase and tensin homolog; RERG, Ras-related and estrogen-regulated growth inhibitor; TKI, tyrosine kinase inhibitor.

### V.2.3 Most suitable cell model - comparison between keratinocytes and fibroblasts

Throughout all experiments and analyses included in this thesis, it has been clearly observed that primary human dermal keratinocytes and primary human dermal fibroblasts greatly differ, with regard to regulation of proteins involved in signaling cascades induced via EGFR as well as with regard to miRNA profiles. This means that the two dermal cell types are not interchangeable as cell models to study areas such as EGFR signaling and EGFRI-induced skin rash. Biomarkers established in one cell type most likely will not be usable in the other one.

*In vitro* effect of erlotinib on EGFR signaling

While for both cell types an optimal concentration of erlotinib to observe changes in cell signaling *in vitro* was found to be between 5 and 10 µM, the inhibitory effect of erlotinib was different for specific signaling proteins in keratinocytes and fibroblasts. In keratinocytes the MAPK JNK seemed to play a more important role in the EGFR signaling pathway than the MAPK ERK, while in fibroblasts it was the other way around. In addition, in fibroblasts *in vitro* treatment with erlotinib had a very strong inhibitory effect on proteins of the PI3K/Akt pathway (Akt (1/2/3) and TOR), while in keratinocytes erlotinib did not seem to have such a considerable inhibitory effect on this pathway. These results are in accordance with a study from 2002, in which strong activity of ERK1/2 and Akt was verified *in vitro* in fibroblasts in early as well as late passages (but not in senescent cells)[179], suggesting an important role of these two pathways in proliferating fibroblasts. In contrast to the results described here, in some publications activity of ERK1/2 and Akt has also been described in dermal keratinocytes and was shown to be important for proliferation and differentiation in this cell type. For example, PI3K/Akt signaling has been shown to be essential in keratinocyte differentiation in mice *in vivo*[180]*.* Nevertheless, in human dermal keratinocytes the PI3K/Akt and ERK1/2 pathways might be more importantly regulated via other receptors than via EGFR, as also suggested in the study by Sadagurski and colleagues[181], in which the insulin-like growth factor 1 receptor (IGF-1R) very strongly mediated activation (phosphorylation) or inhibition of the signaling proteins ERK1/2 and Akt in primary mouse keratinocytes. Another explanation might be that the two signaling cascades are differentially active depending on the specific conditions present at a given time. Akt and ERK1/2 have for example been shown to become activated by mechanical stretching in human dermal keratinocytes[182], indicating that external stimuli might change the activity of certain signaling molecules and therefore most likely also the effect of specific inhibitors on their activity.

At this time in the literature data about differences in specific EGFR signaling cascades in different human dermal cell types, such as keratinocytes and fibroblasts, is scarce.

miRNA profiles

With regard to identification of gene regulatory biomarkers it has been clearly shown in the NGS experiments described here that in both dermal skin types, keratinocytes as well as fibroblasts, differences in miRNA profiles between erlotinib-sensitive and -insensitive cells are much greater when looking at precursor (hairpin) miRNA molecules than at mature miRNAs. This should be kept in mind for all further investigations concerning miRNAs as biomarkers. It could be speculated that because precursor miRNAs are simply longer than mature miRNA molecules, they are more stable throughout experiments and allow for design of more specific primers and increased primer optimization options, which might yield better sequencing and PCR results. In addition, precursor miRNA levels might show earlier responses to changes within a cell than mature miRNAs, which are further down-stream in the miRNA biogenesis process[183]. However, it also has to be kept in mind that differences in miRNA processing might only be evident in mature miRNAs and hence, depending on the research question, it should be carefully evaluated whether expression of precursor or mature miRNAs will be investigated in future biomarker studies.

Those miRNAs which were identified in this study as significantly differentially expressed in keratinocytes were not significantly differentially expressed in fibroblasts and *vice versa*, again indicating large differences in cellular processes in these two dermal cell types. Regulation of **mir-34a** and its mature form **miR-34a-5p** even seemed to be opposite in the two cell types. While in fibroblasts expression of **mir-34a** and **miR-34a-5p** was up-regulated in erlotinib-sensitive cells (mir-34a significantly, miR-34a-5p non-significantly), in keratinocytes the two miRNAs were rather down-regulated in erlotinib-sensitive cells (both not significantly). The same was observed for **mir-146a** and its mature form **miR-146a-5p**, which was significantly down-regulated in erlotinib-sensitive keratinocytes as compared to the -insensitive ones but rather up-regulated in the respective fibroblast groups (not significant). The reasons for these differences cannot be explained so far but highlight the fact that miRNA profiles are highly specific with respect to cell type, treatment and time point and it remains a challenge to further elucidate the exact mechanisms of regulation under different conditions.

Taken together, in this study different miRNAs have been identified which show promising potential in predicting the efficacy of EGFR inhibition by erlotinib in keratinocytes or fibroblasts. The identified miRNAs were different in the two dermal cell types. Hence it is

suggested that further investigations about the clinical suitability of the identified miRNAs as predictive biomarkers should be performed in both cell types. However, it always has to be considered that the isolation of keratinocytes from patients might be easier than obtaining fibroblasts, since keratinocytes are part of the epidermis, which is more superficial than the dermis, from which fibroblasts originate. Therefore, if there are suitable biomarkers identified in both cell types, the ones determinable in keratinocytes might be preferred for establishment in clinical practice.

It should be noted that some of the discussed miRNAs might also have a therapeutic potential and could possibly be applied together with EGFRIs to increase inhibition of proliferative signaling cascades via additional targets. However, such therapeutic potential is investigated by other research groups and is not part of the scope of this thesis.

## V.3 Conclusion

In this study analysis of patient plasma from the Dermatoxgen study showed that the concentration of the EGFRI cetuximab was not significantly associated with the occurrence of EGFRI-induced skin rash. In a previous publication by our research group a metabolic ratio of erlotinib (erlotinib concentration divided by O-desmethylerlotinib) was shown to be significantly correlated with occurrence of EGFRI-induced rash and therefore is thought to be a promising predictive biomarker, especially with regard to optimization of dosage. However, this seems to be relevant only for TKIs and cannot be transferred to anti-EGFR mAbs, since they have no known/measurable metabolites.
While the investigated analytes AREG and 25-OH-vitamin D also failed to show a correlation with the rash, the MET ligand HGF showed very promising results in this study. The plasma concentration of HGF was inversely correlated with severity of EGFRI-induced skin rash. This inverse correlation was also seen with OS in patients who developed EGFRI-induced rash but not in patients with no rash. HGF seems to be a promising biomarker, whose predictive and/or prognostic value should definitely be confirmed/validated in a larger and well-controlled patient cohort.
It was further shown in this study that primary human dermal keratinocytes and primary human dermal fibroblasts can be successfully cultured and can be sensitive to *in vitro* treatment with erlotinib, which can be determined by measuring the decrease in amount of phosphorylated EGFR in keratinocytes and phosphorylated ERK1/2 in fibroblasts, respectively, using specific ELISAs. In this study both dermal cell types have proven their suitability to be used as cell models to further study EGFRI-induced skin rash. However, it was also clearly shown that both cell types greatly differ with regard to regulation of

signaling cascades down-stream of EGFR, as well as with regard to miRNA profiles under specific conditions. Comparison of miRNA profiles between cells identified as rather erlotinib-sensitive and cells identified as rather erlotinib-insensitive combined with a literature review to identify the miRNAs with the most supporting data, led to identification of the precursor miRNAs mir-146a, mir-31, mir-221, mir-520e and mir-944 as most promising predictive biomarkers in keratinocytes for efficacy of EGFRIs. Of these, mir-146a, mir-520e and mir-944 have known targets (EGFR and SOCS4, respectively) and a suggested mechanism of action which can plausibly explain their predictive potential, while mir-31 and mir-221 do not have such known targets but instead have already been shown to be associated with sensitivity to an EGFRI in at least one previously published study. In fibroblasts the precursor miRNA mir-34a has been identified as the by far most promising predictive biomarker with MET reported as direct target and an associated plausible mechanism of action and two confirmatory previous studies about a synergistic effect with TKIs in cancer cells and a xenograft model. Further identified promising predictive precursor miRNAs in fibroblasts were mir-382, mir-494 and mir-520e with the plausible suggested targets PTEN and RERG, PTEN and p190B and EGFR, respectively. Mir-7-1 also showed positive results with the plausible suggested targets EGFR and Ras and a confirmatory previous study showing an association with sensitivity to cetuximab in cancer cells. Taken together, the predictive potential of all these miRNAs is worth further confirming in larger, well-controlled patient cohorts in future studies.

Overall, as final conclusion of this study it is suggested that it might be possible to develop a kind of “predictive profile” consisting of several biomarkers which taken together may have a predictive value on individual extent of EGFR inhibition in patients. Such a predictive profile should include several parameters. At this time the results of this study indicate that next to the metabolic ratio of erlotinib, the plasma concentration of HGF, the expression of mir-146a and mir-31 in dermal keratinocytes and the expression of mir-34a in dermal fibroblasts are promising parameters to include in such a predictive score, as also illustrated in figure 33.

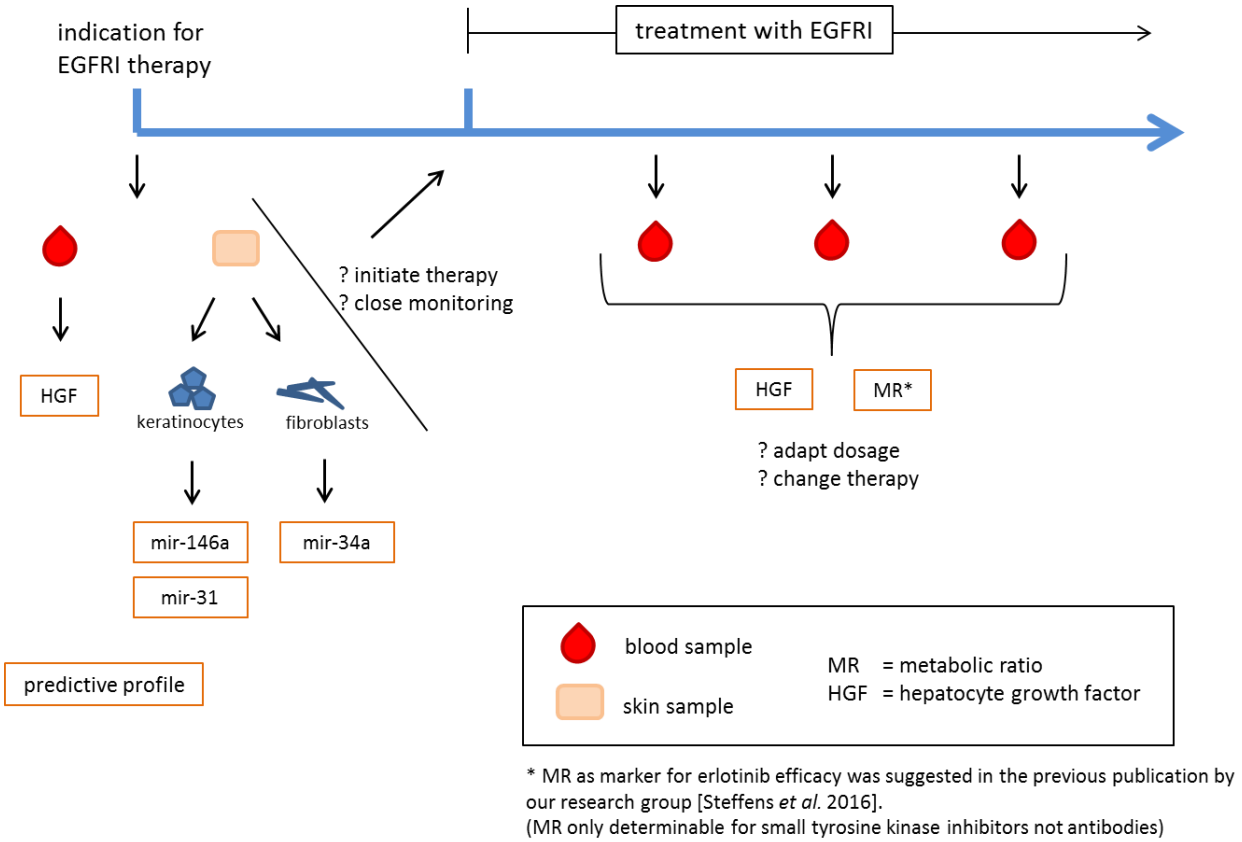


**Figure 33 Suggested predictive score for efficacy of EGFRIs**

If therapy with an EGFRI is indicated, prior to initiation of treatment blood and skin samples could be isolated from the patient to determine a predictive score consisting of the concentration of HGF in plasma and the expression of mir-146a and mir-31 in keratinocytes and mir-34a in fibroblasts. Based on the results it could be reconsidered if the therapy has promising efficacy and should indeed be initiated, whether closer monitoring of efficacy e.g. by tumor imaging should be performed due to questionable predicted efficacy etc. During the course of treatment blood samples could be drawn to determine changes in any of the parameters to monitor requirements for dosage optimization.

## V.4 Limitations

The study population for this thesis (the Dermatoxgen cohort) has the limitation that all patients received an EGFRI and there was no control group of untreated patients or rather a group of patients who received chemotherapy alone, without an EGFRI. This renders it difficult to draw definite conclusions about purely prognostic or predictive biomarkers. However, if the concentration of a certain substance is correlated with outcome in patients who developed skin rash but not in the ones who did not develop rash, it can be assumed that this parameter is rather specifically predictive for EGFRI efficacy, because

development of the rash is thought to be mainly associated with the specific mechanism of action of the drug[184].

A further limitation with regard to the patient samples used in this study is that blood samples were only available from one time point for each patient, four weeks after initiation of EGFRI therapy. Control samples from before initiation of treatment and further samples drawn along the course of therapy would be helpful to check stability and reliability of potential biomarkers more efficiently.

It also has to be noted that this study focused on biomarkers for efficacy of inhibition of EGFR signaling, irrespective of the type of EGFRI used (erlotinib, gefitinib, cetuximab or panitumumab). Different types of EGFRIs might have different additional off-target effects and respective additional predictive/prognostic biomarkers, which cannot be identified in the patient cohort investigated in this study.

Concerning cell culture experiments a limitation is the unavailability of skin samples from patients treated with an EGFRI. Skin samples from healthy donors had to be used for all experiments. The work presented in this thesis represents first characterizations of skin cells as *in vitro* models to study EGFRI-induced skin rash and first investigations about the suitability of miRNA profiles of skin cells as predictive biomarkers. Conclusions drawn from this work should be further studied/validated in a clinical setting using skin samples from patients receiving EGFRI therapy.

With regard to NGS experiments it was noted that detection of very slight differences in miRNA profiles is hampered by severe inter-run differences, meaning that the elaborate sample preparation procedure seems to result in different conditions in each individual sequencing run, which influence the sequencing results. In order to reliably detect also slight differences in miRNA profiles involving only low copy numbers of miRNAs, sample preparation has to be further standardized and samples which are to be compared should be sequenced one after the other as rapidly as possible.

It was further noted that the miRNA PCR assays used in this study (miScript Precursor/Primer Assays by Qiagen) were not completely suitable to verify the differences in miRNA profiles determined by NGS. Even though, those miRNAs which were significantly up- or down-regulated in the NGS analyses were mainly also determined as up- or down-regulated in the PCR analyses, respectively, in the PCR analyses the differences in expression were not significant for any of the tested miRNAs, regardless of the significance in NGS experiments. Since the manufacturer does not provide the sequences of the primers, optimization of primers is not possible. Different assays might have to be tested for future experiments.

## V.5 Outlook

Today there are still new EGFRIs developed for the treatment of various types of cancers. The first-generation EGFRI TKIs erlotinib and gefitinib are still treatment standard, e.g. in NSCLC. However, when resistance mutations arise, such as the T790M mutation, alternative treatments become necessary. Hence, second-generation EGFRIs were developed, such as afatinib, which also targets EGFR with the T790M mutation[185]. However, since the second-generation EGFRIs also target WT EGFR, they still induce dose-limiting toxicity in patients[186]. Therefore, there is still need for development of new EGFRIs with increased specificity for mutant compared to WT EGFR. While the third-generation EGFRI osimertinib has already been approved in the EU in 2016[8], numerous others, e.g. rociletinib, olmutinib, nazartinib and avitinib, are currently still under development and tested in clinical studies[186]. Considering the high amount of available established and new EGFRIs, biomarkers which can be used to predict the efficacy of EGFRIs are of very high importance to select patients which can really benefit from this type of treatment. Previous studies have shown that the markers in place today, e.g. mutation status of *EGFR* and *KRAS*, are not sufficient to select patients for efficient EGFRI therapy[27,29]. Therefore, new biomarkers are still needed. The potential predictive biomarkers identified in this study, namely plasma concentration of HGF and expression of several precursor miRNAs in skin cells, are very promising and their predictive properties should be further investigated in clinical settings in future studies. The precursor miRNAs mentioned in the conclusion were found to be worth investigating in skin samples of patients for the first time. Plasma levels of HGF and erlotinib metabolic ratio proved promising in the Dermatoxgen patient cohort and should definitely be further studied/validated in a larger patient cohort with a suitable control arm to confirm their predictive as compared to a rather prognostic value. This would also allow to stratify according to tumor type and type of EGFRI used to search for differences in predictive potential under different conditions.

Later steps in biomarker development should then also be to establish thresholds for each biomarker to define which values represent “high” or “low” presence of the respective parameter. Following definition of such thresholds the next step will be to define consequences for results of biomarker measurements, e.g. change in dosage of a specific EGFRI, closer monitoring of therapy efficacy by more frequent tumor imaging or maybe even change in therapy away from using an EGFRI or at least adding an adjuvant drug to the EGFRI therapy, e.g. an anti-HGF or anti-MET substance in case of high HGF levels determined in a patient’s plasma.

A further idea to better study EGFRI-induced skin rash *in vitro* in future might be to use a 3D skin model, e.g. like the ones described by Sadagurski et al[181] and Commandeur et al (skin equivalents)[139]. In such models keratinocytes and fibroblasts are cultured together and could therefore be studied in parallel, which might be beneficial considering that the two cell types probably also interact *in vivo*.

With regard to the miRNA experiments described in this thesis, the developed method should be further optimized and sample handling better standardized to allow to also detect smaller differences in miRNA profiles in the future. Moreover, investigations should be carried out in skin samples from patients treated with an EGFRI to validate the first results drawn from the experiments in skin cells from healthy donors. The method might also be used to identify miRNAs with a therapeutic potential, when patient samples from responders and non-responders are used. Over the next years miRNAs will become increasingly important in the area of biomarkers as well as in therapeutics in oncology.

# Chapter VI: References


1. Ma Q, Lu AY. Pharmacogenetics, pharmacogenomics, and individualized medicine. *Pharmacol Rev.* 2011;63(2):437-459.

2. Baudino TA. Targeted Cancer Therapy: The Next Generation of Cancer Treatment. *Curr Drug Discov Technol.* 2015;12(1):3-20.

3. Honeywell RJ, Hitzerd S, Kathmann I, Peters GJ. Transport of six tyrosine kinase inhibitors: active or passive? *Admet & Dmpk.* 2016;4(1).

4. Minematsu T, Giacomini KM. Interactions of tyrosine kinase inhibitors with organic cation transporters and multidrug and toxic compound extrusion proteins. *Mol Cancer Ther.* 2011;10(3):531-539.

5. Elmeliegy MA, Carcaboso AM, Tagen M, Bai F, Stewart CF. Role of ATP-binding cassette and solute carrier transporters in erlotinib CNS penetration and intracellular accumulation. *Clin Cancer Res.* 2011;17(1):89-99.

6. de Vries NA, Buckle T, Zhao J, Beijnen JH, Schellens JH, van Tellingen O. Restricted brain penetration of the tyrosine kinase inhibitor erlotinib due to the drug transporters P-gp and BCRP. *Invest New Drugs.* 2012;30(2):443-449.

7. Gridelli C, Bareschino MA, Schettino C, Rossi A, Maione P, Ciardiello F. Erlotinib in non-small cell lung cancer treatment: current status and future development. *Oncologist.* 2007;12(7):840-849.

8. European Medicines Agency. Human medicines, European Public Assessment Reports. 2017; http://www.ema.europa.eu/.

9. Stewart EL, Tan SZ, Liu G, Tsao MS. Known and putative mechanisms of resistance to EGFR targeted therapies in NSCLC patients with EGFR mutations-a review. *Transl Lung Cancer Res.* 2015;4(1):67-81.

10. Bokemeyer C, Bondarenko I, Makhson A, et al. Fluorouracil, leucovorin, and oxaliplatin with and without cetuximab in the first-line treatment of metastatic colorectal cancer. *J Clin Oncol.* 2009;27(5):663-671.

11. Van Cutsem E, Kohne CH, Hitre E, et al. Cetuximab and chemotherapy as initial treatment for metastatic colorectal cancer. *N Engl J Med.* 2009;360(14):1408-1417.

12. Peeters M, Price TJ, Cervantes A, et al. Randomized phase III study of panitumumab with fluorouracil, leucovorin, and irinotecan (FOLFIRI) compared with FOLFIRI alone as second-line treatment in patients with metastatic colorectal cancer. *J Clin Oncol.* 2010;28(31):4706-4713.

13. Douillard JY, Siena S, Cassidy J, et al. Randomized, phase III trial of panitumumab with infusional fluorouracil, leucovorin, and oxaliplatin (FOLFOX4) versus FOLFOX4 alone as first-line treatment in patients with previously untreated metastatic colorectal cancer: the PRIME study. *J Clin Oncol.* 2010;28(31):4697-4705.

14. Rana P, Sridhar SS. Efficacy and tolerability of lapatinib in the management of breast cancer. *Breast Cancer (Auckl).* 2012;6:67-77.

15. Dungo RT, Keating GM. Afatinib: first global approval. *Drugs.* 2013;73(13):1503-1515.

16. Boix-Perales H, Borregaard J, Jensen KB, et al. The European Medicines Agency Review of Pertuzumab for the Treatment of Adult Patients With HER2-Positive Metastatic or Locally Recurrent Unresectable Breast Cancer: Summary of the Scientific Assessment of the Committee for Medicinal Products for Human Use. *The Oncologist.* 2014;19(7):766-773.

17. Garnock-Jones KP. Necitumumab: First Global Approval. *Drugs.* 2016;76(2):283-289.

18. Italiano A. Prognostic or predictive? It's time to get back to definitions! *J Clin Oncol.* 2011;29(35):4718; author reply 4718-4719.

19. Ballman KV. Biomarker: Predictive or Prognostic? *J Clin Oncol.* 2015;33(33):3968-3971.

20. World Health Organization. *Biomarkers In Risk Assessment: Validity And Validation; Environmental Health Criteria 222.* Geneva 2001.

21. Badila E, Japie C, Bartos D. Cancer biomarkers in clinical practice. *Rom J Intern Med.* 2014;52(4):223-232.

22. Sturgeon CM, Duffy MJ, Stenman UH, et al. National Academy of Clinical Biochemistry laboratory medicine practice guidelines for use of tumor markers in testicular, prostate, colorectal, breast, and ovarian cancers. *Clin Chem.* 2008;54(12):e11-79.

23. Chung KY, Shia J, Kemeny NE, et al. Cetuximab Shows Activity in Colorectal Cancer Patients With Tumors That Do Not Express the Epidermal Growth Factor Receptor by Immunohistochemistry. *Journal of Clinical Oncology.* 2005;23(9):1803-1810.

24. Burtness B, Goldwasser MA, Flood W, Mattar B, Forastiere AA. Phase III Randomized Trial of Cisplatin Plus Placebo Compared With Cisplatin Plus Cetuximab in Metastatic/Recurrent Head and Neck Cancer: An Eastern Cooperative Oncology Group Study. *Journal of Clinical Oncology.* 2005;23(34):8646-8654.

25. Bailey R, Kris M, Wolf M, et al. O-242 Gefitinib (‘Iressa’, ZD1839) monotherapy for pretreated advanced non-small-cell lung cancer in IDEAL 1 and 2: tumor response is not clinically relevantly predictable from tumor EGFR membrane staining alone. *Lung Cancer.*41:S71.

26. Vijayalakshmi R, Krishnamurthy A. Targetable “Driver” Mutations in Non Small Cell Lung Cancer. *Indian Journal of Surgical Oncology.* 2011;2(3):178-188.

27. Rosell R, Moran T, Cardenal F, et al. Predictive biomarkers in the management of EGFR mutant lung cancer. *Ann N Y Acad Sci.* 2010;1210:45-52.

28. De Stefano A, Carlomagno C. Beyond KRAS: Predictive factors of the efficacy of anti-EGFR monoclonal antibodies in the treatment of metastatic colorectal cancer. *World J Gastroenterol.* 2014;20(29):9732-9743.

29. Lievre A, Bachet JB, Le Corre D, et al. KRAS mutation status is predictive of response to cetuximab therapy in colorectal cancer. *Cancer Res.* 2006;66(8):3992-3995.

30. Tveit KM, Guren T, Glimelius B, et al. Phase III trial of cetuximab with continuous or intermittent fluorouracil, leucovorin, and oxaliplatin (Nordic FLOX) versus FLOX alone in first-line treatment of metastatic colorectal cancer: the NORDIC-VII study. *J Clin Oncol.* 2012;30(15):1755-1762.

31. Hirsh V, Blais N, Burkes R, Verma S, Croitoru K. Management of diarrhea induced by epidermal growth factor receptor tyrosine kinase inhibitors. *Current Oncology.* 2014;21(6):329-336.

32. Perez-Soler R, Chachoua A, Hammond LA, et al. Determinants of tumor response and survival with erlotinib in patients with non--small-cell lung cancer. *J Clin Oncol.* 2004;22(16):3238-3247.

33. Fox LP. Nail toxicity associated with epidermal growth factor receptor inhibitor therapy. *J Am Acad Dermatol.* 2007;56(3):460-465.

34. Burtness B, Anadkat M, Basti S, et al. NCCN Task Force Report: Management of dermatologic and other toxicities associated with EGFR inhibition in patients with cancer. *J Natl Compr Canc Netw.* 2009;7 Suppl 1:S5-21; quiz S22-24.

35. Lacouture ME, Anadkat MJ, Bensadoun RJ, et al. Clinical practice guidelines for the prevention and treatment of EGFR inhibitor-associated dermatologic toxicities. *Support Care Cancer.* 2011;19(8):1079-1095.

36. Hichert V, Paul T, Scholl C, Stingl J. Untersuchungen zu genregulatorischen Biomarkern für EGFR-Inhibitor-vermittelte Hautreaktionen. *Bulletin zur Arzneimittelsicherheit, Informationen aus BfArM und PEI.* 2014;3:29-33.

37. Saltz LB, Meropol NJ, Loehrer PJ, Sr., Needle MN, Kopit J, Mayer RJ. Phase II trial of cetuximab in patients with refractory colorectal cancer that expresses the epidermal growth factor receptor. *J Clin Oncol.* 2004;22(7):1201-1208.

38. Wacker B, Nagrani T, Weinberg J, Witt K, Clark G, Cagnoni PJ. Correlation between development of rash and efficacy in patients treated with the epidermal growth factor receptor tyrosine kinase inhibitor erlotinib in two large phase III studies. *Clin Cancer Res.* 2007;13(13):3913-3921.

39. Perez-Soler R, Van Cutsem E. Clinical research of EGFR inhibitors and related dermatologic toxicities. *Oncology (Williston Park).* 2007;21(11 Suppl 5):10-16.

40. Van Cutsem E, Tejpar S, Vanbeckevoort D, et al. Intrapatient cetuximab dose escalation in metastatic colorectal cancer according to the grade of early skin reactions: the randomized EVEREST study. *J Clin Oncol.* 2012;30(23):2861-2868.

41. Van Cutsem E, Li CP, Nowara E, et al. Dose escalation to rash for erlotinib plus gemcitabine for metastatic pancreatic cancer: the phase II RACHEL study. *British Journal of Cancer.* 2014;111(11):2067-2075.

42. Brown J, Su Y, Nelleson D, Shankar P, Mayo C. Management of epidermal growth factor receptor inhibitor-associated rash: a systematic review. *J Community Support Oncol.* 2016;14(1):21-28.

43. Perez-Soler R, Delord JP, Halpern A, et al. HER1/EGFR inhibitor-associated rash: future directions for management and investigation outcomes from the HER1/EGFR inhibitor rash management forum. *Oncologist.* 2005;10(5):345-356.

44. Citri A, Yarden Y. EGF-ERBB signalling: towards the systems level. *Nat Rev Mol Cell Biol.* 2006;7(7):505-516.

45. Yarden Y, Pines G. The ERBB network: at last, cancer therapy meets systems biology. *Nat Rev Cancer.* 2012;12(8):553-563.

46. Tebbutt N, Pedersen MW, Johns TG. Targeting the ERBB family in cancer: couples therapy. *Nat Rev Cancer.* 2013;13(9):663-673.

47. Stoll SW, Johnson JL, Bhasin A, et al. Metalloproteinase-mediated, context-dependent function of amphiregulin and HB-EGF in human keratinocytes and skin. *J Invest Dermatol.* 2010;130(1):295-304.

48. Sanderson MP, Dempsey PJ, Dunbar AJ. Control of ErbB signaling through metalloprotease mediated ectodomain shedding of EGF-like factors. *Growth Factors.* 2006;24(2):121-136.

49. Yarden Y. The EGFR family and its ligands in human cancer. signalling mechanisms and therapeutic opportunities. *Eur J Cancer.* 2001;37 Suppl 4:S3-8.

50. Scaltriti M, Baselga J. The epidermal growth factor receptor pathway: a model for targeted therapy. *Clin Cancer Res.* 2006;12(18):5268-5272.

51. Zhao HF, Wang J, Tony To SS. The phosphatidylinositol 3-kinase/Akt and c-Jun N-terminal kinase signaling in cancer: Alliance or contradiction? (Review). *Int J Oncol.* 2015;47(2):429-436.

52. Johnson GL, Lapadat R. Mitogen-activated protein kinase pathways mediated by ERK, JNK, and p38 protein kinases. *Science.* 2002;298(5600):1911-1912.

53. Miyamoto Y, Suyama K, Baba H. Recent Advances in Targeting the EGFR Signaling Pathway for the Treatment of Metastatic Colorectal Cancer. *Int J Mol Sci.* 2017;18(4).

54. Horn D, Hess J, Freier K, Hoffmann J, Freudlsperger C. Targeting EGFR-PI3K-AKT-mTOR signaling enhances radiosensitivity in head and neck squamous cell carcinoma. *Expert Opin Ther Targets.* 2015;19(6):795-805.

55. Betz C, Hall MN. Where is mTOR and what is it doing there? *J Cell Biol.* 2013;203(4):563-574.

56. Shao H, Cheng HY, Cook RG, Tweardy DJ. Identification and characterization of signal transducer and activator of transcription 3 recruitment sites within the epidermal growth factor receptor. *Cancer Res.* 2003;63(14):3923-3930.

57. Patterson RL, van Rossum DB, Nikolaidis N, Gill DL, Snyder SH. Phospholipase C-gamma: diverse roles in receptor-mediated calcium signaling. *Trends Biochem Sci.* 2005;30(12):688-697.

58. Lacouture ME. Mechanisms of cutaneous toxicities to EGFR inhibitors. *Nat Rev Cancer.* 2006;6(10):803-812.

59. Bensouilah J, Buck P. *Aromadermatology: Aromatherapy in the Treatment and Care of Common Skin Conditions.* Radcliffe Publishing; 2006.

60. Alberts B, Johnson A, Lewis J, Raff M, Roberts K, Walter P. *Molecular Biology of the Cell.* 4th ed: Garland Science; 2002.

61. Nanba D, Toki F, Barrandon Y, Higashiyama S. Recent advances in the epidermal growth factor receptor/ligand system biology on skin homeostasis and keratinocyte stem cell regulation. *J Dermatol Sci.* 2013;72(2):81-86.

62. Iizuka H. Epidermal turnover time. *J Dermatol Sci.* 1994;8(3):215-217.

63. Jost M, Kari C, Rodeck U. The EGF receptor - an essential regulator of multiple epidermal functions. *Eur J Dermatol.* 2000;10(7):505-510.

64. Lichtenberger BM, Gerber PA, Holcmann M, et al. Epidermal EGFR controls cutaneous host defense and prevents inflammation. *Sci Transl Med.* 2013;5(199):199ra111.

65. Stoll SW, Johnson JL, Li Y, Rittie L, Elder JT. Amphiregulin carboxy-terminal domain is required for autocrine keratinocyte growth. *J Invest Dermatol.* 2010;130(8):2031-2040.

66. Rittie L, Varani J, Kang S, Voorhees JJ, Fisher GJ. Retinoid-induced epidermal hyperplasia is mediated by epidermal growth factor receptor activation via specific induction of its ligands heparin-binding EGF and amphiregulin in human skin in vivo. *J Invest Dermatol.* 2006;126(4):732-739.

67. Ishikawa N, Daigo Y, Takano A, et al. Increases of amphiregulin and transforming growth factor-alpha in serum as predictors of poor response to gefitinib among patients with advanced non-small cell lung cancers. *Cancer Res.* 2005;65(20):9176-9184.

68. Gusenbauer S, Vlaicu P, Ullrich A. HGF induces novel EGFR functions involved in resistance formation to tyrosine kinase inhibitors. *Oncogene.* 2013;32(33):3846-3856.

69. Organ SL, Tsao MS. An overview of the c-MET signaling pathway. *Ther Adv Med Oncol.* 2011;3(1 Suppl):S7-s19.

70. Bevan D, Gherardi E, Fan TP, Edwards D, Warn R. Diverse and potent activities of HGF/SF in skin wound repair. *J Pathol.* 2004;203(3):831-838.

71. Conway K, Price P, Harding KG, Jiang WG. The molecular and clinical impact of hepatocyte growth factor, its receptor, activators, and inhibitors in wound healing. *Wound Repair Regen.* 2006;14(1):2-10.

72. Huh CG, Factor VM, Sanchez A, Uchida K, Conner EA, Thorgeirsson SS. Hepatocyte growth factor/c-met signaling pathway is required for efficient liver regeneration and repair. *Proc Natl Acad Sci U S A.* 2004;101(13):4477-4482.

73. Puri N, Salgia R. Synergism of EGFR and c-Met pathways, cross-talk and inhibition, in non-small cell lung cancer. *J Carcinog.* 2008;7:9.

74. Hammond DE, Hyde R, Kratchmarova I, Beynon RJ, Blagoev B, Clague MJ. Quantitative analysis of HGF and EGF-dependent phosphotyrosine signaling networks. *J Proteome Res.* 2010;9(5):2734-2742.

75. Di Renzo MF, Olivero M, Giacomini A, et al. Overexpression and amplification of the met/HGF receptor gene during the progression of colorectal cancer. *Clin Cancer Res.* 1995;1(2):147-154.

76. Di Renzo MF, Olivero M, Martone T, et al. Somatic mutations of the MET oncogene are selected during metastatic spread of human HNSC carcinomas. *Oncogene.* 2000;19(12):1547-1555.

77. Danilkovitch-Miagkova A, Zbar B. Dysregulation of Met receptor tyrosine kinase activity in invasive tumors. *J Clin Invest.* 2002;109(7):863-867.

78. Matsumoto R, Tsuda M, Wang L, et al. Adaptor protein CRK induces epithelial-mesenchymal transition and metastasis of bladder cancer cells through HGF/c-Met feedback loop. *Cancer Sci.* 2015;106(6):709-717.

79. Takahashi N, Yamada Y, Furuta K, et al. Association between serum ligands and the skin toxicity of anti-epidermal growth factor receptor antibody in metastatic colorectal cancer. *Cancer Sci.* 2015;106(5):604-610.

80. Gonzalez EA, Disthabanchong S, Kowalewski R, Martin KJ. Mechanisms of the regulation of EGF receptor gene expression by calcitriol and parathyroid hormone in UMR 106-01 cells. *Kidney Int.* 2002;61(5):1627-1634.

81. McGaffin KR, Acktinson LE, Chrysogelos SA. Growth and EGFR regulation in breast cancer cells by vitamin D and retinoid compounds. *Breast Cancer Res Treat.* 2004;86(1):55-73.

82. McGaffin KR, Chrysogelos SA. Identification and characterization of a response element in the EGFR promoter that mediates transcriptional repression by 1,25-dihydroxyvitamin D3 in breast cancer cells. *Journal of Molecular Endocrinology.* 2005;35(1):117-133.

83. Shen Z, Zhang X, Tang J, et al. The coupling of epidermal growth factor receptor down regulation by 1alpha,25-dihydroxyvitamin D3 to the hormone-induced cell cycle arrest at the G1-S checkpoint in ovarian cancer cells. *Molecular and cellular endocrinology.* 2011;338(1-2):58-67.

84. Zehnder D, Bland R, Williams MC, et al. Extrarenal expression of 25-hydroxyvitamin d(3)-1 alpha-hydroxylase. *J Clin Endocrinol Metab.* 2001;86(2):888-894.

85. Lehmann B, Genehr T, Knuschke P, Pietzsch J, Meurer M. UVB-induced conversion of 7-dehydrocholesterol to 1alpha,25-dihydroxyvitamin D3 in an in vitro human skin equivalent model. *J Invest Dermatol.* 2001;117(5):1179-1185.

86. Lehmann B, Meurer M. Extrarenal sites of calcitriol synthesis: the particular role of the skin. *Recent Results Cancer Res.* 2003;164:135-145.

87. Bartel DP. MicroRNAs: target recognition and regulatory functions. *Cell.* 2009;136(2):215-233.

88. Gregory RI, Yan KP, Amuthan G, et al. The Microprocessor complex mediates the genesis of microRNAs. *Nature.* 2004;432(7014):235-240.

89. Gregory RI, Chendrimada TP, Cooch N, Shiekhattar R. Human RISC couples microRNA biogenesis and posttranscriptional gene silencing. *Cell.* 2005;123(4):631-640.

90. Rukov JL, Shomron N. MicroRNA pharmacogenomics: post-transcriptional regulation of drug response. *Trends Mol Med.* 2011;17(8):412-423.

91. Griffiths-Jones S, Grocock RJ, van Dongen S, Bateman A, Enright AJ. miRBase: microRNA sequences, targets and gene nomenclature. *Nucleic Acids Res.* 2006;34(Database issue):D140-144.

92. Kozomara A, Griffiths-Jones S. miRBase: annotating high confidence microRNAs using deep sequencing data. *Nucleic Acids Res.* 2014;42(Database issue):D68-73.

93. Calin GA, Dumitru CD, Shimizu M, et al. Frequent deletions and down-regulation of micro- RNA genes miR15 and miR16 at 13q14 in chronic lymphocytic leukemia. *Proc Natl Acad Sci U S A.* 2002;99(24):15524-15529.

94. Bhattacharya A, Ziebarth JD, Cui Y. SomamiR: a database for somatic mutations impacting microRNA function in cancer. *Nucleic Acids Res.* 2013;41(Database issue):D977-982.

95. Ohtsuka M, Ling H, Doki Y, Mori M, Calin GA. MicroRNA Processing and Human Cancer. *J Clin Med.* 2015;4(8):1651-1667.

96. Gomez GG, Wykosky J, Zanca C, Furnari FB, Cavenee WK. Therapeutic resistance in cancer: microRNA regulation of EGFR signaling networks. *Cancer Biol Med.* 2013;10(4):192-205.

97. Yang S, Li Y, Gao J, et al. MicroRNA-34 suppresses breast cancer invasion and metastasis by directly targeting Fra-1. *Oncogene.* 2013;32(36):4294-4303.

98. Ma ZL, Hou PP, Li YL, et al. MicroRNA-34a inhibits the proliferation and promotes the apoptosis of non-small cell lung cancer H1299 cell line by targeting TGFbetaR2. *Tumour Biol.* 2015;36(4):2481-2490.

99. Gao J, Li N, Dong Y, et al. miR-34a-5p suppresses colorectal cancer metastasis and predicts recurrence in patients with stage II/III colorectal cancer. *Oncogene.* 2015;34(31):4142-4152.

100. Kasinski AL, Slack FJ. miRNA-34 prevents cancer initiation and progression in a therapeutically resistant K-ras and p53-induced mouse model of lung adenocarcinoma. *Cancer Res.* 2012;72(21):5576-5587.

101. Suto T, Yokobori T, Yajima R, et al. MicroRNA-7 expression in colorectal cancer is associated with poor prognosis and regulates cetuximab sensitivity via EGFR regulation. *Carcinogenesis.* 2015;36(3):338-345.

102. Kalinowski FC, Giles KM, Candy PA, et al. Regulation of epidermal growth factor receptor signaling and erlotinib sensitivity in head and neck cancer cells by miR-7. *PLoS One.* 2012;7(10):e47067.

103. Fuerst D, Parmar S, Schumann C, et al. HLA polymorphisms influence the development of skin rash arising from treatment with EGF receptor inhibitors. *Pharmacogenomics.* 2012;13(13):1469-1476.

104. Parmar S, Schumann C, Rudiger S, et al. Pharmacogenetic predictors for EGFR-inhibitor-associated skin toxicity. *Pharmacogenomics J.* 2013;13(2):181-188.

105. Hasheminasab SM, Tzvetkov MV, Schumann C, et al. High-throughput screening identified inherited genetic variations in the EGFR pathway contributing to skin toxicity of EGFR inhibitors. *Pharmacogenomics.* 2015;16(14):1605-1619.

106. Paul T, Schumann C, Rudiger S, et al. Cytokine regulation by epidermal growth factor receptor inhibitors and epidermal growth factor receptor inhibitor associated skin toxicity in cancer patients. *Eur J Cancer.* 2014;50(11):1855-1863.

107. Steffens M, Paul T, Hichert V, et al. Dosing to rash?--The role of erlotinib metabolic ratio from patient serum in the search of predictive biomarkers for EGFR inhibitor-mediated skin rash. *Eur J Cancer.* 2016;55:131-139.

108. Pinheiro J, Bates D, DebRoy S, Sarkar D, R Core Team. nlme: Linear and Nonlinear Mixed Effects Models. 2016.

109. Martin M. Cutadapt removes adapter sequences from high-throughput sequencing reads. *EMBnetjournal; Vol 17, No 1: Next Generation Sequencing Data Analysis.* 2011.

110. Langmead B, Trapnell C, Pop M, Salzberg SL. Ultrafast and memory-efficient alignment of short DNA sequences to the human genome. *Genome Biol.* 2009;10(3):R25.

111. Love MI, Huber W, Anders S. Moderated estimation of fold change and dispersion for RNA-seq data with DESeq2. *Genome Biol.* 2014;15(12):550.

112. Cancer Therapy Evaluation Program. *Common Terminology Criteria for Adverse Events v3.0 (CTCAE).* DCTD, NCI, NIH, DHHS 2006.

113. Aasen T, Izpisua Belmonte JC. Isolation and cultivation of human keratinocytes from skin or plucked hair for the generation of induced pluripotent stem cells. *Nat Protoc.* 2010;5(2):371-382.

114. Chomczynski P, Sacchi N. Single-step method of RNA isolation by acid guanidinium thiocyanate-phenol-chloroform extraction. *Anal Biochem.* 1987;162(1):156-159.

115. Hichert V, Scholl C, Steffens M, et al. Predictive blood plasma biomarkers for EGFR inhibitor-induced skin rash. *Oncotarget.* 2017;8(21):35193-35204.

116. Institute of Medicine Committee to Review Dietary Reference Intakes for Vitamin D, Calcium. The National Academies Collection: Reports funded by National Institutes of Health. In: Ross AC, Taylor CL, Yaktine AL, Del Valle HB, eds. *Dietary Reference Intakes for Calcium and Vitamin D.* Washington (DC): National Academies Press (US), National Academy of Sciences.; 2011.

117. Hansen KE, Johnson RE, Chambers KR, et al. Treatment of Vitamin D Insufficiency in Postmenopausal Women: A Randomized Clinical Trial. *JAMA Intern Med.* 2015;175(10):1612-1621.

118. Maier GS, Horas K, Kurth AA, Lazovic D, Seeger JB, Maus U. Prevalence of Vitamin D Deficiency in Patients with Bone Metastases and Multiple Myeloma. *Anticancer Res.* 2015;35(11):6281-6285.

119. Williams JD, Aggarwal A, Swami S, et al. Tumor Autonomous Effects of Vitamin D Deficiency Promote Breast Cancer Metastasis. *Endocrinology.* 2016;157(4):1341-1347.

120. Keizer RJ, Huitema AD, Schellens JH, Beijnen JH. Clinical pharmacokinetics of therapeutic monoclonal antibodies. *Clin Pharmacokinet.* 2010;49(8):493-507.

121. Takahashi N, Yamada Y, Furuta K, et al. Serum levels of hepatocyte growth factor and epiregulin are associated with the prognosis on anti-EGFR antibody treatment in KRAS wild-type metastatic colorectal cancer. *Br J Cancer.* 2014;110(11):2716-2727.

122. Wang L, Wu H, Wang L, et al. Expression of amphiregulin predicts poor outcome in patients with pancreatic ductal adenocarcinoma. *Diagn Pathol.* 2016;11(1):60.

123. Llovet P, Sastre J, Ortega JS, et al. Prognostic Value of BRAF, PI3K, PTEN, EGFR Copy Number, Amphiregulin and Epiregulin Status in Patients with KRAS Codon 12 Wild-Type Metastatic Colorectal Cancer Receiving First-Line Chemotherapy with Anti-EGFR Therapy. *Mol Diagn Ther.* 2015;19(6):397-408.

124. Yonesaka K, Takegawa N, Satoh T, et al. Combined Analysis of Plasma Amphiregulin and Heregulin Predicts Response to Cetuximab in Metastatic Colorectal Cancer. *PLoS One.* 2015;10(11):e0143132.

125. Engelman JA, Zejnullahu K, Mitsudomi T, et al. MET amplification leads to gefitinib resistance in lung cancer by activating ERBB3 signaling. *Science.* 2007;316(5827):1039-1043.

126. Gou LY, Li AN, Yang JJ, et al. The coexistence of MET over-expression and an EGFR T790M mutation is related to acquired resistance to EGFR tyrosine kinase inhibitors in advanced non-small cell lung cancer. *Oncotarget.* 2016.

127. Troiani T, Martinelli E, Napolitano S, et al. Increased TGF-alpha as a mechanism of acquired resistance to the anti-EGFR inhibitor cetuximab through EGFR-MET interaction and activation of MET signaling in colon cancer cells. *Clin Cancer Res.* 2013;19(24):6751-6765.

128. Corso S, Comoglio PM, Giordano S. Cancer therapy: can the challenge be MET? *Trends Mol Med.* 2005;11(6):284-292.

129. Spix JK, Chay EY, Block ER, Klarlund JK. Hepatocyte growth factor induces epithelial cell motility through transactivation of the epidermal growth factor receptor. *Exp Cell Res.* 2007;313(15):3319-3325.

130. Stintzing S, Kapaun C, Laubender RP, et al. Prognostic value of cetuximab-related skin toxicity in metastatic colorectal cancer patients and its correlation with parameters of the epidermal growth factor receptor signal transduction pathway: results from a randomized trial of the GERMAN AIO CRC Study Group. *Int J Cancer.* 2013;132(1):236-245.

131. Van Cutsem E, Eng C, Nowara E, et al. Randomized phase Ib/II trial of rilotumumab or ganitumab with panitumumab versus panitumumab alone in patients with wild-type KRAS metastatic colorectal cancer. *Clin Cancer Res.* 2014;20(16):4240-4250.

132. Imtiaz S, Siddiqui N, Raza SA, Loya A, Muhammad A. Vitamin D deficiency in newly diagnosed breast cancer patients. *Indian J Endocrinol Metab.* 2012;16(3):409-413.

133. Garland CF, Kim JJ, Mohr SB, et al. Meta-analysis of all-cause mortality according to serum 25-hydroxyvitamin D. *Am J Public Health.* 2014;104(8):e43-50.

134. Holick MF, Binkley NC, Bischoff-Ferrari HA, et al. Evaluation, Treatment, and Prevention of Vitamin D Deficiency: an Endocrine Society Clinical Practice Guideline. *The Journal of Clinical Endocrinology & Metabolism.* 2011;96(7):1911-1930.

135. Heidrich J. Vitamin D messen. *Deutsche Apotheker Zeitung.* 2016;154(48):44-47.

136. Thierfelder W, Roth Heinz J, Laussmann D, et al. Vitamin D und Parathormon: Ein Weg zur Bestimmung methodenabhängiger unterer Grenzwerte für Vitamin D / Vitamin D and parathyroid hormone: a tool to determine assay-specific cutoff values for vitamin D. In. *LaboratoriumsMedizin.* Vol 322008:456.

137. Eckert RL. Structure, function, and differentiation of the keratinocyte. *Physiol Rev.* 1989;69(4):1316-1346.

138. Lankheet NA, Schaake EE, Burgers SA, et al. Concentrations of Erlotinib in Tumor Tissue and Plasma in Non-Small-Cell Lung Cancer Patients After Neoadjuvant Therapy. *Clin Lung Cancer.* 2015;16(4):320-324.

139. Commandeur S, van Drongelen V, de Gruijl FR, El Ghalbzouri A. Epidermal growth factor receptor activation and inhibition in 3D in vitro models of normal skin and human cutaneous squamous cell carcinoma. *Cancer Sci.* 2012;103(12):2120-2126.

140. Miyazaki R, Anayama T, Hirohashi K, Okada H, Kume M, Orihashi K. In Vitro Drug Sensitivity Tests to Predict Molecular Target Drug Responses in Surgically Resected Lung Cancer. *PLoS One.* 2016;11(4):e0152665.

141. Parsons SJ, Parsons JT. Src family kinases, key regulators of signal transduction. *Oncogene.* 2004;23(48):7906-7909.

142. Guo D, Cloughesy TF, Radu CG, Mischel PS. AMPK: A metabolic checkpoint that regulates the growth of EGFR activated glioblastomas. *Cell Cycle.* 2010;9(2):211-212.

143. Jhaveri TZ, Woo J, Shang X, Park BH, Gabrielson E. AMP-activated kinase (AMPK) regulates activity of HER2 and EGFR in breast cancer. *Oncotarget.* 2015;6(17):14754-14765.

144. Chen G, Umelo IA, Lv S, et al. miR-146a inhibits cell growth, cell migration and induces apoptosis in non-small cell lung cancer cells. *PLoS One.* 2013;8(3):e60317.

145. Ali S, Ahmad A, Aboukameel A, et al. Deregulation of miR-146a expression in a mouse model of pancreatic cancer affecting EGFR signaling. *Cancer Lett.* 2014;351(1):134-142.

146. Huang W-T, Cen W-L, He R-Q, et al. Effect of miR-146a-5p on tumor growth in NSCLC using chick chorioallantoic membrane assay and bioinformatics investigation. *Molecular Medicine Reports.* 2017;16(6):8781-8792.

147. Li Y, Vandenboom TG, 2nd, Wang Z, et al. miR-146a suppresses invasion of pancreatic cancer cells. *Cancer Res.* 2010;70(4):1486-1495.

148. Huang S, He R, Rong M, Dang Y, Chen G. Synergistic effect of MiR-146a mimic and cetuximab on hepatocellular carcinoma cells. *Biomed Res Int.* 2014;2014:384121.

149. Mosakhani N, Lahti L, Borze I, et al. MicroRNA profiling predicts survival in anti-EGFR treated chemorefractory metastatic colorectal cancer patients with wild-type KRAS and BRAF. *Cancer Genet.* 2012;205(11):545-551.

150. Manceau G, Imbeaud S, Thiebaut R, et al. Hsa-miR-31-3p expression is linked to progression-free survival in patients with KRAS wild-type metastatic colorectal cancer treated with anti-EGFR therapy. *Clin Cancer Res.* 2014;20(12):3338-3347.

151. Igarashi H, Kurihara H, Mitsuhashi K, et al. Association of MicroRNA-31-5p with Clinical Efficacy of Anti-EGFR Therapy in Patients with Metastatic Colorectal Cancer. *Ann Surg Oncol.* 2015;22(8):2640-2648.

152. Mlcochova J, Faltejskova-Vychytilova P, Ferracin M, et al. MicroRNA expression profiling identifies miR-31-5p/3p as associated with time to progression in wild-type RAS metastatic colorectal cancer treated with cetuximab. *Oncotarget.* 2015;6(36):38695-38704.

153. Gao Y, Fan X, Li W, Ping W, Deng Y, Fu X. miR-138-5p reverses gefitinib resistance in non-small cell lung cancer cells via negatively regulating G protein-coupled receptor 124. *Biochem Biophys Res Commun.* 2014;446(1):179-186.

154. Li B, Yang XX, Wang D, Ji HK. MicroRNA-138 inhibits proliferation of cervical cancer cells by targeting c-Met. *Eur Rev Med Pharmacol Sci.* 2016;20(6):1109-1114.

155. Garofalo M, Romano G, Di Leva G, et al. EGFR and MET receptor tyrosine kinase-altered microRNA expression induces tumorigenesis and gefitinib resistance in lung cancers. *Nat Med.* 2011;18(1):74-82.

156. Deng WG, Kwon J, Ekmekcioglu S, Poindexter NJ, Grimm EA. IL-24 gene transfer sensitizes melanoma cells to erlotinib through modulation of the Apaf-1 and Akt signaling pathways. *Melanoma Res.* 2011;21(1):44-56.

157. Li S, Zhang H, Ning T, et al. MiR-520b/e Regulates Proliferation and Migration by Simultaneously Targeting EGFR in Gastric Cancer. *Cell Physiol Biochem.* 2016;40(6):1303-1315.

158. Flores-Perez A, Marchat LA, Rodriguez-Cuevas S, et al. Suppression of cell migration is promoted by miR-944 through targeting of SIAH1 and PTP4A1 in breast cancer cells. *BMC Cancer.* 2016;16:379.

159. Ma J, Mannoor K, Gao L, et al. Characterization of microRNA transcriptome in lung cancer by next-generation deep sequencing. *Mol Oncol.* 2014;8(7):1208-1219.

160. Kario E, Marmor MD, Adamsky K, et al. Suppressors of cytokine signaling 4 and 5 regulate epidermal growth factor receptor signaling. *J Biol Chem.* 2005;280(8):7038-7048.

161. Liu M, Zhou K, Cao Y. MicroRNA-944 Affects Cell Growth by Targeting EPHA7 in Non-Small Cell Lung Cancer. *Int J Mol Sci.* 2016;17(10).

162. Bouffi C, Bony C, Jorgensen C, Noel D. Skin fibroblasts are potent suppressors of inflammation in experimental arthritis. *Ann Rheum Dis.* 2011;70(9):1671-1676.

163. Van Linthout S, Miteva K, Tschope C. Crosstalk between fibroblasts and inflammatory cells. *Cardiovasc Res.* 2014;102(2):258-269.

164. Zhou JY, Chen X, Zhao J, et al. MicroRNA-34a overcomes HGF-mediated gefitinib resistance in EGFR mutant lung cancer cells partly by targeting MET. *Cancer Lett.* 2014;351(2):265-271.

165. Zhao J, Guerrero A, Kelnar K, Peltier HJ, Bader AG. Synergy between next generation EGFR tyrosine kinase inhibitors and miR-34a in the inhibition of non-small cell lung cancer. *Lung Cancer.* 2017;108:96-102.

166. Gong J, He L, Ma J, Zhang J, Wang L, Wang J. The relationship between miR-17-5p, miR-92a, and let-7b expression with non-small cell lung cancer targeted drug resistance. *J buon.* 2017;22(2):454-461.

167. Zhang W, Lin J, Wang P, Sun J. miR-17-5p down-regulation contributes to erlotinib resistance in non-small cell lung cancer cells. *J Drug Target.* 2017;25(2):125-131.

168. Zhao J, Fu W, Liao H, et al. The regulatory and predictive functions of miR-17 and miR-92 families on cisplatin resistance of non-small cell lung cancer. *BMC Cancer.* 2015;15:731.

169. Cragg MS, Kuroda J, Puthalakath H, Huang DC, Strasser A. Gefitinib-induced killing of NSCLC cell lines expressing mutant EGFR requires BIM and can be enhanced by BH3 mimetics. *PLoS Med.* 2007;4(10):1681-1689; discussion 1690.

170. Gu YF, Zhang H, Su D, et al. miR-30b and miR-30c expression predicted response to tyrosine kinase inhibitors as first line treatment in non-small cell lung cancer. *Chin Med J (Engl).* 2013;126(23):4435-4439.

171. Ho JY, Hsu RJ, Liu JM, et al. MicroRNA-382-5p aggravates breast cancer progression by regulating the RERG/Ras/ERK signaling axis. *Oncotarget.* 2017;8(14):22443-22459.

172. Zhang S, Ge W, Zou G, et al. MiR-382 targets GOLM1 to inhibit metastasis of hepatocellular carcinoma and its down-regulation predicts a poor survival. *American Journal of Cancer Research.* 2018;8(1):120-131.

173. Bei Y, Song Y, Wang F, et al. miR-382 targeting PTEN-Akt axis promotes liver regeneration. *Oncotarget.* 2016;7(2):1584-1597.

174. Sun HB, Chen X, Ji H, et al. miR494 is an independent prognostic factor and promotes cell migration and invasion in colorectal cancer by directly targeting PTEN. *Int J Oncol.* 2014;45(6):2486-2494.

175. Wang J, Chen H, Liao Y, et al. Expression and clinical evidence of miR-494 and PTEN in non-small cell lung cancer. *Tumour Biol.* 2015;36(9):6965-6972.

176. Kwak SY, Yang JS, Kim BY, Bae IH, Han YH. Ionizing radiation-inducible miR-494 promotes glioma cell invasion through EGFR stabilization by targeting p190B rhoGAP. *Biochim Biophys Acta.* 2014;1843(3):508-516.

177. Romano G, Acunzo M, Garofalo M, et al. MiR-494 is regulated by ERK1/2 and modulates TRAIL-induced apoptosis in non-small-cell lung cancer through BIM down-regulation. *Proc Natl Acad Sci U S A.* 2012;109(41):16570-16575.

178. Webster RJ, Giles KM, Price KJ, Zhang PM, Mattick JS, Leedman PJ. Regulation of epidermal growth factor receptor signaling in human cancer cells by microRNA-7. *J Biol Chem.* 2009;284(9):5731-5741.

179. Lorenzini A, Tresini M, Mawal-Dewan M, et al. Role of the Raf/MEK/ERK and the PI3K/Akt(PKB) pathways in fibroblast senescence. *Exp Gerontol.* 2002;37(10-11):1149-1156.

180. Calautti E, Li J, Saoncella S, Brissette JL, Goetinck PF. Phosphoinositide 3-kinase signaling to Akt promotes keratinocyte differentiation versus death. *J Biol Chem.* 2005;280(38):32856-32865.

181. Sadagurski M, Yakar S, Weingarten G, et al. Insulin-like growth factor 1 receptor signaling regulates skin development and inhibits skin keratinocyte differentiation. *Mol Cell Biol.* 2006;26(7):2675-2687.

182. Yano S, Komine M, Fujimoto M, Okochi H, Tamaki K. Activation of Akt by mechanical stretching in human epidermal keratinocytes. *Exp Dermatol.* 2006;15(5):356-361.

183. Chugh P, Dittmer DP. Potential pitfalls in microRNA profiling. *Wiley Interdiscip Rev RNA.* 2012;3(5):601-616.

184. Segaert S, Van Cutsem E. Clinical signs, pathophysiology and management of skin toxicity during therapy with epidermal growth factor receptor inhibitors. *Ann Oncol.* 2005;16(9):1425-1433.

185. Nelson V, Ziehr J, Agulnik M, Johnson M. Afatinib: emerging next-generation tyrosine kinase inhibitor for NSCLC. *Onco Targets Ther.* 2013;6:135-143.

186. Sullivan I, Planchard D. Next-Generation EGFR Tyrosine Kinase Inhibitors for Treating EGFR-Mutant Lung Cancer beyond First Line. *Front Med (Lausanne).* 2016;3:76.

# Chapter VII: Danksagung (Acknowledgements)

Ich danke Frau Prof. Julia Stingl für die Aufnahme in ihre Arbeitsgruppe am BfArM, die Möglichkeit zur Bearbeitung meines spannenden Forschungsprojekts und die Betreuung meiner Arbeit. Mein Dank gilt außerdem Herrn Prof. Ulrich Jaehde von der Universität Bonn für die Betreuung als Zweitgutachter und viele hilfreiche Diskussionen in den Seminaren. Auch bei Herrn Prof. Bendas und Frau Prof. Weltermann bedanke ich mich herzlich für ihre Arbeit als Prüfer.

Besonders bedanken möchte ich mich bei Dr. Catharina Scholl für die Betreuung in allen Situationen im Labor und beim Schreiben der Arbeit und die vielen wertvollen Diskussionen. Danke auch an Dr. Michael Steffens für die Durchführung statistischer Auswertungen. Ich möchte mich zudem herzlich bei Kerstin Brandenburg und Martina Wiertz bedanken für die vielfältige Unterstützung im Labor. An Kerstin außerdem vielen Dank, dass sie sich immer so gut um meine Gesundheit gekümmert hat (die physische und die psychische…). Meine Untersuchungen an Keratinozyten wären ohne Dr. Kazumasa Iwamoto und Tim Stroich (Dermatologie und Allergologie, Universitätsklinikum Bonn) und ihre zahlreichen Hautproben nicht möglich gewesen. Kazu and Tim, thank you for your time and effort! Dank außerdem an Bärbel Reiser für die Pflege der Datenbank und an alle Kollegen in den Dermatoxgen Studienzentren für die Probengewinnung und Erhebung der klinischen Daten.

Natürlich danke ich auch den weiteren Kollegen aus der Forschungsabteilung im BfArM, vor allem Anna, Simone, Miriam, Alva, Karim und Tatjana für die gute Arbeitsatmosphäre, ihre motivierenden Worte und die schöne Zeit, auch außerhalb des BfArMs. Ganz besonders hervorheben möchte ich meinen Bürokollegen Jörg Breitfeld, der mich zwar mit seinem unerschütterlichen Optimismus des Öfteren an den Rand des Wahnsinns getrieben hat, aber auch in jeder Situation das passende Getränk bereit hielt (Kaffee, Magen-Darm-Tee, Rotwein…) und meinen Lieblingspraktikanten Marcel Struß, der meine tiefe Begeisterung für Fibroblasten teilt und mir so manchen Arbeitstag erleichtert und verschönert hat.
Zudem danke ich Tonia und Annkathrin, die einfach immer ein offenes Ohr für mich haben.

Mein tiefster Dank gilt meinen Eltern und Großeltern und meiner Schwester Sonja für ihr Verständnis, ihren Rat und ihre bedingungslose Unterstützung, ohne die ich diese Arbeit nicht hätte schreiben können. Soni, du bist der einzige Mensch, der alle 200 (bzw. dann nur noch 197) Seiten dieser Arbeit am Stück durchgesehen hat, Danke dafür!
Auch meinem Verlobten Matthias Molitor danke ich für seine vielseitige Unterstützung und sein Verständnis für meine langen Arbeitszeiten, meine unberechenbaren Launen und meine Abwesenheit bei vielen Veranstaltungen.

DANKE!

# Appendix

## A) Keratinocytes

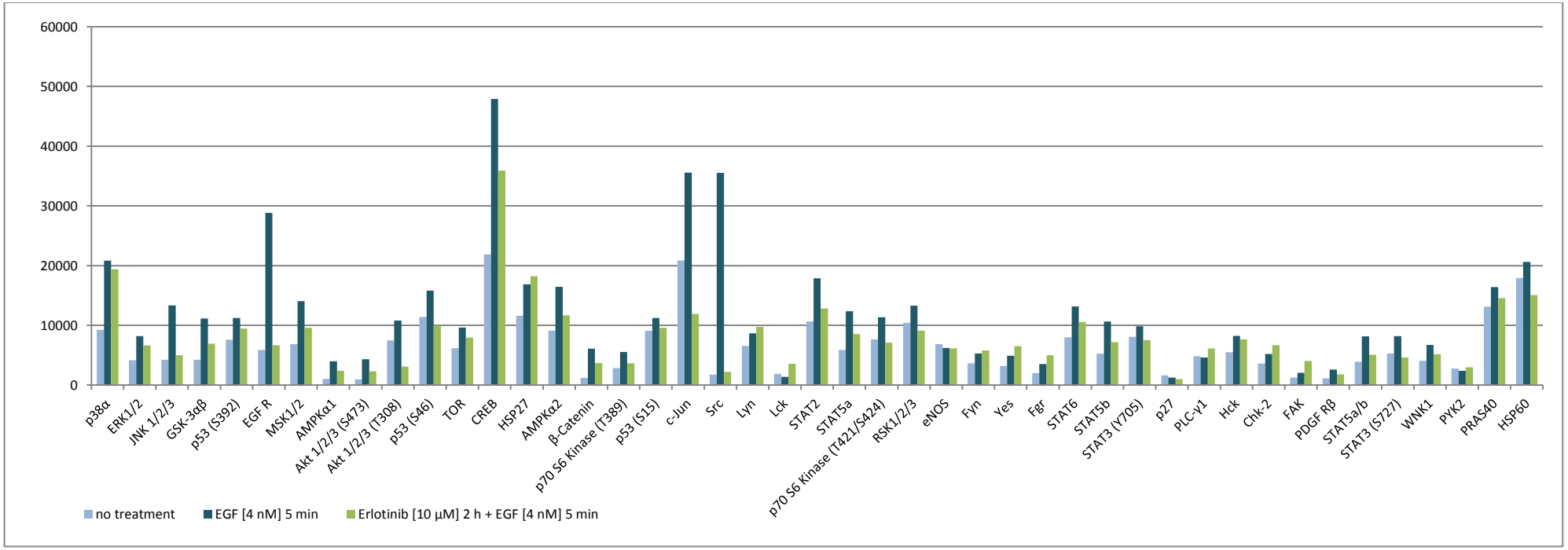


**Figure 34 Quantification of *in vitro* effect of erlotinib on phosphorylation of proteins involved in EGFR signaling in keratinocytes**

Human phospho kinase arrays were conducted with keratinocyte cell lysates of HK3 p6. The mean pixel density after chemiluminescent visualization of the 45 different phosphorylated proteins is shown. Light blue: no treatment. Dark blue: stimulated with 4 nM EGF for 5 min. Green: incubated with 10 µM erlotinib for 2 h then stimulated with 4 nM EGF for 5 min. A stronger signal (pixel density) corresponds to higher amounts of phosphorylated protein present and stronger signaling activity.

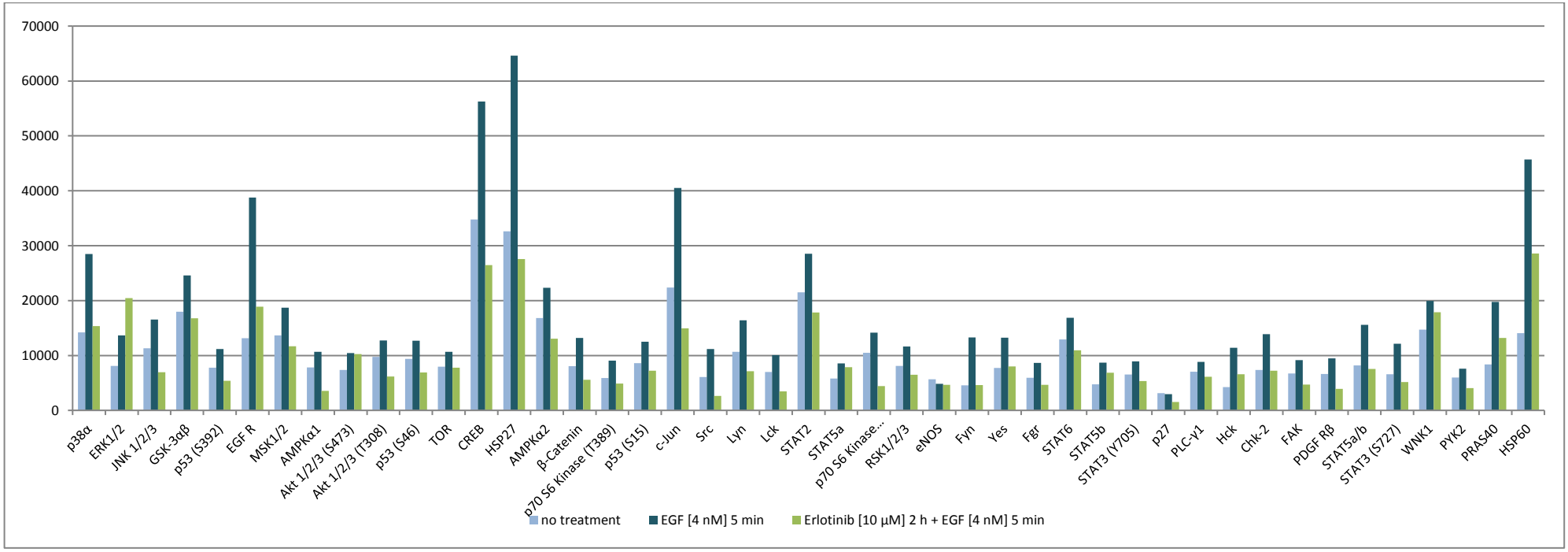


**Figure 35 Quantification of *in vitro* effect of erlotinib on phosphorylation of proteins involved in EGFR signaling in keratinocytes**

Human phospho kinase arrays were conducted with keratinocyte cell lysates of HK4 p5. The mean pixel density after chemiluminescent visualization of the 45 different phosphorylated proteins is shown. Light blue: no treatment. Dark blue: stimulated with 4 nM EGF for 5 min. Green: incubated with 10 µM erlotinib for 2 h then stimulated with 4 nM EGF for 5 min. A stronger signal (pixel density) corresponds to higher amounts of phosphorylated protein present and stronger signaling activity.

**Table 35 Mean pixel density for all proteins from human phospho-kinase arrays of 3 different keratinocyte samples**

Human phospho-kinase arrays were conducted with three different keratinocyte cell samples (HK3 p6, HK4 p5, HK4 p8) following three *in vitro* treatment conditions (no treatment, 4 nM EGF for 5 min and 10 µM erlotinib for 2 h + 4 nM EGF for 5 min). For clearer comparison of the stimulating effect of EGF and the inhibitory effect of erlotinib between the different cell samples, ratios were calculated (EGF/no treatment and erlotinib/EGF).

| | mean pixel density for HK3 p6 | | | | | mean pixel density for HK4 p5 | | | | | mean pixel density for HK4 p8 | | | | |
|---|---|---|---|---|---|---|---|---|---|---|---|---|---|---|---|
| **protein** | **no treatment** | **EGF** | **erlotinib** | **EGF/no treatment** | **erlotinib/ EGF** | **no treatment** | **EGF** | **erlotinib** | **EGF/no treatment** | **erlotinib/ EGF** | **no treatment** | **EGF** | **erlotinib** | **EGF/no treatment** | **erlotinib/ EGF** |
| p38α | 9257 | 20834 | 19411 | 2.25 | 0.93 | 14197 | 28490 | 15365 | 2.01 | 0.54 | 23003 | 25044 | 26302 | 1.09 | 1.05 |
| ERK1/2 | 4146 | 8193 | 6648 | 1.98 | 0.81 | 8088 | 13640 | 20449 | 1.69 | 1.50 | 6320 | 9400 | 12042 | 1.49 | 1.28 |
| JNK 1/2/3 | 4254 | 13344 | 4993 | 3.14 | 0.37 | 11292 | 16537 | 6933 | 1.46 | 0.42 | 9328 | 15247 | 8401 | 1.63 | 0.55 |
| GSK-3αβ | 4257 | 11144 | 6919 | 2.62 | 0.62 | 17955 | 24583 | 16753 | 1.37 | 0.68 | 14265 | 20224 | 11439 | 1.42 | 0.57 |
| p53 (S392) | 7604 | 11215 | 9440 | 1.47 | 0.84 | 7784 | 11159 | 5389 | 1.43 | 0.48 | 11360 | 13210 | 17600 | 1.16 | 1.33 |
| EGF R | 5884 | 28853 | 6687 | 4.90 | 0.23 | 13143 | 38779 | 18868 | 2.95 | 0.49 | 9225 | 26717 | 17661 | 2.90 | 0.66 |
| MSK1/2 | 6851 | 14030 | 9594 | 2.05 | 0.68 | 13645 | 18716 | 11666 | 1.37 | 0.62 | 9848 | 13096 | 9683 | 1.33 | 0.74 |
| AMPKα1 | 1052 | 4001 | 2370 | 3.80 | 0.59 | 7833 | 10667 | 3559 | 1.36 | 0.33 | 4752 | 8422 | 4465 | 1.77 | 0.53 |
| Akt 1/2/3 (S473) | 961 | 4329 | 2307 | 4.51 | 0.53 | 7371 | 10431 | 10278 | 1.42 | 0.99 | 5837 | 9662 | 5788 | 1.66 | 0.60 |
| Akt 1/2/3 (T308) | 7468 | 10801 | 3089 | 1.45 | 0.29 | 9737 | 12734 | 6152 | 1.31 | 0.48 | 9025 | 7851 | 8112 | 0.87 | 1.03 |
| p53 (S46) | 11411 | 15837 | 9948 | 1.39 | 0.63 | 9365 | 12674 | 6908 | 1.35 | 0.55 | 10314 | 11117 | 13412 | 1.08 | 1.21 |
| TOR | 6194 | 9612 | 7924 | 1.55 | 0.82 | 7981 | 10659 | 7795 | 1.34 | 0.73 | 6737 | 8726 | 5491 | 1.30 | 0.63 |
| CREB | 21876 | 47905 | 35917 | 2.19 | 0.75 | 34769 | 56251 | 26441 | 1.62 | 0.47 | 29126 | 39759 | 36996 | 1.37 | 0.93 |
| HSP27 | 11619 | 16861 | 18218 | 1.45 | 1.08 | 32599 | 64615 | 27547 | 1.98 | 0.43 | 36671 | 52802 | 38228 | 1.44 | 0.72 |
| AMPKα2 | 9104 | 16454 | 11697 | 1.81 | 0.71 | 16823 | 22308 | 13063 | 1.33 | 0.59 | 11567 | 17321 | 12701 | 1.50 | 0.73 |
| β-Catenin | 1188 | 6082 | 3689 | 5.12 | 0.61 | 8032 | 13209 | 5571 | 1.64 | 0.42 | 7497 | 12559 | 8644 | 1.68 | 0.69 |
| p70 S6 Kinase (T389) | 2829 | 5531 | 3632 | 1.96 | 0.66 | 5889 | 9046 | 4870 | 1.54 | 0.54 | 6288 | 8158 | 6935 | 1.30 | 0.85 |
| p53 (S15) | 9070 | 11242 | 9569 | 1.24 | 0.85 | 8587 | 12514 | 7244 | 1.46 | 0.58 | 7149 | 8645 | 9444 | 1.21 | 1.09 |
| c-Jun | 20885 | 35552 | 11892 | 1.70 | 0.33 | 22371 | 40513 | 14939 | 1.81 | 0.37 | 17372 | 27373 | 13679 | 1.58 | 0.50 |
| Src | 1772 | 35532 | 2232 | 20.05 | 0.06 | 6088 | 11194 | 2641 | 1.84 | 0.24 | 5823 | 6115 | 5262 | 1.05 | 0.86 |
| Lyn | 6535 | 8673 | 9738 | 1.33 | 1.12 | 10681 | 16419 | 7128 | 1.54 | 0.43 | 10610 | 11926 | 10205 | 1.12 | 0.86 |
| Lck | 1884 | 1367 | 3573 | 0.73 | 2.61 | 6984 | 10070 | 3472 | 1.44 | 0.34 | 5946 | 6710 | 4582 | 1.13 | 0.68 |

| | | | | | | | | | | | | | | | |
|---|---|---|---|---|---|---|---|---|---|---|---|---|---|---|---|
| STAT2 | 10656 | 17886 | 12811 | 1.68 | 0.72 | 21517 | 28507 | 17830 | 1.32 | 0.63 | 13986 | 19978 | 14816 | 1.43 | 0.74 |
| STAT5a | 5886 | 12383 | 8532 | 2.10 | 0.69 | 5799 | 8561 | 7891 | 1.48 | 0.92 | 4821 | 7515 | 5708 | 1.56 | 0.76 |
| p70 S6 Kinase (T421/S424) | 7654 | 11372 | 7104 | 1.49 | 0.62 | 10490 | 14143 | 4438 | 1.35 | 0.31 | 9455 | 11731 | 9768 | 1.24 | 0.83 |
| RSK1/2/3 | 10418 | 13291 | 9113 | 1.28 | 0.69 | 8092 | 11622 | 6495 | 1.44 | 0.56 | 8183 | 10719 | 8876 | 1.31 | 0.83 |
| eNOS | 6839 | 6205 | 6146 | 0.91 | 0.99 | 5642 | 4851 | 4650 | 0.86 | 0.96 | 5073 | 6622 | 5890 | 1.31 | 0.89 |
| Fyn | 3654 | 5283 | 5801 | 1.45 | 1.10 | 4578 | 13271 | 4596 | 2.90 | 0.35 | 6256 | 7909 | 6565 | 1.26 | 0.83 |
| Yes | 3198 | 4904 | 6517 | 1.53 | 1.33 | 7714 | 13232 | 7997 | 1.72 | 0.60 | 7640 | 8695 | 7142 | 1.14 | 0.82 |
| Fgr | 1993 | 3529 | 5000 | 1.77 | 1.42 | 5958 | 8667 | 4632 | 1.45 | 0.53 | 3935 | 4901 | 3489 | 1.25 | 0.71 |
| STAT6 | 7997 | 13154 | 10542 | 1.64 | 0.80 | 12898 | 16882 | 10946 | 1.31 | 0.65 | 8485 | 12311 | 8581 | 1.45 | 0.70 |
| STAT5b | 5269 | 10659 | 7190 | 2.02 | 0.67 | 4740 | 8702 | 6866 | 1.84 | 0.79 | 3667 | 5785 | 4539 | 1.58 | 0.78 |
| STAT3 (Y705) | 8084 | 9852 | 7505 | 1.22 | 0.76 | 6527 | 8941 | 5334 | 1.37 | 0.60 | 6858 | 8830 | 7490 | 1.29 | 0.85 |
| p27 | 1614 | 1235 | 984 | 0.77 | 0.80 | 3136 | 2956 | 1520 | 0.94 | 0.51 | 2329 | 2998 | 2689 | 1.29 | 0.90 |
| PLC-γ1 | 4823 | 4627 | 6131 | 0.96 | 1.32 | 7026 | 8822 | 6120 | 1.26 | 0.69 | 4998 | 6546 | 5084 | 1.31 | 0.78 |
| Hck | 5520 | 8245 | 7635 | 1.49 | 0.93 | 4264 | 11387 | 6576 | 2.67 | 0.58 | 6600 | 7100 | 6018 | 1.08 | 0.85 |
| Chk-2 | 3595 | 5224 | 6670 | 1.45 | 1.28 | 7381 | 13872 | 7230 | 1.88 | 0.52 | 8310 | 10288 | 8768 | 1.24 | 0.85 |
| FAK | 1246 | 2031 | 4023 | 1.63 | 1.98 | 6742 | 9168 | 4701 | 1.36 | 0.51 | 4885 | 6708 | 4938 | 1.37 | 0.74 |
| PDGF Rβ | 1122 | 2612 | 1778 | 2.33 | 0.68 | 6614 | 9461 | 3930 | 1.43 | 0.42 | 3837 | 6274 | 4550 | 1.64 | 0.73 |
| STAT5a/b | 3904 | 8139 | 5073 | 2.09 | 0.62 | 8170 | 15592 | 7540 | 1.91 | 0.48 | 6131 | 10003 | 7504 | 1.63 | 0.75 |
| STAT3 (S727) | 5283 | 8195 | 4634 | 1.55 | 0.57 | 6604 | 12134 | 5164 | 1.84 | 0.43 | 6612 | 10912 | 8433 | 1.65 | 0.77 |
| WNK1 | 4069 | 6723 | 5172 | 1.65 | 0.77 | 14725 | 19949 | 17859 | 1.35 | 0.90 | 8923 | 12783 | 9401 | 1.43 | 0.74 |
| PYK2 | 2756 | 2373 | 2959 | 0.86 | 1.25 | 5980 | 7615 | 4063 | 1.27 | 0.53 | 4775 | 6329 | 5323 | 1.33 | 0.84 |
| PRAS40 | 13122 | 16425 | 14567 | 1.25 | 0.89 | 8383 | 19763 | 13207 | 2.36 | 0.67 | 9501 | 11435 | 11182 | 1.20 | 0.98 |
| HSP60 | 17917 | 20612 | 15047 | 1.15 | 0.73 | 14059 | 45695 | 28590 | 3.25 | 0.63 | 17490 | 31426 | 21905 | 1.80 | 0.70 |

**Table 36 Differentially expressed miRNAs in erlotinib-sensitive as compared to -insensitive keratinocytes (incubation: EGF)**

Differentially expressed precursor and mature miRNAs in erlotinib-sensitive as compared to -insensitive keratinocytes (n = 6 in each group) previously stimulated with 4 nM EGF were determined by NGS and the program DESeq2. In vitro sensitivity towards erlotinib was previously determined by EGFR-ELISA. MiRNAs with a p-value < 0.05 and a fold change of ≥ 1.50 (up-regulated in erlotinib-sensitive cells) or ≤ 0.66 (down-regulated in erlotinib-sensitive) respectively, are listed. The fold change as logarithm of the basis 2 (log2 fold change) is given with its standard error (lfcSE, log fold change standard error). The result of the statistic Wald test (stat) together with the corresponding p-value is also listed.

| | erlotinib-sensitive vs. -insensitive incubation: EGF | | | | |
|---|---|---|---|---|---|
| **precursor miRNA (hairpin)** | **log2 fold change** | **lfcSE** | **fold change** | **stat** | **p-value** |
| hsa-mir-1181 | -0.9241 | 0.3209 | 0.5270 | -2.8800 | 3.98E-03 |
| hsa-mir-4284 | -0.8849 | 0.3271 | 0.5415 | -2.7051 | 6.83E-03 |
| hsa-mir-4461 | 0.9550 | 0.3545 | 1.9386 | 2.6944 | 7.05E-03 |
| hsa-mir-944 | 0.6490 | 0.2529 | 1.5681 | 2.5665 | 1.03E-02 |
| hsa-mir-9-3 | -0.8497 | 0.3471 | 0.5549 | -2.4482 | 1.44E-02 |
| hsa-mir-8082 | -0.8114 | 0.3336 | 0.5698 | -2.4322 | 1.50E-02 |
| hsa-mir-5000 | -0.6807 | 0.2893 | 0.6239 | -2.3527 | 1.86E-02 |
| hsa-mir-203b | -0.6924 | 0.3094 | 0.6188 | -2.2374 | 2.53E-02 |
| hsa-mir-203a | -0.6441 | 0.2905 | 0.6399 | -2.2173 | 2.66E-02 |
| hsa-mir-877 | -0.7405 | 0.3433 | 0.5985 | -2.1568 | 3.10E-02 |
| hsa-mir-3138 | -0.6805 | 0.3234 | 0.6239 | -2.1042 | 3.54E-02 |
| hsa-mir-3973 | -0.6342 | 0.3134 | 0.6443 | -2.0238 | 4.30E-02 |
| hsa-mir-146a | -0.6885 | 0.3418 | 0.6205 | -2.0143 | 4.40E-02 |
| hsa-mir-6797 | -0.6631 | 0.3359 | 0.6315 | -1.9740 | 4.84E-02 |
| hsa-mir-548ao | 0.6478 | 0.3285 | 1.5668 | 1.9718 | 4.86E-02 |
| hsa-mir-1246 | -0.6296 | 0.3200 | 0.6464 | -1.9676 | 4.91E-02 |
| | | | | | |
| **mature miRNA** | | | | | |
| hsa-miR-146a-5p | -0.8212 | 0.2957 | 0.5660 | -2.7771 | 5.49E-03 |
| hsa-miR-199a-3p | -0.7039 | 0.3021 | 0.6139 | -2.3297 | 1.98E-02 |
| hsa-miR-203a | -0.6213 | 0.2780 | 0.6501 | -2.2354 | 2.54E-02 |
| hsa-miR-328-3p | -0.6625 | 0.3139 | 0.6318 | -2.1106 | 3.48E-02 |
| hsa-miR-744-3p | 0.6363 | 0.3109 | 1.5544 | 2.0469 | 4.07E-02 |

There were 13 precursor and four mature miRNAs significantly down-regulated and three precursor miRNAs and one mature miRNA significantly up-regulated in the erlotinib-sensitive cells. Fold changes ranged between 1.55 and 1.94 (0.65 and 0.53 for down-regulation respectively).

**Table 37 Differentially expressed miRNAs in erlotinib-sensitive as compared to -insensitive keratinocytes (incubation: erlotinib + EGF)**

Differentially expressed precursor and mature miRNAs in erlotinib-sensitive as compared to -insensitive keratinocytes (n = 6 in each group) previously incubated with 5 µM erlotinib and 4 nM EGF were determined by NGS and the program DESeq2. In vitro sensitivity towards erlotinib was previously determined by EGFR-ELISA. MiRNAs with a p-value < 0.02 and fold change of ≥ 1.50 (up-regulated in erlotinib-sensitive cells) or ≤ 0.66 (down-regulated in erlotinib-sensitive) respectively, are listed. Fold change as logarithm of the basis 2 (log2 fold change) is given with its standard error (lfcSE, log fold change standard error). The result of the statistic Wald test (stat) with the corresponding p-value is also listed.

| | erlotinib-sensitive vs. -insensitive incubation: erlotinib + EGF | | | | |
|---|---|---|---|---|---|
| **precursor miRNA (hairpin)** | **log2 fold change** | **lfcSE** | **fold change** | **stat** | **p-value** |
| hsa-mir-520e | -2.4886 | 0.3985 | 0.1782 | -6.2441 | 4.26E-10 |
| hsa-mir-138-2 | -1.3058 | 0.3455 | 0.4045 | -3.7797 | 1.57E-04 |
| hsa-mir-944 | 0.7424 | 0.2406 | 1.6730 | 3.0851 | 2.03E-03 |
| hsa-mir-585 | 1.1030 | 0.3904 | 2.1480 | 2.8256 | 4.72E-03 |
| hsa-mir-1263 | -1.0450 | 0.3955 | 0.4847 | -2.6424 | 8.23E-03 |
| hsa-mir-31 | -0.6154 | 0.2375 | 0.6527 | -2.5913 | 9.56E-03 |
| hsa-mir-615 | 0.8141 | 0.3202 | 1.7582 | 2.5422 | 1.10E-02 |
| hsa-mir-203b | -0.8346 | 0.3355 | 0.5607 | -2.4879 | 1.29E-02 |
| hsa-mir-5690 | -0.8531 | 0.3517 | 0.5536 | -2.4252 | 1.53E-02 |
| hsa-mir-3615 | -0.6497 | 0.2686 | 0.6374 | -2.4186 | 1.56E-02 |
| hsa-mir-3911 | -0.8821 | 0.3655 | 0.5426 | -2.4132 | 1.58E-02 |
| hsa-mir-942 | 0.8371 | 0.3500 | 1.7865 | 2.3915 | 1.68E-02 |
| hsa-mir-137 | -0.9345 | 0.3931 | 0.5232 | -2.3774 | 1.74E-02 |
| **mature miRNA** | | | | | |
| hsa-miR-520e | -1.4014 | 0.3285 | 0.3786 | -4.2660 | 1.99E-05 |
| hsa-miR-138-5p | -1.1798 | 0.3404 | 0.4414 | -3.4664 | 5.27E-04 |
| hsa-miR-221-3p | -0.5960 | 0.1954 | 0.6616 | -3.0494 | 2.29E-03 |
| hsa-miR-146a-5p | -1.0023 | 0.3481 | 0.4992 | -2.8792 | 3.99E-03 |
| hsa-miR-138-2-3p | -0.9914 | 0.3508 | 0.5030 | -2.8261 | 4.71E-03 |
| hsa-miR-944 | 0.6969 | 0.2507 | 1.6210 | 2.7800 | 5.44E-03 |
| hsa-miR-16-2-3p | 0.8118 | 0.2991 | 1.7554 | 2.7139 | 6.65E-03 |
| hsa-let-7e-3p | -0.8953 | 0.3595 | 0.5376 | -2.4907 | 1.27E-02 |
| hsa-miR-615-3p | 0.7502 | 0.3100 | 1.6820 | 2.4197 | 1.55E-02 |
| hsa-miR-210-3p | -0.8384 | 0.3530 | 0.5593 | -2.3752 | 1.75E-02 |

In keratinocytes which were incubated with erlotinib and then stimulated with EGF prior to sequencing, the list of significantly differentially expressed miRNAs is substantially longer than for untreated and only EGF-stimulated cells (when comparing erlotinib-sensitive to -insensitive cells). Therefore, in 37 only the most significant miRNAs with a p-value < 0.02

are listed. This restriction results in a list of nine precursor and seven mature miRNAs down-regulated and four precursor and three mature miRNAs up-regulated in the erlotinib-sensitive cells. Fold changes ranged between 1.62 and 2.15 (0.66 and 0.18 for down-regulation respectively).

**Table 38 Overview of literature search for miRNAs found to be significantly differentially expressed in erlotinib-sensitive as compared to -insensitive keratinocytes by NGS**

Specific miRNAs which were significantly differentially expressed (p-value < 0.05) in all three *in vitro* treatment groups (none, 4 nM EGF or 5 µM erlotinib plus 4 nM EGF) represent a "baseline" difference between erlotinib-sensitive and -insensitive cells and are called "overlap miRNAs" here. Specific miRNAs which were only significantly differentially expressed in cells treated with erlotinib are called "erlotinib only" miRNAs here. For the "overlap" and the "erlotinib only" miRNAs a thorough literature search was conducted and publications concerning their association with cancer, EGFR or other tyrosine kinases, erlotinib or other EGFRIs, fibroblasts and keratinocytes were reviewed. √ means at least one publication has been found. (√) means a closely related or superordinate miRNA has been found in this context (e.g. hsa-mir-7 instead of hsa-mir-7-1). In the lists for mature miRNAs those miRNAs already listed for precursors are not included again. MiRNAs chosen for further analyses are marked in bold.

**"overlap miRNAs"**

| | *cue for literature search* | | | | | | | |
|---|---|---|---|---|---|---|---|---|
| **miRNA name** | **miRNA** | **cancer** | **EGFR** | **tyrosine kinase** | **erlotinib** | **keratinocytes** | **fibroblasts** | **comment** |
| **hsa-mir-146a** | √ | √ | √ | √ | √ | √ | √ | interesting |

**"erlotinib only miRNAs"**

| | *cue for literature search* | | | | | | | |
|---|---|---|---|---|---|---|---|---|
| **miRNA name** | **miRNA** | **cancer** | **EGFR** | **tyrosine kinase** | **erlotinib** | **keratinocytes** | **fibroblasts** | **comment** |
| **precursors** | | | | | | | | |
| hsa-mir-1263 | - | - | - | - | - | - | - | |
| hsa-mir-137 | √ | √ | - | √ | - | √ | - | |
| **hsa-mir-138-2** | √ | (√) | (√) | (√) | (gefitinib) | (√) | (√) | (mir-138), interesting |
| hsa-mir-197 | √ | √ | - | √ | - | √ | - | |
| **hsa-mir-31** | √ | √ | √ | √ | (cetuximab) | √ | √ | interesting |
| hsa-mir-3615 | √ | √ | - | - | - | - | - | |
| hsa-mir-5195 | - | - | - | - | - | - | - | |
| **hsa-mir-520e** | √ | √ | √ | √ | - | - | - | interesting, also for FB! |
| hsa-mir-5690 | - | - | - | - | - | - | - | |
| hsa-mir-585 | √ | √ | - | - | - | - | - | |
| hsa-mir-609 | √ | - | - | - | - | - | - | |
| hsa-mir-615 | √ | √ | - | (√) | - | - | - | |

| | | | | | | | | |
|---|---|---|---|---|---|---|---|---|
| hsa-mir-622 | √ | √ | - | √ | - | - | - | |
| hsa-mir-6510 | - | - | - | - | - | - | - | |
| hsa-mir-675 | √ | √ | (√) | √ | - | √ | √ | (H19 = long non-coding precursor of miR-675) |
| hsa-mir-6780b | √ | √ | - | - | - | - | - | |
| hsa-mir-711 | √ | √ | - | - | - | - | - | |
| hsa-mir-875 | (√) | √ | - | - | - | (√) | - | |
| hsa-mir-942 | √ | √ | - | - | - | - | - | |
| | | | | | | | | |
| **mature** | | | | | | | | |
| hsa-let-7e-3p | √ | √ | √ | √ | - | - | - | |
| hsa-miR-1282 | √ | √ | - | - | - | - | - | |
| hsa-miR-1299 | √ | √ | - | - | - | - | - | |
| hsa-miR-138-5p | √ | (√) | √ | √ | (gefitinib) | √ | √ | interesting, mir-138-2 chosen |
| hsa-miR-16-2-3p | √ | (√) | (√) | (√) | - | (√) | (√) | |
| hsa-miR-210-3p | √ | √ | (√) | (√) | - | (√) | (√) | |
| **hsa-miR-221-3p** | √ | √ | √ | (√) | - | (√) | (√) | interesting |
| hsa-miR-7641 | √ | √ | - | - | - | - | - | |
| **hsa-miR-944** | √ | √ | - | √ | - | √ | - | |

## B) Fibroblasts

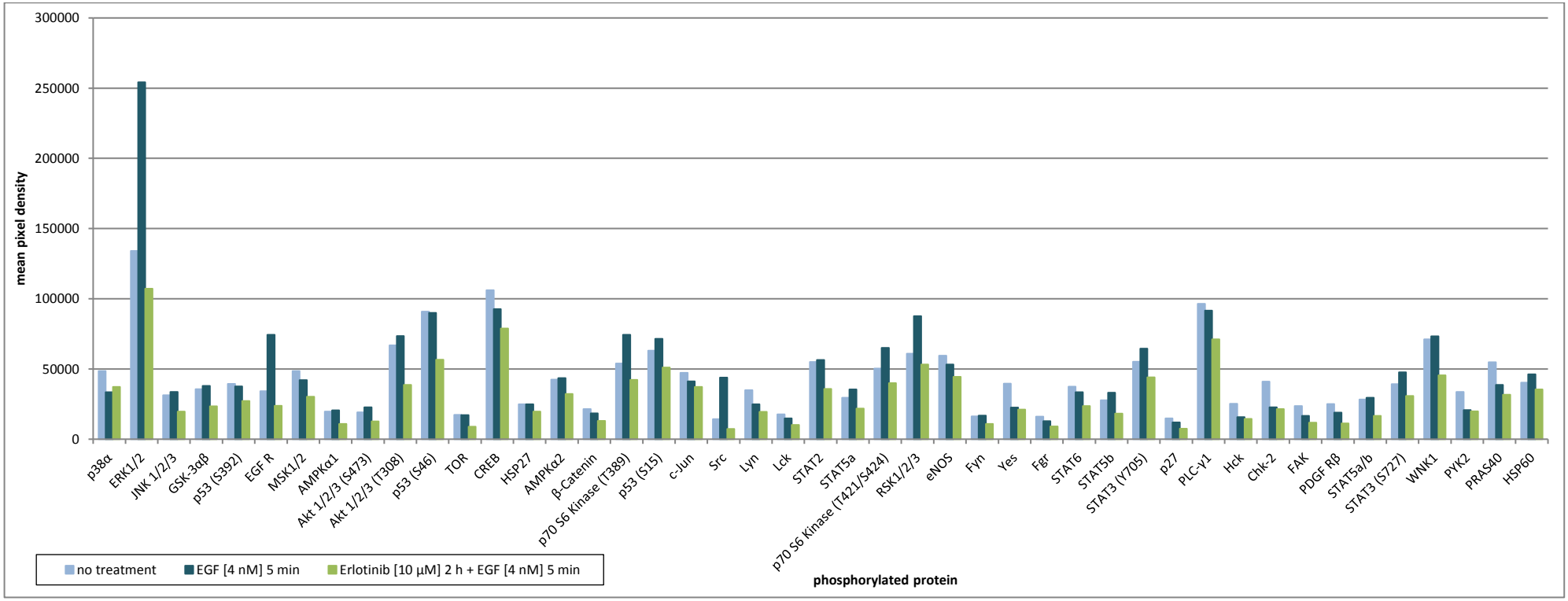


**Figure 36 Quantification of *in vitro* effect of erlotinib on phosphorylation of proteins involved in EGFR signaling in fibroblasts**

Human phospho kinase arrays were conducted with dermal fibroblast cell lysates of FB64 p7. The mean pixel density after chemiluminescent visualization of the 45 different phosphorylated proteins is shown. Light blue: no treatment. Dark blue: stimulated with 4 nM EGF for 5 min. Green: incubated with 10 µM erlotinib for 2 h then stimulated with 4 nM EGF for 5 min. A stronger signal (pixel density) corresponds to higher amounts of phosphorylated protein present and stronger signaling activity.

**Table 39 Mean pixel density for all proteins from human phospho-kinase arrays of two different fibroblast samples**

Human phospho-kinase arrays were conducted with two different fibroblast cell samples (FB64 p7 and FB120 p8) following three *in vitro* treatment conditions (no treatment, 4 nM EGF for 5 min and 10 µM erlotinib for 2 h + 4 nM EGF for 5 min). For clearer comparison of the stimulating effect of EGF and the inhibitory effect of erlotinib between the different cell samples, ratios were calculated (EGF/no treatment and erlotinib/EGF).

| | mean pixel density for FB64 p7 | | | | | mean pixel density for FB120 p8 | | | | |
|---|---|---|---|---|---|---|---|---|---|---|
| **protein** | **no treatment** | **EGF** | **erlotinib** | **EGF/no treatment** | **erlotinib/ EGF** | **no treatment** | **EGF** | **erlotinib** | **EGF/no treatment** | **erlotinib/ EGF** |
| p38α | 48455 | 33452 | 37262 | 0.69 | 1.11 | 16413 | 15591 | 8104 | 0.95 | 0.52 |
| ERK1/2 | 134053 | 254220 | 107268 | 1.90 | 0.42 | 64331 | 182975 | 33812 | 2.84 | 0.18 |
| JNK 1/2/3 | 31304 | 33636 | 19622 | 1.07 | 0.58 | 6889 | 8930 | 4786 | 1.30 | 0.54 |
| GSK-3αβ | 35587 | 37931 | 23447 | 1.07 | 0.62 | 14108 | 19551 | 10494 | 1.39 | 0.54 |
| p53 (S392) | 39400 | 37560 | 27196 | 0.95 | 0.72 | 10888 | 10334 | 9604 | 0.95 | 0.93 |
| EGF R | 34264 | 74409 | 23720 | 2.17 | 0.32 | 7628 | 24849 | 4612 | 3.26 | 0.19 |
| MSK1/2 | 48500 | 42084 | 30278 | 0.87 | 0.72 | 10066 | 13658 | 5942 | 1.36 | 0.44 |
| AMPKα1 | 19637 | 20536 | 10839 | 1.05 | 0.53 | 4540 | 6167 | 3295 | 1.36 | 0.53 |
| Akt 1/2/3 (S473) | 19079 | 22766 | 12611 | 1.19 | 0.55 | 4629 | 11388 | 3942 | 2.46 | 0.35 |
| Akt 1/2/3 (T308) | 66851 | 73386 | 38726 | 1.10 | 0.53 | 11092 | 15493 | 10034 | 1.40 | 0.65 |
| p53 (S46) | 90862 | 89905 | 56668 | 0.99 | 0.63 | 14209 | 16816 | 11888 | 1.18 | 0.71 |
| TOR | 17408 | 17158 | 8974 | 0.99 | 0.52 | 5835 | 8063 | 2370 | 1.38 | 0.29 |
| CREB | 106105 | 92573 | 78798 | 0.87 | 0.85 | 28362 | 30446 | 19193 | 1.07 | 0.63 |
| HSP27 | 24846 | 24911 | 19649 | 1.00 | 0.79 | 6881 | 11764 | 4508 | 1.71 | 0.38 |
| AMPKα2 | 42436 | 43524 | 32276 | 1.03 | 0.74 | 12909 | 19528 | 10526 | 1.51 | 0.54 |
| β-Catenin | 21551 | 18328 | 12956 | 0.85 | 0.71 | 3458 | 5233 | 3355 | 1.51 | 0.64 |
| p70 S6 Kinase (T389) | 53872 | 74366 | 42203 | 1.38 | 0.57 | 6868 | 12281 | 5201 | 1.79 | 0.42 |
| p53 (S15) | 63097 | 71452 | 50963 | 1.13 | 0.71 | 9070 | 11694 | 7106 | 1.29 | 0.61 |
| c-Jun | 47208 | 41204 | 37222 | 0.87 | 0.90 | 7833 | 10276 | 5877 | 1.31 | 0.57 |
| Src | 14331 | 43802 | 7245 | 3.06 | 0.17 | 5677 | 7299 | 1791 | 1.29 | 0.25 |
| Lyn | 34875 | 24861 | 19574 | 0.71 | 0.79 | 9440 | 12425 | 5558 | 1.32 | 0.45 |
| Lck | 17672 | 14847 | 10124 | 0.84 | 0.68 | 3958 | 6676 | 2784 | 1.69 | 0.42 |

| | | | | | | | | | | |
|---|---|---|---|---|---|---|---|---|---|---|
| STAT2 | 55007 | 56417 | 35881 | 1.03 | 0.64 | 15206 | 21569 | 11657 | 1.42 | 0.54 |
| STAT5a | 29578 | 35512 | 21838 | 1.20 | 0.61 | 5226 | 8992 | 4143 | 1.72 | 0.46 |
| p70 S6 Kinase (T421/S424) | 50392 | 65028 | 39881 | 1.29 | 0.61 | 13615 | 18662 | 10030 | 1.37 | 0.54 |
| RSK1/2/3 | 60980 | 87714 | 53284 | 1.44 | 0.61 | 12037 | 18244 | 8482 | 1.52 | 0.46 |
| eNOS | 59493 | 53156 | 44472 | 0.89 | 0.84 | 5608 | 6911 | 4304 | 1.23 | 0.62 |
| Fyn | 16314 | 16881 | 10913 | 1.03 | 0.65 | 5271 | 7356 | 3779 | 1.40 | 0.51 |
| Yes | 39636 | 22497 | 21097 | 0.57 | 0.94 | 6502 | 9564 | 4961 | 1.47 | 0.52 |
| Fgr | 15996 | 12807 | 9173 | 0.80 | 0.72 | 3094 | 5588 | 2839 | 1.81 | 0.51 |
| STAT6 | 37348 | 33422 | 23655 | 0.89 | 0.71 | 8813 | 15219 | 6981 | 1.73 | 0.46 |
| STAT5b | 27802 | 33193 | 18316 | 1.19 | 0.55 | 4966 | 10092 | 4374 | 2.03 | 0.43 |
| STAT3 (Y705) | 55209 | 64578 | 44114 | 1.17 | 0.68 | 8816 | 12867 | 6591 | 1.46 | 0.51 |
| p27 | 14853 | 12045 | 7530 | 0.81 | 0.63 | 2985 | 3197 | 1616 | 1.07 | 0.51 |
| PLC-γ1 | 96466 | 91609 | 71067 | 0.95 | 0.78 | 7595 | 9793 | 5630 | 1.29 | 0.57 |
| Hck | 25273 | 15717 | 14407 | 0.62 | 0.92 | 5396 | 7576 | 4313 | 1.40 | 0.57 |
| Chk-2 | 41064 | 22688 | 21420 | 0.55 | 0.94 | 7866 | 11194 | 6144 | 1.42 | 0.55 |
| FAK | 23624 | 16607 | 11723 | 0.70 | 0.71 | 3811 | 5907 | 2959 | 1.55 | 0.50 |
| PDGF Rβ | 25026 | 18932 | 11300 | 0.76 | 0.60 | 4638 | 6810 | 4207 | 1.47 | 0.62 |
| STAT5a/b | 28200 | 29490 | 16658 | 1.05 | 0.56 | 6289 | 10251 | 5878 | 1.63 | 0.57 |
| STAT3 (S727) | 39278 | 47581 | 30870 | 1.21 | 0.65 | 11053 | 18198 | 9715 | 1.65 | 0.53 |
| WNK1 | 71225 | 73212 | 45498 | 1.03 | 0.62 | 11438 | 16083 | 7915 | 1.41 | 0.49 |
| PYK2 | 33731 | 20784 | 19913 | 0.62 | 0.96 | 6705 | 9206 | 4484 | 1.37 | 0.49 |
| PRAS40 | 54826 | 38643 | 31747 | 0.70 | 0.82 | 8383 | 12462 | 6479 | 1.49 | 0.52 |
| HSP60 | 40293 | 46245 | 35509 | 1.15 | 0.77 | 17836 | 25243 | 20169 | 1.42 | 0.80 |

**Table 40 Differentially expressed miRNAs in erlotinib-sensitive as compared to -insensitive fibroblasts (incubation: EGF)**

Differentially expressed precursor and mature miRNAs in erlotinib-sensitive as compared to -insensitive fibroblasts (n = 4 in each group) previously stimulated with 4 nM EGF were determined by NGS and the program DESeq2. *In vitro* sensitivity towards erlotinib was previously determined by ERK 1/2-ELISA. MiRNAs with a p-value < 0.02 and a fold change of ≥ 1.50 (up-regulated in erlotinib-sensitive cells) or ≤ 0.66 (down-regulated in erlotinib-sensitive) respectively, are listed. The fold change as logarithm of the basis 2 (log2 fold change) is given with its standard error (lfcSE, log fold change standard error). The result of the statistic Wald test (stat) together with the corresponding p-value is also listed.

| | erlotinib-sensitive vs. -insensitive incubation: EGF | | | | |
|---|---|---|---|---|---|
| **precursor miRNA (hairpin)** | **log2 fold change** | **lfcSE** | **fold change** | **stat** | **p-value** |
| hsa-mir-30b | 1.1489 | 0.3009 | 2.2175 | 3.8184 | 1.34E-04 |
| hsa-mir-199b | 1.0110 | 0.3004 | 2.0153 | 3.3649 | 7.66E-04 |
| hsa-mir-1273a | -1.0836 | 0.3259 | 0.4718 | -3.3247 | 8.85E-04 |
| hsa-mir-1273g | -1.0559 | 0.3179 | 0.4810 | -3.3210 | 8.97E-04 |
| hsa-mir-382 | 1.2671 | 0.3910 | 2.4068 | 3.2407 | 1.19E-03 |
| hsa-mir-342 | 1.2297 | 0.3967 | 2.3452 | 3.0997 | 1.94E-03 |
| hsa-mir-452 | 1.2955 | 0.4188 | 2.4547 | 3.0931 | 1.98E-03 |
| hsa-mir-450b | 0.9669 | 0.3128 | 1.9546 | 3.0907 | 2.00E-03 |
| hsa-mir-148b | 0.7591 | 0.2486 | 1.6924 | 3.0535 | 2.26E-03 |
| hsa-mir-494 | 1.3173 | 0.4433 | 2.4921 | 2.9715 | 2.96E-03 |
| hsa-mir-107 | 0.8711 | 0.3032 | 1.8290 | 2.8733 | 4.06E-03 |
| hsa-mir-4510 | -0.8290 | 0.2934 | 0.5629 | -2.8257 | 4.72E-03 |
| hsa-mir-127 | 1.2327 | 0.4442 | 2.3501 | 2.7754 | 5.51E-03 |
| hsa-mir-585 | 1.0837 | 0.3935 | 2.1195 | 2.7537 | 5.89E-03 |
| hsa-mir-615 | -0.7948 | 0.2902 | 0.5764 | -2.7387 | 6.17E-03 |
| hsa-mir-155 | 0.9491 | 0.3468 | 1.9307 | 2.7364 | 6.21E-03 |
| hsa-mir-34a | 0.8328 | 0.3049 | 1.7811 | 2.7311 | 6.31E-03 |
| hsa-mir-148a | 1.1817 | 0.4360 | 2.2684 | 2.7103 | 6.72E-03 |
| hsa-mir-379 | 1.1840 | 0.4379 | 2.2720 | 2.7040 | 6.85E-03 |
| hsa-mir-20a | 0.9481 | 0.3541 | 1.9294 | 2.6773 | 7.42E-03 |
| hsa-mir-106b | 0.7494 | 0.2825 | 1.6811 | 2.6531 | 7.98E-03 |
| hsa-mir-4508 | -1.2907 | 0.4898 | 0.4088 | -2.6350 | 8.41E-03 |
| hsa-mir-101-2 | 0.8362 | 0.3189 | 1.7853 | 2.6221 | 8.74E-03 |
| hsa-mir-3120 | 0.8283 | 0.3179 | 1.7755 | 2.6053 | 9.18E-03 |
| hsa-mir-374b | 0.7545 | 0.2898 | 1.6870 | 2.6038 | 9.22E-03 |
| hsa-mir-25 | 0.6959 | 0.2754 | 1.6199 | 2.5272 | 1.15E-02 |
| hsa-mir-6838 | -1.0350 | 0.4154 | 0.4880 | -2.4913 | 1.27E-02 |
| hsa-mir-101-1 | 0.7985 | 0.3218 | 1.7393 | 2.4814 | 1.31E-02 |
| hsa-mir-19b-1 | 1.1539 | 0.4675 | 2.2251 | 2.4682 | 1.36E-02 |
| hsa-mir-300 | 1.3163 | 0.5340 | 2.4903 | 2.4651 | 1.37E-02 |
| hsa-mir-299 | 1.1065 | 0.4508 | 2.1532 | 2.4543 | 1.41E-02 |
| hsa-mir-103a-2 | 0.6920 | 0.2827 | 1.6155 | 2.4481 | 1.44E-02 |

| | | | | | |
|---|---|---|---|---|---|
| hsa-mir-329-1 | 1.0451 | 0.4295 | 2.0635 | 2.4334 | 1.50E-02 |
| hsa-mir-4419a | -0.8746 | 0.3670 | 0.5454 | -2.3830 | 1.72E-02 |
| hsa-mir-196a-1 | -0.9705 | 0.4082 | 0.5103 | -2.3777 | 1.74E-02 |
| hsa-mir-889 | 0.9951 | 0.4191 | 1.9932 | 2.3742 | 1.76E-02 |
| hsa-mir-3529 | 0.8237 | 0.3485 | 1.7699 | 2.3632 | 1.81E-02 |
| hsa-mir-103a-1 | 0.6677 | 0.2827 | 1.5885 | 2.3619 | 1.82E-02 |
| hsa-mir-134 | 0.9904 | 0.4195 | 1.9867 | 2.3606 | 1.82E-02 |
| | | | | | |
| **mature miRNA** | | | | | |
| hsa-miR-22-3p | -0.7501 | 0.1344 | 0.5946 | -5.5822 | 2.38E-08 |
| hsa-miR-452-5p | 2.1789 | 0.5188 | 4.5281 | 4.1996 | 2.67E-05 |
| hsa-miR-4510 | -1.1409 | 0.2933 | 0.4535 | -3.8894 | 1.00E-04 |
| hsa-miR-450b-5p | 0.7362 | 0.1999 | 1.6657 | 3.6821 | 2.31E-04 |
| hsa-let-7d-3p | -0.9480 | 0.2886 | 0.5184 | -3.2844 | 1.02E-03 |
| hsa-miR-125b-1-3p | -0.6121 | 0.1879 | 0.6542 | -3.2578 | 1.12E-03 |
| hsa-miR-1285-5p | -1.8478 | 0.5681 | 0.2778 | -3.2526 | 1.14E-03 |
| hsa-miR-5684 | -1.5474 | 0.4891 | 0.3421 | -3.1640 | 1.56E-03 |
| hsa-miR-1827 | -1.5010 | 0.4786 | 0.3533 | -3.1366 | 1.71E-03 |
| hsa-miR-1273g-3p | -1.4620 | 0.4768 | 0.3630 | -3.0659 | 2.17E-03 |
| hsa-miR-127-5p | 1.4988 | 0.4916 | 2.8260 | 3.0488 | 2.30E-03 |
| hsa-miR-138-5p | -0.8402 | 0.2803 | 0.5585 | -2.9980 | 2.72E-03 |
| hsa-miR-615-3p | -1.1127 | 0.3722 | 0.4624 | -2.9898 | 2.79E-03 |
| hsa-miR-1273d | -1.8095 | 0.6157 | 0.2853 | -2.9392 | 3.29E-03 |
| hsa-miR-299-3p | 1.2538 | 0.4284 | 2.3847 | 2.9266 | 3.43E-03 |
| hsa-miR-20a-5p | 0.8014 | 0.2760 | 1.7428 | 2.9033 | 3.69E-03 |
| hsa-miR-30b-5p | 0.9882 | 0.3418 | 1.9837 | 2.8910 | 3.84E-03 |
| hsa-miR-300 | 1.9305 | 0.6801 | 3.8119 | 2.8386 | 4.53E-03 |
| hsa-miR-490-3p | -1.9406 | 0.6875 | 0.2605 | -2.8227 | 4.76E-03 |
| hsa-miR-199b-5p | 1.3917 | 0.4942 | 2.6238 | 2.8160 | 4.86E-03 |
| hsa-miR-4648 | -1.9378 | 0.6898 | 0.2610 | -2.8091 | 4.97E-03 |
| hsa-miR-22-5p | -0.7864 | 0.2813 | 0.5798 | -2.7957 | 5.18E-03 |
| hsa-miR-3135b | -1.1090 | 0.3982 | 0.4636 | -2.7848 | 5.36E-03 |
| hsa-miR-149-3p | -1.8630 | 0.6870 | 0.2749 | -2.7117 | 6.69E-03 |
| hsa-miR-548h-5p | 1.6784 | 0.6260 | 3.2007 | 2.6813 | 7.33E-03 |
| hsa-miR-653-3p | -1.5127 | 0.5678 | 0.3504 | -2.6644 | 7.71E-03 |
| hsa-miR-1303 | -1.0440 | 0.3972 | 0.4850 | -2.6282 | 8.58E-03 |
| hsa-miR-5585-3p | -1.2743 | 0.4878 | 0.4134 | -2.6127 | 8.98E-03 |
| hsa-miR-4508 | -1.6642 | 0.6494 | 0.3155 | -2.5627 | 1.04E-02 |
| hsa-miR-125b-2-3p | 1.1948 | 0.4681 | 2.2891 | 2.5525 | 1.07E-02 |
| hsa-miR-655-3p | 1.2337 | 0.4882 | 2.3518 | 2.5271 | 1.15E-02 |
| hsa-miR-145-3p | -1.3832 | 0.5476 | 0.3834 | -2.5256 | 1.15E-02 |
| hsa-miR-7851-3p | -1.5984 | 0.6351 | 0.3302 | -2.5166 | 1.18E-02 |
| hsa-miR-6780a-3p | -1.6601 | 0.6606 | 0.3164 | -2.5128 | 1.20E-02 |
| hsa-miR-3925-5p | -1.7267 | 0.6943 | 0.3021 | -2.4870 | 1.29E-02 |
| hsa-miR-17-5p | 0.7216 | 0.2919 | 1.6490 | 2.4723 | 1.34E-02 |

| | | | | | |
|---|---|---|---|---|---|
| hsa-miR-4492 | -1.7022 | 0.6942 | 0.3073 | -2.4519 | 1.42E-02 |
| hsa-miR-708-5p | -0.8588 | 0.3606 | 0.5514 | -2.3817 | 1.72E-02 |
| hsa-miR-548k | 1.3489 | 0.5675 | 2.5472 | 2.3768 | 1.75E-02 |
| hsa-miR-3667-3p | -1.6472 | 0.6935 | 0.3193 | -2.3751 | 1.75E-02 |
| hsa-miR-27b-5p | -0.9829 | 0.4186 | 0.5060 | -2.3480 | 1.89E-02 |

There were eight precursor and 28 mature miRNAs significantly down-regulated and 31 precursor and 13 mature miRNA significantly up-regulated in the erlotinib-sensitive cells. Fold changes ranged between 1.59 and 4.53 (0.65 and 0.26 for down-regulation respectively).

**Table 41 Differentially expressed miRNAs in erlotinib-sensitive as compared to -insensitive fibroblasts (incubation: erlotinib + EGF)**

Differentially expressed precursor and mature miRNAs in erlotinib-sensitive as compared to -insensitive fibroblasts (n = 4 in each group) previously incubated with 5 µM erlotinib and 4 nM EGF were determined by NGS and the program DESeq2. *In vitro* sensitivity towards erlotinib was previously determined by ERK 1/2-ELISA. MiRNAs with a p-value < 0.02 and a fold change of ≥ 1.50 (up-regulated in erlotinib-sensitive cells) or ≤ 0.66 (down-regulated in erlotinib-sensitive) respectively, are listed. The fold change as logarithm of the basis 2 (log2 fold change) is given with its standard error (lfcSE, log fold change standard error). The result of the statistic Wald test (stat) together with the corresponding p-value is also listed.

| | erlotinib-sensitive vs. -insensitive incubation: erlotinib + EGF | | | | |
|---|---|---|---|---|---|
| **precursor miRNA (hairpin)** | **log2 fold change** | **lfcSE** | **fold change** | **stat** | **p-value** |
| hsa-mir-106b | 1.0262 | 0.2807 | 2.0366 | 3.6563 | 2.56E-04 |
| hsa-mir-127 | 1.4375 | 0.4011 | 2.7086 | 3.5838 | 3.39E-04 |
| hsa-mir-494 | 1.4315 | 0.4098 | 2.6972 | 3.4932 | 4.77E-04 |
| hsa-mir-299 | 1.3938 | 0.4011 | 2.6276 | 3.4747 | 5.12E-04 |
| hsa-mir-199b | 1.0230 | 0.2949 | 2.0322 | 3.4686 | 5.23E-04 |
| hsa-mir-379 | 1.3438 | 0.3884 | 2.5382 | 3.4602 | 5.40E-04 |
| hsa-mir-7158 | 1.2695 | 0.3799 | 2.4108 | 3.3420 | 8.32E-04 |
| hsa-mir-452 | 1.2786 | 0.3878 | 2.4260 | 3.2967 | 9.78E-04 |
| hsa-mir-4510 | -1.0039 | 0.3184 | 0.4986 | -3.1533 | 1.61E-03 |
| hsa-mir-889 | 1.2018 | 0.3869 | 2.3003 | 3.1064 | 1.89E-03 |
| hsa-mir-30b | 0.9932 | 0.3202 | 1.9906 | 3.1018 | 1.92E-03 |
| hsa-mir-155 | 1.0103 | 0.3260 | 2.0144 | 3.0997 | 1.94E-03 |
| hsa-mir-134 | 1.2560 | 0.4053 | 2.3883 | 3.0989 | 1.94E-03 |
| hsa-mir-20a | 1.0117 | 0.3329 | 2.0163 | 3.0394 | 2.37E-03 |
| hsa-mir-148a | 1.2421 | 0.4102 | 2.3654 | 3.0277 | 2.46E-03 |
| hsa-mir-1-2 | -1.5491 | 0.5265 | 0.3417 | -2.9422 | 3.26E-03 |
| hsa-mir-136 | 1.2104 | 0.4145 | 2.3141 | 2.9202 | 3.50E-03 |
| hsa-mir-382 | 1.2349 | 0.4269 | 2.3536 | 2.8924 | 3.82E-03 |
| hsa-mir-1-1 | -1.5349 | 0.5341 | 0.3451 | -2.8739 | 4.05E-03 |
| hsa-mir-323a | 1.1258 | 0.3971 | 2.1822 | 2.8353 | 4.58E-03 |
| hsa-mir-550a-3 | -1.3207 | 0.4665 | 0.4003 | -2.8311 | 4.64E-03 |
| hsa-mir-146b | 1.0194 | 0.3750 | 2.0270 | 2.7185 | 6.56E-03 |
| hsa-mir-711 | 0.8425 | 0.3109 | 1.7932 | 2.7103 | 6.72E-03 |
| hsa-mir-585 | 1.0465 | 0.3947 | 2.0655 | 2.6516 | 8.01E-03 |
| hsa-mir-101-2 | 0.7650 | 0.2895 | 1.6994 | 2.6422 | 8.24E-03 |
| hsa-mir-25 | 0.7389 | 0.2809 | 1.6689 | 2.6301 | 8.54E-03 |
| hsa-mir-101-1 | 0.7615 | 0.2896 | 1.6953 | 2.6294 | 8.55E-03 |
| hsa-mir-103b-2 | 0.8183 | 0.3116 | 1.7633 | 2.6264 | 8.63E-03 |
| hsa-mir-409 | 1.1184 | 0.4274 | 2.1711 | 2.6171 | 8.87E-03 |
| hsa-mir-374c | 0.8991 | 0.3491 | 1.8649 | 2.5755 | 1.00E-02 |
| hsa-mir-654 | 1.0299 | 0.4009 | 2.0419 | 2.5689 | 1.02E-02 |
| hsa-mir-224 | 0.9229 | 0.3593 | 1.8960 | 2.5685 | 1.02E-02 |

| | | | | | |
|---|---|---|---|---|---|
| hsa-mir-199a-2 | 0.7221 | 0.2812 | 1.6496 | 2.5678 | 1.02E-02 |
| hsa-mir-199a-1 | 0.7099 | 0.2768 | 1.6357 | 2.5652 | 1.03E-02 |
| hsa-mir-17 | 0.8907 | 0.3494 | 1.8541 | 2.5492 | 1.08E-02 |
| hsa-mir-22 | -0.6463 | 0.2556 | 0.6389 | -2.5283 | 1.15E-02 |
| hsa-mir-154 | 1.3097 | 0.5187 | 2.4789 | 2.5248 | 1.16E-02 |
| hsa-mir-34a | 0.8391 | 0.3329 | 1.7890 | 2.5206 | 1.17E-02 |
| hsa-mir-93 | 0.8001 | 0.3191 | 1.7413 | 2.5078 | 1.21E-02 |
| hsa-mir-520e | -1.3333 | 0.5358 | 0.3969 | -2.4884 | 1.28E-02 |
| hsa-mir-660 | 0.7458 | 0.3006 | 1.6769 | 2.4812 | 1.31E-02 |
| hsa-mir-450b | 0.7777 | 0.3162 | 1.7143 | 2.4594 | 1.39E-02 |
| hsa-mir-107 | 0.7683 | 0.3139 | 1.7032 | 2.4477 | 1.44E-02 |
| hsa-mir-4284 | -1.2944 | 0.5289 | 0.4077 | -2.4474 | 1.44E-02 |
| hsa-mir-3529 | 0.7369 | 0.3027 | 1.6666 | 2.4342 | 1.49E-02 |
| hsa-mir-92a-2 | 0.7317 | 0.3019 | 1.6606 | 2.4238 | 1.54E-02 |
| hsa-mir-629 | 0.7785 | 0.3241 | 1.7154 | 2.4018 | 1.63E-02 |
| hsa-mir-4497 | 0.9083 | 0.3852 | 1.8769 | 2.3581 | 1.84E-02 |
| hsa-mir-615 | -0.7262 | 0.3081 | 0.6045 | -2.3571 | 1.84E-02 |
| hsa-mir-370 | 0.9735 | 0.4152 | 1.9636 | 2.3449 | 1.90E-02 |
| hsa-mir-376c | 1.0974 | 0.4684 | 2.1397 | 2.3429 | 1.91E-02 |
| **mature miRNA** | | | | | |
| hsa-miR-4510 | -1.2655 | 0.2400 | 0.4160 | -5.2723 | 1.35E-07 |
| hsa-miR-22-3p | -0.8717 | 0.1743 | 0.5465 | -5.0022 | 5.67E-07 |
| hsa-miR-140-5p | -0.8504 | 0.1892 | 0.5546 | -4.4955 | 6.94E-06 |
| hsa-miR-299-3p | 1.5046 | 0.3531 | 2.8374 | 4.2614 | 2.03E-05 |
| hsa-miR-106b-3p | 0.7647 | 0.2263 | 1.6990 | 3.3785 | 7.29E-04 |
| hsa-miR-22-5p | -0.8358 | 0.2485 | 0.5603 | -3.3640 | 7.68E-04 |
| hsa-miR-361-3p | 0.7875 | 0.2383 | 1.7261 | 3.3044 | 9.52E-04 |
| hsa-miR-1290 | -1.1422 | 0.3725 | 0.4531 | -3.0665 | 2.17E-03 |
| hsa-miR-20a-5p | 0.8984 | 0.2994 | 1.8640 | 3.0005 | 2.70E-03 |
| hsa-miR-1827 | -1.3873 | 0.4655 | 0.3823 | -2.9804 | 2.88E-03 |
| hsa-miR-138-5p | -0.8444 | 0.2907 | 0.5569 | -2.9046 | 3.68E-03 |
| hsa-miR-3976 | -0.9261 | 0.3258 | 0.5263 | -2.8427 | 4.47E-03 |
| hsa-miR-17-5p | 0.8752 | 0.3163 | 1.8342 | 2.7672 | 5.65E-03 |
| hsa-miR-758-3p | 0.9601 | 0.3473 | 1.9454 | 2.7644 | 5.70E-03 |
| hsa-miR-30b-5p | 0.8301 | 0.3118 | 1.7778 | 2.6625 | 7.76E-03 |
| hsa-miR-628-5p | -1.5003 | 0.5660 | 0.3535 | -2.6508 | 8.03E-03 |
| hsa-miR-1282 | -1.1942 | 0.4506 | 0.4370 | -2.6501 | 8.05E-03 |
| hsa-miR-127-5p | 1.1813 | 0.4509 | 2.2678 | 2.6200 | 8.79E-03 |
| hsa-miR-409-5p | 1.3147 | 0.5021 | 2.4874 | 2.6183 | 8.84E-03 |
| hsa-miR-4765 | -1.2239 | 0.4704 | 0.4281 | -2.6016 | 9.28E-03 |
| hsa-miR-145-3p | -1.2037 | 0.4631 | 0.4342 | -2.5989 | 9.35E-03 |
| hsa-miR-653-3p | -1.0836 | 0.4287 | 0.4718 | -2.5275 | 1.15E-02 |
| hsa-miR-379-3p | 1.1485 | 0.4549 | 2.2168 | 2.5249 | 1.16E-02 |
| hsa-miR-199b-5p | 1.2094 | 0.4878 | 2.3124 | 2.4795 | 1.32E-02 |

| | | | | | |
|---|---|---|---|---|---|
| hsa-miR-615-3p | -0.8787 | 0.3586 | 0.5439 | -2.4501 | 1.43E-02 |
| hsa-miR-618 | -0.9569 | 0.3911 | 0.5152 | -2.4466 | 1.44E-02 |
| hsa-miR-93-5p | 0.6571 | 0.2710 | 1.5769 | 2.4249 | 1.53E-02 |
| hsa-miR-127-3p | 1.0631 | 0.4387 | 2.0894 | 2.4232 | 1.54E-02 |
| hsa-miR-450b-5p | 0.5940 | 0.2460 | 1.5094 | 2.4143 | 1.58E-02 |
| hsa-miR-589-5p | -0.8448 | 0.3511 | 0.5568 | -2.4058 | 1.61E-02 |
| hsa-miR-25-3p | 0.5853 | 0.2449 | 1.5003 | 2.3897 | 1.69E-02 |
| hsa-miR-708-3p | -1.0520 | 0.4435 | 0.4823 | -2.3720 | 1.77E-02 |
| hsa-miR-3074-3p | -1.3518 | 0.5708 | 0.3918 | -2.3684 | 1.79E-02 |
| hsa-miR-4429 | -1.3181 | 0.5591 | 0.4011 | -2.3577 | 1.84E-02 |

Eight precursor and 19 mature miRNAs were down-regulated and 43 precursor and 15 mature miRNAs up-regulated in the erlotinib-sensitive cells. Fold changes ranged between 1.50 and 2.84 (0.64 and 0.34 for down-regulation, respectively).

**Table 42 Overview of literature search for miRNAs found to be significantly differentially expressed in erlotinib-sensitive as compared to -insensitive fibroblasts by NGS**

Specific miRNAs which were significantly differentially expressed (p-value < 0.05) in all three *in vitro* treatment groups (none, 4 nM EGF or 5 µM erlotinib plus 4 nM EGF) represent a "baseline" difference between erlotinib-sensitive and -insensitive cells and are called "overlap miRNAs" here. Specific miRNAs which were only significantly differentially expressed in cells treated with erlotinib are called "erlotinib only" miRNAs here. For the "overlap" and the "erlotinib only" miRNAs a thorough literature search was conducted and publications concerning their association with cancer, EGFR or other tyrosine kinases, erlotinib or other EGFRIs, fibroblasts and keratinocytes were reviewed. √ means at least one publication has been found. (√) means a closely related or superordinate miRNA has been found in this context (e.g. hsa-mir-7 instead of hsa-mir-7-1). In the lists for mature miRNAs those miRNAs already listed for precursors are not included again. MiRNAs chosen for further analyses are marked in bold.

**"overlap miRNAs"**

| | *cue for literature search* | | | | | | | |
|---|---|---|---|---|---|---|---|---|
| **miRNA name** | **miRNA** | **cancer** | **EGFR** | **tyrosine kinase** | **erlotinib** | **keratinocytes** | **fibroblasts** | **comment** |
| **precursor** | | | | | | | | |
| hsa-mir-101-1 | √ | √ | - | - | - | - | - | |
| hsa-mir-101-2 | √ | √ | - | - | - | - | - | |
| hsa-mir-106b | √ | √ | - | - | - | - | √ | |
| hsa-mir-107 | √ | √ | √ | √ | - | √ | - | |
| hsa-mir-127 | √ | √ | - | - | - | - | √ | |
| hsa-mir-136 | √ | √ | - | - | - | - | √ | |
| hsa-mir-146b | √ | √ | √ | √ | - | - | - | interesting, see 146a in HK list |
| hsa-mir-148a | √ | √ | √ | √ | - | - | - | |
| hsa-mir-148b | √ | √ | - | √ | - | - | - | |
| hsa-mir-155 | √ | √ | √ | √ | - | √ | √ | |
| **hsa-mir-17** | √ | (√) | - | √ | √ | √ | √ | interesting (also mature) |
| hsa-mir-196a-2 | √ | √ | - | - | - | - | - | |
| hsa-mir-199a-1 | √ | (√) | - | - | - | - | - | |
| hsa-mir-199a-2 | √ | (√) | - | - | - | - | - | |
| hsa-mir-199b | √ | √ | - | √ | - | - | - | |
| hsa-mir-20a | √ | √ | - | √ | - | - | √ | |
| hsa-mir-299 | √ | √ | - | - | - | - | - | |
| **hsa-mir-30b** | √ | (√) | √ | √ | - | - | √ | interesting (also mature) |
| hsa-mir-323a | √ | √ | - | - | - | - | - | |

| | | | | | | | | |
|---|---|---|---|---|---|---|---|---|
| hsa-mir-329-1 | √ | √ | - | - | - | - | - | |
| **hsa-mir-34a** | √ | √ | √ | √ | √ | √ | √ | interesting |
| hsa-mir-379 | √ | √ | - | - | - | - | - | |
| **hsa-mir-382** | √ | √ | - | - | - | - | - | one very interesting publication |
| hsa-mir-450b | √ | - | - | - | - | - | - | |
| hsa-mir-4510 | - | - | - | - | - | - | - | |
| hsa-mir-452 | √ | √ | - | (√) | - | - | - | |
| **hsa-mir-494** | √ | √ | √ | √ | - | - | √ | interesting |
| **hsa-mir-520e** | √ | √ | √ | √ | - | - | - | interesting, also for HK! |
| hsa-mir-585 | √ | √ | - | - | - | - | - | |
| hsa-mir-660 | √ | √ | - | - | - | - | - | |
| hsa-mir-7158 | - | - | - | - | - | - | - | |
| hsa-mir-758 | √ | - | - | - | - | - | - | |
| hsa-mir-889 | √ | √ | - | - | - | - | - | |
| hsa-mir-93 | √ | √ | (√) | √ | - | - | √ | |
| | | | | | | | | |
| **mature** | | | | | | | | |
| hsa-miR-1303 | √ | √ | - | √ | - | - | - | |
| hsa-miR-138-5p | √ | √ | √ | √ | - | √ | √ | interesting, see HK list |
| hsa-miR-145-3p | √ | √ | √ | √ | - | √ | √ | |
| hsa-miR-22-5p | √ | √ | √ | √ | - | √ | √ | |
| hsa-miR-615-3p | √ | √ | - | - | - | - | - | |
| hsa-miR-708-5p | √ | √ | - | - | - | - | √ | |
| | | | | | | | | |
| | | | | | | | | |
| | | | | | | | | |
| **"erlotinib only miRNAs"** | | | | | | | | |
| | ***cue for literature search*** | | | | | | | |
| **miRNA name** | **miRNA** | **cancer** | **EGFR** | **tyrosine kinase** | **erlotinib** | **keratinocytes** | **fibroblasts** | **comment** |
| **precursors** | | | | | | | | |
| hsa-mir-1185-1 | (√) | (√) | - | - | - | - | - | |

| | | | | | | | | |
|---|---|---|---|---|---|---|---|---|
| hsa-mir-1-2 | √ | √ | (√) | (√) | - | - | (√) | publications no interesting results |
| hsa-mir-1290 | √ | √ | - | √ | - | - | - | |
| hsa-mir-152 | √ | √ | - | √ | - | - | √ | |
| hsa-mir-186 | √ | √ | √ | - | - | - | √ | |
| hsa-mir-19b-2 | (√) | (√) | (√) | - | - | - | - | |
| hsa-mir-204 | √ | √ | √ | √ | - | - | √ | |
| **hsa-mir-31** | √ | √ | √ | √ | - | √ | √ | interesting |
| hsa-mir-320c-2 | (√) | (√) | - | (√) | - | - | - | |
| hsa-mir-345 | √ | √ | - | - | - | √ | - | |
| hsa-mir-370 | √ | √ | √ | √ | - | √ | - | |
| hsa-mir-374c | (√) | (√) | - | (√) | (√) | - | - | |
| hsa-mir-409 | √ | √ | - | √ | - | - | √ | |
| hsa-mir-4497 | √ | - | - | - | - | - | - | |
| hsa-mir-485 | √ | √ | - | - | - | - | - | |
| hsa-mir-500a | √ | √ | - | - | √ | - | - | |
| hsa-mir-628 | √ | √ | - | - | - | - | - | |
| hsa-mir-6779 | - | - | - | - | - | - | - | |
| **hsa-mir-7-1** | (√) | (√) | (√) | (√) | (√) | - | - | mir-7 interesting |
| hsa-mir-711 | √ | √ | - | - | - | - | (√) | |
| hsa-mir-7-2 | √ | √ | (√) | (√) | (√) | - | - | mir-7 interesting |
| hsa-mir-7641-2 | (√) | - | - | - | - | - | - | |
| hsa-mir-769 | √ | √ | √ | √ | - | - | - | |
| hsa-mir-92a-1 | √ | √ | (√) | - | - | (√) | (√) | |
| hsa-mir-92a-2 | (√) | (√) | (√) | - | - | (√) | (√) | |
| hsa-mir-941-1 | (√) | (√) | - | - | - | - | - | |
| hsa-mir-941-2 | (√) | (√) | - | - | - | - | - | |
| | | | | | | | | |
| **mature** | | | | | | | | |
| hsa-let-7c-3p | √ | √ | √ | - | - | - | - | |
| hsa-miR-106b-3p | √ | √ | - | - | - | √ | √ | |
| hsa-miR-126-5p | √ | √ | √ | √ | - | - | √ | |
| hsa-miR-1282 | √ | - | - | - | - | - | - | |

| | | | | | | | | |
|---|---|---|---|---|---|---|---|---|
| hsa-miR-137 | √ | √ | √ | √ | √ | √ | | |
| hsa-miR-140-5p | √ | √ | √ | √ | - | - | √ | |
| hsa-miR-155-5p | √ | √ | √ | √ | (√) | √ | √ | |
| hsa-miR-193a-3p | √ | √ | - | √ | - | | | |
| hsa-miR-25-3p | √ | √ | - | (√) | - | √ | - | |
| hsa-miR-3074-3p | (√) | - | - | - | - | - | - | |
| hsa-miR-3607-3p | √ | √ | - | - | - | - | - | |
| hsa-miR-3919 | - | - | - | - | - | - | - | |
| hsa-miR-3976 | √ | √ | - | - | - | - | - | |
| hsa-miR-4327 | - | - | - | - | - | - | - | |
| hsa-miR-4429 | √ | - | - | - | - | - | - | |
| hsa-miR-4652-3p | - | - | - | - | - | - | - | |
| hsa-miR-4765 | - | - | - | - | - | - | - | |
| hsa-miR-4792 | √ | √ | - | - | - | - | - | |
| hsa-miR-5088-3p | √ | - | - | - | - | - | - | |
| hsa-miR-618 | √ | √ | - | - | - | - | - | |
| hsa-miR-628-5p | √ | √ | - | √ | - | - | - | |
| hsa-miR-93-5p | √ | √ | - | √ | - | - | √ | |

# List of Publications

### Research articles

Hichert V, Scholl C, Steffens M, Paul T, Schumann C, Rüdiger S, Boeck S, Heinemann V, Kächele V, Seufferlein T, Stingl J. Predictive blood plasma biomarkers for EGFR inhibitor-induced skin rash. *Oncotarget.* 2017; 8(21):35193-35204.

Steffens M, Paul T, Hichert V, Scholl C, von Mallek D, Stelzer C, Sörgel F, Reiser B, Schumann C, Rüdiger S, Boeck S, Heinemann V, Kächele V, Seufferlein T, Stingl J. Dosing to rash?--The role of erlotinib metabolic ratio from patient serum in the search of predictive biomarkers for EGFR inhibitor-mediated skin rash. *Eur J Cancer*. 2016; 55:131-9.

Hichert V, Steffens M, Paul T, Scholl C, Parmar S, Rüdiger S, Schumann C, Seufferlein T, Stingl JC. Gene regulatory biomarker identification for skin toxicities induced by EGFR inhibitor treatment. *Int J Clin Pharmacol Ther*. 2015; 53(12):1056-8.

Hasheminasab SM, Tzvetkov MV, Schumann C, Rüdiger S, Boeck S, Heinemann V, Kächele V, Steffens M, Scholl C, Hichert V, Seufferlein T, Brockmöller J, Stingl JC. High-throughput screening identified inherited genetic variations in the EGFR pathway contributing to skin toxicity of EGFR inhibitors. *Pharmacogenomics.* 2015; 16(14):1605-19.

Hichert V, Paul T, Scholl C, Steffens M, Stingl J. Untersuchungen zu genregulatorischen Biomarkern für EGFR-Inhibitor-vermittelte Hautreaktionen. *Bulletin zur Arzneimittelsicherheit - Informationen aus BfArM und PEI*. 2014; 3:29-33.

Paul T, Schumann C, Rüdiger S, Boeck S, Heinemann V, Kächele V, Steffens M, Scholl C, Hichert V, Seufferlein T, Stingl JC. Cytokine regulation by epidermal growth factor receptor inhibitors and epidermal growth factor receptor inhibitor associated skin toxicity in cancer patients. *Eur J Cancer.* 2014; 50(11):1855-1863.

**Conference talks**

Hichert V, Steffens M, Paul T, Scholl C, Rüdiger S, Schumann C, Seufferlein T, Stingl J. Pharmacogenomics and predictive biomarkers of epidermal growth factor receptor inhibitor-induced skin toxicity. *Retreat on Biomedical Research of the Paul Ehrlich Institute 2015*, Heidelberg, Germany.

Hichert V, Steffens M, Paul T, Scholl C, Lehmann M-L, Rüdiger S, Schumann C, Seufferlein T, Stingl J. Gene regulatory biomarker identification for EGFR Inhibitor treatment-induced skin toxicities. *Central European Society for Anticancer Drug Research (CESAR) Annual Meeting, 2014*, Bonn, Germany.

**Poster presentations**

Hichert V, Struß M, Steffens M, Scholl C, Stingl J. Gene regulatory biomarker identification for EGFR inhibitor treatment-induced skin toxicity in a cell model. *Retreat on Biomedical Research of the Paul Ehrlich Institute 2016*, Heidelberg, Germany.